Real-time quantum many-body dynamics

by

Øyvind Sigmundson Schøyen

Thesis

for the degree of

Master of Science

Faculty of Mathematics and Natural Sciences
University of Oslo

September 2019

Abstract

Solutions to the time-dependent Schrödinger equation are central to the understanding of the interaction between particles and external probes. The increasing availability of intense laser fields in experiments has spawned an interest in the study of the dynamics of many-body systems interacting with strong laser pulses. However, the complexity of the many-body problem quickly becomes a significant roadblock in the exploration of larger atoms and molecules, thus limiting the size of the systems that can be explored. Real-time *ab initio* electronic structure theory provides promising methods for investigating the dynamics of matter-field interactions and we have implemented several many-body methods which we use to analyze atoms and molecules subject to intense laser fields.

We implement three different *ab initio* real-time methods: Hartree-Fock, configuration interaction, and coupled-cluster which we apply to systems of atoms and molecules. A thorough theory section outlines the foundation of our work. We demonstrate the strengths of the implemented methods and highlight the applicability of the orbital-adaptive time-dependent coupled-cluster method with doubles excitations by showcasing how this method is stable where the more conventional time-dependent coupled-cluster method with singles-and-doubles excitations fail. We demonstrate the first dipole allowed transition energy for Neon and Argon in the aug-cc-pVDZ basis to be 19.4327 eV and 12.7275 eV, respectively. Finally, we end this thesis demonstrating the versatility of our implemented methods by exhibiting simulations of exotic systems with spin-dependent laser fields and ionization of the one-dimensional Beryllium atom.

Acknowledgements

This thesis would not have come about were it not for my two excellent supervisors: Håkon and Morten. I would like to thank Håkon for allowing me to continue on his work, and for including me in his research. Your open-mindedness towards new suggestions on any topic is truly mind-boggling and inspiring for someone as stubborn as myself. I am indebted to your counsel and friendship throughout this work. I would also like to thank Morten for providing me with such an interesting topic, and for all the guidance you have given me throughout the work with this thesis. Your insight, fascination, and knowledge on all things related to many-body physics and computations are awe-inspiring. Not to mention your passion for teaching and the well-being of students at the computational physics group. I look forward to continuing to collaborate with both of you.

Working with Sebastian on this topic have made the last couple of years a truly valuable experience. I believe that we together have achieved so much more than what would have been possible if we went our separate ways. Your excellent humor and work ethic makes the long days of work immensely more enjoyable. So many hours have been spent at the old computational physics group and most of them were with my long-time office partners Alocias, Magnus, and Vilde. Thank you all for an exciting and memorable time. A huge thanks to all the people at computational physics for making my time here so pleasant. I would also like to thank the guys and gals at OSI Elvepadling for bringing me along on adventures to the rivers all over Norway.

To my brother, Vemund, for being a truly wonderful guy! To my parents, Helle and Sigmund, for always being there and always rooting for Vemund and me. To Jenny, for your love, support, and patience throughout these last months. Your presence always make the days a little brighter, and I feel truly lucky to have you in my life. I cannot wait to explore the future with you.

Finally, to the reader of this text, wherein there are no statements of topics or derivations being “easy”, “simple”, or “trivial”. If a topic takes you several years of advanced physics study to understand, then it is *emphatically not* easy [1].

Contents

Chapter 1

Introduction

Quantum mechanics is a theory that describes the microscopic realm of nature. Given the wave function $\psi(x,t)$ we can in principle compute all there is to know about the underlying system described by the Hamiltonian $\hat{H}(x,t)$, where x is a spatial coordinate and t the time. If we know the wave function at a given initial time t_0 we can from the time-dependent Schrödinger equation,

$$i\hbar \frac{\partial}{\partial t} \psi(x,t) = \hat{H}(x,t)\psi(x,t), \tag{1.1}$$

compute all there is to know about the system for all future and earlier times. Analytical solutions to the time-dependent Schrödinger equation are truly rare, and often idealized. This means that we must resort to numerical methods for more complex systems. However, moving to the time-independent Schrödinger equation we can find the spectrum of wave functions by solving the eigenvalue equation,

$$\hat{H}\psi_k(x) = E_k\psi_k(x), \tag{1.2}$$

where E_k is the eigenenergy of the eigenstate $\psi_k(x)$. We can then build the time-dependent wave function from a linear combination of these stationary states. The inclusion of many particles – or the so-called many-body problem – is of great interest in many fields of physics and quantum chemistry, but this severely complicates the matter of solving the time-independent Schrödinger equation, and not to say, the time-dependent Schrödinger equation. As a result there exists a plethora of approximate methods, e.g., Hartree-Fock [2, 3], density functional [4], variational Monte-Carlo [5], configuration interaction [6], and coupled-cluster theory [7], which lets us locate the ground state, i.e., the eigenstate of the time-independent Schrödinger equation with the lowest eigenenergy, with various degrees of accuracy. Some of these methods allow for a description of higher excited states, and we often categorize a spectrum

of the time-independent Schrödinger equation as a solved system. However, such a description fails to explain the dynamics of a system.

Real-time methods let us simulate experiments and describe the physics as they occur. These methods provide a way to explore the evolution of particles in time as they respond to interactions from external stimuli [8]. Real-time simulations can be described as a way of preparing a system in a specific configuration, i.e., choosing an initial state $\psi(x)$, before evolving the system in time using the time-dependent Schrödinger equation by including time-dependent interactions in the Hamiltonian. With the evolution of attosecond physics and the invention of several bright light sources, our numerical experiments more and more resemble experiments done in the laboratory [9]. Due to the interest being in the many-body realm – as we study atoms and molecules – we must use an appropriate many-body method. However, for interacting fermionic systems under the influence of strong, time-dependent, external pertubations, e.g., intense laser pulses, many of the widely used many-body methods like perturbation theory fail to describe the physics of the systems. This leads us to study more advanced *ab initio* methods like coupled-cluster theory. Coupled-cluster theory allows for a systematic inclusion of many-body correlations. Compared to for example large scale diagonalization methods coupled-cluster theory resums to infinite order selected and important correlations, allowing us to study larger basis sets and a higher number of interacting particles.

1.1 Goals

Studies of time-dependent quantum mechanical systems present several challenges to traditional many-body methods, and the main goal of this thesis is thus to implement a stable and efficient approach to time-evolving systems. We have chosen to work with coupled-cluster theory, a widely used and popular method in several fields of physics and quantum chemistry [5–7, 10–15]. In particular we have implemented – for the first time – the orbital-adaptive time-dependent coupled-cluster method with doubles excitations (OATDCCD) [14]. We have developed a versatile framework which allows to study several types of quantum mechanical systems. In this thesis we focus on studies of atoms and molecules subject to intense laser pulses. To simulate a time-evolving system we need an initial condition to start the simulation. Typically we choose the ground state of the system to be our initial condition. We therefore need to implement ground state solutions to the many-body problem. As the OATDCCD-method is an extension of other time-dependent coupled-cluster methods we have also implemented the coupled-cluster doubles (CCD), and the coupled-cluster singles-and-doubles (CCSD) ground state and time-dependent solvers. Furthermore, the time-dependent Hartree-Fock

(TDHF) and time-dependent configuration interaction (TDCI) methods have been implemented for comparison.

1.2 Our contribution

There already exists a plethora of many-body codes, but almost none concerning real-time solutions to the electronic many-body problem. To the author's knowledge there are no existing implementations of the orbital-adaptive time-dependent coupled-cluster method applicable to general many-body problems. Our main contribution is therefore an implementation of this novel solver along with time-dependent coupled-cluster solvers in the doubles and singles-and-doubles approximation. As part of this work we have implemented several Hartree-Fock methods. We have implemented general, restricted, and unrestricted Hartree-Fock methods [3]. We have also implemented a time-dependent general Hartree-Fock method [16]. We have implemented the time-dependent configuration interaction method to arbitrary truncation level. We have implented one-dimensional quantum systems with arbitrary potentials, two-dimensional quantum dots in single and double wells along with magnetic fields [17]. We have implemented interfaces towards the libraries PySCF [18] and Psi4 [19]. This opens for usage of different types of basis sets and systems. The time evolution of our systems is general, but we have only implemented a description of an external laser field in the dipole approximation. This should be extensible to other types of time evolution, e.g., a time-dependent potential.

1.3 Thesis structure

This thesis has been structured into four parts:

I. A theory part reviewing central parts of quantum mechanics and many-body quantum mechanics that we deem important for an understanding of what has been done in this thesis. The three last chapters of this part describe both the ground state and time-dependent theories for the Hartree-Fock, the configuration interaction, and the coupled-cluster many-body methods. We have tried to keep these chapters as general as possible without a discussion of numerical and computational implementations.

II. In part two we discuss computational aspects, implementation of quantum systems and many-body solvers. We try to describe the most central

parts of the implementation, but leave out the bulk of the implementations as the sheer size[1] of the libraries would clutter this entire thesis.

III. Part three contains the results and discussions from the work in this thesis. The first chapter demonstrates the validity of our code. In the second chapter we discuss the stability of the novel OATDCCD-method. In the third chapter we display the quality of the implemented code by studying systems explored in the literature. We demonstrate how the methods can be used to explore exotic effects such as spin-dependent laser fields and ionization.

A note to the expert reader; a large part of this thesis has been dedicated to the author's desire at understanding much of the underlying theory and mathematics of the implemented methods. This has led to a rather extensive tome of work without necessarily highlighting the important discoveries done. The expert reader can therefore consider chapters 2 and 3 more as a review of known quantum mechanics and many-body theories.

1.4 Disclaimer

There is only so much that can be done in a year as a master's student, and indeed much of the code has been developed in collaboration with other students and researchers. Much of our work builds on the work done by Kristiansen [20]. Kristiansen has provided invaluable guidance and help as a supervisor. Both the work done by Winther-Larsen [17] and myself use the same many-body methods developed in collaboration, but our work has diverged in terms of focus and results. However, the collaboration has proved fruitful in the sense that we have arguably reached further in our work as a team than going our separate ways. The novelty and applicability of the libraries we have developed has spawned interest with researchers at the Hylleraas Center at the University of Oslo. This has led to several researchers using the code, and as a consequence they have provided us with valuable feedback. thus making the implementation more robust. Furthermore, we have received working implementations of the non-orthogonal coupled-cluster doubles (NOCCD) method [21], the direct-inversion of the iterative subspace (DIIS) acceleration [21], and the Gauss-Legendre [22] integrator which we have integrated in our framework.

[1] We have implemented approximately 15000 lines of code according to `cloc` (`http://cloc.sourceforge.net/`).

Part I

Theory

Chapter 2

Quantum mechanics

We start our journey by reviewing parts of quantum mechanics that we deem necessary in order to understand the thesis. We will in this chapter discuss the general theory of quantum mechanics without any concern for the number of particles in a specific system. In the following chapters we move on to more specialized theories that will utilize many of the results from this chapter.

2.1 The postulates of quantum mechanics

In order to make sure that we have a common understanding of how to understand and interpret quantum mechanics we begin by introducing the postulates of quantum mechanics. The postulates were originally developed by Dirac [23] and Neumann [24], but have since been subject to interpretation. This has lead to many versions of the postulates, both in the number of postulates, and in the accuracy of their description. We will base our definition of the postulates of quantum mechanics on the representation given in the book *Quantum Physics of Light and Matter* by Salasnich [25] and the lecture notes by Leinaas [26].

1. A state $|\psi\rangle$ – denoted a "ket" [27] – is a unitary vector defined on a separably complex Hilbert space. The state can be expanded in any complete set of basis vectors $|i\rangle$ on the Hilbert space by

$$|\psi\rangle = \sum_i c_i |i\rangle , \tag{2.1}$$

where $c_i \in \mathbb{C}$. For any state $|\psi\rangle$ there is a corresponding dual state $\langle\psi|$ which can be found by the anti-linear mapping

$$|\psi\rangle \to \langle\psi| = \sum_i \langle i| c_i^* . \tag{2.2}$$

The dual state is denoted a "bra" and the inner product of a ket and a bra is given by $\langle\psi_1|\psi_2\rangle \in \mathbb{C}$.

2. A physical observable is described by a Hermitian operator $\hat{Q}$ acting on the Hilbert space of state vectors. The spectrum of the operator $\hat{Q}$ spans the Hilbert space. For a discrete spectrum we get orthogonal eigenfunctions which can be made orthonormal. The eigenfunctions form a complete basis set which can be seen through the resolution of the identity, viz.

$$\sum_i |i\rangle\langle i| = \mathbb{1}, \tag{2.3}$$

where $\mathbb{1}$ is the unit operator.

3. The eigenvalue q of the observable $\hat{Q}$ represents its measurable values. That is,

$$\hat{Q}\,|q\rangle = q\,|q\rangle\,, \tag{2.4}$$

where $(q, |q\rangle)$ are the eigenpairs of the observable. We can measure the probability p of finding the normalized state $|\psi\rangle$ in the normalized eigenstate $|q\rangle$ by

$$p = \left|\langle q|\psi\rangle\right|^2. \tag{2.5}$$

As a consequence p also gives the probability of measuring the eigenvalue q. The expectation value of the observable $\hat{Q}$ for the state $|\psi\rangle$ can be measured by

$$\langle Q\rangle = \langle\psi|\hat{Q}|\psi\rangle\,. \tag{2.6}$$

4. The time evolution of a state $|\psi(t)\rangle$ is defined by the Schrödinger equation

$$i\hbar\,\frac{d}{dt}\,|\psi(t)\rangle = \hat{H}\,|\psi(t)\rangle\,, \tag{2.7}$$

where the Hamiltonian of the system $\hat{H}$ is a linear, Hermitian operator. The Hamiltonian describes a unitary time evolution of the state $|\psi(t)\rangle$.

5. The ideal measurement of $\hat{Q}$ on a state $|\psi\rangle$ projects the state onto the subspace spanned by the eigenstates of $\hat{Q}$. We have

$$|\psi\rangle \to |\psi'\rangle = \hat{Q}\,|\psi\rangle\,, \tag{2.8}$$

which is often denoted a "wave function collapse".

2.2 Time-independent Schrödinger equation

The abstract Dirac notation utilized in the postulates are useful for a coordinate independent description of quantum mechanics. However, we will often work with wave functions formulated in either position $\mathbf{r}$ or momentum $\mathbf{p}$ space. We define

$$\Psi(\mathbf{r}, t) \equiv \langle \mathbf{r} | \Psi(t) \rangle \,, \tag{2.9}$$

as the position space representation of the state vector $|\Psi(t)\rangle$, and similarly for the momentum space with $\mathbf{r}$ replaced by $\mathbf{p}$. The coordinate representation of the time-dependent Schrödinger equation thus becomes

$$i\hbar \frac{\partial}{\partial t} \Psi(\mathbf{r}, t) = -\frac{\hbar^2}{2m} \boldsymbol{\nabla}^2 \Psi(\mathbf{r}, t) + \hat{v}(\mathbf{r}, t) \Psi(\mathbf{r}, t), \tag{2.10}$$

where the total time-derivative in the Schrödinger equation has been replaced by a partial derivative with respect to time. The Hamiltonian is replaced by the kinetic term represented as a Laplace operator and we have included the external potential $\hat{v}(\mathbf{r}, t)$. For a time-independent potential $\hat{v}(\mathbf{r})$ we can solve the Schrödinger equation in Equation 2.10 using the method of separation of variables, viz.

$$\Psi(\mathbf{r}, t) = \psi(\mathbf{r}) \phi(t), \tag{2.11}$$

where $\psi(\mathbf{r})$ is a spatial function and $\phi(t)$ is purely time-dependent. Inserted into the Schrödinger equation and dividing through by $\Psi(\mathbf{r}, t)$ on both sides we get

$$i\hbar \frac{1}{\phi} \frac{d\phi}{dt} = -\frac{\hbar^2}{2m} \frac{1}{\psi} \boldsymbol{\nabla}^2 \psi + \hat{v}(\mathbf{r}). \tag{2.12}$$

As both sides are functions of their own separate variable, they must be connected through a constant, E. This means that

$$i\hbar \frac{1}{\phi} \frac{d\phi}{dt} = E, \tag{2.13}$$

$$-\frac{\hbar^2}{2m} \frac{1}{\psi} \boldsymbol{\nabla}^2 \psi + \hat{v}(\mathbf{r}) = E, \tag{2.14}$$

and we can solve the two equations independently. The former equation can be solved as a first-order, ordinary differential equation. The solution is given by

$$\phi(t) = \exp\left(-\frac{iEt}{\hbar} \right). \tag{2.15}$$

This is a solution which we will discuss in more depth in section 2.7. Multiplying by $\psi(\mathbf{r})$ on both sides in the second equation we find the *time-independent Schrödinger equation*,

$$-\frac{\hbar^2}{2m}\boldsymbol{\nabla}^2\psi + \hat{v}(\mathbf{r})\psi = E\psi. \tag{2.16}$$

We recognize the left-hand side of the latter equation as the time-independent Hamiltonian. We therefore write the time-independent Schrödinger equation on the form

$$\hat{H}\psi = E\psi, \tag{2.17}$$

and we interpret the constant E as the energy of the state ψ in the system described by the Hamiltonian $\hat{H}$. The time-independent Schrödinger equation is an eigenvalue equation, and by diagonalizing the Hamiltonian we find the spectrum of the system with the eigenpairs (ψ_n, E_n). Once the spectrum is found we say that the problem is solved as the time evolution of the wave function can be expressed as a linear combination of the eigenstates ψ_n. However, we will see in this thesis that finding the spectrum of a many-body Hamiltonian proves a challenge indeed and therefore complicates the matter of the time evolution.

2.3 Density operators

From the probability interpretation of quantum mechanics we have that a quantum state described by a single state vector $|\psi\rangle$ – denoted *pure state* – contains the maximum amount of available information about a system. Thus, as discussed in the postulates we have that a measurement on the state leads to a collapse of the wave function and therefore altering the original state. Often a single pure state is not known and instead we consider an ensemble of n pure states $\{\psi_k\}$ with a corresponding *classical probability* $\{p_k\}$ denoting the probability for the system to be in a given pure state. A system described by an ensemble of states is said to be in a *mixed state* [26]. To properly describe such a state we introduce the *density operator*

$$\hat{\rho} = \sum_{k=1}^{n} p_k \, |\psi_k\rangle\langle\psi_k| \, . \tag{2.18}$$

Let $\{\phi_i\}$ be a basis of orthonormal states, we can then compute the matrix elements of the density matrix $\boldsymbol{\rho}$ by

$$\rho_{ij} = \sum_{k=1}^{n} p_k \, \langle\phi_i|\psi_k\rangle \, \langle\psi_k|\phi_j\rangle \, . \tag{2.19}$$

From the density operator we can then compute the expectation value of operators in the mixed state by

$$\langle Q \rangle = \sum_{k=1}^{n} p_k \sum_i \langle \psi_k | \hat{Q} | \phi_i \rangle \langle \phi_i | \psi_k \rangle \equiv \mathrm{tr}\Big(\hat{\rho}\hat{Q}\Big). \tag{2.20}$$

The density operator $\hat{\rho}$ must satisfy the properties of being Hermitian, which means that $p_k \in \mathbb{R}$; positivity leading to the density matrix being *positive semidefinite*; and finally normalization of the probabilities. The latter requirement means that the trace of the density operator in any orthonormal basis must be unity. A special case of the density operator for a mixed state is

$$\hat{\rho} = |\psi\rangle\langle\psi|\,, \tag{2.21}$$

where $|\psi\rangle$ is a pure state [26]. In this thesis we will only work with pure states, but we shall see examples of states which do not satisfy the hermiticity requirement of the density operators.

2.4 The variational principle

The variational principle tells us that the "true" ground state energy E_1, i.e., the lowest energy eigenvalue of the Hamiltonian $\hat{H}$, will always be the lower bound on the energy of the system. This means that all approximate wave functions – that are determined variationally – will serve as an upper bound to the ground state energy [28].

Theorem 2.1. *Given a Hamiltonian $\hat{H}$ describing the system we are examining, and a normalized wave function $|\psi\rangle$, we have that*

$$E_1 \leqslant E[\psi, \psi^*] = \langle \psi | \hat{H} | \psi \rangle = \int dx \psi^*(x) \hat{H} \psi(x), \tag{2.22}$$

where $E[\psi, \psi^*]$ is an energy functional dependent on the shape of the wave function $|\psi\rangle$ and x is a set of coordinates. Here E_1 represents the true ground state of the Hamiltonian.

The variational principle guarantees that any wave function $|\psi\rangle$ will overestimate the ground state energy unless we have the true ground state function.

Proof. The eigenstates of the Hamiltonian will form a complete basis set for the Hilbert space they are a part of. This means that we can construct any state $|\psi\rangle$ as a linear combination of these basis functions

$$|\psi\rangle = \sum_{i=1}^{N} c_i \, |\phi_i\rangle\,, \tag{2.23}$$

where the N basis functions $\{\phi_i\}$ are eigenstates of the Hamiltonian

$$\hat{H}\,|\phi_i\rangle = E_i\,|\phi_i\rangle\,, \tag{2.24}$$

such that $E_1 \leqslant E_2 \leqslant \cdots \leqslant E_N$. Furthermore, in our formulation of the variational principle, i.e., for normalized wave functions, we require that the basis functions are orthornomal.

$$\langle\phi_i|\phi_j\rangle = \delta_{ij}, \tag{2.25}$$

and that the coefficients yield

$$|\mathbf{c}|^2 = \sum_{i=1}^{N} c_i^* c_i = 1. \tag{2.26}$$

Inserting the state $|\psi\rangle$ into the energy function[1] in Equation 2.22 we find

$$E(\mathbf{c}) = \sum_{i=1}^{N}\sum_{j=1}^{N} c_i^*\,\langle\phi_i|\hat{H}|\phi_j\rangle\,c_j = \sum_{i=1}^{N}\sum_{j=1}^{N} c_i^* c_j E_j \delta_{ij} = \sum_{i=1}^{N} |c_i|^2 E_i. \tag{2.27}$$

However, by definition E_1 is the smallest eigenvalue of the Hamiltonian, i.e., $E_1 \leqslant E_i$, for all $i \in \{1, \ldots, N\}$. We obtain

$$E(\mathbf{c}) = \sum_{i=1}^{N} |c_i|^2 E_i \geqslant E_1 \sum_{i=1}^{N} |c_i|^2 = E_1, \tag{2.28}$$

which shows that E_1 serves as a lower bound for the energy of the system under observation. □

An arguably more important result is that the stationary condition of the energy functional in the variational principle will be an eigenstate of the time-independent Schrödinger equation.

Proof. Consider a small first-order variation in the trial wave function

$$|\tilde{\psi}\rangle = |\psi\rangle + |\delta\psi\rangle\,, \tag{2.29}$$

with a corresponding adjoint equation. We denote $\delta\psi(x) \equiv \epsilon\eta(x)$, where x represents an arbitrary set of coordinates. The function $\eta(x)$ is arbitrary and ϵ is a small number. Expanding the energy functional in orders of the parameter ϵ, i.e., Taylor expanding the energy functional, we can write

$$E[\tilde{\psi}, \tilde{\psi}^*] = E[\psi, \psi^*] + \left.\frac{\partial E[\tilde{\psi}, \psi^*]}{\partial \epsilon}\right|_{\epsilon=0} \epsilon + \left.\frac{\partial E[\psi, \tilde{\psi}^*]}{\partial \epsilon}\right|_{\epsilon=0} \epsilon + \ldots. \tag{2.30}$$

[1] The energy functional is no longer dependent on a function and is therefore realized as a function instead.

Using the method of *functional derivatives* [29], we can write the derivatives of the energy functionals, and hence the stationary conditions to be

$$\left.\frac{\partial E[\tilde{\psi},\psi^*]}{\partial \epsilon}\right|_{\epsilon=0} = \int dx \frac{\delta E[\tilde{\psi},\psi^*]}{\delta \psi(x)}\eta(x) = 0, \tag{2.31}$$

$$\left.\frac{\partial E[\psi,\tilde{\psi}^*]}{\partial \epsilon}\right|_{\epsilon=0} = \int dx \frac{\delta E[\psi,\tilde{\psi}^*]}{\delta \psi^*(x)}\eta^*(x) = 0. \tag{2.32}$$

A word on notation, on the right-hand sides the integrals are over the same coordinates as for the expectation value of the Hamiltonian. This means that we move $\delta\psi(x)$ and $\eta(x)$ into the integral over the expectation value. Treating $\epsilon \in \mathbb{R}$ but allowing $\eta(x)$ to be complex, we have

$$\delta\psi(x) = \epsilon\eta(x), \qquad \delta\psi^*(x) = \epsilon\eta^*(x). \tag{2.33}$$

The variations in the energy functional are given by

$$\delta E[\tilde{\psi},\psi^*] = E[\tilde{\psi},\psi^*] - E[\psi,\psi^*], \tag{2.34}$$

$$\delta E[\psi,\tilde{\psi}^*] = E[\psi,\tilde{\psi}^*] - E[\psi,\psi^*]. \tag{2.35}$$

We find expressions for the variations by inserting Equation 2.29 into the definition of the energy functional. We have

$$E[\tilde{\psi},\psi^*] = \frac{\langle\psi|\hat{H}|\psi\rangle + \langle\psi|\hat{H}|\delta\psi\rangle}{\langle\psi|\psi\rangle + \langle\psi|\delta\psi\rangle} \tag{2.36}$$

$$= \frac{\langle\psi|\hat{H}|\psi\rangle + \langle\psi|\hat{H}|\delta\psi\rangle}{\langle\psi|\psi\rangle}\left[1 - \frac{\langle\psi|\delta\psi\rangle}{\langle\psi|\psi\rangle} + \dots\right], \tag{2.37}$$

where we no longer require that the wave functions are normalized, and we have used the relation

$$\frac{1}{1+x} = 1 - x + \mathcal{O}(x^2). \tag{2.38}$$

Keeping only first-order variations in $\delta\psi$ we can write the energy functional as

$$E[\tilde{\psi},\psi^*] = E[\psi,\psi^*] + \frac{\langle\psi|\hat{H}|\delta\psi\rangle}{\langle\psi|\psi\rangle} - E[\psi,\psi^*]\frac{\langle\psi|\delta\psi\rangle}{\langle\psi|\psi\rangle} + \dots \tag{2.39}$$

$$= E + \frac{\langle\psi|(\hat{H}-E)|\delta\psi\rangle}{\langle\psi|\psi\rangle}, \tag{2.40}$$

where for brevity we have written $E = E[\psi,\psi^*]$. The energy functional with the adjoint variation is given by

$$E[\psi,\tilde{\psi}^*] = E + \frac{\langle\delta\psi|(\hat{H}-E)|\psi\rangle}{\langle\psi|\psi\rangle}. \tag{2.41}$$

Subtracting E from the above equation the functionals yield the variations $\delta E[\tilde{\psi}, \psi^*]$ and $\delta E[\psi, \tilde{\psi}^*]$. Inserting into the stationary conditions we find

$$\int dx \frac{\delta E[\psi, \tilde{\psi}^*]}{\delta \psi^*(x)} \eta^*(x) = \frac{1}{\langle \psi | \psi \rangle} \int dx \frac{\epsilon \eta^*(x)(\hat{H} - E)\psi(x)}{\epsilon \eta^*(x)} \eta^*(x) \tag{2.42}$$

$$= \frac{\langle \eta | (\hat{H} - E) | \psi \rangle}{\langle \psi | \psi \rangle} = 0, \tag{2.43}$$

where we look at the variations over the adjoint wave function to recover the time-independent Schrödinger equation instead of the adjoint formulation. From the fundamental lemma of calculus of variations [30], we have that the stationary condition is fullfilled for all $\eta^*(x)$ as long as

$$\hat{H} |\psi\rangle = E |\psi\rangle , \tag{2.44}$$

which is just the time-independent Schrödinger equation. Looking at the stationary condition for the adjoint wave function we will find

$$\langle \psi | \hat{H} = \langle \psi | E, \tag{2.45}$$

i.e., the adjoint time-independent Schrödinger equation. We have therefore found that the stationary condition for the variational energy functional is satisfied as long as $(|\psi\rangle, E[\psi, \psi^*])$ is an eigenpair of the time-independent Schrödinger equation. This means that we can find the eigenstate $|\psi\rangle$ by optimizing the functional $E[\psi, \psi^*]$. □

The variational principle can then be summarized as follows: the stationary conditions of the variational energy functional will yield the eigenstates of the Hamiltonian.

2.4.1 The variational method

We will now look at a formulation of the variational method using wave functions that are linear combinations of a known basis set as this is a much applicable technique for our work. Given a Hermitian model Hamiltonian $\hat{H}$ and a normalized trial wave function $|\psi\rangle$ that is constructed as a linear combination of finite set of L known normalized wave functions $|\chi_\alpha\rangle$, viz.

$$|\psi\rangle = \sum_{\alpha=0}^{L} c_\alpha |\chi_\alpha\rangle , \tag{2.46}$$

where $\mathbf{c}$ is the set of coefficients c_α, we construct the variational energy function $E(\mathbf{c})$ by

$$E(\mathbf{c}) = \langle \psi | \hat{H} | \psi \rangle . \tag{2.47}$$

Optimizing the energy function is now done by finding the stationary points with respect to the variational parameters c_α. We do this by demanding that

$$\frac{\partial E(\mathbf{c})}{\partial c_\alpha} = 0, \qquad \frac{\partial^2 E(\mathbf{c})}{\partial c_\alpha \partial c_\beta} = 0, \tag{2.48}$$

where the first variation locates the stationary point and the second variation gives the Hessian matrix elements which categorizes the point as a minimum, maxmimum, or saddle [6]. However, looking at the first variation we have

$$\frac{\partial}{\partial c_\alpha} \langle \psi | \hat{H} | \psi \rangle = 0, \tag{2.49}$$

which is not solvable as the equations stand [3] as they are unbounded. In order to construct equations which can be optimized, we use Lagrange's method of undetermined multipliers to construct a new function $G(\mathbf{c})$ given by [3, 6]

$$G(\mathbf{c}) = \langle \psi | \hat{H} | \psi \rangle - E(\mathbf{c}) \left(\langle \psi | \psi \rangle - 1 \right), \tag{2.50}$$

where we have introduced the normalization condition for the trial wave function as a constraint. Optimizing this function for the first variation we find

$$\begin{aligned} \frac{\partial G(\mathbf{c})}{\partial c_\alpha} = &\left[\frac{\partial}{\partial c_\alpha} \langle \psi | \right] \hat{H} | \psi \rangle + \langle \psi | \hat{H} \left[\frac{\partial}{\partial c_\alpha} | \psi \rangle \right] - \langle \psi | \psi \rangle \frac{\partial E(\mathbf{c})}{\partial c_\alpha} \\ &- E(\mathbf{c}) \left[\frac{\partial}{\partial c_\alpha} \langle \psi | \right] | \psi \rangle - \langle \psi | \left[\frac{\partial}{\partial c_\alpha} | \psi \rangle \right] \qquad (2.51) \\ = &\, 2 \langle \chi_\alpha | \hat{H} | \psi \rangle - 0 - 2E(\mathbf{c}) \langle \chi_\alpha | \psi \rangle = 0, \qquad (2.52) \end{aligned}$$

where the first variation in the energy function becomes zero due to the conditions imposed on the stationary point. Furthermore, due to the hermiticity of the Hamiltonian, we have collected equal terms. Inserting the expansion for the trial wave function on both sides, we find

$$\sum_{\beta=0}^{L} \langle \chi_\alpha | \hat{H} | \chi_\beta \rangle c_\beta - E(\mathbf{c}) \sum_{\beta=0}^{L} \langle \chi_\alpha | \chi_\beta \rangle c_\beta = 0 \tag{2.53}$$

$$\implies \sum_{\beta=0}^{L} H_{\alpha\beta} c_\beta = E(\mathbf{c}) \sum_{\beta=0}^{L} s_{\alpha\beta} c_\beta \tag{2.54}$$

$$\implies \mathbf{H}\mathbf{c} = E(\mathbf{c}) \mathbf{S}\mathbf{c}, \tag{2.55}$$

where we have defined the overlap matrix $\boldsymbol{S}$ from the overlap integrals between the known basis elements $|\chi_\alpha\rangle$ by

$$s_{\alpha\beta} \equiv \langle \chi_\alpha | \chi_\beta \rangle \tag{2.56}$$

We have now reduced the task of optimizing the energy function to the problem of solving the generalized eigenvalue equation in Equation 2.55. In other words, by creating the Hamiltonian matrix $\mathbf{H}$ and the overlap matrix $\mathbf{S}$ from the basis of known basis elements, we can diagonalize the matrices, i.e., solve the generalized eigenvalue equation, and extract the optimal eigenpair $(E, \mathbf{c})$ as the eigenvalue and eigenvector respectively. This procedure will be used extensively as a procedure to transform from a known to an unknown basis. See the book *Molecular Electronic-Structure Theory* by Helgaker *et al.* [6] for a derivation of the Hessian matrix elements.

2.5 The Hellmann-Feynman theorem

The Hellmann-Feynman theorem provides us with a method of calculating first-order changes (also known as a first-order property) in the energy due to a perturbation [6].

Theorem 2.2. *If $|\psi\rangle$ is a normalized eigenstate of the Hamiltonian $\hat{H}$, or $|\psi\rangle$ is variationally determined from the Hamiltonian $\hat{H}$, the Hellmann-Feynman theorem [31] states that*

$$\left.\frac{dE(\alpha)}{d\alpha}\right|_{\alpha=0} = \left.\frac{\partial}{\partial\alpha}\langle\psi_\alpha|\,\hat{H} + \alpha\hat{V}\,|\psi_\alpha\rangle\right|_{\alpha=0} = \langle\psi|\,\hat{V}\,|\psi\rangle\,, \tag{2.57}$$

where α is a perturbational parameter and $\hat{V}$ the perturbation operator. The wave function $|\psi_\alpha\rangle$ is given by

$$|\psi_\alpha\rangle = N(|\psi\rangle + \alpha\,|\delta\psi\rangle), \tag{2.58}$$

where N is a normalization factor. For approximate wave functions, they must be optimized with respect to the same variational parameter α as in the theorem.

Proof. The underlying assumption is that

$$\hat{H}\,|\psi\rangle = E\,|\psi\rangle\,, \tag{2.59}$$

regardless if we have an exact or a variationally determined wave function $|\psi\rangle$. Furthermore, both perturbed and unperturbed wave functions are normalized, viz.

$$\langle\psi|\psi\rangle = \langle\psi_\alpha|\psi_\alpha\rangle = 1 \implies \frac{\partial}{\partial\alpha}\langle\psi_\alpha|\psi_\alpha\rangle = 0. \tag{2.60}$$

See reference [6] for a proof where the normalization of the perturbed wave function is relaxed. We now prove Equation 2.57 directly.

$$\left.\frac{dE(\alpha)}{d\alpha}\right|_{\alpha=0} = \left.\frac{\partial}{\partial\alpha}\langle\psi_\alpha|\hat{H}+\alpha\hat{V}|\psi_\alpha\rangle\right|_{\alpha=0} \tag{2.61}$$

$$= \langle\delta\psi|\hat{H}|\psi\rangle + \langle\psi|\hat{V}|\psi\rangle + \langle\psi|\hat{H}|\delta\psi\rangle \tag{2.62}$$

$$= E\left[\langle\delta\psi|\psi\rangle + \langle\psi|\delta\psi\rangle\right] + \langle\psi|\hat{V}|\psi\rangle \tag{2.63}$$

$$= E\frac{\partial}{\partial\alpha}\langle\psi|\psi\rangle + \langle\psi|\hat{V}|\psi\rangle \tag{2.64}$$

$$= \langle\psi|\hat{V}|\psi\rangle\,, \tag{2.65}$$

which is what we wanted to show. □

A consequence of the Hellmann-Feynman theorem is that it provides us with a technique for computing expectation values of other quantities than the energy once we have variatonally determined the optimal state for a given system. For example, the expectation value of the operator $\hat{O}$ can be found by

$$\langle O\rangle = \langle\psi|\hat{O}|\psi\rangle = \frac{\partial}{\partial\alpha}\left.\langle\psi_\alpha|\hat{H}+\alpha\hat{O}|\psi_\alpha\rangle\right|_{\alpha=0} = \left.\frac{\partial E(\alpha)}{\partial\alpha}\right|_{\alpha=0}. \tag{2.66}$$

This avoids the need of having to variationally determine every expectation value that we wish to measure as finding the optimal parameters for the energy is enough.

2.6 The time-dependent Schrödinger equation

Moving to the time domain, the dynamics of an isolated quantum system is described by the Schrödinger equation

$$i\hbar\frac{d}{dt}|\psi(t)\rangle = \hat{H}(t)|\psi(t)\rangle\,. \tag{2.67}$$

Given an initial state $|\psi(t_0)\rangle$ at an initial time t_0, we can use the time-dependent Schrödinger equation to determine $|\psi(t)\rangle$ for all earlier and later times. A point to note is that the time-dependent Schrödinger equation does not require that the initial state $|\psi(t)\rangle$ be a "meaningfull state", the equation will evolve this state – whatever it is – in time governed by the time-dependent Hamiltonian $\hat{H}(t)$. This is an important point in the sense that solving the time-dependent Schrödinger equation for a specific Hamiltonian can prove a great challenge. The approach that we take in this thesis is to choose an initial state, most often the approximation we have for the ground state of the

time-independent Schrödinger equation, and evolve this state in time. This can be thought of as "preparing" a system in the ground state and then perturbing the system with an external interaction which triggers a reaction in the dynamics of the system.

2.7 The time evolution operators

Any solution to the time-dependent Schrödinger equation is given by

$$|\psi(t)\rangle = \hat{U}(t, t_0)\,|\psi(t_0)\rangle\,, \tag{2.68}$$

where $\hat{U}(t, t_0)$ is the time evolution operator that acts on the initial state $|\psi(t_0)\rangle$, and yields the state $|\psi(t)\rangle$ at some other time t. The time evolution operators are unitary at common times, viz.

$$\hat{U}^\dagger(t, t_0)\hat{U}(t, t_0) = \mathbb{1}. \tag{2.69}$$

This means that we can go "backwards in time" in the sense that going from $|\psi(t)\rangle \to |\psi(t_0)\rangle$ is done by

$$|\psi(t_0)\rangle = \hat{U}^\dagger(t, t_0)\,|\psi(t)\rangle\,. \tag{2.70}$$

Furthermore, we can compose a time evolution operator from other time evolution operators as

$$\hat{U}(t_2, t_0) = \hat{U}(t_2, t_1)\hat{U}(t_1, t_0). \tag{2.71}$$

One way to realize this is that we are allowed to have intermediate states between two points in time t_2 and t_0. This seemingly benign result is important for our numerical time propagation schemes as we make use of this property to move between two time points using many small intermediate steps, where smaller steps in general yields lower errors. The time evolution operator can be found by solving the time-dependent Schrödinger equation

$$i\,\frac{\partial}{\partial t}\,\hat{U}(t, t_0) = \hat{H}(t)\hat{U}(t, t_0). \tag{2.72}$$

Now, if the Hamiltonian is time-independent the time evolution operator takes on the closed form solution

$$\hat{U}(t, t_0) = \exp\left(\frac{-i\hat{H}}{\hbar}(t - t_0)\right). \tag{2.73}$$

Assuming we have found the spectrum of our time-independent Hamiltonian, where (E_n, ψ_n) are the eigenpairs, and we use an eigenstate from the the spectrum as our initial state, we find that

$$|\psi_n(t)\rangle = \exp\left(\frac{-i\hat{H}}{\hbar}(t-t_0)\right)|\psi_n\rangle = \exp\left(\frac{-iE_n}{\hbar}(t-t_0)\right)|\psi_n\rangle\,, \tag{2.74}$$

where $|\psi_n(t)\rangle$ is a *stationary state*. This means that all expectation values are stationary in time as can be seen from

$$\langle O(t)\rangle = \sum_n \langle\psi_n(t)|\hat{O}|\psi_n(t)\rangle = \sum_n \langle\psi_n|\hat{O}|\psi_n\rangle = \langle O\rangle\,, \tag{2.75}$$

where the time dependence cancels. However, a general time-dependent state $|\psi(t)\rangle$ can be written as a linear combination of the eigenstates, viz.

$$|\psi(t)\rangle = \sum_n c_n(t)\,|\psi_n\rangle\,, \tag{2.76}$$

where we have absorbed the time-dependency into the coefficients, and require that the squared sum of the coefficients should equal unity. This means that even though the Hamiltonian is time-independent, the states themselves are not stationary. All observables that commute with the time-independent Hamiltonian will still be time-independent for $|\psi(t)\rangle$. We can see this by looking at a time-independent observable $\hat{Q}$ which commutes with the time-independent Hamiltonian such that the eigenstate of the Hamiltonian will be eigenstates of $\hat{Q}$ with eigenvalues q_n. We then have

$$\langle Q(t)\rangle = \langle\psi(t)|\hat{Q}|\psi(t)\rangle = \sum_{n,m} c_n^*(t)c_m(t)\,\langle\psi_n|\hat{Q}|\psi_m\rangle \tag{2.77}$$

$$= \sum_{n,m} c_n^*(t)c_m(t)q_n\delta_{nm} = \sum_n \left|c_n(t)\right|^2 q_n = \sum_n q_n, \tag{2.78}$$

which shows that the observables that commute with the time-independent Hamiltonian are time-independent.

In the case of a time-dependent Hamiltonian, the time evolution operator takes on a more complicated shape.

$$\hat{U}(t,t_0) = \mathcal{T}\exp\left(-\frac{i}{\hbar}\int_{t_0}^{t} d\tau\hat{H}(\tau)\right), \tag{2.79}$$

where $\mathcal{T}$ is the time-ordering operator. As an extra complicating factor, the time-dependent Hamiltonian might not commute with itself at different times. The time evolution operator shown in Equation 2.79 serve as a theoretical foundation for the time evolution. However, we will see later in the thesis how one can approximate this operator using known numerical integration methods.

2.8 The time-dependent variational principle

We now wish to extend the variational principle to the time-domain. This is done by the time-dependent variational principle by considering the action functional

$$S = \int_{t_1}^{t_2} dt L[\psi, \psi^*], \tag{2.80}$$

where $L[\psi, \psi^*]$ is a Lagrangian functional of the trial wave function ψ and its adjoint. In the case of normalized trial wave functions in time, the Lagrangian is given by

$$L[\psi, \psi^*] = \langle \psi(t) | \Big(i\hbar\partial_t - \hat{H}(t) \Big) | \psi(t) \rangle \,, \tag{2.81}$$

where we for the sake of brevity have introduced the short-hand notation ∂_t for the partial derivative with respect to time. If the wave functions are not required to be normalized in time the Lagrangian takes on a more complicated form to ensure that the action stays real as the differential operator $i\partial_t$ does not stay Hermitian along with the normalization condition [32]. By requiring that the first-order variations

$$\delta S = \int_{t_1}^{t_2} dt \delta L = 0, \tag{2.82}$$

are stationary we recover the time-dependent Schrödinger equation.

Proof. Performing variations in a similar fashion as in section 2.4,

$$\tilde{\psi}(x, t) = \psi(x, t) + \epsilon\eta(x, t), \tag{2.83}$$

and the adjoint equation with $\epsilon \in \mathbb{R}$ and $\eta(x, t)$ a complex function. Note that we now include time-dependent variations as we no longer restrict ourselves to stationary states. The stationary condition in Equation 2.82 results in the requirements that

$$\delta L[\tilde{\psi}, \psi^*] = \langle \psi(t) | \Big(i\hbar\partial_t - \hat{H}(t) \Big) | \delta\psi(t) \rangle = 0, \tag{2.84}$$

$$\delta L[\psi, \tilde{\psi}^*] = \langle \delta\psi(t) | \Big(i\hbar\partial_t - \hat{H}(t) \Big) | \psi(t) \rangle = 0. \tag{2.85}$$

The latter of these two equations is known as the Dirac-Frenkel variational principle. Letting $\delta\psi(x, t)$ be arbitrary variations vanishing at the endpoints $t = t_1$ and $t = t_2$, we recover the time-dependent Schrödinger equation and the complex conjugate formulation from the fundamental lemma of calculus of variations [30, 33]. □

2.9 Electrodynamics

In vacuum the classical electromagnetic field is described by Maxwell's equations without sources.

$$\nabla \cdot \mathbf{E} = 0, \tag{2.86}$$

$$\nabla \cdot \mathbf{B} = 0, \tag{2.87}$$

$$\nabla \times \mathbf{E} = -\frac{\partial}{\partial t}\mathbf{B}, \tag{2.88}$$

$$\nabla \times \mathbf{B} = \frac{1}{c^2}\frac{\partial}{\partial t}\mathbf{E}, \tag{2.89}$$

where $\mathbf{E}(\mathbf{r}, t)$ and $\mathbf{B}(\mathbf{r}, t)$ are the electric and magnetic fields respectively. Here "without sources" translates to the charge density ρ and the current density $\mathbf{j}$ being set to zero. The electric and magnetic fields can be described by the scalar and vector potentials $\phi(\mathbf{r}, t)$ and $\mathbf{A}(\mathbf{r}, t)$, respectively, by the relations

$$\mathbf{E} = -\nabla\phi - \frac{\partial}{\partial t}\mathbf{A}, \tag{2.90}$$

$$\mathbf{B} = \nabla \times \mathbf{A}. \tag{2.91}$$

In addition to Maxwell's equations, the potentials and the electric and magnetic fields satisfy the homogeneous wave equation [9]

$$\nabla^2\mathbf{A} = \frac{1}{c^2}\frac{\partial^2}{\partial t^2}\mathbf{A}. \tag{2.92}$$

Maxwell's equations and the wave equation does not uniquely define the scalar and vector potentials as the electric and magnetic field are invariant under the gauge transformations

$$\mathbf{A} \to \mathbf{A}' = \mathbf{A} + \nabla f, \tag{2.93}$$

$$\phi \to \phi' = \phi + \frac{\partial f}{\partial t}, \tag{2.94}$$

where f is a differentiable, real function of $\mathbf{r}$ and t. To go from here we choose a gauge fixing condition such that we are able to remove non-physical degrees of freedom [26]. We will strictly be working in the non-relativistic limit such that the Lorenz gauge[2] is unnecessary. We will be using the Coulomb gauge given by

$$\nabla \cdot \mathbf{A} = 0. \tag{2.95}$$

[2]Yes, this is *actually* spelled "the Lorenz gauge", named after the Danish physicist Ludvig Lorenz and is *not* to be confused with the misnamed "Lorentz gauge" after Hendrik Lorentz. However, the Lorenz gauge is a Lorentz invariant condition where the two terms frequently coincide and is therefore quite often interchanged [34].

Without sources this means that $\phi = 0$ and the electric and magnetic fields are found by

$$\mathbf{E} = -\frac{\partial}{\partial t}\mathbf{A}, \tag{2.96}$$

$$\mathbf{B} = \boldsymbol{\nabla} \times \mathbf{A}. \tag{2.97}$$

A solution to the wave equation in Equation 2.92 for the vector potential $\mathbf{A}$ is the monochromatic plane wave solutions with wave number $\mathbf{k} = 2\pi/\lambda$, and angular frequency $\omega_k = |\mathbf{k}|c$. That is,

$$\mathbf{A}(\mathbf{r}, t) = \mathbf{A}_0 \exp\left[i(\mathbf{k}\cdot\mathbf{r} - \omega_k t)\right] + \mathbf{A}_0^* \exp\left[-i(\mathbf{k}\cdot\mathbf{r} - \omega_k t)\right], \tag{2.98}$$

where the first term represents the positive frequency solution and the second term the negative frequency solution. The amplitudes $\mathbf{A}_0$ are given by

$$\mathbf{A}_0 = \boldsymbol{\epsilon} A_0, \tag{2.99}$$

where $\boldsymbol{\epsilon}$ is the polarization vector, and we have that $\boldsymbol{\epsilon}\cdot\boldsymbol{\epsilon}^* = 1$. If the polarization vector is real and time-independent, we say that the electromagnetic field is linearly polarized. The Coulomb gauge condition is satisfied if

$$\mathbf{k}\cdot\boldsymbol{\epsilon} = 0, \tag{2.100}$$

that is, the wave is transversal and the polarization is perpendicular to the propagation direction. In three dimensions we can in general write the plane wave solution as a linear combination of two linearly independent polarization vectors $\boldsymbol{\epsilon}_1$ and $\boldsymbol{\epsilon}_2$ which both are orthogonal to the wave vector $\mathbf{k}$ thus forming a three-dimensional coordinate system. This opens up for elliptical polarization of the electromagnetic field. However, we will in this thesis limit ourselves to the case of linearly polarized fields with real polarization vectors.

Now, Equation 2.98 describes a classical plane wave solution to the wave equation. It is possible to quantize the plane wave solution and introduce Fock states for the electromagnetic vector potential. The laser fields we will be working with will have such a high photoncount that the classical description of the field will dominate over quantum fluctuations arising from quantization of the fields [9]. An alternative is to describe the radiation from the laser field as a coherent state, which will allow us to use the quantum mechanical description of the electromagnetic field [9, 26]. However, we will in the following remain in the classical description of the electromagnetic fields yielding a semi-classical approach to describing interactions between particles and electromagnetic fields.

2.9.1 Particle-field interactions

In a quantum description of the electromagnetic field, we have the full Hamiltonian of a particle in a potential $v(\mathbf{r})$ given by

$$\hat{H} = \hat{H}_p + \hat{H}_e + \hat{H}_{ep}, \tag{2.101}$$

where we have denoted the particle (or, matter) contribution by $\hat{H}_p$, the electromagnetic contribution by $\hat{H}_e$ and finally the interaction between particles and the electromagnetic field by $\hat{H}_{ep}$. In the classical description of the electromagnetic field, the free-field Hamiltonian takes on the form

$$H(t) = \frac{1}{2}\int d^3\mathbf{r}\left[\epsilon_0 \mathbf{E}^2(\mathbf{r},t) + \frac{1}{\mu_0}\mathbf{B}^2(\mathbf{r},t)\right], \tag{2.102}$$

where ϵ_0 is the vacuum permittivity and μ_0 the magnetic permeability. The free-field contribution to the total Hamiltonian is necessary to include in order to keep the system of particles and fields conservative. This term allows for interchange of energy between the particles and the electromagnetic fields thus conserving the total energy. In the semi-classical description we use, the free-field Hamiltonian will reduce to a time-dependent constant as the electric and magnetic fields are classical quantities which do not act as operators on the quantum states. We will ignore the free-field Hamiltonian in the rest of this text and treat the particle-field interaction $\hat{H}_{ep}$ as a perturbation to the particle Hamiltonian $\hat{H}_p$, viz

$$\hat{H} = \hat{H}_p + \hat{H}_{ep}, \tag{2.103}$$

which means that the total energy will *not* be conserved while the field is active. The particle contribution to the Hamiltonian is given by

$$\hat{H}_p = \frac{\hat{\mathbf{p}}^2}{2m} + v(\mathbf{r}), \tag{2.104}$$

where we have ignored particle-particle interaction in this discussion. However, when we do include the Coulomb interaction in the chapter on many-body quantum mechanics, this will be included to $\hat{H}_p$ without any extra concern for the particle-field interaction $\hat{H}_{ep}$. The particle-field interaction term $\hat{H}_{ep}$ is typically found by describing a system with free particles subject to an external electromagnetic field in terms of a Lagrangian. This Hamiltonian is given by

$$\hat{H}_f = \frac{1}{2m}\left[\hat{\mathbf{p}} - q\boldsymbol{A}\right]^2 + q\phi, \tag{2.105}$$

where q is the charge of the particles. To get rid of the extra kinetic term we therefore find $\hat{H}_{ep}$ by

$$\hat{H}_{ep} = \hat{H}_f - \frac{\hat{\mathbf{p}}^2}{2m} = -\frac{q}{2m}\left[\hat{\mathbf{p}}\cdot\mathbf{A} + \mathbf{A}\cdot\hat{\mathbf{p}}\right] + \frac{q^2}{2m}\mathbf{A}^2 + q\phi. \tag{2.106}$$

However, this form comes from a classical description of the Hamiltonian and therefore does not include spin. This can be added by

$$\hat{H}_s = \frac{gq}{2m}\hat{\mathbf{S}}\cdot\mathbf{B}, \tag{2.107}$$

where g is the g-factor of the particle. The spin-coupling term is small compared to the other two particle-field interactions [26]. Furthermore, when we move to the dipole approximation, this term will disappear completely and we will therefore ignore the spin-coupling. Working in the Coulomb gauge, we can make the first term in Equation 2.106 a little shorter. If we consider a test function $f = f(\mathbf{r})$, we see that

$$\hat{\mathbf{p}}\cdot\mathbf{A}f = -i\hbar\boldsymbol{\nabla}\cdot(\mathbf{A}f) = -i\hbar\left(f\boldsymbol{\nabla}\cdot\mathbf{A} + \mathbf{A}\boldsymbol{\nabla}f\right) = -i\hbar\mathbf{A}\boldsymbol{\nabla}f = \mathbf{A}\cdot\hat{\mathbf{p}}f, \tag{2.108}$$

where going from the second to the third equality we used the Coulomb gauge condition that the divergence of $\mathbf{A}$ should be zero. Thus, the particle-field interaction term should be

$$\hat{H}_{ep} = -\frac{q}{m}\mathbf{A}\cdot\hat{\mathbf{p}} + \frac{q^2}{2m}\mathbf{A}^2 + q\phi \tag{2.109}$$

without the spin-coupling. Now, the full Hamiltonian in Equation 2.103, without the spin-coupling, will be invariant under the the quantum mechanical gauge transformations [9]

$$\mathbf{A} \to \mathbf{A}' = \mathbf{A} + \boldsymbol{\nabla}f, \tag{2.110}$$

$$\phi \to \phi' = \phi - \frac{\partial f}{\partial t}, \tag{2.111}$$

$$\psi \to \psi' = \exp\left[\frac{iq}{\hbar}f\right]\psi, \tag{2.112}$$

where $f = f(\mathbf{r}, t)$ is a real, differentiable function and $\psi = \psi(\mathbf{r}, t)$ is a solution to the time-dependent Schrödinger equation. A demonstration of the invariance of the Hamiltonian from Equation 2.103 under the listed gauge transformations is shown in section A.1.

2.9.2 The dipole approximation

If we assume that the wavelength λ of the field is much larger than the size of the quantum system, that is, if

$$\lambda \gg |\mathbf{r}| \implies \mathbf{k}\cdot\mathbf{r} \ll 1, \tag{2.113}$$

the spatial variations of the electromagnetic field will be small compared to the time variations. When looking at atomic particles with sizes on the order of nanometers, this approximation can be good when the electromagnetic field is in the low frequency domain, e.g., infrared light with wave lengths of the order of 700 nm to 1 mm. Looking at the plane wave solution in Equation 2.98 we see that

$$\exp[\pm i\mathbf{k}\cdot\mathbf{r}] = 1 \pm i\mathbf{k}\cdot\mathbf{r} - \frac{1}{2}(\mathbf{k}\cdot\mathbf{r})^2 + \ldots, \tag{2.114}$$

where the first term will dominate. The *dipole approximation* consists of choosing this term as the only contribution to the spatial variations, i.e.,

$$\exp[\pm i\mathbf{k}\cdot\mathbf{r}] \approx 1. \tag{2.115}$$

This means that $\mathbf{A}(\mathbf{r}, t) \approx \mathbf{A}(t)$ and we get a spatially uniform electromagnetic field. In the Coulomb gauge this means that

$$\mathbf{E} = -\frac{d}{dt}\mathbf{A}, \tag{2.116}$$

$$\mathbf{B} = \boldsymbol{\nabla}\times\mathbf{A} = 0, \tag{2.117}$$

and as promised, the magnetic field and therefore the spin-coupling disappears in the particle-field interaction from Equation 2.107.

In the dipole approximation we can write the vector potential as

$$\mathbf{A}(t) = \mathbf{A}_0 e^{-i\omega_k t} + \mathbf{A}_0^* e^{i\omega_k t} = \boldsymbol{\epsilon}\left[A_0 e^{-i\omega_k t} + A_0^* e^{i\omega_k t}\right]. \tag{2.118}$$

In the case of a quantized electromagnetic field where the amplitudes are photon creation and annihilation operators and all operators are expressed in the interaction picture, it is common to split the particle-field interaction Hamiltonian into an emission part related to the negative frequency solutions and an absorption part for the positive frequency solutions. It is then possible to observe quantum effects such as spontaneous emission where a system will be able to emit a photon even if there are no electromagnetic fields present. However, as stated, we work in the semi-classical approximation and we will assume that quantum fluctuations such as spontaneous emission are small compared to classical effects. We will therefore collect both the positive and the negative frequency solutions into a single term.

$$\mathbf{A}(t) = \boldsymbol{\epsilon}\mathcal{A}_0 \sin(\omega_k t + \phi), \tag{2.119}$$

where ϕ is a phase factor and we have defined

$$2\,\mathrm{Re}(A_0) = \mathcal{A}_0 \sin(\phi), \tag{2.120}$$

$$2\,\mathrm{Im}(A_0) = \mathcal{A}_0 \cos(\phi), \tag{2.121}$$

and used the exponential identities for the sine and cosine. To go from here we introduce the gauge function

$$f \equiv -\mathbf{A}(t) \cdot \mathbf{r}, \tag{2.122}$$

and insert it into the gauge transformations from Equation 2.110 to Equation 2.112 with $\phi = 0$. This yields

$$\mathbf{A}' = \mathbf{A} + \boldsymbol{\nabla} f = 0, \tag{2.123}$$

$$\phi' = -\frac{\partial f}{\partial t} = -\mathbf{r} \cdot \mathbf{E}, \tag{2.124}$$

$$\psi' = \exp\left[-\frac{iq}{\hbar}\mathbf{A}(t) \cdot \mathbf{r}\right]\psi, \tag{2.125}$$

where we have inserted the electric field $-\mathbf{E} = \dot{\mathbf{A}}$ in the dipole approximation in the gauge transformation for the scalar potential. Inserted into the time-dependent Schrödinger equation we then find

$$i\hbar \frac{\partial}{\partial t}\psi' = \left[\hat{H}_p - q\hat{\mathbf{r}} \cdot \mathbf{E}\right]\psi'. \tag{2.126}$$

This transformation is known as the *length gauge* due to the position operator $\hat{\mathbf{r}}$ [9]. Collecting the position operator and the electric charge q we find the *electric dipole moment* given by

$$\hat{\mathbf{d}} \equiv q\hat{\mathbf{r}}, \tag{2.127}$$

For the plane-wave solution of the vector potential we get the corresponding electric field

$$\mathbf{E} = \boldsymbol{\epsilon}\mathcal{E}_0 \cos(\omega_k t + \phi), \tag{2.128}$$

where we have defined the constant

$$\mathcal{E}_0 = -\omega_k \mathcal{A}_0. \tag{2.129}$$

This in total yields the particle-field interaction of the Hamiltonian to be

$$\hat{H}_{ep} = -\hat{\mathbf{d}} \cdot \boldsymbol{\epsilon}\mathcal{E}_0 \cos(\omega_k t + \phi). \tag{2.130}$$

2.9.3 Selection rules

Computing the matrix elements of the particle-field interaction term of the Hamiltonian between two states $|\psi_a\rangle$ and $|\psi_b\rangle$ we find

$$\langle\psi_a|\hat{H}_{ep}(t)|\psi_b\rangle = -\langle\psi_a|\hat{\mathbf{d}}|\psi_b\rangle \cdot \mathbf{E}(t), \tag{2.131}$$

where the matrix elements of the dipole moment decides which transitions are allowed as a consequence of conservation of spin and parity [26]. In short, only non-zero matrix elements for the dipole moment will contribute to the total Hamiltonian. We will discuss selection rules in more detail when we look at specific quantum systems. It is worth mentioning that the selection rules only apply for the dipole effects. This means that an experiment might yield transitions which are deemed forbidden in the dipole regime occuring from higher multipole expansions in the exponential plane wave solution.

2.10 Laser fields

The topic of lasers and laser fields interacting with atomic systems is a vast subject, and we will skim lightly at the edge of this field, discussing the more important aspects that are related to our simulations. Now, a linearly polarized, monochromatic laser field in the dipole approximation can be described by a vector potential on the form [9]

$$\mathbf{A}(t) = \boldsymbol{\epsilon}\mathcal{A}_0 \sin(\omega_k t + \phi). \tag{2.132}$$

$$\tag{2.133}$$

From Equation 2.116 we find the corresponding expression for the electric field to be

$$\mathbf{E}(t) = \boldsymbol{\epsilon}\mathcal{E}_0 \cos(\omega_k t + \phi), \tag{2.134}$$

where $\mathcal{E}_0$ is defined as in Equation 2.129. These two equations describe a spatially homogeneous electric field oscillating in time. Furthermore, they describe a laser that is "switched on" for the entire simulation. However, we are often interested in firing a short laser pulse at the system before turning it off. Thus we can observe how the system reacts after the laser is switched off and we avoid driving the system in time.

A linearly polarized laser pulse in the dipole approximation can be described by the vector potential [9]

$$\mathbf{A}(t) = \boldsymbol{\epsilon}\mathcal{A}_0 \int_{-\infty}^{t} dt' F(t') \cos\big(\omega_k t' + \phi\big), \tag{2.135}$$

where we treat ω_k and ϕ constant in time over the response of the system. The function $F(t) \in [0, 1]$ is known as the *envelope* of the pulse and we will discuss it in due time. We find the electric field of the dipole laser from Equation 2.116.

$$\mathbf{E}(t) = \boldsymbol{\epsilon}\mathcal{E}_0 F(t) \cos(\omega_k t + \phi). \tag{2.136}$$

We see that by setting $F(t) = 1$ we recover the expression for the monochromatic, linearly polarized, laser field.

2.10.1 Envelope

The purpose of the envelope function $F(t)$ is to ensure that the laser pulse goes smoothly to zero outside some defined region such that the electric field disappears at $t \to \pm\infty$. Furthermore it defines the temporal shape of the field. There are different models for the envelope function defined to replicate real laser pulses. Common choices are the cosine-squared, Gaussian, and the hyperbolic secant functions [9]. The cosine-squared envelope function is given by

$$F(t) = \begin{cases} \cos^2\left[\pi t/T\right], & t \in [-T/2, T/2], \\ 0, & \text{else}, \end{cases} \tag{2.137}$$

where T decides how long the envelope should last. We define a cycle of the laser pulse to be $2\pi/\omega_k$. It is common to choose $T = 2n\pi/\omega_k$, where $n \in \mathbb{N} \setminus 0$ to ensure that we fit n cycles of the laser pulse inside the envelope, but this is strictly not necessary and we can choose any value for T. As the cosine-squared envelope is a periodic function, we have to define a region where the function should be cut off and yield zero. On the other hand, the hyperbolic secant and the Gaussian envelopes will remove the pulse gradually,

$$F(t) = \operatorname{sech}\left[\frac{\pi t}{T}\right], \tag{2.138}$$

$$F(t) = \exp\left[-\frac{(\pi t)^2}{2T^2}\right]. \tag{2.139}$$

These functions are however harder to turn on and off as they are small, but non-zero, for a wide range of time points both before and after the peak intensity. In accordance with much of the literature, we will almost exclusively use the sine-squared envelope function given by

$$F(t) = \begin{cases} \sin^2\left[\pi t/T\right], & t \in [0, T], \\ 0, & \text{else}. \end{cases} \tag{2.140}$$

This envelope shares the same properties as the cosine-squared envelope, but it is often more convenient to start in $t_0 = 0$ by turning on the laser instead of setting $t_0 < 0$. A plot of the different envelope functions during a pulse is shown in Figure 2.1.

2.10.2 Measuring energy transitions

To see the usefulness of laser induced dynamics, we consider a system described by a Hamiltonian

$$\hat{H}(t) = \hat{H}_p + \hat{H}_{ep}(t), \tag{2.141}$$

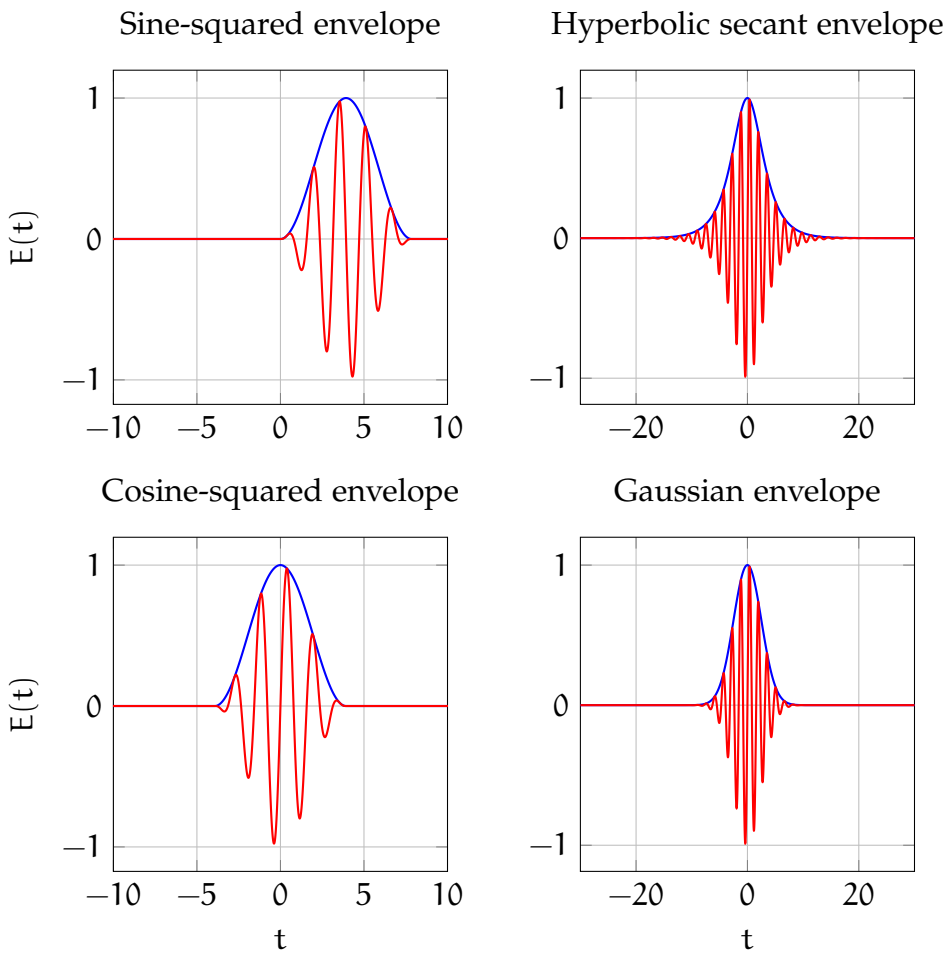

Figure 2.1: In these figures we plot the sine-squared, cosine-squared, hyperbolic secant, and Gaussian envelope functions $F(t)$ along with an electric field $E(t)$ under the envelope. We have used $\mathcal{E}_0 = 1$, $\omega_k = 4$, $T = 10\pi/\omega_k$ (giving five cycles of the laser pulse inside the envelope) on a grid with $t \in [-30, 30]$ in dimensionless units. The choice of the strength $\mathcal{E}_0$ and the frequency is such that the figures look presentable. Note that the figures for the sine- and cosine-squared envelopes are plotted in a shorter time-scale than the other two functions to bring out more details. The phase factor in the cosine of the electric field is set to $\phi = -\pi/2$ to give a sine function.

where the time-dependence is kept in the particle-field interaction. The scenarios we will consider consist of describing the system before and after the laser pulse is active. At $t = 0$ we have the time-independent Schrödinger equation

$$\hat{H}(0)\,|\phi_k\rangle = \hat{H}_p\,|\phi_k\rangle = E_k\,|\phi_k\rangle\,, \tag{2.142}$$

where $(E_k, |\phi_k\rangle)$ are the eigenpairs of the time-independent Hamiltonian, and the eigenstates are orthonormal. Now, if we choose a particular $|\phi_k\rangle$ as our initial state[3] we can "turn on" the laser pulse for $t \in [0, T]$ using an envelope function. We can in some ways consider the laser as a thermalization step where we move from an initial state that might be slightly unphysical in the sense that the pure eigenstates are very unlikely states to find a system in. For $t \geqslant T$ we have $\hat{H}(t \geqslant T) = \hat{H}(0)$, that is, $\hat{H}(t \geqslant T)$ has the same spectrum as $\hat{H}(0)$. At $t = T$ we can then write the evolved state as

$$\big|\psi(T)\big\rangle = \sum_{k=0}^{\infty} c_k(T)\,|\phi_k\rangle\,, \tag{2.143}$$

In terms of measurements, the state $\big|\psi(T)\big\rangle$ will be our initial state as this is a thermalized state from some initial eigenstate $|\phi_k\rangle$. The time evolution of an arbitrary state $\big|\psi(t)\big\rangle$ can be described by

$$\big|\psi(t \geqslant T)\big\rangle = \sum_{k=0}^{\infty} c_k(t)\,|\phi_k\rangle = \sum_{k=0}^{\infty} c_k(T) e^{-iE_k t/\hbar}\,|\phi_k\rangle\,, \tag{2.144}$$

where the time evolution is kept in the coefficients. There are now two quantities which are of interest as they provide information on the energy transitions in a system and we will look at these separately.

Autocorrelation

We define the autocorrelation as the overlap between the time-evolved stated $|\psi(t)\rangle$ with the initial state $|\psi(T)\rangle$ for $t \geqslant T$ [22, 35],[4]

$$A(t,T) = \langle\psi(t)|\psi(T)\rangle = \sum_{i=0}^{\infty}\sum_{j=0}^{\infty} c_i^*(t)c_j(T)\,\langle\phi_i|\phi_j\rangle \tag{2.145}$$

$$= \sum_{i=0}^{\infty}\sum_{j=0}^{\infty} c_i^*(T)c_j(T)e^{-iE_i t/\hbar}\delta_{ij} = \sum_{i=0}^{\infty}\big|c_i(T)\big|^2 e^{-iE_i t/\hbar}, \tag{2.146}$$

where we have used that the eigenstates of the time-independent Hamiltonian are orthonormal.

[3] We will always choose the ground state as our starting point in this thesis.

[4] Note that the autocorrelation can be computed for arbitrary states, but we use it in a specific way for measurements.

Dipole moment

Computing the expectation value of the dipole moment for $t \geqslant T$ we have

$$\langle \mathbf{d}(t) \rangle = \langle \psi(t) | \hat{\mathbf{d}} | \psi(t) \rangle = c_i^*(t) c_j(t) \langle \phi_i | \hat{\mathbf{d}} | \phi_j \rangle \tag{2.147}$$

$$= c_i^*(T) c_j(T) e^{iE_i t/\hbar} e^{-iE_j t/\hbar} \mathbf{d}_{ij} = c_i^*(0) c_j(0) e^{i\omega_{ij} t} \mathbf{d}_{ij}, \tag{2.148}$$

where we have defined the energy transition frequency by

$$\omega_{ij} \equiv \frac{E_i - E_j}{\hbar}, \tag{2.149}$$

and the matrix elements of the dipole moment using the eigenstates by $\mathbf{d}_{ij}$. Note that we typically measure along one direction in the dipole moment, but we have kept the vector notation to demonstrate that we can choose whichever axis of the dipole moment we like.

Now, we often do not have access to the spectrum of the time-independent system and the right-hand sides of the expectation value of the dipole moment and the autocorrelation is not something we can evaluate directly. However, by inspection we see that the right-hand sides bears resemblance to the *discrete Fourier transform*. This inspires the calculation of the Fourier transform of the autocorrelation and the dipole moment. The peaks in the Fourier spectrum can then be interpreted as the excited state E_i from the autocorrelation. The peaks in the Fourier spectrum of the dipole moment yields the energy transitions ω_{ij}. Note that we often sample the dipole moment and the autocorrelation from $T = 0$ while the laser is active, but we ignore all values of the autocorrelation that are generated while the laser is active.

Time-dependent overlap

In this thesis we will not compute the autocorrelation as it stands, but rather compute the time-dependent overlap. This is given by

$$P(t, t_0) = \left| \langle \psi(t) | \psi(t_0) \rangle \right|^2. \tag{2.150}$$

Instead of taking the Fourier transform of this quantity we use it as a measure of the transition probability to go from state $|\psi(t_0)\rangle$ to $|\psi(t)\rangle$. It can also be interpreted as the "amount" of $|\psi(t_0)\rangle$ in state $|\psi(t)\rangle$. This can be used as a measure of how much the state changes in time from some initial configuration.

2.11 Atomic units

When doing large calculations on quantum mechanical systems, the constants related to the physical units quickly becomes quite populous and can lead to

Table 2.1: In this table we list some of derived atomic units from working in Hartree atomic units [2, 9].

Dimension	Expression
Length	$a_0 = 4\pi\epsilon_0\hbar^2/(m_e e^2)$
Energy	$E_h = m_e e^4/(4\pi\epsilon_0\hbar)^2$
Time	$t_a = \hbar/E_h$
Frequency	$\omega_a = E_h/\hbar$
Momentum	$p_a = \hbar/a_0$
Electric field	$\mathcal{E}_a = E_h/(e a_0)$
Intensity	$I_a = \frac{1}{2}\epsilon_0 c\mathcal{E}_a^2$

numerical errors and might overshadow the important concepts of the theory. As a consequence, we tend to set most units to unity thus eliminating them from the equations. However, this means that in order to recover physical expressions, we must re-insert the constants to get the proper units and magnitudes. We will for the most part use Hartree atomic units [2] where we set the following quantities to unity:

- Reduced Planck's constant $\hbar = 1$.
- The magnitude of the charge of the electron $e = 1$.
- The electron rest mass $m_e = 1$.
- The Coulomb force constant $k_e = (4\pi\epsilon_0)^{-1} = 1$.

As a consequence of converting to atomic units, we now measure various physical units in a scaled system. A list of the derived units and how they can be scaled are shown in Table 2.1.

Chapter 3

Many-body quantum mechanics

Having discussed the rather general formulation of quantum mechanics we now move to the more specialized field of many-body quantum mechanics. In this chapter we will consider explicit wave functions and systems of more than a single particle. The results from the previous chapter are still applicable, but now we extend on the theory by introducing a more convenient formalism.

3.1 Summation convention

We will throughout this thesis use a summation convention that resembles the Einstein summation convention, but with slight variations. As we will be dealing with matrix elements with many indices and will perform quite a significant amount of contractions over these indices, we will refrain from writing the sums explicitly. The first difference from the Einstein summation convention is that our indices run over basis sets and not coordinates in a metric space. Furthermore, we will use different index sets for different sums, e.g., some sums run over a shorter limit than others[1], or different basis sets are used[2], etc. Whenever this is the case, we will inform the reader in advance.

We will often diagonalize a matrix, and to avoid writing out the sums explicitly due to three indices being repeated we will introduce the "rank 3 Kronecker-Delta" defined by

$$\delta^{i}_{jk} = \begin{cases} 1 & i = j = k, \\ 0 & \text{else}, \end{cases} \tag{3.1}$$

as this allows us to write a diagonal matrix $\mathbf{A}$ with diagonal elements a_i on

[1] In particular, see the section on the Fermi vacuum.

[2] For example, when we transform from one basis to another using the variational method.

index form, viz.

$$A_{ij} = \delta^n_{ij} a_n, \tag{3.2}$$

where we see that we have preserved the rank of the tensor A_{ij} on both sides of the equality after we have performed the contraction along index n. The reason for using this index notation is two-fold. First, we remove the clutter of the summation signs, and second, the index notation resembles the implementation in Python as we use tensor contractions where the axes are specified. Thus, no explicit sums in the form of for-loops are done in the code.

3.2 Particle statistics

The particles we concern ourselves with are *identical*. This means that it is not possible to discern two particles of the same type from one another. This statement yields quite profound results in the sense that the ordering of the particles in a many-body wave function is in some sense arbitrary; the wave functions are the same up to a complex phase factor regardless of the ordering of the particles. As a consequence the probability density of our state must be permutation invariant since we are not able to distinguish between the ordering of identical particles. We define $\sigma \in S_N$ as a permutation of N indices $\mathbf{x} = (x_1, \ldots, x_N) \in X^N$ wherein X^N is a coordinate space where both spin and position is incorporated. Furthermore, S_N is the group of all permutations σ where S_N has $N!$ distinct permutations. We denote the permutation of the indices by

$$\mathbf{x} = (x_1, \ldots, x_N) \to \mathbf{x}_\sigma = (x_{\sigma(1)}, \ldots, x_{\sigma(N)}). \tag{3.3}$$

We can then formulate particle indistinguishability by [29, 36]

$$\left|\psi(\mathbf{x})\right|^2 = \left|\psi(\mathbf{x}_\sigma)\right|^2. \tag{3.4}$$

This can be formulated as [29]

$$\psi(\mathbf{x}) = \exp\left[i\alpha(\sigma)\right]\psi(\mathbf{x}_\sigma), \tag{3.5}$$

where $\alpha(\sigma) \in \mathbb{R}$ depends on σ. A transposition $\tau_{ij} \in S_N$ is a permutation exchanging a single pair $(i, j) \to (j, i)$ where $i \neq j$. We denote the transposition of two indices in a similar manner as in Equation 3.3, but where $\mathbf{x}_{ij}$ signifies that all indices in $\mathbf{x}$ are the same except for the pair (i, j). We can construct any permutation σ as a product of an even or an odd number of transpositions [37]

$$\sigma = \prod_{k=1}^{n} \tau_{i_k, j_k}, \tag{3.6}$$

where $|\sigma| \equiv n$ counts the number of transpositions and is always either even or odd. Stated differently, a permutation σ created from a product of transpositions is not unique as the same permutation can be achieved from a different product of transpositions, however, all products are either even or odd. A permutation created from a even product of transpositions is said to have *even parity* whereas a permutation created from an odd product of transpositions is said to have *odd parity*. We define the *exchange operator* $\hat{P}_{ij}$ as the operator that interchanges a pair of indices by

$$\hat{P}_{ij}\psi(\mathbf{x}) = \psi(\mathbf{x}_{ij}). \tag{3.7}$$

From this definition we can then see that

$$\hat{P}_{ij}^2\psi(\mathbf{x}) = \hat{P}_{ij}\psi(\mathbf{x}_{ij}) = \psi(\mathbf{x}), \tag{3.8}$$

which means that the eigenvalues of $\hat{P}_{ij}$ is $p_{ij} = \pm 1$, that is,

$$\hat{P}_{ij}\psi(\mathbf{x}) = \psi(\mathbf{x}_{ij}) = p_{ij}\psi(\mathbf{x}). \tag{3.9}$$

As pointed out by Leinaas & Myrheim in their seminal paper "On the theory of identical particles" [36], this is only part of the truth as two-dimensional systems allow an infinite amount of eigenstates for the exchange operator. However, we will not concern ourselves with other eigenvalues for the exchange operator. Now, it is possible to write a transposition τ_{ij} as a product of three transpositions via an arbitrary index $k \neq i \neq j$. An illustration of this fact can be seen in Figure 3.1. As we can replace the action of a single exchange operator with three other exchange operators, we have that

$$\hat{P}_{jk}\psi(\mathbf{x}) = \hat{P}_{ij}\hat{P}_{ik}\hat{P}_{ij}\psi(\mathbf{x}) = p_{ij}p_{ik}p_{ij}\psi(\mathbf{x}) = p_{ij}^2 p_{ik}\psi(\mathbf{x}) = p_{ik}\psi(\mathbf{x}) = p_{jk}\psi(\mathbf{x}), \tag{3.10}$$

which tells us that the eigenvalues of all the exchange operators are the same. Thus we have $p_{ij} = p_{jk} \equiv p = \pm 1$. A consequence of this is that the eigenvalue of an exchange operator is a charateristic of the wave function $\psi(\mathbf{x})$. Furthermore, by constructing a *permutation operator* $\hat{P}_\sigma$ as a product of exchange operators, that is,

$$\hat{P}_\sigma = \prod_{k=1}^{n} \hat{P}_{i_k j_k}, \tag{3.11}$$

we find that the eigenvalue of the permutation operator is

$$\hat{P}_\sigma\psi(\mathbf{x}) = p^{|\sigma|}\psi(\mathbf{x}). \tag{3.12}$$

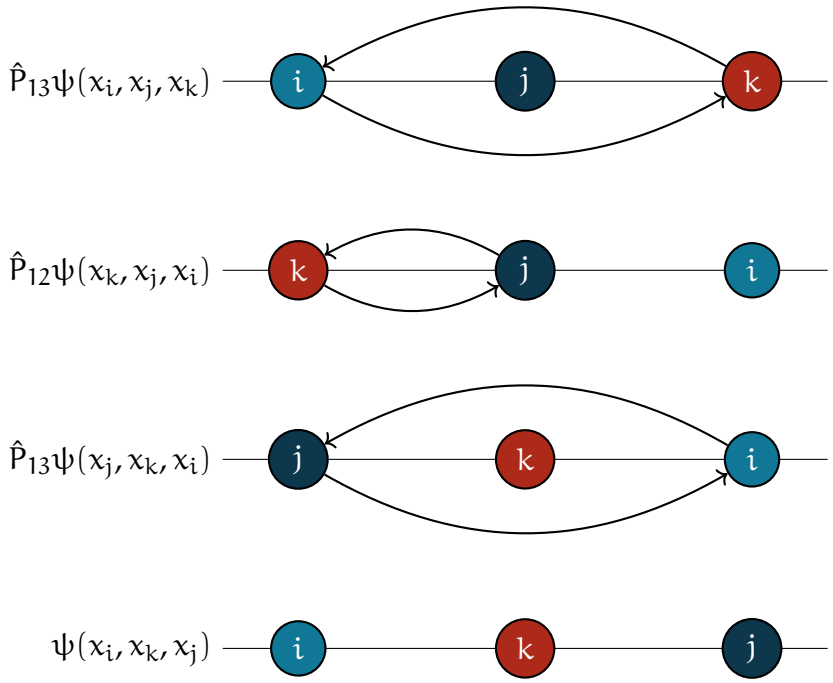

Figure 3.1: Here we illustrate how a single transposition τ_{jk} can be replaced by a product of three transpositions $\tau_{ij}\tau_{ik}\tau_{ij}$. In this figure the numbers represent a position inside the wave function arguments, that is, the exchange operators shuffle the ordering, and the labels i, j, and k along with their colored spheres are there to distinguish the three coordinates from another. The arrows represent the action of the exchange operator from one line to the next (before the exchange has occured). Take care not to mistake the circles to mean particles, the particles are indistinguishable after all and such a labelling is not possible.

Now, depending on the wave function we can get two different situations. If $p = +1$, then we call $\psi(\mathbf{x})$ symmetric as $p^{|\sigma|} = 1$ regardless of the parity of the permutation operator. A symmetric wave function describes a system of *bosons*, e.g., photons. On the other hand, if $p = -1$, then $\psi(\mathbf{x})$ is antisymmetric and

$$p^{|\sigma|} = \begin{cases} +1 & \text{even parity,} \\ -1 & \text{odd parity.} \end{cases} \tag{3.13}$$

Particles described by an antisymmetric wave function are called *fermions*, e.g., electrons.

3.2.1 Pauli exclusion principle

An interesting result of the antisymmetric property of fermions is that we can never have a system containing two fermions *in the same state*. We demonstrate this by considering an antisymmetric wave function $\psi(\mathbf{x})$ where $\mathbf{x} = (x_1, \ldots, x_N) \in X^N$ represents the coordinates of the N particles in the system. We now have that the eigenvalue of $\hat{P}_{ij}$ on $\psi(\mathbf{x})$ will be $p = -1$, that is,

$$\hat{P}_{ij}\psi(\mathbf{x}) = \psi(\mathbf{x}_{ij}) = -\psi(\mathbf{x}), \tag{3.14}$$

where we interpret $\mathbf{x}_{ij}$ as the same collection of coordinates as $\mathbf{x}$ but with x_i and x_j interchanged. Now, if $x_i = x_j$ in $\mathbf{x}$ we have

$$\hat{P}_{ij}\psi(\mathbf{x}) = \psi(\mathbf{x}_{ij}) = \psi(\mathbf{x}) = -\psi(\mathbf{x}), \tag{3.15}$$

which means that $\psi(\mathbf{x}) = 0$ for the equation to be satisified. This observation is known as the *Pauli exclusion principle*. It is not so much that fermions aren't *allowed* to be in the same state, but a fact of life that such things do not exist as they would immediately annihilate one another.

3.3 Second quantization

So far, we have worked with quantum mechanics formulated in first quantization where observables are operators acting on states that are functions defined on some space. Moving to second quantization we will express wave functions as products of creation and annihilation operators acting on the vacuum state. These operators provide a way to express many-body wave functions[3] as a product of operators where each operator represents a particle state.[4] Depending on the algebra for the operators, we can look at antisymmetric fermions or symmetric bosons. Expressing the first quantized observables in the same creation and annihilation operators, we are able to unify much of quantum mechanics to a single set of elementary operators [6].

3.3.1 Fock space

In second quantization, we express a general many-body wave function as a vector in the abstract linear vector space called *Fock space*.

[3] Or more precisely, configurations of many-body wave functions.

[4] It is not strictly a particle as we can not say that a particle is in this or that state, but it is a state which particles can occupy.

Definition 3.1. *For a given single-particle Hilbert space* H*, we define Fock space as the direct sum of the tensor products of copies* H*, viz. [29]*

$$F_\nu = \bigoplus_{n=0}^{\infty} S_\nu H^{\otimes n} = \mathbb{C} \oplus H \oplus \left[S_\nu (H \otimes H)\right] \oplus \dots, \tag{3.16}$$

where S_ν *is an operator which symmetrizes or antisymmetrizes the tensor product of Hilbert spaces depending on whether or not the system consists of bosons* $\nu \equiv +$ *or fermions* $\nu \equiv -$ *respectively.*

We will be working with a finite basis set of L orthonormal single-particle states $\{|p\rangle\}$, which means that we truncate the infinite direct sum over the tensor products of H constructing the truncated Fock space $F_\nu(L)$. A Fock state[5] $|\mathbf{n}\rangle \in F_\nu(L)$ is denoted

$$|\mathbf{n}\rangle \equiv |n_1, n_2, \dots, n_L\rangle, \tag{3.17}$$

where n_i denotes how many of state $|i\rangle$ are contained in $|\mathbf{n}\rangle$.[6] We have defined the set $\mathbf{n}$ as the set containing all n_i. This formulation of the Fock states lets us incorporate the particle statistics depending on the system we are exploring by choosing the allowed values of n_i.

$$n_i = \begin{cases} 0, 1 & \text{fermions} \iff \nu = -, \\ 0, 1, 2, \dots & \text{bosons} \iff \nu = +, \end{cases} \tag{3.18}$$

where $n_i = 0$ means that the state is unoccupied and $n_i \geqslant 1$ means that state $|i\rangle$ can be occupied by that amount of particles. We can decompose the truncated Fock space $F_\nu(L)$ into a direct sum of subspaces $F_\nu(L, N)$

$$F_\nu(L) = \bigoplus_{N=0}^{L} F_\nu(L, N), \tag{3.19}$$

where $F_\nu(L, N)$ is the Fock space with all Fock states $|\mathbf{n}\rangle$ where $|\mathbf{n}| = N$, i.e., all states where all N particles have been distributed among all L basis states [6]. Due to the particles being indistinguishable we have

$$\dim[F_+(L, N)] = \binom{L+N}{N}, \tag{3.20}$$

$$\dim[F_-(L, N)] = \binom{L}{N}, \tag{3.21}$$

[5] Also known as an occupation number vector [6].

[6] This must not be confused with a *product state* as $|\mathbf{n}\rangle$ is either a symmetric ($\nu = +$) or an antisymmetric ($\nu = -$) state.

where the bosonic Fock states are in a much greater number as they are not subject to the Pauli exclusion principle. The inner product between two Fock states $|\mathbf{n}\rangle, |\mathbf{m}\rangle \in F_\nu(L)$ is given by

$$\langle \mathbf{n}|\mathbf{m}\rangle = \prod_{i=1}^{L} \delta_{pq} \equiv \delta_{\mathbf{nm}}. \tag{3.22}$$

One of the convenient consequences of the Fock space formulation is that it opens up for a description of the inner product between two Fock states with an unequal amount of particles.[7] From Equation 3.22 we can see that two Fock states with an unequal number of particles will yield a zero-overlap. Furthermore, we can construct the identity by

$$\mathbb{1} = |\mathbf{n}\rangle\langle\mathbf{n}|, \tag{3.23}$$

where we sum over over all $|\mathbf{n}\rangle \in F_\nu(L)$. Of particular interest is the *vacuum state* $|-\rangle \in F_\nu(L, 0)$ as the state with no particles.

$$|-\rangle \equiv |\mathbf{0}\rangle = |0_1, 0_2, \ldots, 0_L\rangle. \tag{3.24}$$

From Equation 3.22 we have that the vacuum state is normalized to unity.

3.3.2 Creation and annihilation operators

We now introduce the *creation* and *annihilation* operators which act on Fock states by adding or removing single particle states.

Definition 3.2. *A* creation *operator* $\hat{a}_p^\dagger$ *is an operator acting on Fock states in* $F_\nu(L)$. *It is a mapping* $\hat{a}_p^\dagger : F_\nu(L, N) \mapsto F_\nu(L, N+1)$. *Its action on a Fock state* $|\mathbf{n}\rangle \in F_\nu(L, N)$ *is defined as*

$$\hat{a}_p^\dagger |\mathbf{n}\rangle = (\Gamma_\nu)_p^{\mathbf{n}} \sqrt{n_p + 1}\, |n_1, \ldots, n_p + 1, \ldots, n_L\rangle = (\Gamma_\nu)_p^{\mathbf{n}} \sqrt{n_p + 1}\, |\mathbf{n}'\rangle, \tag{3.25}$$

where $(\Gamma_\nu)_p^{\mathbf{n}}$ *is a phase factor which depends on the particle type* ν.

$$(\Gamma_+)_p^{\mathbf{n}} = 1, \tag{3.26}$$

$$(\Gamma_-)_p^{\mathbf{n}} = \prod_{q=1}^{p-1} (-1)^{n_q}. \tag{3.27}$$

We will denote fermionic creation operators by $\hat{c}_p^\dagger$ *and the corresponding bosonic creation operators by* $\hat{b}_p^\dagger$.

[7] The two Fock states must however be defined from the same basis set of L basis functions.

The phase factor is again a way of incorporating the particle statistics of the system we are exploring. A bosonic wave function is symmetric with respect to its particles and its phase is therefore constant regardless of the ordering of the creation of its particle states. For a fermionic wave function, the interchange of two particles will incur a sign change as discussed in section 3.2. The fact that the ordering of the indices in a fermionic Fock state will depend on the overall sign of the state can lead to ambiguity. We therefore introduce *canonical ordering* with respect to the particle indices,

$$|\mathbf{n}\rangle \equiv \left[\prod_{p=1}^{L} \left(\hat{c}_p^\dagger\right)^{n_p}\right] |-\rangle = \left(\hat{c}_1^\dagger\right)^{n_1} \dots \left(\hat{c}_L^\dagger\right)^{n_L} |-\rangle\,, \tag{3.28}$$

that is, we order the single-particle states in an increasing order. Recalling the Pauli exclusion principle that $n_p \in \{0, 1\}$ for a fermionic wave function, we have that

$$\hat{c}_p^\dagger \hat{c}_p^\dagger = 0, \tag{3.29}$$

and the normalization factor $\sqrt{n_p + 1}$ will always be 1 as long as the state is not annihilated by inserting an already existing state. From the phase in Definition 3.2 we have the commutation relation

$$\left[\hat{b}_p^\dagger, \hat{b}_q^\dagger\right] = \hat{b}_p^\dagger \hat{b}_q^\dagger - \hat{b}_q^\dagger \hat{b}_p^\dagger = 0, \tag{3.30}$$

for the bosonic system as the ordering of the creation of particle states in a bosonic wave function is arbitrary. Fermionic creation operators satisfy the anticommutation relation

$$\left\{\hat{c}_p^\dagger, \hat{c}_q^\dagger\right\} = \hat{c}_p^\dagger \hat{c}_q^\dagger + \hat{c}_q^\dagger \hat{c}_p^\dagger = 0, \tag{3.31}$$

as $p > q$ or $q > p$ and the phase factor will give a sign change by inserting one before the other thus yielding the same state with an opposite sign.

We define the *annihilation operator* as the adjoint of the creation operator. The action can be inferred by utilizing the spectral decomposition of the identity in Equation 3.23.

$$\hat{a}_p |\mathbf{n}\rangle = |\mathbf{m}\rangle \langle \mathbf{m}|\hat{a}_p|\mathbf{n}\rangle = |\mathbf{m}\rangle \left(\langle \mathbf{n}|\hat{a}_p^\dagger|\mathbf{m}\rangle\right)^* = (\Gamma_\nu)_p^{\mathbf{m}}\, \delta_{\mathbf{n}\mathbf{m}'} \sqrt{m_p + 1}\, |\mathbf{m}\rangle\,, \tag{3.32}$$

where

$$\hat{a}_p^\dagger |\mathbf{m}\rangle = (\Gamma_\nu)_p^{\mathbf{m}} \sqrt{m_p + 1}\, |\mathbf{m}'\rangle\,. \tag{3.33}$$

In order for the overlap between $|\mathbf{n}\rangle$ and $\hat{a}_p^\dagger |\mathbf{m}\rangle$ to be non-zero we have to have $|\mathbf{n} - \mathbf{m}| = 1$, that is, the two states $|\mathbf{n}\rangle$ and $|\mathbf{m}\rangle$ can only differ by a single state. Furthermore, as we are acting on $|\mathbf{m}\rangle$ with $\hat{a}_p^\dagger$ we have that $n_p = m_p + 1$, i.e., $|\mathbf{n}\rangle$ has one more particle state $|p\rangle$ than $|\mathbf{m}\rangle$. As all other states in $|\mathbf{n}\rangle$ and $|\mathbf{m}\rangle$ are the same, we have that $(\Gamma_\nu)_p^{\mathbf{m}} = (\Gamma_\nu)_p^{\mathbf{n}}$ and $\sqrt{n_p} = \sqrt{m_p + 1}$. This means that

$$(\Gamma_\nu)_p^{\mathbf{m}} \delta_{\mathbf{n}\mathbf{m}'} \sqrt{m_p + 1} = \Big(\langle \mathbf{n} | \hat{a}_p^\dagger | \mathbf{m} \rangle \Big)^* = \langle \mathbf{m} | \hat{a}_p | \mathbf{n} \rangle = (\Gamma_\nu)_p^{\mathbf{n}} \sqrt{n_p} \delta_{\mathbf{n}'\mathbf{m}}, \tag{3.34}$$

where $|\mathbf{n}'\rangle$ is the state $|\mathbf{n}\rangle$ with state $|p\rangle$ removed. We are thus left with our annihilation operator.

Definition 3.3. *An* annihilation *operator* $\hat{a}_p$ *is an operator acting on Fock states in* $F_\nu(L)$. *It is a mapping* $\hat{a}_p : F_\nu(L, N) \mapsto F_\nu(L, N-1)$. *Its action on a Fock state* $|\mathbf{n}\rangle \in F_\nu(L, N)$ *is defined as*

$$\hat{a}_p |\mathbf{n}\rangle = (\Gamma_\nu)_p^{\mathbf{n}} \sqrt{n_p} \, |n_1, \ldots, n_p - 1, \ldots, n_L\rangle = (\Gamma_\nu)_p^{\mathbf{n}} \sqrt{n_p} \, |\mathbf{n}'\rangle \,, \tag{3.35}$$

where $(\Gamma_\nu)_p^{\mathbf{n}}$ *is the same phase factor as in Definition 3.2. We will denote fermionic annihilation operators by* $\hat{c}_p$ *and the corresponding bosonic annihilation operators by* $\hat{b}_p$.

From the definition of the annihilation operator we have that

$$\hat{c}_p \hat{c}_p = 0, \tag{3.36}$$

as there can only be one particle state of type p in a given fermionic state. Furthermore, we have the commutation relation

$$\Big[\hat{b}_p, \hat{b}_q \Big] = \hat{b}_p \hat{b}_q - \hat{b}_q \hat{b}_p = 0, \tag{3.37}$$

for the bosonic states and the anticommutation relation

$$\big\{ \hat{c}_p, \hat{c}_q \big\} = \hat{c}_p \hat{c}_q + \hat{c}_q \hat{c}_p = 0, \tag{3.38}$$

for the fermionic system. These relations can be seen by taking the Hermitian conjugate of the commutation and anitcommutation relation for the creation operators. If the annihilation operator $\hat{a}_p$ acts on a Fock state $|\mathbf{n}\rangle$ which does not contain the state $|p\rangle$, then

$$\hat{a}_p |\mathbf{n}\rangle = \hat{a}_p \, |n_1, \ldots, 0_p, \ldots, n_L\rangle = 0. \tag{3.39}$$

As a consequence, any annihilation operator will annihilate the vacuum.

Now, in order to derive the fundamental properties of the second quantized operators we look at the combined action of a creation and an annihilation operator acting on a state in combination. For the bosonic operators we have

$$\left.\begin{aligned}\hat{b}_p\hat{b}_p^\dagger|\mathbf{n}\rangle &= (n_p+1)|\mathbf{n}\rangle\\ \hat{b}_p^\dagger\hat{b}_p|\mathbf{n}\rangle &= n_p|\mathbf{n}\rangle\end{aligned}\right\} \implies \left[\hat{b}_p,\hat{b}_p^\dagger\right] = (n_p+1)-n_p = 1, \tag{3.40}$$

when we create and remove the same particle state $|p\rangle$. When $p \neq q$ we have

$$\left.\begin{aligned}\hat{b}_p\hat{b}_q^\dagger|\mathbf{n}\rangle &= \sqrt{n_p}\sqrt{n_q+1}|\mathbf{n}'\rangle\\ \hat{b}_q^\dagger\hat{b}_p|\mathbf{n}\rangle &= \sqrt{n_p}\sqrt{n_q+1}|\mathbf{n}'\rangle\end{aligned}\right\} \implies \left[\hat{b}_p,\hat{b}_q^\dagger\right] = 0. \tag{3.41}$$

Collecting all three commutation relations for the bosonic states we find

$$\left[\hat{b}_p,\hat{b}_q\right] = 0, \tag{3.42}$$

$$\left[\hat{b}_p^\dagger,\hat{b}_q^\dagger\right] = 0, \tag{3.43}$$

$$\left[\hat{b}_p,\hat{b}_q^\dagger\right] = \delta_{pq}. \tag{3.44}$$

Repeating this exercise for the fermionic states we start by noting that the fermionic phase factor squared is 1.

$$\left.\begin{aligned}\hat{c}_p\hat{c}_p^\dagger|\mathbf{n}\rangle &= \delta_{n_p0}|\mathbf{n}\rangle\\ \hat{c}_p^\dagger\hat{c}_p|\mathbf{n}\rangle &= \delta_{n_p1}|\mathbf{n}\rangle\end{aligned}\right\} \implies \left\{\hat{c}_p,\hat{c}_p^\dagger\right\} = \delta_{n_p0}+\delta_{n_p1} = 1, \tag{3.45}$$

where n_p in the Kronecker-Deltas following the anticommutator expression are dummy indices. When $p \neq q$ we have

$$\hat{c}_p\hat{c}_q^\dagger|\mathbf{n}\rangle = (\Gamma_+)_p^{\mathbf{n}^{(1)}}(\Gamma_+)_q^{\mathbf{n}}\delta_{n_p1}\delta_{n_q0}|\mathbf{n}^{(3)}\rangle \tag{3.46}$$

$$\hat{c}_q^\dagger\hat{c}_p|\mathbf{n}\rangle = (\Gamma_+)_q^{\mathbf{n}^{(2)}}(\Gamma_+)_p^{\mathbf{n}}\delta_{n_q0}\delta_{n_p1}|\mathbf{n}^{(3)}\rangle \tag{3.47}$$

where we have defined the state $|\mathbf{n}^{(3)}\rangle$ as state $|\mathbf{n}\rangle$ with the single-particle states $|q\rangle$ added and $|p\rangle$ removed. Collecting the creation and annihilation pair into an anticommutator relation we have

$$\left\{\hat{c}_p,\hat{c}_q^\dagger\right\} = \delta_{n_q0}\delta_{n_p1}\left[(\Gamma_+)_p^{\mathbf{n}^{(1)}}(\Gamma_+)_q^{\mathbf{n}}+(\Gamma_+)_q^{\mathbf{n}^{(2)}}(\Gamma_+)_p^{\mathbf{n}}\right]. \tag{3.48}$$

In order to get a final expression for this anticommutator we need to find expressions for the phases $(\Gamma_+)_p^{\mathbf{n}^{(1)}}$ and $(\Gamma_+)_q^{\mathbf{n}^{(2)}}$ relative to the original state

$|\mathbf{n}\rangle$. We have two situations that needs to be explored, namely when $p > q$ and the opposite situation when $p < q$. Now, when $p > q$ we have

$$(\Gamma_+)_p^{\mathbf{n}^{(1)}}(\Gamma_+)_q^{\mathbf{n}} = -(\Gamma_+)_p^{\mathbf{n}}(\Gamma_+)_q^{\mathbf{n}}, \tag{3.49}$$

as $\hat{c}_q^\dagger$ inserts an extra state $|q\rangle$ between n_1 and n_p. Conversely, this sign change does not occur for the reverse situation when $\hat{c}_q^\dagger \hat{c}_p$ acts on $|\mathbf{n}\rangle$ and we get $(\Gamma_+)_p^{\mathbf{n}^{(2)}} = (\Gamma_+)_p^{\mathbf{n}}$. Thus, in total we have

$$\left\{\hat{c}_p, \hat{c}_q^\dagger\right\} = 0, \tag{3.50}$$

for $p > q$. When $p < q$ we get the same result as can be seen by taking the Hermitian conjugate of the anticommutator and reversing the dummy indices p and q. In total we have the fundamental anticommutation relations

$$\left\{\hat{c}_p, \hat{c}_q\right\} = 0, \tag{3.51}$$

$$\left\{\hat{c}_p^\dagger, \hat{c}_q^\dagger\right\} = 0, \tag{3.52}$$

$$\left\{\hat{c}_p, \hat{c}_q^\dagger\right\} = \delta_{pq}. \tag{3.53}$$

As stated at the start of this section on second quantization, the fundamental commutation relations for bosons and the fundamental anticommutation relations for fermions completely specifies the system we are exploring. In the rest of this thesis we will only look at fermions as we will be exploring electrons and electronic particles, but we wanted to include the discussion of both sets of creation and annihilation operators as it provides insight on how one would go about formulating the many-body methods we will explore for bosons as well. By replacing the fundamental anticommutation relations with the symmetric fundamental commutation relations[8] one can look at bosonic systems.

3.4 Wick's theorem

We will discover that the evaluation of products of many-body operators quickly will yield large products of second quantized operators which will have to be evaluated using the anticommutation relations from Equation 3.51 to Equation 3.53. To alleviate this process we introduce *Wick's theorem*, first introduced by Wick [38].

[8] And performing a substantial amount of algebra.

Definition 3.4. *The* normal-ordered form *of a string of second quantized operators is defined as a form where all the annihilation operators are placed to the right of all the creation operators. For an operator $\hat{A}$ containing a string of creation and annihilation operators, we denote the normal-ordered form by $\{\hat{A}\}$.*

To see the usefulness of Definition 3.4, consider an operator $\hat{A}$ containing a string of creation and annihilation operators on normal-ordered form, that is, $\hat{A} = \{\hat{A}\}$, we will then have

$$\{\hat{A}\}|-\rangle = 0, \tag{3.54}$$

as all the annihilation operators will annihilate the vacuum. Note that the normal-ordered form is not unique. However, whilst in the normal-ordered form, a permutation of the operators will at most yield a sign change and thus no consideration of the Kronecker-Delta in Equation 3.53 needs to be taken.

Definition 3.5. *We define a* contraction *between two arbitrary second quantized operators $\hat{A}$ and $\hat{B}$ to be*

$$\hat{A}\hat{B} = \hat{A}\hat{B} - \{\hat{A}\hat{B}\}, \tag{3.55}$$

where $\{\hat{A}\hat{B}\}$ is the normal-ordered form of the operator pair $\hat{A}\hat{B}$ relative to the vacuum state $|-\rangle$.

Similarly to the anticommutation relations, we can find contraction relations for the second quantized operators.

$$\hat{c}_p\hat{c}_q = \hat{c}_p\hat{c}_q - \{\hat{c}_p\hat{c}_q\} = \hat{c}_p\hat{c}_q - \hat{c}_p\hat{c}_q = 0, \tag{3.56}$$

$$\hat{c}_p^\dagger\hat{c}_q^\dagger = \hat{c}_p^\dagger\hat{c}_q^\dagger - \{\hat{c}_p^\dagger\hat{c}_q^\dagger\} = \hat{c}_p^\dagger\hat{c}_q^\dagger - \hat{c}_p^\dagger\hat{c}_q^\dagger = 0, \tag{3.57}$$

$$\hat{c}_p^\dagger\hat{c}_q = \hat{c}_p^\dagger\hat{c}_q - \{\hat{c}_p^\dagger\hat{c}_q\} = \hat{c}_p^\dagger\hat{c}_q - \hat{c}_p^\dagger\hat{c}_q = 0, \tag{3.58}$$

where these three contractions all yield zero because they are already on normal-ordered form. The only-nonzero contraction is

$$\hat{c}_p\hat{c}_q^\dagger = \hat{c}_p\hat{c}_q^\dagger - \{\hat{c}_p\hat{c}_q^\dagger\} = \hat{c}_p\hat{c}_q^\dagger + \hat{c}_q^\dagger\hat{c}_p = \left\{\hat{c}_p, \hat{c}_q^\dagger\right\} = \delta_{pq}, \tag{3.59}$$

where the sign-change comes from re-ordering of the operators to normal-ordered form. Wick's theorem provides a method of re-writing a string of creation and annihilation operators as a sum of normal-ordered strings.

Theorem 3.1. *Let* $\hat{A}\hat{B}\ldots\hat{Z}$ *be a string of second quantized operators, then*

$$\hat{A}\hat{B}\ldots\hat{Z} = \{\hat{A}\hat{B}\ldots\hat{Z}\} + \sum_{singles} \{\hat{A}\hat{B}\ldots\hat{Z}\} + \sum_{doubles} \{\hat{A}\hat{B}\ldots\hat{Y}\hat{Z}\} + \ldots, \quad (3.60)$$

where the sums run over all singly, doubly, and higher, contracted normal-ordered strings.

Contractions inside normal-ordered braces are performed by permuting the two operators together where each permutation between operators introduce a sign-change. Once the pair has been collected, the contraction can be evaluated. We see that only Equation 3.59 will provide a non-zero contraction.

3.4.1 Generalized Wick's theorem

An extension to Wick's theorem is the product of several normal-oredered operator strings.

Theorem 3.2. *Let* $\{\hat{A}\hat{B}\ldots\}$ *and* $\{\hat{X}\hat{Y}\ldots\}$ *be two normal-ordered strings of second quantized operators, then*

$$\{\hat{A}\hat{B}\ldots\}\{\hat{X}\hat{Y}\ldots\} = \{\hat{A}\hat{B}\ldots\hat{X}\hat{Y}\ldots\} + \sum_{singles} \{\hat{A}\hat{B}\ldots\hat{X}\hat{Y}\ldots\} + \sum_{doubles} \{\hat{A}\hat{B}\ldots\hat{X}\hat{Y}\ldots\} + \ldots, \quad (3.61)$$

where the contractions are only done between the two normal-ordered strings.

To see the usefulness of Wick's theorem, we consider the evaluation of a matrix element between two Fock states $|\mathbf{k}\rangle, |\mathbf{n}\rangle \in F_-(L,N)$ on the operator $\hat{A}$ consisting of a string of creation and annihilation operators. We have that

$$|\mathbf{n}\rangle = \left[\prod_{p=1}^{L} \left(\hat{c}_p^\dagger\right)^{n_p}\right] |-\rangle, \quad (3.62)$$

which is already on normal-ordered form. The Hermitian conjugate of this state is also on normal-ordered form. Now, the matrix element of $\hat{A}$ is given by

$$\langle\mathbf{k}|\hat{A}|\mathbf{n}\rangle = \langle -| \left[\prod_{p=1}^{L} \left(\hat{c}_p\right)^{k_p}\right] \hat{A} \left[\prod_{p=1}^{L} \left(\hat{c}_p^\dagger\right)^{n_p}\right] |-\rangle. \quad (3.63)$$

Using Wick's generalized theorem on the operator $\hat{A}$ we see that only the *fully contracted* terms will survive, as any "left-over" normal-ordered strings will annihilate the vacuum state.

3.5 Spin-orbitals

As discussed in the previous section on Fock space, we build our many-body wave function by combining single-particle states from an underlying basis. Since we're exploring systems of fermions, we will limit our attention to particles with spin-1/2 and our single-particle states must incorporate the spin. It is often more convenient to express the single-particle states as functions defined on position or momentum space and in a spin-basis. We call the spatial representation of the single-particle functions an *orbital* and combined with spin, we have the *spin-orbital*,

$$\langle x|\psi\rangle = \psi(x) \equiv \psi(\mathbf{r}, m_s) = \langle \mathbf{r}, m_s|\psi\rangle\,, \tag{3.64}$$

where $x = (\mathbf{r}, m_s)$ is a generalized coordinate of both position, $\mathbf{r}$, and spin quantum number, m_s. For fermions we have only two allowed spin states

$$s_z = \pm\frac{1}{2}\hbar, \tag{3.65}$$

where s_z is the spin along the z-direction. As there are only two allowed states we have that $m_s \in \{\uparrow, \downarrow\}$, where a positive value for s_z corresponds to $m_s = \uparrow$, i.e., spin up, and a negative value for s_z to $m_s = \downarrow$, i.e., spin down. We denote

$$\psi_1(\mathbf{r}) \equiv \psi\left(\mathbf{r}, \uparrow\right), \qquad \psi_2(\mathbf{r}) \equiv \psi\left(\mathbf{r}, \downarrow\right), \tag{3.66}$$

for the two different spin directions. We can thus represent the generalized spin-orbital $\psi(x)$ as a two-dimensional vector

$$\psi(x) = \begin{pmatrix} c_1\psi_1(\mathbf{r}) \\ c_2\psi_2(\mathbf{r}) \end{pmatrix}, \tag{3.67}$$

where $c_i \in \mathbb{C}$ are coefficients satisfying $|c_1|^2 + |c_2|^2 = 1$. We separate the spin dependence from the spatial part of the spin-orbitals by introducing separate spin functions for spin-up and spin-down. For example, choosing the spin-basis

$$\alpha \equiv \alpha(m_s) = \begin{pmatrix} 1 \\ 0 \end{pmatrix}, \qquad \beta \equiv \beta(m_s) = \begin{pmatrix} 0 \\ 1 \end{pmatrix}, \tag{3.68}$$

we use the same convention as in much of the many-body quantum mechanics literature in labelling α as spin up and β as spin down in the z-direction. Evaluating the spin functions thus yields

$$\alpha\left(\uparrow\right) = 1, \qquad \alpha\left(\downarrow\right) = 0, \tag{3.69}$$

$$\beta\left(\uparrow\right) = 0, \qquad \beta\left(\downarrow\right) = 1. \tag{3.70}$$

Using Equation 3.68 we see that we can write the generalized spin-orbital as a linear combination of the spin basis functions by

$$\psi(x) = c_1\psi_1(\mathbf{r})\alpha(m_s) + c_2\psi_2(\mathbf{r})\beta(m_s). \tag{3.71}$$

We will for the most part work with spin-orbitals in a definite spin direction, viz.

$$\psi(x) = \phi(\mathbf{r})\sigma(m_s), \tag{3.72}$$

where $\sigma(m_s)$ is either spin up $\alpha(m_s)$ or spin down $\beta(m_s)$ and we have denoted the spatial orbital by $\phi(\mathbf{r})$. The reason we avoid using a general spin-orbital as in Equation 3.71 is reduction of computational complexity. It is more convenient to generate a basis of spin-orbitals where we use a definite basis of analytical orbitals, e.g., harmonic oscillator basis functions, Gauss functions, etc, before tacking on the spin direction of each orbital. When labelling the different spin-orbitals from Equation 3.72 we use the notation

$$\psi_P(x) = \phi_p(\mathbf{r})\sigma(m_s), \tag{3.73}$$

where $P = (p, \sigma)$ is a composite index with p labelling a specific orbital and σ a specific spin-function. In the spin basis shown in Equation 3.68 we have that the inner product of two spin functions is given by

$$\langle\sigma|\tau\rangle = \sigma(\uparrow)\tau(\uparrow) + \sigma(\downarrow)\tau(\downarrow) = \delta_{\sigma\tau}, \tag{3.74}$$

that is, they are orthonormal. The inner product of two spin-orbitals from Equation 3.72 is then separated into an orbital and a spin inner product,

$$\langle\psi_P|\psi_Q\rangle = \langle\phi_p|\phi_q\rangle\ \langle\sigma|\tau\rangle = \delta_{\sigma\tau}\int d\mathbf{r}\phi_p^*(\mathbf{r})\phi_q(\mathbf{r}). \tag{3.75}$$

This equation is quite suggestive in the sense that we can see that the spin decouples from the spatial part of the wave function. Spin-1/2 is a two-level system that can be represented as a vector in a two-dimensional Hilbert space. Unless an operator contains a spin-coupling, the two spin directions are completely independent of one another. For example, given a spin-independent operator, $\hat{O}$, the matrix element between two spin-orbitals become

$$\langle\psi_P|\hat{O}|\psi_Q\rangle = \langle\phi_p|\hat{O}|\phi_q\rangle\ \langle\sigma|\tau\rangle = \delta_{\sigma\tau}\int d\mathbf{r}\phi_p^*(\mathbf{r})O(\mathbf{r})\phi_q(\mathbf{r}). \tag{3.76}$$

This motivates the coordinate independent notation

$$|\psi_P\rangle = |\phi_p\rangle \otimes |\sigma\rangle\,, \tag{3.77}$$

where the tensor product combines the two-dimensional Hilbert space from the spin $|\sigma\rangle$ and the one-dimensional Hilbert space containing the orbital basis function. A general operator on the combined Hilbert space can thus be represented by

$$\hat{O} = \hat{R}_i \otimes \hat{S}_j, \tag{3.78}$$

where $\hat{R}_i$ is an operator on the one-dimensional Hilbert space containing the orbitals and $\hat{S}_j$ an operator on the two-dimensional Hilbert space containing the spin functions. The matrix elements of this operator can be computed by

$$\langle \psi_P | \hat{O} | \psi_Q \rangle = \langle \phi_p | \hat{R}_i | \phi_q \rangle \langle \sigma | \hat{S}_j | \tau \rangle . \tag{3.79}$$

Looking back at Equation 3.76 we see that a spin-independent operator $\hat{O}$ corresponds to $\hat{S}_j = \mathbb{1}$.

3.5.1 Restrictions on the choice of spin-orbitals

Many-body methods are often defined by restrictions on the spin-orbitals. Below we list some of the more common restrictions.

1. The general spin-orbital is on the form

$$\psi(x,t) = c_1\psi_1(\mathbf{r},t)\alpha(m_s) + c_2\psi_2(\mathbf{r},t)\beta(m_s). \tag{3.80}$$

   These spin-orbitals can lead to mixing between both spin directions, known as spin-contamination, that is, the spin-orbitals are no longer eigenstates of the spin-projection operator $\hat{S}_z$. This is often an unwanted effect as this greatly limits some of the optimizations that can be employed on some of the computational methods.

2. The spin-unrestricted spin-orbital is on the form

$$\psi(x,t) = \psi_\sigma(\mathbf{r},t)\sigma(m_s), \tag{3.81}$$

   where the orbital ψ_σ depends on the spin direction σ. Often this type of spin-orbitals are dubbed unrestricted spin-orbitals, which is somewhat of a misnomer as the spin-orbitals are restricted in the choice of spin direction as opposed to the (truly) unrestricted generalized spin-orbitals shown in Equation 3.80.

3. The spin-restricted spin-orbital is given by

$$\psi(x,t) = \psi(\mathbf{r},t)\sigma(m_s), \tag{3.82}$$

   where each orbital is doubly occupied. If the system we are exploring exhibits no spin-effects, then choosing restricted spin-orbitals can often reduce the complexity of the problem. Furthermore, the system remains eigenstates of the spin-projection operator.

3.5.2 Basis transformations

Much of what will be done in this thesis boils down to basis transformations of spin-orbitals. For a given basis of L spin-orbitals $\{\chi_\alpha\}$, a basis transformation to a new basis of K spin-orbitals $\{\phi_i\}$ is done by

$$|\phi_i\rangle = C_{\alpha i} |\chi_\alpha\rangle , \tag{3.83}$$

where we for the sake of generality allow the two basis sets to be of differing sizes. The coefficient matrix $\mathbf{C} \in \mathbb{C}^{L\times K}$, defines the transformation. We will often denote the known set of spin-orbitals as *atomic orbitals* as done in the field of quantum chemistry.

Lemma 3.1. *Let $\{\xi_\mu\}$ be an orthonormal set of L spin-orbitals. Performing a unitary transformation of this basis set will yield a new basis set $\{\phi_p\}$ of L orthonormal spin-orbitals.*

Proof. Performing a unitary transformation from the orthonormal basis of L atomic orbitals $\{\xi_\mu\}$ to a new basis set of L atomic orbitals $\{\phi_p\}$ is done via

$$|\phi_p\rangle = U_{\mu p} |\xi_\mu\rangle , \tag{3.84}$$

where $U_{\mu p}$ is an element in the unitary matrix $\mathbf{U} \in \mathbb{C}^{L\times L}$. As the atomic orbitals are orthonormal, we find

$$\langle\phi_p|\phi_q\rangle = U^*_{\mu p} \langle\xi_\mu|\xi_\nu\rangle U_{\nu q} = U^*_{\mu p} U_{\mu q} = \delta_{pq}, \tag{3.85}$$

due to the unitarity of the matrix $\mathbf{U}$. This proves Lemma 3.1. □

3.6 Slater determinants

We have established that the full many-body wave function of a fermionic system should be antisymmetric with respect to its particles. The creation and annihilation operators for the Fock space representation of many-body configurations incorporates the anti-symmetry requirement, but we are no closer to establishing what our many-body wave function looks like in a coordinate representation making it hard to compute integrals in order to find matrix elements.

A start is to consider a system of non-interacting particles with a Hamiltonian on the form

$$\hat{H} = \sum_{i=1}^{N} \hat{h}_i, \tag{3.86}$$

where $\hat{h}_i$ is a one-body Hamiltonian acting on particle i. We are able to find the spectrum of $\hat{h}$, and we can use the N first eigenstates $|\psi_i\rangle$ as a basis of spin-orbitals. This lets us construct a many-body wave function as a product state from these spin-orbitals, viz.

$$|\Psi\rangle = \bigotimes_{i=1}^{N} |\psi_i\rangle = |\psi_1\rangle \otimes \cdots \otimes |\psi_n\rangle \,. \tag{3.87}$$

The coordinate representation of this state can be found by

$$\langle x_1, \ldots, x_n | \Psi \rangle = \psi_1(x_1) \ldots \psi_n(x_n), \tag{3.88}$$

where $\psi_i(x_i)$ is the coordinate representation of the spin-orbitals. Since each eigenstate $|\psi_i\rangle$ is an eigenstate of the one-body Hamiltonian with eigenenergy ϵ_i we can find the total energy of the full Hamiltonian by

$$\hat{H} |\Psi\rangle = E |\Psi\rangle = \left[\sum_{i=1}^{N} \epsilon_i \right] |\Psi\rangle \,. \tag{3.89}$$

This particular product state is in quantum chemistry and nuclear physics often known as the *Hartree product*. However, a product state is neither symmetric nor antisymmetric with respect to exchange of particles as a product state is not an eigenstate of the exchange operator. A way to introduce particle indistinguishability and the anti-symmetry requirement to the product state is to create a linear combination of product states using the permutation operator $\hat{P}_\sigma$ defined in a similar manner as in section 3.2. Defining the action of the permutation operator on the product state to be

$$\hat{P}_\sigma |\Psi\rangle = \hat{P}_\sigma \bigotimes_{i=1}^{N} |\psi_i\rangle = \bigotimes_{i=1}^{N} |\psi_{\sigma(i)}\rangle \,, \tag{3.90}$$

where $\sigma(i)$ is a permutation. Now we construct the *antisymmetrizer* $\hat{A}$ defined as the operator

$$\hat{A} = \frac{1}{N!} \sum_{\sigma \in S_N} \hat{P}_\sigma, \tag{3.91}$$

that is, the operator that performs all $N!$ permutations in S_N. Using the antisymmetrizer we can construct a totally antisymmetric wave function $|\Phi\rangle$ by

$$|\Phi\rangle = \sqrt{N!} \hat{A} |\Psi\rangle = \frac{1}{\sqrt{N!}} \sum_{\sigma \in S_N} \hat{P}_\sigma \bigotimes_{i=1}^{N} |\psi_i\rangle \,, \tag{3.92}$$

where the factor $\sqrt{N!}$ is added to ensure that $|\Phi\rangle$ is normalized. As the non-interacting many-body Hamiltonian only acts on a single spin-orbital at a time, the ordering does not matter. This means that

$$\left[\hat{H}, \hat{P}_\sigma\right] = 0, \tag{3.93}$$

and the state $|\Phi\rangle$ is also an eigenstate of $\hat{H}$ with the same energy E as the product state $|\Psi\rangle$. The coordinate representation of $|\Phi\rangle$ now takes on the familiar form of a determinant,

$$\Phi(x_1, \ldots, x_N) = \langle x_1, \ldots, x_N | \Phi \rangle = \frac{1}{\sqrt{N!}} \sum_{\sigma \in S_N} \prod_{i=1}^{N} \psi_{\sigma(i)}(x_i) \tag{3.94}$$

$$= \frac{1}{\sqrt{N!}} \begin{vmatrix} \psi_1(x_1) & \ldots & \psi_N(x_1) \\ \vdots & \ddots & \vdots \\ \psi_1(x_N) & \ldots & \psi_N(x_N) \end{vmatrix}. \tag{3.95}$$

Here $\Phi(x_1, \ldots, x_N)$ is known as the *Slater determinant* of N particles. Exchanging a row or a column in the determinant results in a sign change as required from the antiysmmetric full wave function for the many-body problem. This means that there can not be two, or more, of the same spin-orbitals in the wave function perfectly encapsulating the Pauli principle as two of the same spin-orbitals translates to two particles being in the same state. The spin-orbitals in a Slater determinant are linearly independent, otherwise $\Phi(x_1, \ldots, x_N) = 0$ and thus constitute a basis. This is a consequence of the properties of a determinant that adding a scalar multiple of a column to another column does not change the determinant.

In Fock space the Slater determinants are represented as the occupation number vectors $|\mathbf{n}\rangle$, that is, projecting the occupation number vectors on a spatial basis yields the Slater determinants. This is somewhat of a misnomer where an abstract occupation number vector is named a Slater determinant which stricly speaking is defined on a coordinate system. However, we will continue this tradition and name the fermionic occupation number vectors Slater determinants. As Slater determinants are the occupation number vectors we see that the creation and annihilation operators build states which are Slater determinants and the Slater determinants will form a basis in Fock space. The action of a creation operator on a Slater determinant will be to add a new column in the determinant, whereas an annihilation operator removes a column.

3.6.1 Reference determinant

When working with many-body methods we typically start from a single Slater determinant $|\Phi\rangle$ called the *reference state* or *reference determinant* and

build a basis of Slater determinants using the creation and annihilation operators to create *excited determinants*. The reference determinant is defined as the determinant with lowest energy in the non-interacting case. Using canonical ordering it is given by

$$|\Phi\rangle = \left[\prod_{i=1}^{N} \hat{c}_i^\dagger\right] |-\rangle = \hat{c}_N^\dagger \dots \hat{c}_1^\dagger |-\rangle , \tag{3.96}$$

where N is the number of particles in the system we are exploring.

3.6.2 Fermi vacuum

Having introduced the reference state as the Slater determinant consisting of the N lowest single-particle states, and being the determinant that all other higher-order determinants are built from, we define a "new vacuum" called the *Fermi vacuum*. That is, for a given basis of L single-particle states $\{\phi_p\}$, we split the basis into an *occupied* basis and a *virtual* basis,

$$\{\phi_p\}_{p=1}^{L} = \{\phi_i\}_{i=1}^{N} \cup \{\phi_a\}_{a=N+1}^{L} , \tag{3.97}$$

where N is the number of particles in our reference determinant $|\Phi\rangle$. The occupied states are single-particle states that are contained in the reference determinant $|\Phi\rangle$. We denote the occupied index set by $o = \{1, \dots, N\}$. The virtual states are all $M = L - N$ other states in the single-particle basis that are not contained in the reference determinant. The virtual index set is denoted by $v = \{N+1, \dots, L\}$. As is the convention in the field of many-body quantum mechanics, we use the indices $i, j, k, l, \dots \in o$ to signify occupied indices. Repeated occupied indices means that we only sum over occupied states. For the virtual indices we use $a, b, c, d, \dots \in v$ and repeated indices are only summed over virtual states. Lastly, we use $p, q, r, s, \dots \in o \cup v$ for general states.

Recalling the definition of the creation and annihilation operator, we have that an annihilation operator destroys the vacuum whereas a creation operator will populate the vacuum. Shifting the vacuum to mean the reference determinant we see that we get a new definition for the creation and the annihilation operators. That is, our new annihilation operators will destroy the reference determinant, whereas the new creation operators will populate the reference determinant. This means that $\hat{c}_i^\dagger$ and $\hat{c}_a$ will be our new annihilation operators as

$$\hat{c}_i^\dagger |\Phi\rangle = \hat{c}_a |\Phi\rangle = 0. \tag{3.98}$$

Our new creation operators will be $\hat{c}_a^\dagger$ and $\hat{c}_i$ as their action on the reference state will either add or remove a single-particle state without annihilating the determinant.

$$\hat{c}_a^\dagger |\Phi\rangle = (\Gamma_-)_a^\Phi \, |\Phi'\rangle \,, \tag{3.99}$$

$$\hat{c}_i |\Phi\rangle = (\Gamma_-)_i^\Phi \, |\Phi''\rangle \,, \tag{3.100}$$

where $|\Phi'\rangle$ is $|\Phi\rangle$ with particle state $|a\rangle$ added and $|\Phi''\rangle$ is $|\Phi\rangle$ with particle state $|i\rangle$ removed.

From the Fermi vacuum formalism we can extend the anticommutation relations by splitting up into occupied and virtual states. We have that

$$\left\{\hat{c}_a, \hat{c}_i^\dagger\right\}_F = \left\{\hat{c}_a^\dagger, \hat{c}_i\right\}_F = 0, \tag{3.101}$$

as $a \neq i$, and similarly for the other virtual and occupied indices. We have denoted the anticommutators by an F to emphasize that we are using Fermi vacuum indices.

3.6.3 Excited determinants

From the reference determinant we can create excited determinants by acting on the reference determinant with a creation operator and an annihilation operator. An excited determinant is defined as a Slater determinant containing the same number of single-particle states N as the reference determinant, but with higher-order single-particle states. That is, in the non-interacting case, an excited determinant will yield a higher, or equal, eigenenergy than the reference state.[9]

Definition 3.6. *An* excitation operator *is defined in terms of creation and annihilation operators as*

$$\hat{X}_i^a \equiv \hat{c}_a^\dagger \hat{c}_i, \tag{3.102}$$

and conversely the relaxation operator *as the Hermitian conjugate of the excitation operator, viz.*

$$\left(\hat{X}_i^a\right)^\dagger = \hat{c}_i^\dagger \hat{c}_a, \tag{3.103}$$

where the indices are defined according to the formalism used for the Fermi vacuum.

[9]It is not necessarily true that the eigenenergy of an excited state will be higher than the eigenenergy of the reference state. If we are dealing with degenerate reference determinants we can very well get the same eigenenergy for an excited determinant as the reference state.

Acting with the excitation operator in Definition 3.6 on the reference state, we get

$$|\Phi_i^a\rangle \equiv \hat{X}_i^a |\Phi\rangle , \tag{3.104}$$

where we denote the excited state by $|\Phi_i^a\rangle$. If $|\Phi\rangle \in F_-(L,N)$ we see that $|\Phi\rangle \in F_-(L,N)$ as we remove state $|i\rangle$ and inserts state $|a\rangle$ thus preserving the number of particles N in the excited state. From the Fermi vacuum formalism we have $i < a$ which means that neither the excitation nor the relaxation operator incurs a sign change. Furthermore, from the fundamental anticommutation relations and with the addition of the Fermi vacuum in Equation 3.101 we see that

$$\left\{\hat{X}_i^a, \hat{X}_j^b\right\} = 0, \tag{3.105}$$

and similarly for the relaxation operators. In fact, as the excitation and relaxation operators consist of an even number of second quantized operators they also commute, viz.

$$\left[\hat{X}_i^a, \hat{X}_j^b\right] = 0. \tag{3.106}$$

By repeating the action of the excitation operator on the reference state, we can create any $|\Phi_\mu\rangle \in F_-(L,N)$, where μ is used as a placeholder for any excitation level. That is,

$$|\Phi_{ijk\ldots}^{abc\ldots}\rangle = \hat{X}_i^a \hat{X}_j^b \hat{X}_k^c \ldots |\Phi\rangle = \hat{X}_{ijk\ldots}^{abc\ldots} |\Phi\rangle , \tag{3.107}$$

where we have defined the compound excitation operator $\hat{X}_{ijk\ldots}^{abc\ldots}$ as the product of several excitation operators. As the excitation operators anticommute we get the following antisymmetry requirements on the compound excitation operators,

$$\hat{X}_{ijk\ldots}^{abc\ldots} = -\hat{X}_{ijk\ldots}^{bac\ldots} = -\hat{X}_{jik\ldots}^{abc\ldots} = \hat{X}_{jik\ldots}^{bac\ldots}. \tag{3.108}$$

Note that we get a natural truncation of N excitation operators on any reference determinant with N particles as $N+1$ excitation operators, or more, will annihilate the reference determinant. As discussed in subsection 3.3.1, if the basis of single-particle states is orthonormal, then all excited states and the reference state will be orthonormal to one another.

3.6.4 Operator representation

Having found the coordinate representation of the Slater determinants we are in a position to determine how we can evaluate the expectation values of an

operator $\hat{Q}$ as an integral, viz.

$$\langle Q \rangle = \langle \Phi | \hat{Q} | \Phi \rangle = \int d\mathbf{x} \Phi^*(\mathbf{x}) \hat{Q} \Phi(\mathbf{x}), \tag{3.109}$$

but this quickly becomes tedious as the dN-dimensional integral – where d is the dimensionality of a single coordinate x – over determinants of single-particle functions is quite involved. Luckily, the second quantized formulation lets us collect any operator $\hat{Q}$ as a sum of N-body operators $\hat{Q}_i$ which we can evaluate using tensor contractions over N-body matrix elements. That is, we can write

$$\hat{Q} = \sum_{i=0}^{N} \hat{Q}_i = q_0 \mathbb{1} + q_q^p \hat{c}_p^\dagger \hat{c}_q + \frac{1}{2!} q_{rs}^{pq} \hat{c}_p^\dagger \hat{c}_q^\dagger \hat{c}_s \hat{c}_r + \ldots, \tag{3.110}$$

where each N-body operator is symmetrical in its indices, and includes a $(N!)^{-1}$ factor to account for double counting. The matrix elements of the N-body operator is given by

$$q_q^p \equiv \langle \phi_p | \hat{Q}_1 | \phi_q \rangle = \int dx \phi_p^*(x) \hat{Q}_1 \phi_q(x), \tag{3.111}$$

$$q_{rs}^{pq} \equiv \langle \phi_p \phi_q | \hat{Q}_2 | \phi_r \phi_s \rangle = \int dx_1 dx_2 \phi_p^*(x_1) \phi_q^*(x_2) \hat{Q}_2 \phi_r(x_1) \phi_s(x_2), \tag{3.112}$$

$$\vdots \tag{3.113}$$

Here we have specified a label for single-particle states, but these expressions are valid for any basis of single-particle states. In this thesis we will limit ourselves to at most two-particle operators. A proof of why this representation of the one- and two-body operators is valid is shown in section A.6.

3.6.5 The Slater-Condon rules

The Slater-Condon rules [39, 40] gives all non-zero contributions to matrix elements of one- and two-body operators over Slater determinants constructed from an orthonormal basis of single-particle states. The notation used to describe these rules are widely different, and the rules are notoriously difficult to express in a straightforward manner. Wikipedia gives a relatively clear description [41], but they give the impression that the rules only apply for a reference determinant and determinants excited at most twice from this reference. Furthermore, the sign of the matrix elements is completely ignored in this description.

We will use the occupation number representation of the Slater determinants to describe the Slater-Condon rules. Thus, $|\mathbf{n}\rangle$ describes a Slater determinant containing the states in the set $\mathbf{n}$. To denote an index being contained

in a given set we use the Kronecker-Delta notation $\delta_{p\in\mathbf{n}}$ which is read as "all states p in the set $\mathbf{n}$". In the jargon of the Fermi vacuum, this corresponds to the occupied states in $|\mathbf{n}\rangle$. The difference in the number of states in two states $|\mathbf{n}\rangle$ and $|\mathbf{m}\rangle$ is given by $|\mathbf{n}-\mathbf{m}|$. Note that we only look at states with the same number of particles N, which means that the difference between two states will always be an even number as an excitation is done by replacing single-particle states. We are now ready to state the Slater-Condon rules.

Lemma 3.2. *Given two Fock states* $|\mathbf{n}\rangle, |\mathbf{m}\rangle \in F_-(L,N)$ *and a one-body operator on the form*

$$\hat{g} = g_q^p \hat{c}_p^\dagger \hat{c}_q, \tag{3.114}$$

the Slater-Condon rules for this operator gives the value of the matrix elements $\langle\mathbf{n}|\hat{g}|\mathbf{m}\rangle$*. The three cases are:*

$$\langle\mathbf{n}|\hat{g}|\mathbf{m}\rangle = \begin{cases} g_p^p \delta_{p\in\mathbf{m}}, & |\mathbf{n}-\mathbf{m}| = 0, \\ g_q^p (\Gamma_-)_p^{\mathbf{n}} (\Gamma_-)_q^{\mathbf{m}} \delta_{p\in\mathbf{n}} \delta_{q\in\mathbf{m}}, & |\mathbf{n}-\mathbf{m}| = 2, \\ 0, & |\mathbf{n}-\mathbf{m}| > 2, \end{cases} \tag{3.115}$$

where the phase $(\Gamma_-)_p^{\mathbf{n}}$ *is the same as in Definition 3.2. Sums are only over repeated indices in the matrix elements.*

From Lemma 3.2 we see that two determinants can differ by at most a single-excitation for the matrix element to be non-zero. This greatly limits the number of matrix elements that needs to evaluated when working with orthonormal Slater determinants acting on one-body operators.

Lemma 3.3. *Given two Fock states* $|\mathbf{n}\rangle, |\mathbf{m}\rangle \in F_-(L,N)$ *and a two-body operator on the form*

$$\hat{g} = \frac{1}{4} g_{rs}^{pq} \hat{c}_p^\dagger \hat{c}_q^\dagger \hat{c}_r \hat{c}_s, \tag{3.116}$$

where we assume that the two-body matrix elements g_{rs}^{pq} *are antisymmetric, that is,*

$$g_{rs}^{pq} = \langle\phi_p\phi_q|\hat{g}|\phi_r\phi_s\rangle - \langle\phi_p\phi_q|\hat{g}|\phi_s\phi_r\rangle\,. \tag{3.117}$$

The Slater-Condon rules for this operator gives the value of the matrix elements $\langle\mathbf{n}|\hat{g}|\mathbf{m}\rangle$*. The four cases are:*

$$\langle\mathbf{n}|\hat{g}|\mathbf{m}\rangle = \begin{cases} \frac{1}{2} g_{pq}^{pq} (1-\delta_{pq}) \delta_{p\in\mathbf{m}} \delta_{q\in\mathbf{m}}, & |\mathbf{n}-\mathbf{m}| = 0, \\ g_{qr}^{pr} (\Gamma_-)_p^{\mathbf{n}} (\Gamma_-)_q^{\mathbf{m}} \delta_{p\in\mathbf{n}} \delta_{q\in\mathbf{m}} \delta_{r\in\mathbf{n}}, & |\mathbf{n}-\mathbf{m}| = 2, \\ g_{rs}^{pq} (\Gamma_-)_p^{\mathbf{n}} (\Gamma_-)_q^{\mathbf{n}} (\Gamma_-)_r^{\mathbf{m}} (\Gamma_-)_s^{\mathbf{m}} \delta_{p,q\in\mathbf{n}} \delta_{r,s\in\mathbf{m}} & |\mathbf{n}-\mathbf{m}| = 4, \\ 0, & |\mathbf{n}-\mathbf{m}| > 4, \end{cases} \tag{3.118}$$

where the phase $(\Gamma_-)_p^n$ *is the same as in Definition 3.2. The factor* $(1-\delta_{pq})$ *in the first case comes about as a consequence of the Pauli exclusion principle where* $\hat{c}_p\hat{c}_p$ *always destroys an antisymmetric state. Pay extra close attention to the Kronecker-Deltas in the evaluation of the matrix elements when* $|\mathbf{n}-\mathbf{m}|=4$ *as we have added the notation* $\delta_{p,q\in\mathbf{n}}$ *denoting that both* i *and* j *must be contained in* $\mathbf{n}$*. Sums are only over repeated indices in the matrix elements.*

3.6.6 Orbital rotations

As demonstrated in Lemma 3.1, a unitary transformation of the spin-orbital basis preserves orthonormality. An extension to this lemma is therefore that the normalization of a Slater determinant built from an orthonormal basis of spin-orbitals is preserved when transforming to a new basis by a unitary transformation.

Lemma 3.4. *Let* $|\Phi\rangle$ *be a Slater determinant built from* N *single-particle states from an orthonormal basis of* L *states* $\{\phi_i\}$*. We can then perform a unitary transformation to a new orthonormal basis of* L *single-particle states* $\{\psi_i\}$ *building a new* N*-particle Slater determinant* $|\Psi\rangle$*, where the single-particle states in* $|\Psi\rangle$ *are obtained by the unitary transformation of the* N *single-particle states in* $|\Phi\rangle$*. This unitary transformation will leave the determinant invariant up to a complex phase.*

See section A.3 for a proof of this lemma. Another important theorem for computational many-body quantum mechanics is *Thouless theorem* as it explains the role and the influence of the singles excitations operators [42].

Theorem 3.3. *Given an* N*-particle Slater determinant* $|\Phi\rangle$*, we can write any other* N*-particle Slater determinant* $|\Psi\rangle$ *where* $\langle\Phi|\Psi\rangle\neq 0$*, by*

$$|\Psi\rangle = \exp(\hat{T})\,|\Phi\rangle\,, \tag{3.119}$$

where $\hat{T}=\tau_i^a\hat{X}_i^a$ *is a singles excitation operator with the coefficients* τ_i^a *determined uniquely.*

Stated in words, Thouless theorem tells us that we can construct any other N-particle determinant $|\Psi\rangle$ from an arbitrary N-particle determinant $|\Phi\rangle$ using an exponential singles excitation operator as long as the two determinants are not orthogonal to one another.

3.6.7 Determinant overlap

So far we have limited our attention to an orthonormal set of basis states, thus making the Slater determinants orthonormal. However, we will discover situations where the determinants no longer are orthonormal. This will mainly

be due to time evolution of the single-particle states. In some sense we are computing the overlap between two determinants in differing bases, but this can be represented as two expansions of the same underlying basis. Consider the two spin-orbital expansions

$$|\phi_i\rangle = C_{\alpha i}\,|\chi_\alpha\rangle\,, \tag{3.120}$$
$$|\psi_i\rangle = D_{\alpha i}\,|\chi_\alpha\rangle\,, \tag{3.121}$$

where $\left\{\,|\chi_\alpha\rangle\right\}_{\alpha=1}^{L}$ is an underlying basis of spin-orbitals with overlap

$$s_{\alpha\beta} = \langle\chi_\alpha|\chi_\beta\rangle\,, \tag{3.122}$$

not necessarily orthonormal. The overlap between the two spin-orbital expansions is thus given by

$$\langle\psi_i|\phi_j\rangle = D^*_{\alpha i}\,\langle\chi_\alpha|\chi_\beta\rangle\,C_{\beta j} = D^*_{\alpha i}s_{\alpha\beta}C_{\beta j} \equiv T_{ij}, \tag{3.123}$$

where we have defined the overlap elements T_{ij}. In matrix notation the overlap matrix $\mathbf{T}$ is found from the coefficient matrices $\mathbf{C}$ and $\mathbf{D}$ along with the overlap matrix $\boldsymbol{S}$ by

$$\mathbf{T} = \mathbf{D}^\dagger\mathbf{S}\mathbf{C}. \tag{3.124}$$

We now construct two Slater determinants $|\Phi\rangle$ and $|\Psi\rangle$ from the N first spin-orbitals $|\phi_i\rangle$ and $|\psi_i\rangle$, respectively. Using the antisymmetrizer, the overlap between the two determinants is given by

$$\langle\Psi|\Phi\rangle = \frac{1}{N!}\sum_{\sigma,\tau\in S_N}(-1)^{|\sigma||\tau|}\prod_{i=1}^{N}\langle\psi_{\sigma(i)}|\phi_{\tau(i)}\rangle \tag{3.125}$$
$$= \frac{1}{N!}\sum_{\sigma,\tau\in S_N}(-1)^{|\sigma||\tau|}\prod_{i=1}^{N}T_{\sigma(i)\tau(i)}, \tag{3.126}$$

where we now have a double sum over all permutations σ and τ. By keeping one of the permutation sums fixed, we see that the product over i will yield all unique combinations of T_{ij}. Thus, summing over both permutations will yield the same terms N! times and we can remove one of the permutation sums at the cost of multiplying by N!. This leaves us with

$$\langle\Psi|\Phi\rangle = \frac{1}{N!}N!\sum_{\sigma\in S_N}(-1)^{|\sigma|}\prod_{i=1}^{N}T_{i\sigma(i)} = \det(\mathbf{T}), \tag{3.127}$$

where we have recognized the determinant of T.

3.7 The many-body Hamiltonian

A general many-body Hamiltonian can be described by

$$\hat{H} \equiv \sum_{i=0}^{\infty} \hat{H}_i, \tag{3.128}$$

where we denote the N-body Hamiltonian by $\hat{H}_i$. From the postulates of quantum mechanics we require that $\hat{H}^\dagger = \hat{H}$, that is, the Hamiltonian should be Hermitian. This in turn implies that $\hat{H}_i^\dagger = \hat{H}_i$ for all N-body terms. We can compute the energy, i.e., the expectation value of the Hamiltonian, by

$$\langle\psi|\hat{H}|\psi\rangle = \sum_{i=0}^{\infty} \langle\psi|\hat{H}_i|\psi\rangle = \langle\psi|\hat{H}_0|\psi\rangle + \langle\psi|\hat{H}_1|\psi\rangle + \langle\psi|\hat{H}_2|\psi\rangle + \ldots, \tag{3.129}$$

where each term involves the *interaction* between i particles. For $i = 0$ we have $\hat{H}_0$ which we take to signify a constant term, e.g., the nuclear repulsion energy of an atomic system where we limit our attention to electrons. This term contributes with a constant energy shift in the expectation value. The one-body term, $\hat{H}_1$, is the familiar Hamiltonian from introductory courses in quantum mechanics. This term describes one-particle contributions, e.g., the kinetic energy, external potentials of the system, external fields, etc. Higher order terms describe interactions between particles in the system. For example, the Coulomb interaction is a two-body interaction between particle pairs and is described by $\hat{H}_2$. More exotic higher-order interactions can occur in nuclear physics and the sort. However, it is common to truncate the interactions in the many-body Hamiltonian as higher-order terms leads to complicated equations which become intractable unless clever approximations are introduced.

Luckily, much of solid-state physics, and almost all of quantum chemistry, can be described by the Coulomb interaction as the dynamics of the system is mainly governed by the electrons. This means that we will truncate the many-body Hamiltonian to second-order interactions. Furthermore, we ignore the constant term in the Hamiltonian as this can always be added when we compute the energy and will not contribute when we look for a solution of the many-body problem. We will denote the general electronic Hamiltonian by

$$\hat{H} = \hat{h} + \hat{u}, \tag{3.130}$$

where $\hat{h}$ is the one-body term and $\hat{u}$ describes two-body interactions, which in our case is the Coulomb interaction.

3.7.1 The Born-Oppenheimer approximation

The Born-Oppenheimer approximation first occured in a seminal paper by Born & Oppenheimer [43]. It is a procedure describing how we can solve a molecular system consisting of electrons and nucleons where we assume that the total wave function can approximately be separated into an electronic and a nuclear part, viz.

$$|\Psi\rangle \approx |\Psi_e\rangle \otimes |\Psi_n\rangle\,, \tag{3.131}$$

where we denote the electronic wave function by $|\Psi_e\rangle$ and the nuclear counterpart as $|\Psi_n\rangle$. This lets us separate the full Hamiltonian in a nuclear Hamiltonian and an electronic Hamiltonian. We say that this approximation is valid as the electrons move much faster than the nucleons and that the electrons therefore experiences the nucleus as having a fixed position in time [44]. The electronic Hamiltonian desribed above therefore only includes the nucleus-nucleus terms as a constant energy shift, the electron-nucleus interaction as a potential well and the rest of the system is described by the Coulomb interaction and the kinetic energy.

3.7.2 One-body Hamiltonian

The one-body Hamiltonian describes the non-interacting system we are examining. In the time-independent case, we typically describe the system by a sum of kinetic and potential terms,

$$\hat{h} = \sum_{i=1}^{N} \hat{h}_i = \sum_{i=1}^{N} \left(\hat{t}_i + \hat{v}_i\right) = \sum_{i=1}^{N} \left(\frac{\hat{p}_i^2}{2m_i} + \hat{v}_i\right), \tag{3.132}$$

where the sum runs over all particles in the system separately. The potential term can come from many different sources, e.g., an external field, mean-field approximations, the electron-nucleon interaction, etc. We will discsuss these more in depth when we start looking at specific systems. Often when solving the many-body problem we seek a solution to the one-body Hamiltonian in terms of a reference Slater determinant. This will in many cases provide us with a good starting guess for the system before using more sophisticated methods such as the Hartree-Fock method to improve on our reference state.

Time-dependency

In general the time-dependency can occur in all the terms in the full many-body Hamiltonian, but the most common scenario is an external interaction occuring in the one-body Hamiltonian, e.g., a laser field, time-varying potential, etc. In this thesis we will only concern ourselves with an external laser

field. We can then write the time-dependent one-body Hamiltonian on the form

$$\hat{h}(t) = \sum_{i=1}^{N} \hat{h}_i(t) = \sum_{i=1}^{N} \left(\hat{t}_i + \hat{v}_i + \hat{f}_i(t) \right), \tag{3.133}$$

where the time-dependence is represented by the time-dependent operator $\hat{f}_i(t)$.

3.7.3 Two-body Hamiltonian

The two-body Hamiltonian provides interactions between pairs of particles. This complicates the matter by introducing a double sum over all particles to include all pairs.

$$\hat{u} = \sum_{i=1}^{N} \sum_{j=1}^{N} \hat{u}_{ij}. \tag{3.134}$$

Often some care must be taken when $i = j$ as this results in self-interaction which can yield unphysical results, but we have for the sake of generality written the full sum. The two-body operator is often the bottle-neck in terms of complexity for the electronic Hamiltonian.

Coulomb interaction

We will in this thesis concern ourselves with electronic interactions and will therefore limit ourselves to the Coulomb interaction as our two-body operator. This operator is given by

$$\hat{u} = \sum_{i=1}^{N} \sum_{j=i+1}^{N} \hat{u}_{ij} = \sum_{i=1}^{N} \sum_{j=1}^{N} \frac{1}{4\epsilon_0 \pi} \frac{e^2}{\left| \hat{\mathbf{r}}_i - \hat{\mathbf{r}}_j \right|}, \tag{3.135}$$

The Coulomb interaction is a quantized version of the Coulomb potential with ϵ_0 representing the vacuum permittivity and e^2 the charge of the particles, which we assume to be of the same type.

3.7.4 Second quantized formulation

Having introduced the second quantized formulation of many-body quantum mechanics we wish to represent the Hamiltonian in this formalism. This introduces a generalization which will prove very useful for the later many-body methods as it removes the explicit grid representation of the operators

and introduces abstract matrix elements as coefficients to the second quantized operators. For a given basis of L orthonormal single-particle states $\{\phi_p\}$ we can write the second quantized formulation of the electronic Hamiltonian as

$$\hat{H} = \hat{h} + \hat{u} = h_q^p \hat{c}_p^\dagger \hat{c}_q + u_{rs}^{pq} \hat{c}_p^\dagger \hat{c}_q^\dagger \hat{c}_s \hat{c}_r, \tag{3.136}$$

where we denote the antisymmetric two-body elements by

$$u_{rs}^{pq} \equiv \langle \phi_p \phi_q | \hat{u} | \phi_r \phi_s \rangle_{AS} = \langle \phi_p \phi_q | \hat{u} | \phi_r \phi_s \rangle - \langle \phi_p \phi_q | \hat{u} | \phi_s \phi_r \rangle . \tag{3.137}$$

The matrix elements of the one- and two-body elements are given by

$$h_q^p \equiv \langle \phi_p | \hat{h} | \phi_q \rangle = \int dx \phi_p^*(x) \hat{h} \phi_q(x), \tag{3.138}$$

$$\langle \phi_p \phi_q | \hat{u} | \phi_r \phi_s \rangle = \int dx_1 dx_2 \phi_p^*(x_1) \phi_q^*(x_2) \hat{u} \phi_r(x_1) \phi_s(x_2), \tag{3.139}$$

where x is a generalized coordinate of spin, and position or momentum.

3.7.5 The reference energy

Given a basis of L orthonormal single-particle states $\{\phi_p\}$ we construct a Slater determinant from the N first states, viz.

$$|\Phi\rangle = |\phi_1 \dots \phi_N\rangle , \tag{3.140}$$

that is, we have N occupied states and $M = L - N$ virtual states using the same convention for the indices as discussed in subsection 3.6.2 on the Fermi vacuum. We dub this state the *reference state* for reasons which will become clear when we start working on the many-body methods. For a general electronic Hamiltonian with one- and two-body operators, we can compute the expectation value of the energy from the reference state.

$$\langle \Phi | \hat{H} | \Phi \rangle = h_q^p \langle \Phi | \hat{c}_p^\dagger \hat{c}_q | \Phi \rangle + \frac{1}{4} u_{rs}^{pq} \langle \Phi | \hat{c}_p^\dagger \hat{c}_q^\dagger \hat{c}_s \hat{c}_r | \Phi \rangle , \tag{3.141}$$

where we use the antisymmetric two-body elements. Using Wick's theorem[10] we can evaluate the overlap strings on the reference state. This yields the *reference energy* given by

$$E_0 \equiv \langle \Phi | \hat{H} | \Phi \rangle = h_i^i + \frac{1}{2} u_{ij}^{ij}. \tag{3.142}$$

The derivation of this expression can be found in section A.4.

[10] Or the anti-commutation rules manually.

3.7.6 The normal-ordered Hamiltonian

Starting from the general electronic Hamiltonian on second quantized form in Equation 3.136, we can write the operators on normal-ordered form relative to the Fermi vacuum. We then get

$$\hat{H}_N = \hat{f}_N + \hat{u}_N = f^p_q\{\hat{c}^\dagger_p\hat{c}_q\} + \frac{1}{4}u^{pq}_{rs}\{\hat{c}^\dagger_p\hat{c}^\dagger_q\hat{c}_s\hat{c}_r\}, \tag{3.143}$$

where the matrix elements of the normal-ordered Fock operator is given by

$$f^p_q = h^p_q + u^{pi}_{qi}. \tag{3.144}$$

The complete derivation of the normal-ordered Hamiltonian is shown in section A.5

3.8 Many-body density matrices

In a seminal paper by Löwdin [45], the concept of a many-body density matrix in terms of the orbitals of a Slater determinant is discussed. These are dubbed N-body density matrices, where N depends on the N-body interaction, that is, the number of particles included in the interaction. Consider the Hermitian operator $\hat{Q}$ from Equation 3.110, then for a normalized, pure state $|\psi\rangle$, we are able to compute the expectation value of the operator $\hat{Q}$ by

$$\langle Q\rangle = \langle\psi|\hat{Q}|\psi\rangle = \mathrm{tr}\Big(\hat{\rho}\hat{Q}\Big), \tag{3.145}$$

where we have introduced the density operator $|\psi\rangle$ by

$$\hat{\rho} = |\psi\rangle\langle\psi|\,. \tag{3.146}$$

Now, if $|\psi\rangle$ is a wave function describing a system of N particles, we can write the expectation value of the operator $\hat{Q}$ as

$$\langle Q\rangle = \mathrm{tr}\Big(\hat{\rho}\hat{Q}\Big) = \langle\psi|\psi\rangle\ \langle\psi|\hat{Q}|\psi\rangle = \sum_{i=0}^{N}\langle\psi|\hat{Q}_i|\psi\rangle \tag{3.147}$$

$$= Q_0\langle\psi|\mathbb{1}|\psi\rangle + Q^p_q\langle\psi|\hat{c}^\dagger_p\hat{c}_q|\psi\rangle + \frac{1}{2!}Q^{pq}_{rs}\langle\psi|\hat{c}^\dagger_p\hat{c}^\dagger_q\hat{c}_s\hat{c}_r|\psi\rangle + \ldots \tag{3.148}$$

$$= Q_0 + Q^p_q\rho^q_p + \frac{1}{2!}Q^{pq}_{rs}\rho^{rs}_{pq} + \ldots, \tag{3.149}$$

where we ask the reader to direct special attention to the index ordering of the N-body density matrix indices ρ as the "opposite" direction of the index ordering from the N-body matrix elements. We thus observe that all

information about the wave function that is needed for the evaluation of the expectation value $\langle Q \rangle$ is contained in the N-body density matrices, where the elements are given by

$$\rho_p^q = \langle \psi | \hat{c}_p^\dagger \hat{c}_q | \psi \rangle , \tag{3.150}$$

$$\rho_{pq}^{rs} = \langle \psi | \hat{c}_p^\dagger \hat{c}_q^\dagger \hat{c}_s \hat{c}_r | \psi \rangle , \tag{3.151}$$

$$\vdots \tag{3.152}$$

Of all the N-body density matrices, the one- and two-body density matrices are the ones that are most applicable for our work as the many-body Hamiltonian we are looking at is limited to two-body interactions and we are only interested in observables expressable as one-body operators.

3.8.1 One-body density matrix

We will denote the one-body density operator by $\hat{\rho}_1$ where the elements are given by Equation 3.150. Comparing the one-body density operator with the general density operator as discussed in section 2.3 we have that $\hat{\rho}_1^\dagger = \hat{\rho}_1$, i.e., it is Hermitian. This can be seen from the elements by

$$(\rho_p^q)^* = \langle \psi | \hat{c}_p^\dagger \hat{c}_q | \psi \rangle^* = \langle \psi | \hat{c}_q^\dagger \hat{c}_p | \psi \rangle = \rho_q^p. \tag{3.153}$$

The one-body density is positive semidefinite, which means it satisifies the positivity condition for density operators. The normalization of the one-body density is however a little different from the general density operator. We have that

$$\mathrm{tr}(\hat{\rho}_1) = \rho_p^p = \langle \psi | \hat{c}_p^\dagger \hat{c}_p | \psi \rangle = N, \tag{3.154}$$

where N is the number of particles contained in $|\psi\rangle$. The formalism of the one-body density operator can also be extended to a mixed many-body states similar to the general density operator.

3.8.2 Particle density

A quantity we will be concerned with is the one-particle density – also known as the first-order reduced density matrix – which describes the simulatanous distribution of all the particles in the system. As an integral it is defined as

$$\rho(x_1) = N \left(\prod_{i=2}^{N} \int dx_i \right) \left| \psi(x_1, x_2, \ldots, x_N) \right|^2, \tag{3.155}$$

where the integral runs over all generalized coordinates x_i except for one [45, 46]. Due to the indistinguishability of the particles, the particle density is a measure of where any particle is located in space under the influence of all the other particles. The one-body density provides insight as to where particles in a system will be positioned, but not which particles are where nor how they behave relative to each other. Using the one-body density matrix we are able to find the distribution of all the particles by the single-particle functions. This is given by

$$\rho(x) = \phi_q^*(x)\rho_p^q\phi_p(x). \tag{3.156}$$

An interesting property of the particle density is that we can define a sort of ad-hoc ionization description. The process of ionization can be described by a bound particle leaving the confinement of either the core of an atom or the a more general potential well. If we define a radius R as the distance from the centre of the well to the edge where the influence of the well is zero, or close to zero, then we can measure the amount of ionization by

$$I(R) = N\int_{|x|\leqslant R} dx\rho(x), \tag{3.157}$$

where N is a normalization factor which we take to be the particle density integrated over the entire coordinate space such that $I(R) \in [0, 1]$. Note that the choice of R depends on the system. Some systems such as the infinite harmonic oscillator will always have bound states and the ionization can thus be interpreted as a measure of how much of the state is still distributed in the centre of the well.

3.8.3 Two-body density matrix

We denote the two-body density operator by $\hat{\rho}_2$ with elements from Equation 3.151. Due to the anticommutation relations between the second quantized operators we have the anti-symmetry

$$\rho_{pq}^{rs} = -\rho_{pq}^{sr} = -\rho_{qp}^{rs} = \rho_{qp}^{sr}. \tag{3.158}$$

As a consequence, the Pauli principle is baked into the elements by

$$\rho_{pq}^{rr} = \rho_{pp}^{rs} = \rho_{p}^{rr} = 0, \tag{3.159}$$

in the same way as the two-body Hamiltonian. The two-body density operator is also Hermitian in the sense that

$$(\rho_{pq}^{rs})^* = \langle\psi|\hat{c}_p^\dagger\hat{c}_q^\dagger\hat{c}_s\hat{c}_r|\psi\rangle^* = \langle\psi|\hat{c}_r^\dagger\hat{c}_s^\dagger\hat{c}_q\hat{c}_p|\psi\rangle = \rho_{rs}^{pq}. \tag{3.160}$$

The two-body density operator is also positive semidefinite in the same manner as the one-body density operator. The normalization of the two-body density operator can be found from

$$\rho_{pq}^{pq} = \langle\psi|\hat{c}_p^\dagger\hat{c}_q^\dagger\hat{c}_q\hat{c}_p|\psi\rangle = -\langle\psi|\hat{c}_p^\dagger\hat{c}_q^\dagger\hat{c}_p\hat{c}_q|\psi\rangle = -\langle\psi|\hat{c}_p^\dagger(\delta_{pq}-\hat{c}_p\hat{c}_q^\dagger)\hat{c}_q|\psi\rangle \tag{3.161}$$

$$= \langle\psi|\hat{N}_p\hat{N}_q|\psi\rangle - \langle\psi|\hat{N}_p|\psi\rangle = N^2 - N = N(N-1). \tag{3.162}$$

The two-body density matrix can used when computing the energy contribution from the two-body Hamiltonian.

3.9 The multireference problem

A common topic in many-body quantum mechanics is the multireference problem. Most many-body methods require a single reference, i.e., a single Fock state, as a starting point and then build higher excited states from this state. In the case of degenerate reference states, we are in the multireference regime. As an example, consider the lithium (Li) atom with three electrons, thus requiring a fourth electron in order to get a closed shell. In the case of a non-interacting Li atom in a given spin-orbital basis $\left\{|\psi_i\rangle\right\}_{i=1}^{L}$, the ground state will consist of the two Slater determinants

$$|\Phi_1\rangle = |\psi_1\psi_2\psi_3\rangle\,, \tag{3.163}$$

$$|\Phi_2\rangle = |\psi_1\psi_2\psi_4\rangle\,, \tag{3.164}$$

where both states will have the same eigenenergy $E_1 = E_2$ from the non-interacting Hamiltonian $\hat{h}$. The true ground state of this system will then be a linear combination of these two Fock states yielding

$$|\Psi\rangle = \frac{1}{\sqrt{2}}\left[|\Phi_1\rangle \pm |\Phi_2\rangle\right]. \tag{3.165}$$

Most second quantized many-body methods rely on the single-reference assumption and will not work in the multireference regime.

Chapter 4

Hartree-Fock theory

One can not tackle the subject of many-body theory without a discussion of the Hartree-Fock method. It serves as an excellent initial approximation, and in many cases the most the favored approximation, to the many-body wave function for a given system. It is a rather cheap method, in terms of computational intensity, and explains much of the underlying physics of a given system of many particles.

4.1 Time-independent Hartree-Fock theory

We start from the time-independent Schrödinger equation,

$$\hat{H}\,|\Psi\rangle = E\,|\Psi\rangle\,, \tag{4.1}$$

where $\hat{H}$ is the electronic Hamiltonian with one- and two-body operators. We know that the ground state of the one-body Hamiltonian will be a single Slater determinant as demonstrated in section 3.6. If the two-body interactions are weak, we can treat these contributions perturbatively and a single Slater determinant will serve as a good approximation to the full many-body wave function.[1] This motivates the approximation that the many-body wave function $|\Psi\rangle$ can be approximated by a single Slater determinant, viz.

$$|\Psi\rangle = |\Phi\rangle = |\phi_1\phi_2\ldots\phi_N\rangle\,, \tag{4.2}$$

where the N *molecular orbitals*[2] $\{\phi_i\}$ are the primary unknowns, subject to the constraint that they are orthonormal,

$$\langle\phi_i|\phi_j\rangle = \delta_{ij} \implies \langle\Phi|\Phi\rangle = 1. \tag{4.3}$$

[1] We will see that it does not take much before the two-body interaction becomes a little more than just a small perturbation.

[2] The term molecular orbitals will be used exclusively to denote the "Hartree-Fock" orbitals.

4.1.1 The non-canonical Hartree-Fock equations

Starting from the variational principle, we define the energy functional

$$E[\Phi, \Phi^*] \equiv \langle \Phi | \hat{H} | \Phi \rangle = \langle \phi_i | \hat{h} | \phi_i \rangle + \frac{1}{2} \langle \phi_i \phi_j | \hat{u} | \phi_i \phi_j \rangle_{AS}, \tag{4.4}$$

found from the definition of the reference energy in subsection 3.7.5. Our task is now to find the molecular orbitals $\{\phi_i\}$ that minimize the energy functional, i.e., we find the stationary points of the energy functional as discussed in section 2.4. As the energy functional $E[\Phi, \Phi^*]$ does not incorporate the constraint that the molecular orbitals should be orthonormal, we use Lagrange's method of undetermined multipliers. This yields the Lagrangian functional

$$L[\Phi, \Phi^*, \lambda] = E[\Phi, \Phi^*] - \lambda_{ji} \left(\langle \phi_i | \phi_j \rangle - \delta_{ij} \right), \tag{4.5}$$

where λ_{ji} are Lagrange multipliers, one for each constraint. As the Lagrangian functional is real and the constraint is Hermitian, the Lagrange multipliers can be chosen Hermitian as well. See section A.7 for a proof of this fact. We are now interested in finding a stationary point of the Lagrangian with respect to small variations in functional dependency, that is, the molecular orbitals and the Lagrange multipliers. The stationary conditions for the Lagrange multipliers yield the constraint that the molecular orbitals should be orthonormal, viz.

$$\frac{\partial}{\partial \lambda_{ji}} L[\Phi, \Phi^*, \lambda] = 0 \implies \langle \phi_i | \phi_j \rangle = \delta_{ij}, \tag{4.6}$$

which are included in the end when we find solutions that are orthonormal as the constraint is included in the variation over the molecular orbitals [29]. The variation over a specific orbital k is given by

$$\tilde{\phi}_i(x) = \phi_i(x) + \delta_{ik} \epsilon \eta(x), \tag{4.7}$$

where $\epsilon \in \mathbb{R}$ is a small number and $\eta(x)$ is a single-particle function over some coordinate x. Note the use of the Kronecker-Delta to ensure that the variation only occurs for a single orbital at a time. This variation is similar for the complex conjugate of the molecular orbitals, but with $\phi_i^*(x)$ and $\eta^*(x)$ instead. To avoid too much clutter, we will denote a variation over the molecular orbitals by a variation over the Slater determinants. That is, we take $\tilde{\Phi}(\mathbf{x})$ to mean a variation over a single orbital $\phi_i(x)$ in $\Phi(\mathbf{x})$, and similarly for the complex conjugate. Taylor expanding the Lagrangian functional,

$$\begin{aligned} L[\tilde{\Phi}, \tilde{\Phi}^*, \lambda] = L[\Phi, \Phi^*, \lambda] &+ \left. \frac{\partial L[\tilde{\Phi}, \Phi^*, \lambda]}{\partial \epsilon} \right|_{\epsilon=0} \epsilon \\ &+ \left. \frac{\partial L[\Phi, \tilde{\Phi}^*, \lambda]}{\partial \epsilon} \right|_{\epsilon=0} \epsilon + \ldots, \end{aligned} \tag{4.8}$$

where the dots represent variations beyond the first-order stationary condition. As discussed in the section on the variational principle, the first order variations does not guarantee that we have found a minimum, but they do it *often enough* for us to not bother with second order variations or more [3]. In lieu of this comforting thought, we proceed on our merry way by finding the stationary points using the method of functional derivatives as dicussed in section 2.4. We will restrict ourselves to the variation over the complex conjugated orbitals as both variations yield the same equation adjointed of one another. This yields

$$L[\Phi, \tilde{\Phi}^*, \lambda] = E[\Phi, \tilde{\Phi}^*] - \lambda_{ji} \left[\langle \phi_i | \phi_j \rangle + \epsilon \delta_{ik} \langle \eta | \phi_j \rangle - \delta_{ij} \right], \tag{4.9}$$

where we used the linearity of the inner product to split ut the variation over the orbital $\phi_i^*(x)$ in the constraint term. Keeping only first-order variations in the energy functional we find

$$E[\Phi, \tilde{\Phi}^*] = E[\Phi, \Phi^*] + \epsilon \left(\langle \eta | \hat{h} | \phi_k \rangle + \langle \eta \phi_j | \hat{u} | \phi_k \phi_j \rangle_{AS} \right) + \mathcal{O}(\epsilon^2), \tag{4.10}$$

where we have used the antisymmetric properties of the two-body elements to collect the two variations over the left-hand side of the matrix elements. Furthermore, we have collapsed one of the sums over the Kronecker-Delta in the variation in all terms. The variation in the Lagrangian functional can now be found by

$$\delta L[\Phi, \tilde{\Phi}^*, \lambda] = L[\Phi, \tilde{\Phi}^*, \lambda] - L[\Phi, \Phi^*, \lambda] \tag{4.11}$$

$$= \epsilon \left[\langle \eta | \hat{h} | \phi_k \rangle + \langle \eta \phi_j | \hat{u} | \phi_k \phi_j \rangle_{AS} - \lambda_{jk} \langle \eta | \phi_j \rangle \right]. \tag{4.12}$$

Having collapsed one of the orbital sums to yield ϕ_k we now restrict the variation over the molecular orbitals to

$$\delta \phi_k^*(x) = \tilde{\phi}_k^*(x) - \phi_k^*(x) = \epsilon \eta^*(x). \tag{4.13}$$

Computing the stationary point of the Lagrangian with variations over $\phi_k^*(x)$ now gives

$$\left. \frac{\partial L[\Phi, \tilde{\Phi}^*, \lambda]}{\partial \epsilon} \right|_{\epsilon=0} = \int dx \frac{\delta L[\Phi, \tilde{\Phi}^*, \lambda]}{\delta \phi_k^*(x)} \eta^*(x) = 0 \tag{4.14}$$

$$\implies \langle \eta | \hat{h} | \phi_k \rangle + \langle \eta \phi_j | \hat{u} | \phi_k \phi_j \rangle_{AS} = \lambda_{jk} \langle \eta | \phi_j \rangle, \tag{4.15}$$

which according to the fundamental lemma of calculus of variations [30] must be valid for all variations $\epsilon \eta^*(x)$. We now introduce the single-particle *Fock operator* by its matrix elements

$$\langle \phi_p | \hat{f} | \phi_q \rangle \equiv \langle \phi_p | \hat{h} | \phi_q \rangle + \langle \phi_p \phi_j | \hat{u} | \phi_q \phi_j \rangle_{AS}, \tag{4.16}$$

where we use the Fermi vacuum formalism for the sums. This lets us write the stationary point of the Lagrangian functional from Equation 4.15 as

$$\hat{f}\,|\phi_k\rangle = \lambda_{jk}\,|\phi_j\rangle\,. \tag{4.17}$$

This equation is known as the *non-canonical Hartree-Fock equations*, where the molecular orbitals ϕ_k are orthonormal.

4.1.2 Canonical Hartree-Fock equations

Now, Equation 4.17 will yield the stationary Hartree-Fock energy, but from Lemma 3.4 we know that a unitary transformation of the Slater determinant $\Phi(\mathbf{x})$ leaves the determinant invariant up to a complex phase. We therefore look for a new set of spin-orbitals $\{\psi_p\}$ which will diagonalize the non-canonical Hartree-Fock equations. We define the unitary transformation from the non-canonical orbitals $\{\phi_p\}$ to the new spin-orbitals by

$$|\psi_p\rangle = U_{qp}\,|\phi_q\rangle \iff |\phi_r\rangle = U^*_{pr}\,|\psi_p\rangle\,, \tag{4.18}$$

where U_{qp} is an element in the unitary matrix $\mathbf{U}$. From Lemma 3.1 we know that the new basis set $\{\psi_p\}$ will preserve the orthonormality of the original basis set $\{\phi_q\}$. We construct the Hermitian matrix $\boldsymbol{\Lambda}$ from the Hermitian Lagrange multipliers λ_{ji}. From the Schur decomposition [47] we can write

$$\boldsymbol{\Lambda} = \mathbf{U}\mathbf{E}\mathbf{U}^\dagger, \tag{4.19}$$

where we from the spectral theorem know that the matrix $\mathbf{E} = \mathrm{diag}(\epsilon_1, \dots)$ will be diagonal with the eigenvalues ϵ_m of $\boldsymbol{\Lambda}$ on the diagonal [47]. Using the Kronecker-Delta of rank 3 defined in Equation 3.1, the Schur decomposition of the Lagrange multipliers then take on the form

$$\lambda_{jk} = U_{ji}E_{il}U^*_{kl} = U_{ji}\delta^m_{il}\epsilon_m U^*_{kl} \implies \delta^m_{il}\epsilon_m = U^*_{ji}\lambda_{jk}U_{kl}. \tag{4.20}$$

Transforming from the non-canonical molecular orbitals in Equation 4.17 to the new spin-orbital basis, we get

$$\hat{f}\,|\phi_k\rangle = \lambda_{jk}\,|\phi_j\rangle \implies \hat{f}U^*_{lk}\,|\psi_l\rangle = \lambda_{jk}U^*_{lj}\,|\psi_l\rangle \tag{4.21}$$

$$\implies U^*_{lk}U_{km}\hat{f}\,|\psi_l\rangle = U^*_{lj}\lambda_{jk}U_{km}\,|\psi_l\rangle \implies \delta_{ml}\hat{f}\,|\psi_l\rangle = \delta^n_{lm}\epsilon_n\,|\psi_l\rangle \tag{4.22}$$

$$\implies \hat{f}\,|\psi_m\rangle = \epsilon_m\,|\psi_m\rangle\,, \tag{4.23}$$

where we are left with the *canonical Hartree-Fock equations*, which constitutes an eigenvalue equation. It is worth re-iterating that the equations were found from first order variations in the variational principle and therefore do not guarantee that we have found a minimum. In order to categorize the stationary point we can perform higher order variations to determine if we have found a minimum, saddle point, or a maximum. However, we will not explore higher-order variations any further.

4.1.3 The mean-field approximation

It is worth discussing the Fock operator defined in Equation 4.16 in more detail.

First, if we look at a non-interacting system, that is, $u_{rs}^{pq} = 0$ for all indices, then the canonical Hartree-Fock equations in Equation 4.23 reduce to the time-independent Schrödinger equation for the orbitals. Furthermore, creating a Slater determinant from the spin-orbitals with the lowest eigenenergy yield the ground state of the non-interacting many-body problem.

Moving back to the interacting system we adopt a common notation used from quantum chemistry [3] by introducing the Coulomb operator

$$\hat{J} = \int dx_2 \phi_j^*(x_2)\hat{u}(x, x_2)\phi_j(x_2), \tag{4.24}$$

where we denote the two-body operator $\hat{u}(x_1, x_2)$ with explicit coordinates to describe which coordinates are to be integrated. The matrix elements of the Coulomb operator are given by

$$\langle \phi_i|\hat{J}|\phi_k\rangle = \int dx_1 dx_2 \phi_i^*(x_1)\phi_j^*(x_2)\hat{u}(x_1, x_2)\phi_k(x_1)\phi_j(x_2) \tag{4.25}$$

$$= \langle \phi_i\phi_j|\hat{u}|\phi_k\phi_j\rangle . \tag{4.26}$$

That is, the Coulomb operator is just the two-body elements, but formulated as a single-particle operator as the inner integral is pre-computed. The interpretation of the Coulomb operator is that all single-particle states $\phi_j(x)$ create an average potential which an individual particle will interact with, hence the name "mean-field potential". Now, the second term arising from the antisymmetric two-body elements yield nonlocal effects as it cannot be described as an average potential in the same way as the Coulomb operator. The exchange potential is therefore defined in terms of its action on a spin-orbital $\phi_k(x)$,

$$\hat{K}|\phi_k\rangle = \left[\int dx_2 \phi_j^*(x_2)\hat{u}(x, x_2)\phi_k(x_2)\right] \phi_j(x). \tag{4.27}$$

The exchange operator represents a strong deviation from classical mechanics as the potential experienced by a single-particle state depends on the value of the single-particle state in all of coordinate space. The matrix elements of the exchange operator are given by

$$\langle \phi_i|\hat{K}|\phi_k\rangle = \int dx_1 dx_2 \phi_i^*(x_1)\phi_j^*(x_2)\hat{u}(x_1, x_2)\phi_j(x_1)\phi_k(x_2) \tag{4.28}$$

$$= \langle \phi_i\phi_j|\hat{u}|\phi_j\phi_k\rangle . \tag{4.29}$$

The Fock operator can now be written as

$$\hat{f} = \hat{h} + \hat{J} - \hat{K}, \tag{4.30}$$

where the Coulomb and exchange operators have reduced the two-particle contributions to a single-particle mean-field potential. These terms are the reason why the Hartree-Fock method is called a mean-field approximation. In terms of three-particle interactions, the Hartree-Fock method can be used in a similar fashion where the mean-field approximation now incorporates the three-particle interactions.

4.1.4 Brillouin's theorem

An important result from the canonical Hartree-Fock equations is Brillouin's theorem.

Theorem 4.1. *Let* $\{\phi_p\}$ *be an orthonormal set of single-particle states found by solving the canonical Hartree-Fock equations, and sorted such that the Fock energies* $\epsilon_1 \leqslant \epsilon_2 \leqslant \ldots$*, then building the reference Slater determinant* $|\Phi\rangle$ *from the* N *first single-particle states, we have that*

$$\langle \Phi | \hat{H} | \Phi_i^a \rangle = 0, \tag{4.31}$$

where $|\Phi_i^a\rangle$ *is a singly-excited determinant. The converse is also true.*

This theorem is important because it tells us that all single excitations from the reference state can be neglected if we choose the Hartree-Fock reference state as our reference determinant. Note that the theorem does not hold for arbitrary excitations and neither for single-excitations from an already excited state.

Proof. We prove the converse of Brillouin's theorem directly by evaluating the matrix elements

$$\langle \Phi | \hat{H} | \Phi_i^a \rangle = \langle \phi_i | \hat{h} | \phi_a \rangle + \langle \phi_i \phi_j | \hat{u} | \phi_a \phi_j \rangle_{AS} = \langle \phi_i | \hat{f} | \phi_a \rangle , \tag{4.32}$$

where we have used the Slater-Condon rules from Lemma 3.2 and Lemma 3.3 to evaluate the matrix elements. As the single-particle basis is represented by the molecular orbitals found from solving the canonical Hartree-Fock equations, the Fock matrix is diagonal. This means that

$$\langle \phi_i | \hat{f} | \phi_a \rangle = \varepsilon_a \langle \phi_a | \phi_i \rangle = 0, \tag{4.33}$$

where we have used that the molecular orbitals are orthonormal by construction. Proving the opposite proposition can be done by starting from the canonical Hartree-Fock equations and then using the Slater-Condon rules in reverse to get the original formulation of Brillouin's theorem. □

4.2 Time-dependent Hartree-Fock theory

Time-dependent Hartree-Fock continues with the ansatz that the full many-body wave function $|\Psi(t)\rangle$ is described by a single Slater determinant of N single-particle states, viz.

$$|\Psi(t)\rangle = |\Phi(t)\rangle = |\phi_1(t)\phi_2(t)\dots\phi_N(t)\rangle\,, \tag{4.34}$$

where $\{\phi_p\}$ is a basis of time-dependent molecular orbitals subject to the constraint that they are orthonormal in time. We now use the time-dependent variational principle as discussed in section 2.8 in order to find the equations of motion for the system. The Lagrangian of the system is given by

$$L[\Phi,\Phi^*,\lambda] = \langle\Phi(t)|\Big(i\hbar\partial_t - \hat{H}(t)\Big)|\Phi(t)\rangle - \lambda_{ji}\left(\langle\phi_i(t)|\phi_j(t)\rangle - \delta_{ij}\right), \tag{4.35}$$

where we keep the orthonormality condition in the time-dependent case as well, and we have ignored the explicit time-dependence in the functional arguments to the Lagrangian. The action functional of the time-dependent variational principle is given by

$$S[\Phi,\Phi^*] = \int dt L[\Phi,\Phi^*,\lambda], \tag{4.36}$$

with the stationary condition over the first-order variations found from

$$\delta S = \int dt \delta L[\Phi,\Phi^*,\lambda] = 0 \implies \delta L[\Phi,\Phi^*,\lambda] = 0. \tag{4.37}$$

Computing the expectation value of the Hamiltonian in Equation 4.35 yields the same expression for the reference energy as in subsection 3.7.5, but now with time-dependent operators and molecular orbitals. As the time-derivative is a Hermitian, single-particle operator, we find the expectation value to be

$$\langle\Phi(t)|\partial_t|\Phi(t)\rangle = \langle\phi_i(t)|\partial_t|\phi_i(t)\rangle\,. \tag{4.38}$$

Performing variations over a single molecular orbital at a time we have

$$\tilde{\phi}_i(x,t) = \phi_i(x,t) + \delta_{ik}\epsilon\eta(x,t), \tag{4.39}$$

where again $\epsilon \in \mathbb{R}$ and $\eta(x,t)$ is a complex function. As done in the time-independent case, we will restrict our attention to variations over the complex conjugate of $\phi_i(x,t)$. Variations over $\phi_i(x,t)$ will yield the adjoint equation. The only new term in the variation over the time-dependent Lagrangian from the time-independent case is the variation over the time-derivative. We find

$$\langle\tilde{\Phi}(t)|\partial_t|\Phi(t)\rangle = \langle\phi_i(t)|\partial_t|\phi_i(t)\rangle + \epsilon\langle\eta(t)|\partial_t|\phi_k(t)\rangle\,. \tag{4.40}$$

From the stationary conditions of the action functional we find

$$\delta L[\Phi, \tilde{\Phi}^*, \lambda] = L[\Phi, \tilde{\Phi}^*, \lambda] - L[\Phi, \Phi^*, \lambda] = 0 \tag{4.41}$$

$$\implies i\hbar \langle \eta | \partial_t | \phi_k \rangle - \langle \eta | \hat{f} | \phi_k \rangle = \lambda_{jk} \langle \eta | \phi_j \rangle , \tag{4.42}$$

where we now for the sake of brevity removed the explicit time-dependence of the orbitals and the operators. Furthermore, we jumped straight from the variation of the energy functional to include the Fock-operator. As $\eta(x,t)$ was arbitrary, this must be valid for all choices of $\eta(x,t)$ and we can formulate the stationary condition as

$$i\hbar\partial_t |\phi_k\rangle - \hat{f} |\phi_k\rangle = \lambda_{jk} |\phi_j\rangle . \tag{4.43}$$

Projecting onto $\phi_l(x,t)$ and applying the constraint that the molecular orbitals are orthonormal we find an equation for the Lagrange multipliers,

$$\lambda_{lk} = i\hbar \langle \phi_l | \partial_t | \phi_k \rangle - \langle \phi_l | \hat{f} | \phi_k \rangle . \tag{4.44}$$

We now insert this expression for the Lagrange multipliers back into the stationary condition in Equation 4.43. This yields

$$\hat{P} \left[i\hbar\partial_t |\phi_k\rangle - \hat{f} |\phi_k\rangle \right] = 0, \tag{4.45}$$

where we have now defined the projection operator

$$\hat{P} \equiv \mathbb{1} - |\phi_i\rangle\langle\phi_i| , \tag{4.46}$$

and we see that we have gotten rid of the Lagrange multipliers. Solving for the time-derivative of the molecular orbitals we find

$$i\hbar\hat{P}\partial_t |\phi_k\rangle = \hat{P}\hat{f} |\phi_k\rangle . \tag{4.47}$$

We now define an arbitrary time-dependent, Hermitian operator $\hat{Q}$ in terms of a unitary transformation [16]

$$i\hbar \langle \phi_i | \partial_t | \phi_j \rangle \equiv \langle \phi_i | \hat{Q} | \phi_j \rangle . \tag{4.48}$$

We know that Slater determinants are invariant up to a complex phase under unitary transformations, as seen in Lemma 3.4, this unitary transformation will leave the time-dependent Lagrangian invariant. Since $\hat{Q}$ was an arbitary, Hermitian operator and the Fock operator is Hermitian, we can choose $\hat{Q} = \hat{f}$. Expanding the projection operator and inserting this choice, we get the time-dependent Hartree-Fock equations

$$i\hbar\partial_t |\phi_k(t)\rangle = \hat{f}(t) |\phi_k(t)\rangle , \tag{4.49}$$

where the molecular orbitals stays orthonormal in time.

Chapter 5

Configuration interaction

The most natural approach to take in quantum mechanics when creating a wave function is to create a linear combination of all possible states contained in the space one is exploring. In configuration interaction theory the many-body wave function is written as a linear combination of all possible Slater determinants in the basis of spin-orbitals,

$$|\Psi\rangle = C\,|\Phi\rangle + C_i^a\,|\Phi_i^a\rangle + \frac{1}{4}C_{ij}^{ab}\,|\Phi_{ij}^{ab}\rangle + \dots. \tag{5.1}$$

The factor 4 in the doubles sum is included to avoid overcounting as both the coefficients and the excited determinants are antisymmetric. By including all excited Slater determinants of N-particles, we get a method which is exact within the given space of single-particle states. When this is the case we call the method *full configuration interaction* (FCI) theory. There is however a significant catch to the configuration interaction method, and that is its computational scaling. The number of Slater determinants N_s for a given basis of L spin-orbitals with N occupied particles will grow as [29]

$$N_s = \binom{L}{N}. \tag{5.2}$$

This is such a significant roadblock that the method very quickly becomes completely infeasible for systems of interest. Significant attempts at lowering the cost of configuration interaction has been explored, but the factorial scaling quickly becomes a bottleneck for large systems.

A word on notation, we will in the following refrain from using explicit excitation indices $a, b, \dots$ and $i, j, \dots$ when labelling excited Slater determinants, but rather label the coefficients and the Slater determinants by capital letters $I, J, K, \dots$. That is, we can write Equation 5.1 on the short form

$$|\Psi\rangle = C_I\,|\Phi_I\rangle = C_I\hat{X}_I\,|\Phi\rangle\,. \tag{5.3}$$

The capital indices will then run over the total number of Slater determinants N_s in the full Slater determinant basis.

5.1 Time-independent configuration interaction

We start with the time-independent Schrödinger equation

$$\hat{H}\,|\Psi_J\rangle = E_J\,|\Psi_J\rangle\,, \tag{5.4}$$

where (E_J, Ψ_J) is an eigenpair of $\hat{H}$. Expanding the CI wave function in a Slater determinant basis,

$$|\Psi_J\rangle = C_{KJ}\,|\Phi_K\rangle\,, \tag{5.5}$$

where C_{KJ} are the amplitudes for a certain excitation K for a specific energy level J. Inserting Equation 5.5 into Equation 5.4 and left projecting on a state $|\Phi_I\rangle$ we get

$$\langle\Phi_I|\hat{H}|\Phi_K\rangle\,C_{KJ} = E_J\,\langle\Phi_I|\Phi_K\rangle\,C_{KJ}. \tag{5.6}$$

We denote the matrix elements of the Hamiltonian by

$$H_{IK} = \langle\Phi_I|\hat{H}|\Phi_J\rangle\,. \tag{5.7}$$

The Hamiltonian matrix will have a dimensionality of $\mathbf{H} \in \mathbb{C}^{N_s \times N_s}$. If the underlying basis of spin-orbitals is non-orthogonal, the overlap between the Slater determinants will be given by the determinant of the overlap integrals between the occupied spin-orbitals in both determinants. We denote the overlap between the determinants by

$$S_{IK} = \langle\Phi_I|\Phi_K\rangle\,. \tag{5.8}$$

The overlap matrix will have the same dimensionality as the Hamiltonian, that is, $\mathbf{S} \in \mathbb{C}^{N_s \times N_s}$. We can thus formulate the generalized eigenvalue equation

$$H_{IK}C_{KJ} = E_J S_{IK} C_{KJ} \tag{5.9}$$

$$\implies \mathbf{HC} = \mathbf{ESC}, \tag{5.10}$$

where $\mathbf{E} = \mathrm{diag}(E_1, \ldots, E_{N_s})$. We recognize this generalized eigenvalue equation as the same equation found in the variational method for a trial wave function expanded as a linear combination of an underlying basis shown in subsection 2.4.1. Solving this eigenvalue equation corresponds to a variational minization procedure with Equation 5.10 as the stationary condition. In fact, the configuration interaction method is a direct implementation of the variational method using a linear combination of Slater determinants.

Now, to avoid the cost of storing and computing the overlap matrix $\mathbf{S}$ we restrict ourselves to an orthonormal basis of single-particle functions which

means that $S_{IK} = \delta_{IK}$. If the original atomic orbital basis is non-orthogonal, we can make the basis orthonormal by either transforming to the Hartree-Fock basis or by performing an orthogonalization procedure, for example, symmetric orthogonalization [3, 48]. Thus, in the remainder of this chapter, we restrict ourselves to orthonormal Slater determinants. The generalized eigenvalue equation therefore reduces to the eigenvalue equation

$$\mathbf{HC} = \mathbf{EC}. \tag{5.11}$$

The configuration interaction method can thus be summarized as follows: construct the Hamiltonian matrix $\mathbf{H}$ from the matrix elements H_{IJ}, then diagonalize the matrix to get the coefficients of the eigenstates $\mathbf{C}_I$ and the eigenenergies E_I [49]. As the diagonalization yields the full spectrum, configuration interaction is a method which yields higher-order states unlike methods such as the coupled-cluster method which requires extra steps in order to get anything but the ground state.

5.1.1 Truncated configuration interaction

As discussed in the beginning of this chapter, the full configuration interaction method quickly encounters exponential scaling and becomes intractable. A common technique utilized to lower the cost of the method is to only include Slater determinants based on their excitation. For example, by only including the doubly excited Slater determinants, we can construct the configuration interaction doubles (CID) wave function by

$$|\Psi\rangle = C\,|\Phi\rangle + \frac{1}{4} C_{ij}^{ab}\,|\Phi_{ij}^{ab}\rangle\,, \tag{5.12}$$

which reduces the number of Slater determinants to

$$N_s = 1 + \left\lfloor \frac{N(N-1)(L-N)(L-N-1)}{4} \right\rfloor, \tag{5.13}$$

where the division is floored to the nearest integer. Defining $M = L - N$ as the number of virtual spin-orbitals, the scaling of the number of Slater determinants in the configuration interaction doubles method is given by

$$N_s = \mathcal{O}(N^2 M^2), \tag{5.14}$$

which is a significant decrease in computational complexity. However, due to the truncation of the wave function not only do we decrease the quality of the method in terms of closeness to the exact energy solution given by the full configuration interaction method, we also lose size-extensivity and size-consistency [6, 50].

5.1.2 Size-consistency

The concept of size-consistency is defined as [51]

$$E(AB) = E(A) + E(B), \tag{5.15}$$

where A and B are two systems which do not interact with one another.[1] This tells us that the sum of the energy of the two constituent parts should equal the total energy of the combined system. A similar concept is size-extensivity [10], which is often a consequence of size-consistency. In fact these two concepts tend to be discussed interchangeably [6, 52]. We will limit our attention to the case of size-consistency. We can then write the idealized compound Hamiltonian as

$$\hat{H}_{AB} = \hat{H}_A + \hat{H}_B, \tag{5.16}$$

where it is understood that the second quantized operators in the two subsystems anticommute, that is,

$$\left\{\hat{c}_{p_A}, \hat{c}^\dagger_{q_B}\right\} = 0, \tag{5.17}$$

and that the Hamiltonian of a given subsystem only contain operators for that system. We can now formulate Equation 5.15 from the expectation value of the Hamiltonian by

$$\langle \Psi^{AB} | \hat{H}_{AB} | \Psi^{AB} \rangle = \langle \Psi^A | \hat{H}_A | \Psi^A \rangle + \langle \Psi^B | \hat{H}_B | \Psi^B \rangle , \tag{5.18}$$

where we assume that both the compound wave function $|\Psi^{AB}\rangle$ and the wave functions of each subsystem $|\Psi^A\rangle$ and $|\Psi^B\rangle$ are normalized. Furthermore, we assume that the energy of the specific systems is given by

$$E(A) = \langle \Psi^A | \hat{H}_A | \Psi^A \rangle , \tag{5.19}$$

for both the systems. We can thus formulate the requirements necessary for a size-consistent method: the energy must be *additively separable*, viz. Equation 5.15; the wave function must be *multiplicately separable* [6]. The latter requirement is formulated by

$$|\Psi^{AB}\rangle = |\Psi^A\rangle \, |\Psi^B\rangle , \tag{5.20}$$

where the product of the two states is understood as each state acting on a subsystem. This last requirement is enough to demonstrate that truncated

[1] Note that the particles in system A and system B internally can include interations. There is just no interaction between the particles in system A with particles in system B, and vice versa.

configuration interaction is *not size-consistent* [6]. Consider the truncated doubles wave function

$$|\Psi\rangle = \left(\mathbb{1} + \hat{C}\right) |\Phi\rangle \,, \tag{5.21}$$

where we have assumed intermediate normalization of the wave function and we have denoted the doubles operator by

$$\hat{C} \equiv \frac{1}{4} C_{ij}^{ab} \hat{X}_{ij}^{ab}, \tag{5.22}$$

for the sake of brevity. Now, looking at the right-hand side of Equation 5.20 we get

$$\begin{aligned} |\Psi^A\rangle \, |\Psi^B\rangle &= \left(\mathbb{1}^A + \hat{C}^A\right) |\Phi^A\rangle \left(\mathbb{1}^B + \hat{C}^B\right) |\Phi^B\rangle & (5.23) \\ &= |\Phi^A\rangle \, |\Phi^B\rangle \pm |\Phi^A\rangle \, \hat{C}^B \, |\Phi^B\rangle + \hat{C}^A \, |\Phi^A\rangle \, |\Phi^B\rangle \\ &\quad \pm \hat{C}^A \, |\Phi^A\rangle \, \hat{C}^B \, |\Phi^B\rangle \,, & (5.24) \end{aligned}$$

where we repeat that the second quantized operators of the two subsystems anticommute and we have included a possible sign change due to an odd number of particles in subsystem A and hence an odd number of creation operators in this determinant. What is important to note in the last equation is that the last term consists of a *quadruply* excited state as both determinants in each subsystem are excited at the same time. For the left-hand side of Equation 5.20 we have that the doubles wave function for the combined subsystem is restricted to

$$\begin{aligned} |\Psi^{AB}\rangle &= \left(\mathbb{1}^{AB} + \hat{C}^{AB}\right) |\Phi^{AB}\rangle = |\Phi^A\rangle \, |\Phi^B\rangle + \left(\hat{C}^A + \hat{C}^B\right) |\Phi^A\rangle \, |\Phi^B\rangle & (5.25) \\ &= |\Phi^A\rangle \, |\Phi^B\rangle + \hat{C}^A \, |\Phi^A\rangle \, |\Phi^B\rangle \pm |\Phi^A\rangle \, \hat{C}^B \, |\Phi^B\rangle \,, & (5.26) \end{aligned}$$

where we have used that the compound doubles excitation operator can at most be a sum of doubles operators for each subsystem. We note that the left-hand side of Equation 5.20 lacks the expected quadruples excitation coming from the doubles excitation of both subsystems at the same time. This situation extends beyond the doubles excitations [52], and we conclude that truncated configuration interaction is not size-consistent. However, if we use a full configuration interaction ansatz corresponding to a full excitation of the combined system, we then recover size consistency as both sides of Equation 5.20 will be fully excited.

5.2 Time-dependent configuration interaction

Starting from the time-dependent Schrödinger equation, we can formulate the time evolution of the configuration interaction wave function as

$$i\hbar \frac{d}{dt} |\Psi(t)\rangle = \hat{H}(t) |\Psi(t)\rangle , \tag{5.27}$$

Here the time-dependent wave function $|\Psi(t)\rangle$ is expanded as a linear combination of a finite number of Slater determinants

$$|\Psi(t)\rangle = c_I(t) |\Phi_I\rangle , \tag{5.28}$$

where the orbitals in the Slater determinants are time-independent. Our choice of initial state $|\Psi(0)\rangle$ is to a large degree arbitrary as long as the coefficients are normalized and the determinants span the entire space we are looking at. For example, we can choose a single Slater determinant from our basis of determinants as an initial guess. In this thesis we will choose $|\Psi(0)\rangle = |\Psi_J\rangle$, where $|\Psi_J\rangle$ is an eigenstate from the time-independent Schrödinger equation in Equation 5.4. Specifically we will choose the ground state as our initial state, that is, $J = 0$. This corresponds to the first column in the coefficient matrix $\mathbf{C} \in \mathbb{C}^{N_s \times N_s}$ in the diagonalization of the Hamiltonian matrix. The coefficient vector is then $\mathbf{c} \in \mathbb{C}^{N_s}$.

Inserting Equation 5.28 into the time-dependent Schrödinger equation we get an equation for the time evolution of the coefficients,

$$i\hbar \frac{d}{dt} c_J(t) |\Phi_J\rangle = \hat{H}(t) c_J(t) |\Phi_J\rangle . \tag{5.29}$$

Left-projecting with a Slater determinant $|\Phi_I\rangle$ then yields

$$i\hbar \frac{d}{dt} c_J(t) = H_{IJ}(t) c_J(t), \tag{5.30}$$

where we have used that the Slater determinants are orthonormal. The matrix elements of the time-dependent Hamiltonian is denoted by $H_{IJ}(t)$. As the initial coefficients $\mathbf{c}(0)$ are known, we need to compute the matrix elements of the time-dependent Hamiltonian at each time step before using a time evolution scheme to solve Equation 5.30.

Chapter 6

Coupled-cluster theory

In the previous chapter on the configuration interaction method we saw how the direct diagonalization of the full Slater determinant space led to an exponential scaling in the number of determinants. In chapter 4 we demonstrated an approximation to the full many-body wave function using a single Slater determinant. The Hartree-Fock and the full configuration interaction methods therefore serve as endpoints to the approximations that can be done for the exact many-body wave function. The former is too simple, whereas the latter proves too challenging. The latter does open up for further approximations by truncating the Slater determinant space, but this leads to a size-inconsistent model which scales badly once we increase the number of particles.

In lieu of these considerations, the coupled-cluster method provides an approximation to the exact many-body wave function by an exponential ansatz. This method provides higher-order correlations beyond the single determinant approximation given in the Hartree-Fock method, and maintains a polynomial scaling for the Slater determinant basis if the cluster operators are truncated. In the untruncated limit the coupled-cluster method recovers the full configuration interaction method. We shall also see how the truncated coupled-cluster method is size-consistent.

6.1 Time-independent coupled-cluster theory

The coupled-cluster method seeks to find a many-body wave function $|\Psi\rangle$ which solves the time-independent Schrödinger equation. Starting from a single reference Slater determinant $|\Phi\rangle$ built from an orthonormal basis of single-particle states[1] coupled-cluster makes the ansatz that the true many-

[1]We often use orthonormal molecular orbitals from the Hartree-Fock minimization procedure as our basis. This is the reason why coupled-cluster is often called a *post Hartree-Fock*

body wave function can be approximated by the exponential ansatz

$$|\Psi\rangle \equiv \exp(\hat{T})\,|\Phi\rangle = \sum_{n=0}^{\infty} \frac{1}{n!}\hat{T}^n\,|\Phi\rangle\,, \tag{6.1}$$

where the *cluster operator* $\hat{T}$ is given by a sum of excitation operators $\hat{X}_\mu$ and cluster amplitudes τ_μ

$$\hat{T} = \sum_{\mu=1}^{\infty} \hat{X}_\mu \tau_\mu = \tau_i^a \hat{c}_a^\dagger \hat{c}_i + \left(\frac{1}{2!}\right)^2 \tau_{ij}^{ab} \hat{c}_a^\dagger \hat{c}_b^\dagger \hat{c}_i \hat{c}_j + \ldots. \tag{6.2}$$

Here the cluster amplitudes are the primary unknowns. Due to the anti-symmetric properties of the excitation operators, the cluster amplitudes will also be antisymmetric with respect to the exchange of two virtual-virtual or occupied-occupied indices as seen in Equation 3.107. Furthermore, the cluster amplitudes commute with one another as the creation and annihilation operators run over non-overlapping sets of indices. Note that interchange of indices from upper to lower, or vice-versa, are not permitted. By inserting Equation 6.1 into the time-independent Schrödinger equation we get

$$\hat{H}\,|\Psi\rangle = \exp(\hat{T})\,|\Phi\rangle = E\exp(\hat{T})\,|\Phi\rangle = E\,|\Psi\rangle\,. \tag{6.3}$$

Projecting onto the reference Slater determinant we are left with

$$\langle\Phi|\hat{H}|\Psi\rangle = E\,\langle\Phi|\exp(\hat{T})|\Phi\rangle = E, \tag{6.4}$$

where the coupled-cluster wave function assumes *intermediate normalization*, viz.

$$\langle\Phi|\Psi\rangle = \langle\Phi|\left(\mathbb{1} + \hat{T} + \frac{1}{2!}\hat{T}^2 + \ldots\right)|\Phi\rangle = 1. \tag{6.5}$$

Using the same projection technique as for the energy equation, we can obtain expressions for the cluster amplitudes. All we have to do is project onto an excited reference state, where the order of the excitation decides which order of the amplitudes we are solving for. That is,

$$\langle\Phi_\mu|\hat{H}\exp(\hat{T})|\Phi\rangle = E\,\langle\Phi_\mu|\exp(\hat{T})|\Phi\rangle\,. \tag{6.6}$$

Here the excitation order μ decides which amplitudes we are solving for, e.g., for the doubles cluster amplitudes τ_{ij}^{ab} we project onto the doubly excited reference state $|\Phi_{ij}^{ab}\rangle$. These equations are non-linear due to the presence of the exponential function creating cross terms with other excited amplitudes.

method.

Furthermore, if we don't truncate the cluster operator $\hat{T}$ we recover the exact wave function as in the full configuration interaction method [7, 53].

By expanding the exponential cluster operator in a power series, as in Equation 6.1, and inserting it into Equation 6.4 we get

$$\langle \Phi | \hat{H} | \Psi \rangle = \langle \Phi | \hat{H} \sum_{n=0}^{\infty} \frac{1}{n!} \hat{T}^n | \Phi \rangle = E. \tag{6.7}$$

Depending on the form of the Hamiltonian, we will get a natural truncation of the cluster operators. A single cluster operator is at least a singles excitation operator and a cluster operator raised to the power of n will at least excite n particles from the reference state. We restrict ourselves to at most two-body interactions in the Hamiltonian and we are therefore at most able to relax two particles from an excited state. As we are projecting onto the reference state the Hamiltonian is forced to relax the excitation done by the cluster operators in order to get a non-zero contribution. Thus, for a Hamiltonian with at most two-body operators the exponential power series truncates at $n = 2$ for the cluster operators. That is

$$\langle \Phi | \hat{H} | \Psi \rangle = \langle \Phi | \hat{H} | \Phi \rangle + \langle \Phi | \hat{H} \hat{T} | \Phi \rangle + \frac{1}{2!} \langle \Phi | \hat{H} \hat{T}^2 | \Phi \rangle = E. \tag{6.8}$$

Note that this result is general irrespective of the truncation level chosen for the cluster operators themselves. This means that all cluster operators higher than doubles excitations will only contribute indirectly to the energy calculation via the singles and doubles amplitudes.

6.1.1 Rewriting the coupled-cluster equations

In order to get amiable equations for the coupled-cluster energy and amplitudes, we left multiply the Hamiltonian by the inverse of the exponential cluster operator. We then get the equations

$$\langle \Phi | \exp(-\hat{T}) \hat{H} \exp(\hat{T}) | \Phi \rangle = E, \tag{6.9}$$

$$\langle \Phi_\mu | \exp(-\hat{T}) \hat{H} \exp(\hat{T}) | \Phi \rangle = 0. \tag{6.10}$$

Even though Equation 6.4 and Equation 6.6 are formally correct, they are not tractable for numerical implementation, unlike Equation 6.9 and Equation 6.10 [50]. Furthermore, the amplitude equations are now decoupled from the energy equation, which will ensure size-extensivity. By applying the Baker-Campbell-Hausdorff formula we get

$$\bar{H} = \exp(-\hat{T}) \hat{H} \exp(\hat{T}) = \hat{H} + \left[\hat{H}, \hat{T} \right] + \frac{1}{2!} \left[\left[\hat{H}, \hat{T} \right], \hat{T} \right] + \ldots. \tag{6.11}$$

We refer to $\bar{H}$ as the *similarity transformed Hamiltonian*. We now introduce the normal-ordered Hamiltonian $\hat{H}_N$ as defined in subsection 3.7.6 with the reference energy from subsection 3.7.5. As the reference energy is just a number, the similarity transformed normal-ordered Hamiltonian takes on the form

$$\bar{H}_N = \exp(-\hat{T})\hat{H}_N \exp(\hat{T}) = \exp(-\hat{T})\hat{H} \exp(\hat{T}) - \langle\Phi|\hat{H}|\Phi\rangle = \bar{H} - E_0. \quad (6.12)$$

If the reference state is the Hartree-Fock state[2] all energy contributions beyond the reference energy are known as contributions to the *correlation energy*. Next, we apply the Baker-Campbell-Hausdorff formula to Equation 6.12 and use the generalized Wick's theorem to contract the Hamiltonian and the cluster operators. The only nonzero terms in this expansion are the terms containing at least one contraction between the normal-ordered Hamiltonian and every cluster operator to their right. This is called the "connected cluster" theorem, and it yields a natural truncation of the Baker-Campbell-Hausdorff expansion [10, 50]. For a Hamiltonian with at most two-body interactions the expansion contains at most four cluster operators to the right of the Hamiltonian,

$$\bar{H}_N = \left[\hat{H}_N + \hat{H}_N\hat{T} + \frac{1}{2!}\hat{H}_N\hat{T}^2 + \frac{1}{3!}\hat{H}_N\hat{T}^3 + \frac{1}{4!}\hat{H}_N\hat{T}^4\right]_c. \quad (6.13)$$

Here the subscript c means that we only include the terms that are connected, i.e., that the Hamiltonian has at least one contraction with every cluster operator to its right. Note that the connected cluster theorem is a statement about the similarity transformed normal-ordered Hamiltonian. It is therefore applicable to the amplitude equations as well [50].

6.1.2 Energy equations

We are now ready to generate equations for the energy of the many-body system using the coupled-cluster method. We do this by computing

$$E = \langle\Phi|\exp(-\hat{T})\hat{H} \exp(\hat{T})|\Phi\rangle = \langle\Phi|\bar{H}_N|\Phi\rangle + \langle\Phi|\hat{H}|\Phi\rangle\,. \quad (6.14)$$

Having already found an expression for the reference energy from subsection 3.7.5, our job is now to compute the expectation value of the similarity transformed normal-ordered Hamiltonian, or more concisely, the coupled-cluster correlation energy. We now insert the expression for the Hamiltonian from Equation 6.13 into Equation 6.14. The first term is the expectation value of the normal-ordered Hamiltonian which is zero by construction, viz.

$$\langle\Phi|\hat{H}_N|\Phi\rangle = 0. \quad (6.15)$$

[2]The reference state is more or less always the Hartree-Fock state in quantum chemistry computations.

From Equation 6.8 we know that all higher powers of the cluster operator than 2 will annihilate the overlap. If we assume that the cluster operators contain at least the singles and doubles cluster operators, that is,

$$\hat{T} = \hat{T}_1 + \hat{T}_2 + \dots, \tag{6.16}$$

we get the energy contributions

$$\langle \Phi | \left[\hat{H}_N \hat{T} \right]_c | \Phi \rangle = f_a^i \tau_i^a + \frac{1}{4} u_{ab}^{ij} \tau_{ij}^{ab}, \tag{6.17}$$

for the lone cluster operator, whereas the squared operator yields

$$\frac{1}{2!} \langle \Phi | \left[\hat{H}_N \hat{T}^2 \right]_c | \Phi \rangle = \frac{1}{2} u_{ab}^{ij} \tau_i^a \tau_j^b. \tag{6.18}$$

For a complete derivation of these expressions see section B.1. Including the reference energy, the total energy equation in the coupled-cluster method is given by

$$E = \langle \Phi | \bar{H} | \Phi \rangle = f_i^i - \frac{1}{2} u_{ij}^{ij} + f_a^i \tau_i^a + \frac{1}{2} u_{ab}^{ij} \left[\frac{1}{2} \tau_{ij}^{ab} + \tau_i^a \tau_j^b \right]. \tag{6.19}$$

Depending on the truncation level of the cluster operators, we can adjust the energy expression in Equation 6.19. For example, in the coupled-cluster doubles (CCD) approximation, we get the energy equation

$$E = \langle \Phi | \exp(-\hat{T}_2) \hat{H} \exp(\hat{T}_2) | \Phi \rangle = f_i^i - \frac{1}{2} u_{ij}^{ij} + \frac{1}{4} u_{ab}^{ij} \tau_{ij}^{ab}. \tag{6.20}$$

As already mentioned, only the reference, singly and doubly excited states contribute to the final energy expression. All higher excitations couple to the energy, but only indirectly through the singles and doubles amplitudes.

6.1.3 Amplitude equations

Using Equation 6.10 and Wick's theorem we find a set of non-linear equations which we solve iteratively to construct the coupled-cluster amplitudes. Unlike the energy equations in Equation 6.9, we are no longer projecting onto the reference state. This means that in addition to the similarity transformed Hamiltonian, we get an extra set of normal-ordered creation and annihilation operators from the excited state we are projecting onto. This seemingly benign inclusion of pairs of operators leads to a significant increase in the number of terms arising from Wick's theorem and can quickly lead to long and winded computations prone to much error. There are several ways to attack this problem, either by direct computation using Wick's theorem [50]

or the more elegant solution of using diagrams [10, 50]. The task at hand is to evaluate the equations

$$\langle \Phi_\mu | \bar{H} | \Phi \rangle = \langle \Phi_\mu | \bar{H}_N | \Phi \rangle = \langle \Phi | \hat{X}_\mu^\dagger \bar{H}_N | \Phi \rangle = 0, \tag{6.21}$$

where we are left with the normal-ordered similarity transformed Hamiltonian as the overlap between the excited state and the reference state is zero. Furthermore, we have expressed the excited determinant via the relaxation operator from Definition 3.6. As the operator $\hat{X}_\mu^\dagger$ relaxes the incoming state from the right by an order μ we need only keep terms from the normal-ordered similarity transformed Hamiltonian that leaves the reference state excited at μ. We will therefore look for terms in Equation 6.13 that yield

$$\bar{H}_N |\Phi\rangle \propto |\Phi_\mu\rangle , \tag{6.22}$$

as all other terms will vanish. For each set of amplitudes we get a corresponding set of amplitude equations. As an example, for the coupled-cluster singles and doubles (CCSD) method we get the pair of amplitude equations

$$\langle \Phi_i^a | \bar{H}_N | \Phi \rangle = \langle \Phi | (\hat{X}_i^a)^\dagger \bar{H}_N | \Phi \rangle = 0, \tag{6.23}$$

$$\langle \Phi_{ij}^{ab} | \bar{H}_N | \Phi \rangle = \langle \Phi | (\hat{X}_{ij}^{ab})^\dagger \bar{H}_N | \Phi \rangle = 0. \tag{6.24}$$

We will describe both the process of finding amplitude equations and how we can solve these equations in section 9.3.

6.1.4 Size-consistency

Having discussed the lack of size-consistency in the truncated configuration interaction method in subsection 5.1.2, we now turn our attention to the exponential ansatz used in the coupled-cluster method. We assume that the Hamiltonian is additively separable as in Equation 5.16, and that the second quantized operators for the two subsystems A and B anticommute with one another. We now need to demonstrate that the compound coupled-cluster wave function $|\Psi^{AB}\rangle$ is multiplicately separable as in Equation 5.20 in order for the method to be size-consistent [6]. Now, as the cluster operators in the exponential ansatz consist of excitation operators – which we from subsection 3.6.3 know to anticommute – we have that

$$\left[\hat{T}_A, \hat{T}_B \right] = 0. \tag{6.25}$$

Furthermore, this extends to the cluster operator in subsystem A commuting with any other second quantized operator in subsystem B due to there being

an even number of anticommutation. The compound wave function can now be found to be

$$|\Psi^{AB}\rangle = \exp(\hat{T}^{AB})\,|\Phi^{AB}\rangle = \exp(\hat{T}^{A})\exp(\hat{T}^{B})\,|\Phi^{A}\rangle\;|\Phi^{B}\rangle \tag{6.26}$$

$$= \exp(\hat{T}^{A})\,|\Phi^{A}\rangle\exp(\hat{T}^{B})\,|\Phi^{B}\rangle = |\Psi^{A}\rangle\;|\Psi^{B}\rangle\,. \tag{6.27}$$

The size-consistent property is retained for all exponential wave function ansatzes due to the separability of the exponential operator [6, 52].

6.1.5 Non-variational coupled-cluster

From the postulates of quantum mechanics we know that every physical observable q is described by a Hermitian operator $\hat{Q}$ acting on the Hilbert space of state vectors. Having defined the coupled-cluster wave function $|\Psi\rangle$ by

$$|\Psi\rangle = \exp(\hat{T})\,|\Phi\rangle\,, \tag{6.28}$$

we would expect to be able to construct a solution to the amplitudes by virtue of the variational principle. That is, by requiring that the amplitudes minimize the functional

$$E[\Psi,\Psi_*] = \frac{\langle\Psi|\hat{H}|\Psi\rangle}{\langle\Psi|\Psi\rangle} = \frac{\langle\Phi|(\exp(\hat{T}))^{\dagger}\hat{H}\exp(\hat{T})|\Phi\rangle}{\langle\Phi|(\exp(\hat{T}))^{\dagger}\exp(\hat{T})|\Phi\rangle}. \tag{6.29}$$

However, there are some serious limitations in Equation 6.29. By computing the series expansion of the exponential operators we find

$$\langle\Phi|(\exp(\hat{T}))^{\dagger}\hat{H}\exp(\hat{T})|\Phi\rangle = \langle\Phi|\Big(\mathbb{1}+\hat{T}^{\dagger}+\ldots\Big)\,\hat{H}\,\Big(\mathbb{1}+\hat{T}+\ldots\Big)|\Phi\rangle\,, \tag{6.30}$$

where the relaxation operators on the left will act as excitation operators on the reference state we are projecting onto. This means that we no longer get a natural truncation with respect to the Hamiltonian [50].

6.1.6 The coupled-cluster Lagrangian

Even though we conclude that the non-variational formulation of the coupled-cluster method yields an exact solution in the untruncated limit, and is accurate enough in the truncated limit that the lack of a bounded energy is not a large problem, we will get problems when looking at other properties than the energy as the conditions for the Hellmann-Feynman theorem are not met [6]. There have been attempts at computing observable quantities by using the variational expectation value for the operator in question [54, 55]

$$\langle O\rangle = \frac{\langle\Psi|\hat{O}|\Psi\rangle}{\langle\Psi|\Psi\rangle} = \frac{\langle\Phi|(\exp(\hat{T}))^{\dagger}\hat{O}\exp(\hat{T})|\Phi\rangle}{\langle\Phi|(\exp(\hat{T}))^{\dagger}\exp(\hat{T})|\Phi\rangle}, \tag{6.31}$$

but as $|\Psi\rangle$ is not found from optimization of the energy using the variational principle in Equation 6.29, we do not necessarily have that the energy found from the variational principle is the same as the energy found from the projected energy equation [15]. Replacing the Hamiltonian in Equation 6.9 with the operator of the observable in question, we do get an expression for the observable. However, we return to the problem of computing first-order properties being a cumbersome problem as the Hellmann-Feynman theorem is still not satisfied [6, 15].

In order for us to conform to the Hellmann-Feynman theorem, we can use a technique where we construct a variational Lagrangian [6, 56]. To motivate the need for a variational Lagrangian, we consider the coupled-cluster energy expression subject to a small perturbation g [53]

$$E(g, \boldsymbol{\tau}) = \langle \Phi | \exp(-\hat{T}(g)) \hat{H}(g) \exp(\hat{T}(g)) | \Phi \rangle , \tag{6.32}$$

where μ denotes an excitation level and $\boldsymbol{\tau}$ is the set of all cluster amplitudes. We also note that as the perturbation is represented on a grid, we will in the second quantized formulation absorb the pertubation in the matrix elements of the wave function instead of the wave function itself [6]. The expansion of the operators will then become [53]

$$\hat{H}(g) = \hat{H} + g\hat{H}^{(1)} + g^2\hat{H}^{(2)} + \ldots, \tag{6.33}$$

$$\hat{T}(g) = \hat{T} + g\hat{T}^{(1)} + g^2\hat{T}^{(2)} + \ldots. \tag{6.34}$$

We find the optimized energy of Equation 6.32 by

$$E(g) = E(g, \boldsymbol{\tau}^*), \tag{6.35}$$

where $\boldsymbol{\tau}^*$ for a given g represents the solution to the set of amplitude equations

$$f_\mu(g, \boldsymbol{\tau}_*) = \langle \Phi_\mu | \exp(-\hat{T}(g)) \hat{H}(g) \exp(\hat{T}(g)) | \Phi \rangle \Big|_{\boldsymbol{\tau}=\boldsymbol{\tau}^*} = 0, \tag{6.36}$$

for all excitations μ. Now, if the coupled-cluster wave function was indeed variational, this condition corresponds to finding the stationary points of the coupled-cluster energy by

$$\left. \frac{\partial E(g, \boldsymbol{\tau})}{\partial \tau_\mu} \right|_{\boldsymbol{\tau}=\boldsymbol{\tau}^*} = 0, \tag{6.37}$$

for every g. In order to satisty Equation 6.37 and the Hellmann-Feynman theorem we use Lagrange's method of undetermined multipliers to introduce a new set of parameters $\boldsymbol{\lambda}$, one for every cluster amplitude [6]. We incorporate the original energy function in Equation 6.32 into a Lagrangian with the set

of amplitude equations in Equation 6.36 multiplied with the multipliers. That is,

$$L(g, \boldsymbol{\tau}, \boldsymbol{\lambda}) = \langle \Phi | (\mathbb{1} + \hat{\Lambda}) \exp(-\hat{T}(g)) \hat{H}(g) \exp(\hat{T}(g)) | \Phi \rangle , \tag{6.38}$$

where we have introduced the relaxation operator $\hat{\Lambda}$ from the Lagrange multipliers along with the string of relaxation operators from the excited state $|\Phi_\mu\rangle$ we project onto in the amplitude equations. That is,

$$\hat{\Lambda} \equiv \lambda_\mu \hat{X}_\mu^\dagger = \lambda_a^i \hat{c}_i^\dagger \hat{c}_a + \frac{1}{4} \lambda_{ab}^{ij} \hat{c}_i^\dagger \hat{c}_a \hat{c}_j^\dagger \hat{c}_b + \cdots \equiv \hat{\Lambda}_1 + \hat{\Lambda}_2 + \ldots , \tag{6.39}$$

with the truncation level μ matching the truncation of the cluster operators $\hat{T}$. Optimizing Equation 6.38 with respect to the parameters $\boldsymbol{\tau}$ and $\boldsymbol{\lambda}$ we get equations which let us find the stationary points $\boldsymbol{\tau}^*$ and $\boldsymbol{\lambda}^*$,

$$\frac{\partial L(g, \boldsymbol{\tau}, \boldsymbol{\lambda})}{\partial \lambda_\mu} = \langle \Phi_\mu | \exp(-\hat{T}(g)) \hat{H}(g) \exp(\hat{T}(g)) | \Phi \rangle = 0, \tag{6.40}$$

$$\frac{\partial L(g, \boldsymbol{\tau}, \boldsymbol{\lambda})}{\partial \tau_\mu} = \langle \Phi | (\mathbb{1} + \hat{\Lambda}) \exp(-\hat{T}(g)) \left[\hat{H}(g), \hat{X}_\mu \right] \exp(\hat{T}(g)) | \Phi \rangle = 0, \tag{6.41}$$

where we note that the first equation in the absence of the perturbation corresponds to the projected amplitude equations in Equation 6.10. The second equation yields the solution to the Lagrange multipliers. This equation is slightly more involved as the extra set of amplitudes generates an increased amount of contractions to be solved. We can use Wick's generalized theorem in order to find equations for the Lagrange multipliers. In the abscence of the perturbation we write the coupled-cluster Lagrangian as

$$L(\boldsymbol{\tau}, \boldsymbol{\lambda}) = \langle \Phi | (\mathbb{1} + \hat{\Lambda}) \exp(-\hat{T}) \hat{H} \exp(\hat{T}) | \Phi \rangle \equiv \langle \tilde{\Psi} | \hat{H} | \Psi \rangle = E(\boldsymbol{\tau}, \boldsymbol{\lambda}), \tag{6.42}$$

which we interpret as the variational coupled-cluster energy function. Here we have denoted the right- and left-hand coupled-cluster wave functions by

$$|\Psi\rangle = \exp(\hat{T}) |\Phi\rangle , \tag{6.43}$$

$$\langle \tilde{\Psi}| = \langle \Phi | (\mathbb{1} + \hat{\Lambda}) \exp(-\hat{T}). \tag{6.44}$$

The stationary points of the cluster amplitudes and the Lagrange multipliers are then

$$\frac{\partial L(\boldsymbol{\tau}, \boldsymbol{\lambda})}{\partial \lambda_\mu} = \langle \Phi_\mu | \exp(-\hat{T}) \hat{H} \exp(\hat{T}) | \Phi \rangle = 0, \tag{6.45}$$

$$\frac{\partial L(\boldsymbol{\tau}, \boldsymbol{\lambda})}{\partial \tau_\mu} = \langle \Phi | (\mathbb{1} + \hat{\Lambda}) \exp(-\hat{T}) \left[\hat{H}, \hat{X}_\mu \right] \exp(\hat{T}) | \Phi \rangle = 0. \tag{6.46}$$

The introduction of the coupled-cluster wave functions in Equation 6.43 and Equation 6.44 motivates the coupled-cluster density operator [15]

$$\hat{\rho} = |\Psi\rangle\langle\tilde{\Psi}| = e^{\hat{T}}\,|\Phi\rangle\langle\Phi|\left(\mathbb{1}+\hat{\Lambda}\right)e^{\hat{T}}. \tag{6.47}$$

Using this definition for the coupled-cluster density operator we have that

$$\mathrm{tr}(\hat{\rho}) = \mathrm{tr}\Big\{\,|\Psi\rangle\langle\tilde{\Psi}|\,\Big\} = \langle\tilde{\Psi}|\Psi\rangle\;\langle\tilde{\Psi}|\Psi\rangle = 1, \tag{6.48}$$

which shows that the probabilities sum up to unity. To see this, observe that the exponentiated cluster operators cancel each other and the $\hat{\Lambda}$-operator destroys the reference. We are thus left left with the overlap between the normalized reference states. Furthermore, we see that

$$\hat{\rho}^2 = \hat{\rho}\hat{\rho} = |\Psi\rangle\;\langle\tilde{\Psi}|\Psi\rangle\;\langle\tilde{\Psi}| = |\Psi\rangle\langle\tilde{\Psi}| = \hat{\rho}, \tag{6.49}$$

making the density operator idempotent. This also means that the coupled-cluster wave function is a pure state wave function. However, not surprisingly, we have that

$$\hat{\rho} \neq \hat{\rho}^{\dagger}. \tag{6.50}$$

The observation that the coupled-cluster ansatz with the Lagrange multipliers describe a pure, non-Hermitian, state leads to the interpretation of the coupled-cluster wave function using the *bi-variational principle* [14, 15, 57, 58] We will expand on this notion when we discuss the orbital-adaptive time-dependent coupled-cluster method later.

6.1.7 Density matrices

The variational energy function in Equation 6.42 can be written in terms of the one- and two-body density matrices,

$$E = \langle\tilde{\Psi}|\hat{H}|\Psi\rangle = h^p_q\,\langle\tilde{\Psi}|\hat{c}^\dagger_p\hat{c}_q|\Psi\rangle + \frac{1}{4}u^{pq}_{rs}\,\langle\tilde{\Psi}|\hat{c}^\dagger_p\hat{c}^\dagger_q\hat{c}_s\hat{c}_r|\Psi\rangle \tag{6.51}$$

$$= h^p_q\rho^q_p + \frac{1}{4}u^{pq}_{rs}\rho^{rs}_{pq}, \tag{6.52}$$

where the density matrices are treated as first-order properties of the energy function. Defining the coupled-cluster one- and two-body density matrices by

$$\rho^q_p \equiv \langle\tilde{\Psi}|\hat{c}^\dagger_p\hat{c}_q|\Psi\rangle\,, \tag{6.53}$$

$$\rho^{rs}_{pq} \equiv \langle\tilde{\Psi}|\hat{c}^\dagger_p\hat{c}^\dagger_q\hat{c}_s\hat{c}_r|\Psi\rangle\,, \tag{6.54}$$

we recognize the ability to compute expectation values of one- and two-body operators from section 3.8. As the cluster amplitudes are now found using a variational technique, these expectation values will conform to the Hellmann-Feynman theorem.

6.1.8 The non-orthogonal coupled-cluster method

Including explicit orbital rotations in the coupled-cluster Lagrangian is a technique to make the coupled-cluster method gauge invariant [59, 60] and have it satisfy Ehrenfest's theorem [21]. There exists several methods that include orbital rotations in the coupled-cluster formalism, such as, the orbital optimized coupled cluster method, and the Brueckner coupled-cluster method. These methods do suffer from certain defects, where the former does not converge to the full configuration interaction method in the untruncated limit, and the latter yields unphysical results in the second order poles in the response function [21]. However, the method we will discuss is the non-orthogonal coupled cluster method [60] in which we relax the requirement that the orbital transformations should be unitary [21]. This method has been demonstrated to converge to the full configuration interaction method in the untruncated limit [21]. This yields biorthogonal orbitals leading to a bi-variational Lagrangian [15] in a formulation resembling that of Arponen [57].

In the non-orthogonal method we introduce a singles operators $\hat{\kappa}$ given by

$$\hat{\kappa} = \kappa_{pq} \hat{a}_p^\dagger \hat{\tilde{a}}_q, \tag{6.55}$$

where $\hat{a}_p^\dagger$ and $\hat{\tilde{a}}_p$ are creation and annihilation operators two biorthogonal Hilbert spaces. They are defined in terms of the original static creation and annihilation operators via the transformation [6, 21]

$$\hat{a}_p^\dagger = \exp(-\hat{\kappa}) \hat{c}_p^\dagger \exp(\hat{\kappa}), \tag{6.56}$$

$$\hat{\tilde{a}}_p = \exp(-\hat{\kappa}) \hat{c}_p \exp(\hat{\kappa}). \tag{6.57}$$

The approach taken in the orthogonal coupled-cluster method is to require that $\hat{\kappa}$ is antihermitian as this yields unitary transformations for the new creation and annihilation operators, and we have that the operators are the adjoint of one another. However, in the non-orthogonal coupled-cluster method, $\hat{\kappa}$ is no longer antihermitian and we have in general

$$\hat{\tilde{a}}_p^\dagger \neq \hat{a}_p^\dagger, \tag{6.58}$$

as can be seen by taking the Hermitian conjugate of Equation 6.56 and see that this is not the same as Equation 6.57 due to $\hat{\kappa}$ not being antihermitian. Luckily even though the operators not being Hermitian conjugates of one another, they still retain their anticommutation relation [58, 61]

$$\left\{ \hat{\tilde{a}}_p, \hat{a}_q^\dagger \right\} = \delta_{pq}, \tag{6.59}$$

and we can still utilize Wick's theorem [14, 21], as long as the original atomic orbital basis is orthonormal. From the orthogonal coupled-cluster method we have that $\kappa_{aa} = \kappa_{ii} = 0$ which lets us separate the orbital rotation operator into two blocks. This property transfers to the non-orthogonal method and we have

$$\hat{\kappa} = \kappa_{ai}\hat{d}_a^\dagger \hat{\bar{d}}_i + \kappa_{ia}\hat{d}_i^\dagger \hat{\bar{d}}_a \equiv \hat{\kappa}^u + \hat{\kappa}^d, \tag{6.60}$$

where we have introduced the labels u and d for up and down respectively [21]. Constructing the bi-variational non-orthogonal coupled-cluster Lagrangian

$$L(\boldsymbol{\tau}, \boldsymbol{\lambda}, \kappa^u, \kappa^d) = \langle \tilde{\Phi}|(\mathbb{1} + \hat{\Lambda}) \exp(-\hat{T}) \exp(-\hat{\kappa}) \hat{H} \exp(\hat{\kappa}) \exp(\hat{T})|\Phi\rangle\,, \tag{6.61}$$

where we have introduced the left reference state

$$\langle \tilde{\Phi}| = \langle \tilde{\phi}_1, \ldots, \tilde{\phi}_N| = \langle -|\, \hat{\bar{d}}_1 \ldots \hat{\bar{d}}_N, \tag{6.62}$$

as the biorthogonal dual state of the right reference state defined in the normal way. It is interesting to compare the exponential operator with $\hat{\kappa}$ to Thouless theorem from Theorem 3.3. Thouless theorem can be compared to the singles amplitudes in regular coupled-cluster theory as the orbital rotations are formulated in a completely analogous way with a singles excitation operator. In the non-orthogonal formulation $\exp[\hat{\kappa}]$ contains both an excitation and an annihilation operator. This makes the method include the singles ampitudes, and opens for more degrees of freedom for the relaxation operator. By including the relaxation operator the method opens up for two sets of spin-orbitals unlike Thouless theorem which only rotates a single set of spin-orbitals [6]. In fact, by incorporating the singles excitations as an orbital transformation of the Hamiltonian, we can ignore the $\hat{T}_1$ and the $\hat{\Lambda}_1$ contributions to the coupled-cluster amplitudes. This also applies for the non-orthogonal formulation and we have that the doubles excitations with $\hat{T}_2$ and $\hat{\Lambda}_2$ will be equally good as the singles-and-doubles excitations.

Returning to the process of finding the stationary conditions of the non-orthogonal coupled-cluster Lagrangian, we require that $\langle\tilde{\Psi}|$ and $|\Psi\rangle$ must satisfy the standard coupled-cluster equations [21]. As $\hat{\kappa}$ does not commute with $\hat{T}$ and $\hat{\Lambda}$ we express the amplitude equations in the optimized basis where $\hat{\kappa} = 0$ [21, 62]. The stationary conditions for τ_μ and λ_μ are thus the same as in Equation 6.45 and Equation 6.46. For the orbital rotations we compute the right-hand sides and set $\hat{\kappa} = 0$ afterwards [62]. This yields the

stationary conditions

$$\left.\frac{\partial L(\boldsymbol{\tau}, \boldsymbol{\lambda}, \kappa^u, \kappa^d)}{\partial \kappa^u}\right|_{\kappa=0} = \langle \tilde{\Phi}|(\mathbb{1} + \hat{\Lambda}) \exp(-\hat{T}) \left[\hat{H}, \hat{a}_a^\dagger \hat{\tilde{a}}_i\right] \exp(\hat{T})|\Phi\rangle\,, \tag{6.63}$$

$$\left.\frac{\partial L(\boldsymbol{\tau}, \boldsymbol{\lambda}, \kappa^u, \kappa^d)}{\partial \kappa^d}\right|_{\kappa=0} = \langle \tilde{\Phi}|(\mathbb{1} + \hat{\Lambda}) \exp(-\hat{T}) \left[\hat{H}, \hat{a}_i^\dagger \hat{\tilde{a}}_a\right] \exp(\hat{T})|\Phi\rangle\,, \tag{6.64}$$

where it is important to note that all creation and annihilation operators in the cluster amplitudes and the Hamiltonian are the biorthogonal operators.

6.2 Time-dependent coupled-cluster theory

Having explored the time-independent coupled-cluster theory, the question now arises how we can move to the time-dependent situation. The formulation of the time-dependent coupled-cluster theory initially started with a non-variational formulation prior to the introduction of the Lagrange multipliers. In 1978 Hoodbhoy & Negele [63, 64] proposed the time-dependent formulation of coupled-cluster theory by inserting the coupled-cluster wave function into the time-dependent Schrödinger equation,

$$i\hbar \exp(-\hat{T}(t))\partial_t \exp(\hat{T}(t))\,|\Phi\rangle = \exp(-\hat{T}(t))\hat{H}(t) \exp(\hat{T}(t))\,|\Phi\rangle\,, \tag{6.65}$$

which in many ways is the "natural" approach to take as this is the analog to the projected time-independent Schrödinger equation for the coupled-cluster wave function. The truncation level of this approach can be done in a similar manner as in the time-independent case, i.e., by projecting onto an excited state $|\Phi_\mu\rangle$, and the right-hand sides lead to the familiar projected amplitude equations in Equation 6.10 and energy equation Equation 6.9. The time-dependence is kept in the wave function by the amplitudes and in the Hamiltonian in accordance with the Schrödinger picture. As the cluster amplitudes commute, we have that the time-derivative of coupled-cluster wave function is given by

$$i\hbar\partial_t \exp(\hat{T}(t))\,|\Phi\rangle = i\hbar \left(\partial_t \tau_\mu(t)\right) \hat{X}_\mu \exp(\hat{T}(t))\,|\Phi\rangle\,. \tag{6.66}$$

Left-projecting with an excited state we find that

$$i\hbar\,\langle\Phi_\mu|\exp(-\hat{T}(t))\partial_t \exp(\hat{T}(t))|\Phi\rangle = i\hbar\partial_t \tau_\mu(t). \tag{6.67}$$

This means that the time evolution of the amplitudes is given by the amplitude equations in time as their right-hand sides. The time-dependent formulation described above suffers in that it is not variational [63–65] and the

process of computing observables in time suffers from the same problems as in the non-variational time-independent case.

To fix this we reuse the variational coupled-cluster Lagrangian in the time-dependent variational principle yielding the time-dependent coupled-cluster action functional [15]

$$S[\Psi,\tilde{\Psi}] = \int dt\, \langle\tilde{\Psi}(t)|\Big(i\hbar\partial_t - \hat{H}(t)\Big)|\Psi(t)\rangle = \int dt L[\Psi,\tilde{\Psi}], \tag{6.68}$$

where the coupled-cluster Lagrangian now includes the time-derivative. We can write the Lagrangian as

$$L[\Psi,\tilde{\Psi}] = i\hbar\lambda_\mu\partial_t\tau_\mu - E[\Psi,\tilde{\Psi}], \tag{6.69}$$

where $E[\Psi,\tilde{\Psi}]$ is the energy functional formulation of the coupled-cluster energy function from Equation 6.42. Finding the stationary conditions for the action functional now consists of solving the two sets of equations

$$\frac{\partial L[\Psi,\tilde{\Psi}]}{\partial\lambda_\mu} = 0, \qquad \frac{\partial L[\Psi,\tilde{\Psi}]}{\partial\tau_\mu} = 0. \tag{6.70}$$

The former equation yields the time evolution of the τ_μ-amplitudes whereas the latter yield the time evolution for the λ_μ-amplitudes. For the former equation we find

$$\frac{\partial L[\Psi,\tilde{\Psi}]}{\partial\lambda_\mu} = i\hbar\partial_t\tau_\mu - \frac{\partial E[\Psi,\tilde{\Psi}]}{\partial\lambda_\mu} = 0 \tag{6.71}$$

$$\implies i\hbar\partial_t\tau_\mu = \frac{\partial E[\Psi,\tilde{\Psi}]}{\partial\lambda_\mu} = \langle\Phi_\mu|\exp(-\hat{T}(t))\hat{H}(t)\exp(\hat{T}(t))|\Phi\rangle\,, \tag{6.72}$$

where the excited determinant comes from the derivative of the $\hat{\Lambda}(t)$ with respect to λ_μ yielding a relaxation operator $\hat{X}^\dagger_\mu$. We see that Equation 6.72 is the familiar projected amplitude equations in the non-variational formulation of the coupled-cluster wave function similar to the method introduced by Hoodbhoy & Negele [63, 64]. The second stationary condition gives

$$\frac{\partial L[\Psi,\tilde{\Psi}]}{\partial\tau_\mu} = i\hbar\,\frac{\partial}{\partial\tau_\mu}\left[\partial_t\left(\lambda_\nu\tau_\nu\right) - \left(\partial_t\lambda_\nu\right)\tau_\nu\right] - \frac{\partial E[\Psi,\tilde{\Psi}]}{\partial\tau_\mu} = 0 \tag{6.73}$$

$$\implies -i\hbar\partial_t\lambda_\mu = \frac{\partial E[\Psi,\tilde{\Psi}]}{\partial\tau_\mu} = \langle\tilde{\Psi}(t)|\Big[\hat{H}(t),\hat{X}_\mu\Big]|\Psi(t)\rangle\,, \tag{6.74}$$

where we in the product rule for the derivatives of the amplitudes used that the boundary term must disappear in accordance with the time-dependent

variational principle. The commutator comes from the left and right exponential cluster operators. Now, Equation 6.72 and Equation 6.74 yield a variational formulation of the time-dependent coupled-cluster methods where μ decides the truncation level. For Equation 6.72 we can reuse the regular $\hat{T}$-amplitudes as the right-hand side, and for Equation 6.74 we use the right-hand sides for the Lagrange multipliers from the time-independent situation.

6.3 Orbital-adaptive formulation

In the article titled "Ab initio quantum dynamics using coupled-cluster" Kvaal [14] employs the bi-variational principle as discussed by Arponen [57] to create a new family of coupled-cluster methods dubbed "orbital-adaptive time-dependent coupled-cluster". They provide an approximation to the multi-configurational time-dependent Hartree-Fock methods, which themselves are approximations to the time-dependent full configuration interaction method. Similar to the non-orthogonal coupled-cluster method discussed in subsection 6.1.8 the orbital-adaptive method opens up for orbital rotations along with the coupled-cluster amplitudes $\hat{T}(t)$ and $\hat{\Lambda}(t)$, with the orbitals subject to the constraint that they are biorthogonal in time, that is,

$$\langle \tilde{\phi}_p(t) | \phi_q(t) \rangle = \delta_{pq} \implies \left\{ \hat{\tilde{a}}_p, \hat{a}_q^\dagger \right\} = \delta_{pq}, \tag{6.75}$$

where we denote the bra states by tilde to distinguish it from the adjoint state. In general we have $|\phi_p(t)\rangle^\dagger \neq \langle \tilde{\phi}_p(t)|$ as the two orbitals are defined in two separate Hilbert spaces [14]. This extends through to the Slater determinants being biorthogonal in time, that is

$$\langle \tilde{\Phi}_\mu(t) | \Phi_\nu(t) \rangle = \delta_{\mu\nu}. \tag{6.76}$$

In order to avoid two sets of second quantized operators, we transform from the atomic orbital basis in a similar fashion as done in the non-orthogonal coupled-cluster method. However, the formulation of the orbital-adaptive method does not contain an explicit single-particle operator as in the non-orthogonal method. Therefore, instead of transforming via Equation 6.56 and Equation 6.57, we use the projection operator of the biorthogonal Slater determinant basis [14]

$$\Pi(t) = |\Phi_\mu(t)\rangle\langle\tilde{\Phi}_\mu(t)|. \tag{6.77}$$

This lets us transform the Hamiltonian to the biorthogonal basis by

$$\langle \tilde{\Psi}(t) | \hat{H}(t) | \Psi(t) \rangle = \langle \tilde{\Psi}(t) | \Pi(t) \hat{H}(t) \Pi(t) | \Psi(t) \rangle, \tag{6.78}$$

where we stress that $\Pi(t) \neq \Pi^{\dagger}(t)$. This corresponds to replacing all static second quantized operators by the biorthogonal operators. Instead of going through a description of the time-dependent bi-variational principle [14, 57], we define the bi-variational form of the coupled-cluster wave functions to be

$$|\Psi(t)\rangle = \exp(\hat{T}(t))\,|\Phi(t)\rangle\,, \tag{6.79}$$

$$\langle\tilde{\Psi}(t)| = \langle\tilde{\Phi}(t)|\,(\mathbb{1} + \hat{\Lambda}(t))\exp(-\hat{T}(t)), \tag{6.80}$$

where we impose the normalization that

$$\langle\tilde{\Psi}(t)|\Psi(t)\rangle = 1. \tag{6.81}$$

From here on and out we remove the explicit time-dependence on the states and operators to avoid too much clutter. We now define the action-like functional[3] by [14, 57]

$$S[\boldsymbol{\tau}, \boldsymbol{\lambda}, \Phi, \tilde{\Phi}] = \int dt\,\langle\tilde{\Psi}|\Big(i\hbar\partial_t - \hat{H}\Big)|\Psi\rangle = \int dt L[\boldsymbol{\tau}, \boldsymbol{\lambda}, \Phi, \tilde{\Phi}], \tag{6.82}$$

which closely resembles the coupled-cluster action functional from Equation 6.68 except that Equation 6.82 opens up for independent variations over the orbitals. To go from here we evaluate the Lagrangian functional. The time-derivative yields

$$\langle\tilde{\Psi}|\partial_t|\Psi\rangle = \langle\tilde{\Psi}|\Big(\partial_t\tau_\mu\hat{X}_\mu + \hat{\eta}\Big)|\Psi\rangle = \lambda_\mu\partial_t\tau_\mu + \langle\tilde{\Psi}|\hat{\eta}|\Psi\rangle\,, \tag{6.83}$$

where the first term comes from the time-derivative of the cluster amplitudes as seen in Equation 6.67, and the second term comes from the time-derivative of the orbitals. This operator is given by

$$\hat{\eta} = \langle\tilde{\phi}_p|\partial_t|\phi_q\rangle\,\hat{a}_p^{\dagger}\hat{\tilde{a}}_q = \eta_q^p\hat{a}_p^{\dagger}\hat{\tilde{a}}_q, \tag{6.84}$$

which is a one-body operator similar to the projected one-body Hamiltonian. We define the time-dependent energy functional by

$$\mathcal{E}[\boldsymbol{\tau}, \boldsymbol{\lambda}, \Phi, \tilde{\Phi}] \equiv \langle\tilde{\Psi}|\Big(\hat{H} - i\hbar\hat{\eta}\Big)|\Psi\rangle\,, \tag{6.85}$$

which should be compared with Equation 6.42. We can now write the Lagrangian functional as

$$L[\boldsymbol{\tau}, \boldsymbol{\lambda}, \Phi, \tilde{\Phi}] = i\hbar\lambda_\mu\partial_t\tau_\mu - \mathcal{E}[\boldsymbol{\tau}, \boldsymbol{\lambda}, \Phi, \tilde{\Phi}]. \tag{6.86}$$

[3] This must not be mistaken for an actual action functional [57].

We are now interested in finding stationary conditions for the action-like functional by performing variations over all dependent variables in the Lagrangian functional. The stationary conditions for the $\hat{\Lambda}$-amplitudes are given by

$$i\hbar\partial_t\tau_\mu = \frac{\partial\mathcal{E}[\tau_\nu,\lambda_\nu\Phi,\tilde{\Phi}]}{\partial\lambda_\mu} = \langle\tilde{\Phi}_\mu|\exp(-\hat{T})\left[\hat{H}-i\hbar\hat{\eta}\right]\exp(\hat{T})|\Phi\rangle\,. \tag{6.87}$$

Comparing this to Equation 6.72 we see that the only difference is the inclusion of the one-body operator $i\hbar\hat{\eta}$. The stationary conditions for the $\hat{T}$-amplitudes then yields

$$-i\hbar\partial_t\lambda_\mu = \frac{\partial\mathcal{E}[\boldsymbol{\tau},\boldsymbol{\lambda},\Phi,\tilde{\Phi}]}{\partial\tau_\mu} = \langle\tilde{\Psi}|\left[\hat{H}-i\hbar\hat{\eta},\hat{X}_\mu\right]|\Psi\rangle\,, \tag{6.88}$$

which is also comparable to the time-dependent coupled-cluster method with stationary orbitals in Equation 6.74.

6.3.1 Orbital rotations

For the variation of the orbitals we start by noting that the four sets of parameters $\hat{T}$, $\hat{\Lambda}$, Φ, and $\tilde{\Phi}$ are overdetermined [14]. This means that we can choose a gauge condition for the orbital rotations in order to remove parametric redundancies. Similarly to the non-orthogonal coupled-cluster method we choose

$$\hat{\eta} = \eta_a^i\hat{d}_i^\dagger\hat{\tilde{d}}_a + \eta_i^a\hat{d}_a^\dagger\hat{\tilde{d}}_i, \tag{6.89}$$

that is, the occupied-occupied and virtual-virtual rotations are set to zero. Furthermore, the orbital rotations makes the singles amplitudes τ_i^a redundant, and to avoid having more parameters in $\langle\tilde{\Psi}|$ than in $|\Psi\rangle$ we set λ_a^i to zero as well [14]. We now perform variations over the orbitals

$$|\phi_p'\rangle = |\phi_p\rangle + |\delta\phi_p\rangle\,, \tag{6.90}$$

and similarly for the dual single-particle state $\langle\tilde{\phi}_p|$. We restrict our attention to the variation $|\delta\phi_p\rangle$ and ignore the full state $|\phi_p'\rangle$. Now, we note that

$$|\delta\phi_p\rangle = \hat{P}\,|\delta\phi_p\rangle + \hat{Q}\,|\delta\phi_p\rangle\,, \tag{6.91}$$

where the single-particle projection operator $\hat{P}$ is given by

$$\hat{P} = |\tilde{\phi}_p\rangle\langle\phi_p| \implies \hat{Q} = \mathbb{1} - \hat{P}. \tag{6.92}$$

Due to the gauge condition imposed on η_q^p we know that we only need to concern ourselves with variations over occupied-virtual and virtual-occupied pairs. We can thus construct the two sets of orbital variations

$$|\delta\phi_i\rangle = \epsilon_i^a |\phi_a\rangle + \hat{Q} |\delta\phi_i\rangle , \tag{6.93}$$

$$|\delta\phi_a\rangle = \epsilon_i^a |\phi_i\rangle + \hat{Q} |\delta\phi_a\rangle , \tag{6.94}$$

where ϵ_i^a is an arbitrary function of time. Furthermore, the functions $\hat{Q} |\delta\phi_p\rangle$ are also arbitrary and independent of ϵ_i^a. We denote the equations from the variations over the first and second term as P-space equations and Q-space equations respectively. We can then perform the variations over the P-space equations independently of the variations over the Q-space equations.

6.3.2 P-space equations

We start by defining the variations over the orbitals to be

$$|\delta\phi_i\rangle = \epsilon |\phi_a\rangle , \qquad |\delta\phi_a\rangle = \epsilon |\phi_i\rangle , \tag{6.95}$$

where $\epsilon(t)$ is now an arbitrary function of time that is independent of the labels i and a. Due to the biorthogonality of the orbitals, we can find the corresponding variations over the dual states

$$0 = \delta \left(\langle \tilde{\phi}_a | \phi_i \rangle \right) = \langle \delta\tilde{\phi}_a | \phi_i \rangle + \langle \tilde{\phi}_a | \delta\phi_i \rangle \tag{6.96}$$

$$\implies \langle \delta\tilde{\phi}_a | \phi_i \rangle = - \langle \tilde{\phi}_a | \delta\phi_i \rangle = -\epsilon, \tag{6.97}$$

which yields

$$\langle \delta\tilde{\phi}_i | = -\epsilon \langle \tilde{\phi}_a | , \qquad \langle \delta\tilde{\phi}_a | = -\epsilon \langle \tilde{\phi}_i | . \tag{6.98}$$

By inspecting the Lagrangian functional from Equation 6.86 we note that only the energy functional depends explicitly on the orbitals. In terms of the biorthogonal second quantized operators we can describe the variation over an orbital in an arbitrary state by the action

$$|\delta\Psi\rangle = \epsilon \left[\hat{a}_a^\dagger \hat{\tilde{a}}_i + \hat{a}_i^\dagger \hat{\tilde{a}}_a \right] |\Psi\rangle , \tag{6.99}$$

$$\langle \delta\tilde{\Psi}| = -\epsilon \langle \tilde{\Psi}| \left[\hat{a}_a^\dagger \hat{\tilde{a}}_i + \hat{a}_i^\dagger \hat{\tilde{a}}_a \right] , \tag{6.100}$$

as the variation is performed by replacing a virtual orbital by an occupied orbital and vice versa. Now, the Hamiltonian and the cluster amplitudes do not explictly depend on the orbitals and will therefore be unaffected by the orbital variation. However, $\hat{\eta}$ will be varied. We see the effect of this variation

by considering the matrix elements η_q^p prior to imposing the gauge condition for the orbital rotations. This yields

$$\begin{aligned}\delta\eta_q^p &= \langle\delta\tilde{\phi}_p|\partial_t|\phi_q\rangle + \langle\tilde{\phi}_p|\partial_t|\delta\phi_q\rangle && (6.101)\\ &= -\epsilon\left[\delta_{pa}\langle\tilde{\phi}_i| + \delta_{pi}\langle\tilde{\phi}_a|\right]\partial_t|\phi_q\rangle \\ &\quad + \langle\tilde{\phi}_p|\,\partial_t\left[\epsilon\delta_{qa}|\phi_i\rangle + \epsilon\delta_{qi}|\phi_a\rangle\right], && (6.102)\end{aligned}$$

where the Kronecker-Deltas run over free indices and should be treated more as running over occupied or virtual indices. Now, due to the gauge conditions, we get

$$\begin{aligned}\delta\eta_q^p &= -\epsilon\left[\delta_{pa}\delta_{qb}\eta_b^i + \delta_{pi}\delta_{qj}\eta_j^a\right] + \partial_t\epsilon\left[\delta_{qa}\delta_{pi} + \delta_{qi}\delta_{pa}\right] \\ &\quad + \epsilon\left[\delta_{qa}\delta_{pb}\eta_i^b + \delta_{qi}\delta_{pj}\eta_j^a\right] && (6.103)\\ &= \partial_t\epsilon\left[\delta_{qa}\delta_{pi} + \delta_{qi}\delta_{pa}\right], && (6.104)\end{aligned}$$

where the two other terms cancel as can be seen by shuffling the free indices. The variation over the full orbital operator is thus given by

$$\delta\hat{\eta} = \delta\eta_q^p\hat{a}_p^\dagger\hat{\tilde{a}}_q = \partial_t\epsilon\left[\hat{a}_a^\dagger\hat{\tilde{a}}_i + \hat{a}_i^\dagger\hat{\tilde{a}}_a\right]. \tag{6.105}$$

We find the expectation value over the variation of $\hat{\eta}$ to be

$$\langle\tilde{\Psi}|\delta\hat{\eta}|\Psi\rangle = (\partial_t\epsilon)\left[\rho_a^i + \rho_i^a\right] = -\epsilon\left[\partial_t\rho_a^i + \partial_t\rho_i^a\right], \tag{6.106}$$

where the boundary term disappears by definition of the variation [14]. Now, as we have set $\lambda_a^i = 0$, we have that

$$\rho_a^i = \langle\tilde{\Psi}|\hat{a}_a^\dagger\hat{\tilde{a}}_i|\Psi\rangle = \lambda_a^i = 0. \tag{6.107}$$

This is however not the case for ρ_i^a as the operator string acts as a relaxtion operator.

The variation over the occupied orbitals and the virtual orbitals can be done independently [14]. This yields two sets of equations for the P-space variations. We start by looking at the variation over the occupied orbitals in the energy functional.

$$\begin{aligned}\delta\mathcal{E} &= \langle\delta\tilde{\Psi}|\hat{H} - i\hbar\hat{\eta}|\Psi\rangle + \langle\tilde{\Psi}|\hat{H} - i\hbar\hat{\eta}|\delta\Psi\rangle - i\hbar\langle\tilde{\Psi}|\delta\hat{\eta}|\Psi\rangle && (6.108)\\ &= \epsilon\langle\tilde{\Psi}|\left[\hat{H} - i\hbar\hat{\eta}, \hat{a}_a^\dagger\hat{\tilde{a}}_i\right]|\Psi\rangle + \epsilon i\hbar\partial_t\rho_a^i = \epsilon\langle\tilde{\Psi}|\left[\hat{H} - i\hbar\hat{\eta}, \hat{a}_a^\dagger\hat{\tilde{a}}_i\right]|\Psi\rangle. && (6.109)\end{aligned}$$

The variation over the virtual orbitals gives

$$\delta\mathcal{E} = \epsilon\langle\tilde{\Psi}|\left[\hat{H} - i\hbar\hat{\eta}, \hat{a}_i^\dagger\hat{\tilde{a}}_a\right]|\Psi\rangle + \epsilon i\hbar\partial_t\rho_i^a, \tag{6.110}$$

where the time-derivative of the one-body density matrix is retained. Recalling that the amplitudes do not depend on the orbital variations directly we can compute the variation over the orbitals in the action-like functional by

$$\delta S = \int dt \delta L = \int dt \delta \mathcal{E} = 0. \tag{6.111}$$

The requirement that δS is zero for all ϵ implies that we can remove the integrand and ϵ as it factors out. This means that we can write Equation 6.109 and Equation 6.110 on the form

$$i\hbar \langle \tilde{\Psi}| \left[\hat{\eta}, \hat{a}_a^\dagger \hat{\tilde{a}}_i\right] |\Psi\rangle = \langle \tilde{\Psi}| \left[\hat{H}, \hat{a}_a^\dagger \hat{\tilde{a}}_i\right] |\Psi\rangle , \tag{6.112}$$

$$i\hbar \langle \tilde{\Psi}| \left[\hat{\eta}, \hat{a}_i^\dagger \hat{\tilde{a}}_a\right] |\Psi\rangle = \langle \tilde{\Psi}| \left[\hat{H}, \hat{a}_i^\dagger \hat{\tilde{a}}_a\right] |\Psi\rangle + \epsilon i\hbar \partial_t \rho_i^a. \tag{6.113}$$

Looking at the gauge condition for $\hat{\eta}$ given in Equation 6.89 we see that the only non-zero terms in the commutators on the left-hand side becomes

$$i\hbar \eta_b^j \langle \tilde{\Psi}| \left[\hat{a}_j^\dagger \hat{\tilde{a}}_b, \hat{a}_a^\dagger \hat{\tilde{a}}_i\right] |\Psi\rangle = i\hbar \eta_b^j \left[\delta_{ba} \rho_j^i - \delta_{ij} \rho_a^b\right] \equiv i\hbar \eta_b^j A_{aj}^{ib}, \tag{6.114}$$

$$i\hbar \eta_j^b \langle \tilde{\Psi}| \left[\hat{a}_b^\dagger \hat{\tilde{a}}_j, \hat{a}_i^\dagger \hat{\tilde{a}}_a\right] |\Psi\rangle = i\hbar \eta_j^b \left[\delta_{ji} \rho_b^a - \delta_{ab} \rho_i^j\right] \equiv -i\hbar \eta_j^b A_{bi}^{ja}, \tag{6.115}$$

where we have defined the coefficient matrix $\mathbf{A}$. What remains is to evaluate the commutators with the Hamiltonian matrix on the right-hand side. For brevity we restrict ourselves to only looking at the operator strings. We have for the one-body Hamiltonian

$$\left[\hat{a}_p^\dagger \hat{\tilde{a}}_q, \hat{a}_a^\dagger \hat{\tilde{a}}_i\right] = \delta_{qa} \hat{a}_p^\dagger \hat{\tilde{a}}_i - \delta_{ip} \hat{a}_a^\dagger \hat{\tilde{a}}_q, \tag{6.116}$$

$$\left[\hat{a}_p^\dagger \hat{\tilde{a}}_q, \hat{a}_i^\dagger \hat{\tilde{a}}_a\right] = \delta_{qi} \hat{a}_p^\dagger \hat{\tilde{a}}_a - \delta_{ap} \hat{a}_i^\dagger \hat{\tilde{a}}_q. \tag{6.117}$$

The expectation value of these operator strings will be made into one-body density matrices. That is, for the one-body Hamiltonian we get

$$\langle \tilde{\Psi}| \left[\hat{h}, \hat{a}_a^\dagger \hat{\tilde{a}}_i\right] |\Psi\rangle = h_a^p \rho_p^i - h_q^i \rho_a^q, \tag{6.118}$$

$$\langle \tilde{\Psi}| \left[\hat{h}, \hat{a}_i^\dagger \hat{\tilde{a}}_a\right] |\Psi\rangle = h_i^p \rho_p^a - h_q^a \rho_i^q. \tag{6.119}$$

For the two-body operator we get

$$\begin{aligned}\left[\hat{a}_p^\dagger \hat{a}_q^\dagger \hat{\tilde{a}}_s \hat{\tilde{a}}_r, \hat{a}_a^\dagger \hat{\tilde{a}}_i\right] &= \delta_{ra} \hat{a}_p^\dagger \hat{a}_q^\dagger \hat{\tilde{a}}_s \hat{\tilde{a}}_i - \delta_{sa} \hat{a}_p^\dagger \hat{a}_q^\dagger \hat{\tilde{a}}_r \hat{\tilde{a}}_i \\ &\quad - \delta_{ip} \hat{a}_a^\dagger \hat{a}_q^\dagger \hat{\tilde{a}}_s \hat{\tilde{a}}_r + \delta_{iq} \hat{a}_a^\dagger \hat{a}_p^\dagger \hat{\tilde{a}}_s \hat{\tilde{a}}_r, \end{aligned} \tag{6.120}$$

$$\begin{aligned}\left[\hat{a}_p^\dagger \hat{a}_q^\dagger \hat{\tilde{a}}_s \hat{\tilde{a}}_r, \hat{a}_i^\dagger \hat{\tilde{a}}_a\right] &= \delta_{ri} \hat{a}_p^\dagger \hat{a}_q^\dagger \hat{\tilde{a}}_s \hat{\tilde{a}}_a - \delta_{si} \hat{a}_p^\dagger \hat{a}_q^\dagger \hat{\tilde{a}}_r \hat{\tilde{a}}_a \\ &\quad - \delta_{ap} \hat{a}_i^\dagger \hat{a}_q^\dagger \hat{\tilde{a}}_s \hat{\tilde{a}}_r + \delta_{aq} \hat{a}_i^\dagger \hat{a}_p^\dagger \hat{\tilde{a}}_s \hat{\tilde{a}}_r. \end{aligned} \tag{6.121}$$

Similarly to the one-body Hamiltonain, the expectation value will yield two-body density matrices for the operator strings. Using the antisymmetry of the two-body matrix elements, we get

$$\langle\tilde{\Psi}|\left[\hat{u}, \hat{d}_a^\dagger \hat{\tilde{d}}_i\right]|\Psi\rangle = \frac{1}{2}u_{is}^{pq}\rho_{pq}^{as} - \frac{1}{2}u_{rs}^{aq}\rho_{iq}^{sr}, \tag{6.122}$$

$$\langle\tilde{\Psi}|\left[\hat{u}, \hat{d}_i^\dagger \hat{\tilde{d}}_a\right]|\Psi\rangle = \frac{1}{2}u_{is}^{pq}\rho_{pq}^{sa} - \frac{1}{2}u_{rs}^{aq}\rho_{iq}^{sr}. \tag{6.123}$$

Putting everything together we get equations for the occupied-virtual part of $\hat{\eta}$ and the virtual-occupied block. The former is given by

$$i\hbar A_{aj}^{ib}\eta_b^j = h_a^p\rho_p^i - h_q^i\rho_a^q + \frac{1}{2}u_{is}^{pq}\rho_{pq}^{as} - \frac{1}{2}u_{rs}^{aq}\rho_{iq}^{sr}. \tag{6.124}$$

This is a linear equation system that can be solved for η_b^j. The virtual-occupied block equation is

$$-i\hbar\eta_j^b A_{bi}^{ja} = h_i^p\rho_p^a - h_q^a\rho_i^q + \frac{1}{2}u_{is}^{pq}\rho_{pq}^{sa} - \frac{1}{2}u_{rs}^{aq}\rho_{iq}^{sr} + i\hbar\partial_t\rho_i^a, \tag{6.125}$$

which resembles a transposed linear equation. Note that the time-derivative of the one-body density matrix does not disappear in the latter equation. Solving both Equation 6.124 and Equation 6.125 we are able to construct the $\boldsymbol{\eta}$ matrix. We shall in the following derivation of the Q-space equations see how this gives an expression for the time evolution of the orbitals.

6.3.3 Q-space equations

For the Q-space equations we define the variation over the orbitals to be

$$|\delta\phi_p\rangle \equiv |\theta\rangle = \hat{Q}\,|\theta\rangle\,, \tag{6.126}$$

$$\langle\delta\tilde{\phi}_p| \equiv \langle\theta| = \langle\theta|\,\hat{Q}, \tag{6.127}$$

where the requirement that $|\theta\rangle$ can be defined in terms of itself acted upon by $\hat{Q}$ yields

$$\langle\theta|\phi_p\rangle = \langle\tilde{\phi}_p|\theta\rangle = 0, \tag{6.128}$$

for all p. This helps explain why we were able to split up the orbital variations over $\hat{P}$ and $\hat{Q}$ as it demonstrates that the Q-space equations are independent of the P-space equations. The variation over Q-space will only apply to the energy functional $\mathcal{E}$ as the amplitude term in the Lagrangian does not explicitly depend on the orbitals. We write the energy functional in terms of one-

and two-body matrices

$$\mathcal{E} = \langle\tilde{\Psi}|\Big(\hat{H} - i\hbar\hat{\eta}\Big)|\Psi\rangle = \rho_p^q \left(h_q^p - i\hbar\eta_q^p\right) + \frac{1}{4}\rho_{pq}^{rs} u_{rs}^{pq} \tag{6.129}$$

$$= \rho_p^q \langle\tilde{\phi}_p|\Big(\hat{h} - i\hbar\partial_t\Big)|\phi_q\rangle + \frac{1}{4}\rho_{pq}^{rs}\langle\tilde{\phi}_p\tilde{\phi}_q|\hat{u}|\phi_r\phi_s\rangle_{AS}\,, \tag{6.130}$$

where we have written out the explicit orbital dependencies in the one- and two-body Hamiltonian and the time-derivative. Requiring that the first-order variations over the orbitals should make the action functional disappear, we have

$$\delta S = \int dt \left[\rho_p^q \langle\theta|\Big(\hat{h} - i\hbar\partial_t\Big)|\phi_q\rangle + \rho_{pq}^{rs}\langle\theta\tilde{\phi}_q|\hat{u}|\phi_r\phi_s\rangle\right] = 0, \tag{6.131}$$

where we stress that p is now a free index, and where the two-body elements no longer are antisymmetric. The factor 1/4 disappeared from the two-body integrals due to the antisymmetric properties of the two-body density matrix and from the symmetric properties of the two-body elements.[4] As the variation must be valid for all $\langle\theta|\,\hat{Q}$ we are left with

$$i\hbar\rho_p^q\hat{Q}\partial_t|\phi_q\rangle = \rho_p^q\hat{Q}\hat{h}|\phi_q\rangle + \rho_{pq}^{rs}\hat{Q}\hat{W}_s^q|\phi_r\rangle\,, \tag{6.132}$$

where we have defined the mean-field potential W_s^q to be [14]

$$\langle\tilde{\phi}_p|\hat{W}_s^q|\phi_r\rangle = \int dx_1 dx_2 \tilde{\phi}_p(x_1)\tilde{\phi}_q(x_2)\hat{u}(x_1,x_2)\phi_s(x_2)\phi_r(x_1), \tag{6.133}$$

similarly to the Coulomb operator in the Hartree-Fock theory. Performing the variations over the ket-side of the energy functional we have

$$\delta S = \int dt \left[\rho_p^q \langle\tilde{\phi}_p|\Big(\hat{h} - i\hbar\partial_t\Big)|\theta\rangle + \rho_{pq}^{rs}\langle\tilde{\phi}_p\tilde{\phi}_q|\hat{u}|\theta\phi_s\rangle\right] = 0, \tag{6.134}$$

where now q in the first term and r in the second term are free indices. This variation must be valid for all $\hat{Q}\,|\theta\rangle$ and we get the equation

$$-i\hbar\rho_p^q\left(\partial_t\langle\tilde{\phi}_p|\right)\hat{Q} = \rho_p^q\langle\tilde{\phi}_p|\,\hat{h}\hat{Q} + \rho_{pq}^{rs}\langle\tilde{\phi}_p|\,\hat{W}_s^q\hat{Q}, \tag{6.135}$$

where we get a change of sign on the left-hand side due to integration by parts and removal of the boundary term. Now Equation 6.132 and Equation 6.135 along with the P-space equations provide the equations of motion for the orbital rotations.

[4] To see this expand the antisymmetric two-body Hamiltonian in its constituent parts, and permute the orbitals using the symmetric properties of the two-body elements.

When Kvaal [14] formulated the orbital-adaptive coupled-cluster method the intention was to provide an approximation to the multi-configuration Hartree-Fock method. The latter method approximates the full configuration interaction method by truncating the single-particle basis beyond the originally truncated basis set. The orbital-adaptive coupled-cluster method approximates the multi-configuration Hartree-Fock method by truncating the Slater determinant space by using the exponential ansatz from coupled-cluster. Thus, we are in a position to do two truncations from the full-configuration method; the Slater basis and the single-particle basis. Now, the former truncation comes from the choice of the cluster operator truncation and the latter from the Q-space equations. We shall discuss this in more detail when we look at the implementation of the orbital-adaptive coupled-cluster method in subsection 9.3.9.

6.4 Normalization

We compute the normalization of the coupled-cluster wave function by

$$\langle\tilde{\Psi}(t)|\Psi(t)\rangle = N(t). \tag{6.136}$$

When using static orbitals this reduces to

$$\langle\tilde{\Psi}(t)|\Psi(t)\rangle = \langle\Phi|(\mathbb{1}+\hat{\Lambda}(t))\exp(-\hat{T}(t))\exp(\hat{T}(t))|\Phi\rangle = \langle\Phi|\Phi\rangle = 1, \tag{6.137}$$

where we assume that the reference determinant is normalized to unity. We can then see that the static formulation of the coupled-cluster methods is, by construction, normalized to unity. However, for the orbital-adaptive methods where the orbitals are allowed to vary in time, the picture changes. We then have

$$\begin{aligned}\langle\tilde{\Psi}(t)|\Psi(t)\rangle &= \langle\tilde{\Phi}(t)|(\mathbb{1}+\hat{\Lambda}(t))\exp(-\hat{T}(t))\exp(\hat{T}(t))|\Phi(t)\rangle &(6.138)\\ &= \langle\tilde{\Phi}(t)|\Phi(t)\rangle = \det\big[\mathbf{T}(t)\big] = N(t), &(6.139)\end{aligned}$$

where we have introduced the matrix $\mathbf{T}(t)$ as the product of the coefficient matrices for occupied indices. That is,

$$T_{ij}(t) = \tilde{C}_{i\alpha}(t)C_{\alpha j}(t) \tag{6.140}$$

where the coefficients are limited to run over the occupied orbitals in the reference Slater determinants, but α runs over all the atomic orbitals[5]. Here we

[5]There is no problem in computing the determinant of the full product between the coefficient matrices as this should yield the identity, but formally only the occupied orbitals are included in the reference states.

observe that the normalization constant can change in time. Mathematically, we construct the product between the coefficients to be the identity, i.e.,

$$\tilde{\mathbf{C}}(t)\mathbf{C}(t) = \mathbb{1}, \tag{6.141}$$

where this product runs over all indices p and q.

6.5 The quality of the reference state in time

When evolving a system in time, we can – and will – get in a situation where our initial state has little overlap with the time-evolved state [22].[6] That is, we can get in a situation where

$$\langle \psi(t)|\psi(0)\rangle \to 0, \tag{6.142}$$

where $|\psi(0)\rangle$ is some initial state and $|\psi(t)\rangle$ is the time-evolved state at a later time t. In time-dependent configuration interaction theory this is handled automatically by the zero-order amplitude, viz.

$$|\Psi(t)\rangle = C_0(t)\,|\Phi\rangle + C_i^a(t)\,|\Phi_i^a\rangle + \cdots \implies \langle\Phi|\Psi(t)\rangle = C_0(t), \tag{6.143}$$

where $|\Phi\rangle$ is the reference determinant and we assume an orthonormal set of single-particle states as our basis. In time-dependent coupled-cluster theory where we assume intermediate normalization, there is however a different story to be told. For the time-dependent coupled-cluster wave function we have that

$$|\Psi(t)\rangle = \exp(\hat{T}(t))\,|\Phi\rangle = \left(\mathbb{1} + \hat{T}(t) + \ldots\right)|\Phi\rangle \implies \langle\Phi|\Psi(t)\rangle = 1. \tag{6.144}$$

This might not look like much, but for strong fields, or long time evolution, we can find states which have very little overlap with the reference state. In numerical simulations the lack of infinite precision leads to numerial problems when the overlap goes to zero. When this is the case the cluster amplitudes are left with the job of both "removing" the reference state from the cluster wave function *and* providing contribution from higher excited determinants [22]. Frustratingly enough the formulation of the time-dependent coupled-cluster method with static spin-orbitals is seemingly not able to solve this problem. When

$$\langle\Phi|\Psi(t)\rangle \to 0, \tag{6.145}$$

[6] Note that even though there might be a nonzero overlap with our initial state, this overlap can be so small that within computational precision it is zero.

the magnitude of the amplitudes sky-rocket, the energy is no longer conserved,[7] and the data produced can no longer be trusted [22]. Luckily, the orbital-adaptive time-dependent coupled-cluster method seems to remove much of these problems. We will in the coming sections demonstrate that the orbital-adaptive formulation of coupled-cluster fixes some of the problems described by Pedersen & Kvaal [22]. However, the orbital-adaptive formulation does not seem to solve all stability problems, and an ongoing study into this is being conducted by Kristiansen *et al.* [66].

But, before we try to solve the problem, we can formulate a "zero-order" amplitude for the time-dependent coupled-cluster wave function which does not solve the problem, but at least lets us measure how good or bad the reference state is in time. This is done by introducing a phase factor $\tau_0(t) \in \mathbb{C}$ which we insert in the exponential ansatz, viz.

$$|\Psi(t)\rangle = \exp(\tau_0(t) + \hat{T}(t))\,|\Phi\rangle\,, \tag{6.146}$$

$$\langle\tilde{\Psi}(t)| = \langle\Phi|\,(\mathbb{1} + \hat{\Lambda}(t))\exp(-\tau_0(t) - \hat{T}(t)), \tag{6.147}$$

where $\tau_0(t)$ is a number and therefore commutes with the cluster operators. Regardless if $\tau_0(t)$ is real or not, the inclusion of the phase does not change any of the equations used in coupled-cluster methods as it oes not couple amplitude equations. However, we can now see that

$$\langle\Phi|\Psi(t)\rangle = \exp(\tau_0(t)), \tag{6.148}$$

$$\langle\tilde{\Psi}(t)|\Phi\rangle = \exp(-\tau_0(t))\left[1 - \langle\Phi|\hat{\Lambda}(t)\hat{T}(t)|\Phi\rangle\right], \tag{6.149}$$

which tells us how much overlap the reference state $|\Phi\rangle$ has with the time-evolved state at a time t. Stated differently, it measures how well the reference state is at approximating the time-evolved state. Note that the inclusion of $\tau_0(t)$ is in no way able to be used as an amplitude to lower the presence of the reference as in the configuration interaction method. We also see that for $\tau_0(t) = 0$ we recover intermediate normalization and the known time-dependent coupled-cluster method. The question remains how we can evaluate $\tau_0(t)$ from the coupled-cluster equations. In general we find the time derivative of the cluster amplitudes from

$$i\hbar\partial_t\tau_\mu = \langle\Phi_\mu|\exp(-\hat{T}(t))\hat{H}(t)\exp(\hat{T}(t))|\Phi\rangle\,, \tag{6.150}$$

where μ denotes the excitation level of the reference slater determinant and the order of the cluster amplitudes as in Equation 6.2. By choosing $\mu = 0$ we are left with

$$i\hbar\partial_t\tau_0 = \langle\Phi|\exp(-\hat{T}(t))\hat{H}(t)\exp(\hat{T}(t))|\Phi\rangle\,, \tag{6.151}$$

[7] When the time-dependence in the Hamiltonian is turned off.

which looks familiar as the equation for the ground state energy in the time-independent coupled-cluster method if the explicit time-dependence is removed from the Hamiltonian and the cluster amplitudes.

Part II

Implementation

Chapter 7

Computational aspects

Along with this thesis we have implemented several quantum-mechanical solvers that are separated into different Github repositiories.[1] These are:

- Quantum systems is a Python library containing modules to set up matrix elements, time evolution operators, and single-particle states to be used by the many-body solvers. Quantum systems provides interfaces to the PySCF [18] and Psi4 [19] systems. The code is located at `https://github.com/Schoyen/quantum-systems` with the documentation at `https://schoyen.github.io/quantum-systems/`.

- Coupled-cluster is a Python library with modules containing ground state and time-dependent coupled-cluster solvers. Currently this package contains doubles (CCD/TDCCD), singles-and-doubles (CCSD/TDCCSD), non-orthogonal coupled-cluster doubles (NOCCD), and the orbital adaptive time-dependent coupled cluster doubles (OATDCCD) methods. The module uses quantum systems to get access to matrix elements. The code is located at `https://github.com/Schoyen/coupled-cluster` with the documentation at `https://schoyen.github.io/coupled-cluster/`.

- Configuration interaction is a library containing ground state and time-dependent configuration interaction solvers. This code supports arbitrary levels of excitations, e.g., singles-and-doubles (CISD/TDCISD), doubles-and-triples (CIDT/TDCIDT), etc, and full configuration interaction (FCI/TDFCI). The module uses quantum systems to get access to matrix elements. The code is located at `https://github.com/Schoyen/configuration-interaction` with the documentation found at `https://schoyen.github.io/configuration-interaction/`.

[1] Due to ongoing publications using the code most of the repositiories are at the time of writing private and access is therefore limited to collaborators. However, please do request access by sending a mail to: o.s.schoyen@fys.uio.no, and we will set you up.

- Hartree-Fock is a library containing ground state and time-dependent Hartree-Fock solvers. We have implemented Hartree-Fock for general (HF/TDHF), restricted (RHF) and unrestricted spin-orbitals (UHF). The module uses quantum systems to get access to matrix elements. The code is located at `https://github.com/Schoyen/hartree-fock` with the documentation at `https://schoyen.github.io/hartree-fock/`.

We will in the rest of this chapter discuss various aspects of the implementation that we deem important to elaborate on, but we will leave a discussion of the quantum systems and the solvers for the next two chapters and the documentation.

7.1 Why Python?

In working with this thesis we have developed a large computational framework for performing real-time quantum mechanics simulations for many-body problems in the programming language Python [67]. The choice of using Python comes with a list of pros and cons. On the pro-side we have that:

- The development time is much lower when using Python as opposed to more verbose, but efficient languages such as C/C++, and Fortran.
- Integration with other Python libraries is relatively easy.
- Libraries such as SciPy [68], NumPy [69], and SymPy [70] provide fast, and efficient interfaces towards – amongst others – BLAS and LAPACK, along with convenient mathematical abstractions.

However, the use of Python comes with the price of less memory control and less scalability. The former is somewhat alleviated by using NumPy as many operations can be performed on already allocated arrays. The drawback is that this requires a keen eye, and can quickly lead to memory leaks which eventually triggers the Python garbage collector. The scalability problem is also somewhat alleviated by NumPy as many of the operations run in parallel via OpenMP. However, large scale computations requires either more sophisticated libraries such as Dask [71] or CuPY [72].

7.2 Computing tensor contractions

Quite a significant amount of computational resources will go into the evaluation of tensor contractions[2] and we will therefore spend some time discussing

[2]We tend to call the matrix elements for tensors, but they more resemble numerical N-dimensional arrays.

how these contractions are performed and how we can speed up the contractions.

Consider the antisymmetric, two-body, Coulomb elements given by

$$u_{rs}^{pq} = \langle \phi_p \phi_q | \hat{u} | \phi_r \phi_s \rangle_{AS}, \tag{7.1}$$

which, along with the two-body density matrix, is the largest tensor in use. This tensor often represents the bottleneck both in terms of memory and contraction time. When we represent these tensors mathematically, the labelling of the indices is in some sense arbitrary and depends on the context in which the tensors are used. On a computer we however need to decide on a specific way of storing memory, and often this choice is related to speed concerns. Some storage schemes show vast improvements in terms of cache hits as opposed to other schemes. However, tensor contractions are notoriously difficult to handle in terms of memory as they often involve change of dimensionality, re-ordering of indices resulting in the need of reshapes, and summation along axes that are inefficiently laid out in memory.

For the sake of generality we therefore ignore much of these problems and have decided to use a fixed layout of the memory and absorb the cost of reshapes and memory allocations. In our programs we read the axis from top-left and moving right before starting on bottom-left and going right. That is,

$$u_{rs}^{pq} \rightarrow \texttt{u[p, q, r, s]} \tag{7.2}$$

where the right-hand side is the representation of the element using NumPy-arrays. This ordering is used consistenly for all tensors in all solver implementations. Other orderings might be smarter due to efficient usage of cache hits, but this clutters much of the implementation and is therefore ignored.

7.2.1 Intermediates

It is common in the coupled-cluster literature to talk about *intermediates* [5, 12], or intermediate computations, as a technique for speeding up tensor contractions involving three or more tensors. The basics of intermediate computations is to treat a tensor contraction as a binary operation and precomputing common factors, or one of the contractions. As an example, consider the D3c term, sans the permutation operator, from the coupled-cluster doubles τ-amplitudes in Table B.1,

$$g_{ij}^{ab} = \tau_{lj}^{ab} \tau_{ik}^{dc} u_{cd}^{kl}, \tag{7.3}$$

where we use the Fermi vacuum formalism for the indices as discussed in subsection 3.6.2 with N the number of occupied states, L the number of basis states, and $M = L - N$ the number of virtual states. The naïve solution

using explicit for-loops yields an $\mathcal{O}(M^4N^4)$-complexity. By first creating the intermediate contraction

$$W_i^l = \tau_{ik}^{dc} u_{cd}^{kl}, \tag{7.4}$$

and then computing the total result from

$$g_{ij}^{ab} = \tau_{lj}^{ab} W_i^l, \tag{7.5}$$

we have reduced the complexity to $\mathcal{O}(M^2N^3)$. This incurs a memory penalty from the temporary storage of W_i^l, but the gain in reduction of the number of FLOPS far exceeds this cost.

The choice of which terms to use when creating intermediates has been explored in some depth, especially in the case of the coupled-cluster singles-and-doubles method as done by Gauss & Stanton [12]. We will however not employ pre-defined intermediates, but rather use the binary operator `np.tensordot` from NumPy to do contractions. This forces us to pre-compute terms with three or more tensors thus lowering the cost. However, some care must be taken as the optimal choice depends on which terms are to be contracted. By inspection we choose the contractions which will yield the lowest amount of computational complexity by counting the number of unique indices and the lowest amount of storage cost. As an example of the converse, consider again the D3c term shown above, where we chose the intermediate W_i^l in Equation 7.4. Another choice for an intermediate would be a contraction with the other τ-amplitude and the two-body elements, viz.

$$W_{lcd}^{abk} = \tau_{lj}^{ab} u_{cd}^{kl}, \tag{7.6}$$

or even worse, the intermediate constructed from both τ-amplitudes

$$W_{ljik}^{abdc} = \tau_{lj}^{ab} \tau_{ik}^{dc}. \tag{7.7}$$

The former expression incurs an extra memory penalty of $\mathcal{O}_M(M^4N^2)$ along with a computational complexity of $\mathcal{O}(M^4N^2)$. The latter takes up $\mathcal{O}_M(M^4N^4)$ memory and $\mathcal{O}(M^4N^2)$ computational complexity. The tactic is thus to choose intermediates which contain the smallest amount of axes and of these as many as possible should be occupied axes as we often have $M > N$.

7.3 Convergence acceleration

When performing optimization techniques such as the quasi-Newton method for the coupled-cluster equations and the self-consistent field iterations in Hartree-Fock, we often find that the solutions can have trouble converging. To alleviate some of these convergence issues we introduce two techniques which often lets us converge faster, or in some cases, converge at all.

7.3.1 Alpha filter

A first-order approximation stems from data estimation theory as an alternative to the more sophisticated Kalman filter [73]. This is a technique which lets us combine a predicted value and a measured value. Given a measurement $\boldsymbol{x}^{(i)}$ at a time i we can create an updated estimate $\bar{\boldsymbol{z}}^{(i)}$ from a predicted estimate $\boldsymbol{z}^{(i)}$ by

$$\bar{\boldsymbol{z}}^{(i)} = (1-\alpha)\boldsymbol{z}^{(i)} + \alpha\boldsymbol{x}^{(i)}, \tag{7.8}$$

where $\alpha \in [0,1]$ is a gain parameter. We have in our implementations perhaps (mis)named this filter for alpha mixing, as we "mix" some of the predicted and measured values in a new estimate. Note that for $\alpha = 0$ we only keep the predicted value $\boldsymbol{z}^{(i)}$ whereas for $\alpha = 1$ we keep the raw measurements $\boldsymbol{x}^{(i)}$. The alpha filter suffers from the fact that finding a good value for α is largely decided by trial and error. In our code we have dubbed the measurement vector by `trial_vector` and the predicted estimate by `direction_vector`.

7.3.2 Direct inversion of the iterative subspace

A more sophisticated acceleration technique is DIIS (direction inversion of the iterative subspace) acceleration [6, 74–76]. In order to estimate a measured vector $\mathbf{p}_{i+1}$ at a certain step $i+1$ we use the linear combination

$$\bar{\mathbf{p}}_{i+1} = \sum_{k=1}^{i} c_k \mathbf{p}_i, \tag{7.9}$$

where $\bar{\mathbf{p}}_{i+1}$ is the estimated value at step $i+1$, and c_k is a set of unknown coefficients subject to the constraint that they should sum up to unity at every step i. In order to find the coefficients, we construct an error vector $\boldsymbol{e}_i$ from $\mathbf{p}_i$. This step is dependent on the solver we are looking at and will be postponed to the implementation chapters on Hartree-Fock and coupled-cluster. For now, consider the extrapolated error vector

$$\bar{\boldsymbol{e}}_{i+1} = \sum_{k=1}^{i} c_k \boldsymbol{e}_k, \tag{7.10}$$

calculated from the measured error vectors. We now wish to minimize the error, and we do this using Lagrange's method of undetermined multipliers in order to include the constraint that the coefficients should sum up to unity, viz.

$$L = \|\bar{\boldsymbol{e}}_i\|^2 - 2\lambda\left(\sum_{k=1}^{i} c_i - 1\right). \tag{7.11}$$

We see that this is a least squares approach where we minimize the error vectors subject to a constraint. The squared norm of the error vectors can be expressed by

$$\|\bar{\mathbf{e}}_i\|^2 = c_k B_{kl} c_l, \tag{7.12}$$

where we have defined the matrix elements

$$B_{kl} \equiv \boldsymbol{e}_k^T \boldsymbol{e}_l. \tag{7.13}$$

Finding the stationary condition of the Lagrangian in Equation 7.11 with respect to the coefficients c_k we get a system of i linear equations. This can be expressed as matrices by

$$\begin{pmatrix} B_{11} & \dots & B_{1i} & -1 \\ \vdots & \ddots & \vdots & \vdots \\ B_{i1} & \dots & B_{ii} & -1 \\ -1 & \dots & -1 & 0 \end{pmatrix} \begin{pmatrix} c_1 \\ \vdots \\ c_i \\ \lambda \end{pmatrix} = \begin{pmatrix} 0 \\ \vdots \\ 0 \\ -1 \end{pmatrix}. \tag{7.14}$$

Solving this equation for the coefficients c_k we are able to compute the estimated quantity $\bar{\mathbf{p}}_i$ from Equation 7.9. An existing implementation of the DIIS algorithm was given to us by Myhre as part of his article "Demonstrating that the nonorthogonal orbital optimized coupled cluster model converges to full configuration interaction" [21] and has been integrated by the author into the libraries we have created. This makes the method available to all Hartree-Fock solvers and all coupled-cluster implementations.

The DIIS method suffers from the fact that we store all i previous measurements in memory. In the case of large systems this can become a problem as we spend all our memory in the acceleration. We can therefore adjust the number of vectors, i.e., i, in order to limit the memory occupied by DIIS.

7.4 Numerical integration

In this section we will review a select few time-integration schemes for solving time-dependent ordinary differential equations and we will discuss the applicability of each scheme.

7.4.1 Problem statement

The problem we are trying to solve can be formulated as

$$\dot{\mathbf{y}}(t) = \mathbf{F}(\mathbf{y}, t), \tag{7.15}$$

where $\dot{\mathbf{y}}(t)$ is the derivative of the vector $\mathbf{y}(t)$ with respect to time. The function $\mathbf{F}(\mathbf{y}, t)$ is a vector valued function evaluating the right-hand side of the first-order differential equation listed above. Most implemented integration schemes assume that the problem can be formulated as in Equation 7.15, but as we have seen the time-dependent Hartree-Fock method is defined in terms of a matrix, and the time-dependet coupled-cluster methods as two sets of amplitudes of different sizes and coefficient matrices for the orbital-adaptive methods. To get around this we let each time-dependent solver class implement a Python dunder method[3] `__call__` which accepts the two parameters `y` and `t` to represent the right-hand side function $\mathbf{F}(\mathbf{y}, t)$. The innards of this method can now be describe by the following steps:

1. Make sure the vector $\mathbf{y}$ is reshaped to the correct formulation as required by the right-hand sides. For configuration interaction this is handled automatically, but for the time-dependent Hartree-Fock method this means that we need to reshape the vector into a coefficient matrix. For the time-dependent coupled-cluster methods this is even more involved and will be discussed in due time.

2. Update the time-dependent Hamiltonian to the current time step `t`.

3. Compute the right-hand sides to get the derivative of the coefficients and amplitudes.

4. Convert the coefficients and amplitudes to a new vector $\dot{\mathbf{y}}$ and return this to the differential equation solver.

Now, the process of stacking all the elements in the coefficient matrices and amplitudes as a single vector is possible as each index is independent of each other in terms of time evolution. However, they do coupled when evaluating the right-hand sides and we therefore need to recover the original shape. Most differential equation libraries [70] [77] assume the right-hand side to be a callable function with a `__call__`-method. Annoyingly enough, there seems to be no consensus of the ordering of the parameters to the function $\mathbf{F}(\mathbf{y}, t)$ which means that each library will require a different definition of the right-hand side functions. In the current implementation of our programs we have chosen the ordering $\mathbf{F}(\mathbf{y}, t)$, but for us to use differential equation solvers from SymPy [70] or diffeqpy [77] we need to reverse the order, or add extra parameters. This process will be discussed more in section 13.1 as we have not implemented an interface towards these libraries in this work.

[3] A "dunder method" is a special Python function denoted with a double underscore in front and behind of the name. These are often magic methods in the sense that they either overwrite operators, such as: `__add__` for addition, `__mul__` for multiplication, etc, or that they define some special functionality, e.g., `__init__` as the constructor for a class.

Discretizing time with a constant step Δt such that $t_n = t_0 + n\Delta t$ for $n \in \{0, N_t\}$, where N_t is the number of time steps and t_0 is the initial time step. Note that we typically choose a time step Δt such that N_t can be found by

$$N_t = \left\lfloor \frac{t_f - t_0}{\Delta t} \right\rfloor + 1, \tag{7.16}$$

where t_f is the final time step. We denote $\mathbf{y}_0 \equiv \mathbf{y}(t_0)$ and $\mathbf{y}_n \equiv \mathbf{y}(t_n)$, where $\mathbf{y}_0$ is the initial value of the problem. In this thesis we will always choose the initial value to be the ground state of the specific solver. This abstraction thus enables us to work with known ordinary differential equation solvers formulated in a familiar way.

As a first approximation to solving the time-dependent equations, we have implemented the Runge-Kutta 4 algorithm. A rendition of this algorithm can be found in *Numerical Algorithms and Digital Representation* [78] and will not be repeated in this text as all results are achieved using the more sophisticated Gauss-Legendre integrator which will be discussed shortly. Runge-Kutta 4 is a fourth-order method with a local numerical error of the order of $\mathcal{O}(h^5)$ and a total error of $\mathcal{O}(h^4)$.

7.4.2 Symplectic integrators

Looking back to section 2.7 we note that for a time-dependent Hamiltonian in the Schrödinger picture, the time evolution of a state $|\psi(t)\rangle$ is described by the time evolution operator shown in Equation 2.79, where the Hamiltonian in general does not commute at different time steps. It is perhaps somewhat naïve to hope for a numerical method such as Runge-Kutta 4 to yield good results without some extra concern for the problem at hand. As discussed by Goings *et al.* [8] the solution to the time-dependent Schrödinger equation can be better approximated by the Magnus expansion [79]. This leads to implicit integration methods that are *symplectic* [8]. These methods will to a much larger degree conserve the energy, normalization, and unitarity of the coefficients and amplitudes as opposed to the explicit schemes such as Runge-Kutta 4 [8, 22]. One of the first approximations to the Magnus expansion is the Crank-Nicolson algorithm [4, 8].

7.4.3 Gauss-Legendre

In an article on the stability of the time-dependent coupled-cluster singles-and-doubles method on atomic systems subject to intense laser pulses, Pedersen & Kvaal [22] used symplectic, implicit Runge-Kutta methods in an attempt to alleviate some of the stability issues they faced. As part of an

ongoing publication on the stability of time-dependent coupled-cluster methods [66] we have been given the implementation of the Gauss-integrator[4] as used by Pedersen & Kvaal [22] to include it in our libraries. This method is described in depth in their text "Symplectic integration and physical interpretation of time-dependent coupled-cluster theory" [22] and will not be renditioned in this work. However, we will state that the order of the Gauss-integrator is determined by a parameter $s \in \{1, 2, 3\}$ deciding the order of the Gauss-Legendre polynomial used in the integrator. Furthermore, the integrator uses fix-point iterations in each time step. This means that we have to set a tolerance ϵ for when the iteration is considered converged.

[4]Note that the name "Gauss-integrator" is a notoriously ambiguous name as this can refer to a multitude of techniques and solvers due to the use of named polynomials such as Legendre, and Laguerre polynomials, etc.

Chapter 8

Quantum systems

In this chapter we will discuss the different quantum systems which will be explored in this thesis. We will discuss how we represent a general quantum system via the class `QuantumSystem` and the methods that this class incorporates. Before delving into the mathematics of quantum dots, and atoms and molecules, we will discuss what we want from our basis sets.

1. For all types of calculations we need access to the one- and two-body matrix elements of the Hamiltonian, and potentially the nuclear repulsion energy. That is, we need to find values for h_q^p and u_{rs}^{pq} as defined in Equation 3.138 and Equation 3.139 respectively. In case of a non-orthonormal basis set we also need the overlap matrix elements s_q^p between the single-particle states.

2. For time evolution, using a dipole laser we need the dipole matrix elements $\mathbf{d}_q^p$ given by

$$\mathbf{d}_q^p = \langle \psi_p | \hat{\mathbf{d}} | \psi_q \rangle \,, \tag{8.1}$$

   as defined in Equation 2.127.

3. For visualization of the particle density we need the single-particle states themselves, or at least the ability to evaluate the single-particle states on some grid.

If our only interest is the ground state energy, we can get far with point 1 listed above. However, for us to include interactions with a laser field we also need the dipole matrix elements as we are working in the dipole approximation. The single-particle states are necessary for visualization of the system on a grid either via the particle density or by themselves. We will visualize some of our systems to get a qualitative description of what we are looking at, but often we are more interested in quanitifying our results and the

single-particle states are not necessarily needed. That is, they are of course needed when computing the integrals for the matrix elements, but an explicit evaluation of the single-particle states on a grid is not always necessary. The Python class `QuantumSystem` therefore builds the basis sets and serves as a container with the necessary matrix elements listed above, and methods for manipulating these elements.

Often the limitation of basis sets comes from the calculation of the two-body matrix elements as these integrals will in many cases be the computational bottleneck. This is the reason why we often seek systems with analytical solutions to the most intensive integrals – or easier integral evaluation – and then do a basis transformation using the variational method, and eventually Hartree-Fock to build more complicated systems. As part of this thesis we have implemented several systems, they are:

1. The one-dimensional quantum dot on a grid supporting arbitrary one-dimensional potentials.

2. The two-dimensional quantum dot in a harmonic oscillator, in a sharp double well, in a smooth double well, and subject to a magnetic field.

In this thesis we will look briefly at the one-dimensional quantum dot. The two-dimensional quantum dots are discussed in the thesis by Winther-Larsen [17]. The main focus in this thesis are atoms and molecules. The subject of atomic and molecular basis sets is a vast topic in quantum chemistry [6]. To avoid reinventing the wheel we have implemented an interface towards the existing libraries PySCF [18] and Psi4 [19] in order to get access to good and efficient basis sets for atoms and molecules. Furthermore, we will explore *bound systems* which we take to mean that the underlying basis set will be trapped in a potential well and that the states will be held fixed in time. All time evolution occurs in the coefficients and amplitudes of the solver methods. This means that we will have a hard time modelling ionization as this requires the inclusion of continuum states to allow particles to move out of the trapping potential. An alternative is the usage of a time-dependent grid solver for the basis set [80], but this has not been implemented in this thesis.

8.1 One-dimensional quantum dots

Artificial atoms, or the so-called quantum dots, constitute a hot topic in condensed matter physics and material sciences [5, 13, 81, 82]. We will be exploring several types of quantum dots in both one and two dimensions in this thesis. The difference between the types of quantum dots is found in the one-body potential. All of the dots share the characteristic of being in an

infinite well which makes the systems *bound*. In our study of systems subject to intense laser fields, this will prove to be a bad approximation when the laser becomes very strong as the particles have no way of being ionized, i.e., escaping the potential well. Even so, for weak laser fields and for ground state calculations, they serve as excellent candidates for our methods.

The time-independent one-dimensional quantum dot can be described by the one-body Hamiltonian

$$h(x) = -\frac{\hbar^2}{2m}\frac{d^2}{dx^2} + v(x), \tag{8.2}$$

where $v(x)$ is a potential function. In one dimension it is quite cheap to define a grid and use finite differences to solve the one-dimensional Schrödinger equation. Furthermore, for the systems we explore, numerically solving the Coulomb integrals is also feasible. This solution has its drawbacks in that we approximate an infinite integral on a finite line, but it also has the advantage of being "blind" to the choice of potential. This makes the solution completely general and opens up for a wide variety of potentials without the need for any extra mathematics.

8.1.1 Discretizing the one-dimensional quantum dot

For a given one-body Hamiltonian $h(x)$ on the form described in Equation 8.2, we wish to find a solution to the time-indepedent Schrödinger equation

$$h(x)\psi(x) = \epsilon\psi(x), \tag{8.3}$$

where we've ignored labels on the eigenpair $(\epsilon, \psi(x))$ for now to avoid clutter. However, be aware that we are looking for the spectrum of the one-body Hamiltonian. We use the central finite difference scheme for the kinetic term in the one-body Hamiltonian, that is,

$$\frac{d^2\psi(x)}{dx^2} = \frac{\psi(x+\Delta x) - 2\psi(x) + \psi(x-\Delta x)}{(\Delta x)^2} + \mathcal{O}\left((\Delta x)^2\right). \tag{8.4}$$

Now we can write the time-independent Schrödinger equation in the fully discretized form

$$h(x)\psi(x) = -\frac{1}{2}\frac{\psi(x+\Delta x) - 2\psi(x) + \psi(x-\Delta x)}{(\Delta x)^2} + v(x)\psi(x) = \epsilon\psi(x), \tag{8.5}$$

where we use atomic units. Introducing the uniformly discretized grid x_i where $i \in \{1, n\}$ and n is the number of grid points, we label the wave function by

$$\psi_i \equiv \psi(x_i), \tag{8.6}$$

and similarly for the one-body Hamiltonian and the potential. By including the entire grid we denote the eigenstate as a vector $\boldsymbol{\psi}$. We have that

$$x_{i+1} = x_i + \Delta x, \tag{8.7}$$

with Δx being the step-size between the grid points. There are smarter grid choices than the uniform grid, but for our simulations the uniform grid is sufficient. Collecting the wave function evaluated at the same grid points in the time-independent Schrödinger equation we can write the equation as

$$h\psi_i = \left(\frac{1}{(\Delta x)^2} + v_i\right)\psi_i - \frac{1}{2(\Delta x)^2}\left(\psi_{i+1} + \psi_{i-1}\right) = \epsilon\psi_i. \tag{8.8}$$

We are now in a position to formulate this equation as an eigenvalue equation on the form

$$\mathbf{h}\boldsymbol{\psi} = \boldsymbol{\epsilon}\boldsymbol{\psi}, \tag{8.9}$$

where the one-body Hamiltonian matrix is a tridiagonal matrix with diagonal elements

$$h_{ii} = \frac{1}{(\Delta x)^2} + v_i \tag{8.10}$$

and off-diagonal elements

$$h_{ij} = -\frac{1}{2(\Delta x)^2}\left(\delta_{(i+1)j} + \delta_{(i-1)j}\right). \tag{8.11}$$

We now wish to diagonalize Equation 8.9 and find all eigenpairs $(\epsilon_k, \boldsymbol{\psi}_k)$. As $\mathbf{h}$ is Hermitian we have that [47]

$$\mathbf{h} = \mathbf{P}^{-1}\mathbf{D}\mathbf{P} = \mathbf{P}^{\dagger}\mathbf{D}\mathbf{P}, \tag{8.12}$$

where $\mathbf{P} \in \mathbb{C}^{n\times n}$ and $\mathbf{D} = \text{diag}(\epsilon_1, \ldots, \epsilon_n)$. The columns of $\mathbf{P}$ will now be the eigenstates $\boldsymbol{\psi}_k$ with the elements indexed by

$$P_{ik} = \psi_k(x_i). \tag{8.13}$$

The quality of the eigenpairs is dependent on the number of grid points n, and ideally we should include many grid points such that $\Delta x \to 0$. However, we are not in a position to utilize all n eigenstates in the later analysis and we will therefore truncate the number of orbitals to the number of basis functions L that we wish to include. Furthermore, the systems we are exploring are spin-independent which means that we only use $L/2$ orbitals from the spectrum of $\mathbf{h}$, thus halving the number of single-particle functions.

We use the function `np.linalg.eigh` from NumPy [69] to solve the eigenvalue equation in Equation 8.9. This means that the eigenstates $\boldsymbol{\psi}_k$ are normalized to unity with respect to the dot-product, that is,

$$\boldsymbol{\psi}_i^\dagger \boldsymbol{\psi}_j = \delta_{ij}. \tag{8.14}$$

However, we wish to normalize the states to unity with respect to the integral inner product. To solve this we compute the normalized eigenstates $\tilde{\mathbf{P}}$ by

$$\tilde{\mathbf{P}} = \frac{\mathbf{P}}{\Delta x}, \tag{8.15}$$

where an elementwise division is assumed. Lastly, we have not discussed the boundary conditions for the eigenstates. We require that $\psi_p(-\infty) = \psi_p(\infty) = 0$. We can realize this by introducing two extra grid points $i = 0$ and $i = n+1$ after we have diagonalized the one-body Hamiltonian matrix and set

$$\psi_p(x_0) = \psi_p(x_{n+1}) = 0. \tag{8.16}$$

Having found the eigenpairs for the one-dimensional Hamiltonian, we construct a new diagonal, one-dimensional Hamiltonian from the eigenenergies. The normalized eigenstates from the eigenvalue equation will be orthonormal.

8.1.2 Constructing the dipole moments

The matrix elements of the dipole moment for the one-dimensional quantum dot is given by

$$d_{pq} = \langle \psi_p | \hat{x} | \psi_q \rangle = \int_{-\infty}^{\infty} dx \psi_p^*(x) x \psi_q(x). \tag{8.17}$$

As we are using a grid based solution, we approximate this integral using a numerical integration scheme on the grid. In our implementation we use the trapezoidal rule. By defining

$$f_{pq}(x) = \psi_p^*(x) x \psi_q(x), \tag{8.18}$$

and given a uniform grid for $x_i \in [a, b]$ where $i \in \{1, n\}$ such that $x_1 = a$ and $x_n = b$ with grid spacing Δx, we approximate the dipole elements by

$$d_{pq} \approx \frac{\Delta x}{2} \sum_{i=2}^{n} \left[f_{pq}(x_i) + f_{pq}(x_{i-1}) \right]. \tag{8.19}$$

The reason for choosing the trapezoidal rule is for its ease of usage and implementation, as well as the method being quite fast and precise. Furthermore, as our implementation is written in pure Python, we use Numba [83] to speed up explicit for-loops, but Numba does not support the usage of already implemented integrators. Thus, by writing the trapezoidal rule by hand and using Numba to *just-in-time*-compile[1] the function, we gain a significant speed-up over regular Python. It is however, not the best integrator there is and more precise solutions should be considered.

8.1.3 Integrating the Coulomb elements

The arguably heaviest computation in setting up a one-dimensional quantum dot system, is the Coulomb integrals. In atomic units the one-dimensional Coulomb interaction can be represented by

$$u(x_i, x_j) = \frac{1}{|x_i - x_j|}. \tag{8.20}$$

Now, there are a few drawbacks of using this interaction. For example, when integrating on a grid, we get numerical instabilities at the singularity when $x_1 = x_2$. This motivates the introduction of a *shielded Coulomb interaction* [85] given by

$$u(x_i, x_j) = \frac{\alpha}{\sqrt{(x_i - x_j)^2 + a^2}}, \tag{8.21}$$

where α is a dimensionless constant and the screening parameter a removes the singularity while retaining the asymptotic behavior when $(x_i - x_j) \to \infty$ [85]. The integral we wish to solve is then

$$\langle \psi_p \psi_q | \hat{u} | \psi_r \psi_s \rangle = \int dx_1 dx_2 \psi_p^*(x_1) \psi_q^*(x_2) u(x_1, x_2) \psi_r(x_1) \psi_s(x_2), \tag{8.22}$$

where $u(x_1, x_2)$ is the shielded Coulomb interaction. We introduce the inner integral $W_{qs}(x_1)$ given by

$$W_{qs}(x_1) = \int dx_2 \psi_q^*(x_2) u(x_1, x_2) \psi_s(x_2), \tag{8.23}$$

[1] Just-in-time compilation, or just "jit" compilation, is a technique where code is compiled during execution. As Python is an interpreted language Numba [83] can be used to compile certain functions to LLVM (Low Level Virtual Machine) [84] once they are encountered. After the initial hold-up from the compilation, this can lead to a truly impressive speed-up of the original code. For a small demonstration of this see: `https://github.com/Schoyen/Mandelbrot`.

that is, we integrate over one of the two spatial integrals in the Coulomb interaction. We can thus write the Coulomb elements as

$$\langle \psi_p \psi_q | \hat{u} | \psi_r \psi_s \rangle = \langle \psi_p | \hat{W}_{qs} | \psi_r \rangle = \int dx_1 \psi_p^*(x_1) W_{qs}(x_1) \psi_r(x_1), \tag{8.24}$$

where we initially compute the inner integral $W_{qs}(x_1)$ on the entire grid and store it as a vector. We define the functions

$$g_{qs}(x_i, x) = \psi_q^*(x) u(x_i, x) \psi_s(x), \tag{8.25}$$

$$v_{rs}^{pq}(x_i) = \psi_p^*(x_i) W_{qs}(x_i) \psi_r(x_i), \tag{8.26}$$

that is, the functions that occur under the integrals in the inner, and the outer Coulomb integral respectively. We can now compute the inner integrals using the trapezoidal rule in the same manner as for the dipole elements. That is, for a given point x_i we have

$$W_{qs}(x_i) \approx \frac{\Delta x}{2} \sum_{j=2}^{n} \left[g_{qs}(x_i, x_j) + g_{qs}(x_i, x_{j-1}) \right]. \tag{8.27}$$

From this we can compute the Coulomb elements by

$$\langle \psi_p \psi_q | \hat{u} | \psi_r \psi_s \rangle \approx \frac{\Delta x}{2} \sum_{i=2}^{n} \left[v_{rs}^{pq}(x_i) + v_{rs}^{pq}(x_{i-1}) \right]. \tag{8.28}$$

Again, we emphasize that the choice of using the trapezoidal rule is based on convenience and can be replaced by a better integrator if it turns out that the integrals are too erroneous.

8.2 Atomic and molecular systems

Having discussed systems of quantum dots, or so-called "artificial atoms", we will now focus on actual atomic and molecular systems. As stated at the start of this chapter we make use of existing libraries to construct atomic and molecular basis sets. We will therefore touch briefly on the topic of atomic and molecular basis sets as much of the work therein will be treated as a black box. The molecular electronic one-body Hamiltonian in the Born-Oppenheimer approximation is given by [16, 86]

$$\hat{h}_i = -\frac{1}{2}\nabla_i^2 - \frac{Z_A}{|\mathbf{R}_A - \mathbf{r}_i|}, \tag{8.29}$$

where atomic units are assumed. Note that we sum over all nuclei A. Here we have left out the internuclear repulsion and the Coulomb interaction. Furthermore, in the Born-Oppenheimer approximation we treat the nuclei as being frozen and therefore ignore the kinetic energy contribution of the nuclear core.

Now, perhaps not surprisingly the exact solution of the full molecular Hamiltonian[2] is a far fetched goal for all but the smallest systems to say the least. We can solve the molecular Hamiltonian in an approximate basis set. We can then diagonalize the one-body Hamiltonian and express the matrix elements in this new basis. As a consequence a lot of effort in the quantum chemistry field has been put into the construction of efficient and good basis sets. We will in this thesis use the following basis sets:

- The minimal Slater-type orbital (STO-kG) basis sets [87]. Here k denotes the number of Gaussian primitive functions used in a single basis function.
- The split-valence (X-YZg) basis sets [88]. Here X denotes the number of primitive Gaussian functions for the core basis functions. The Y and Z tells us that there are two sets of basis functions with Y and Z basis functions for the valence orbitals respectively.
- The correlation-consistent polarized valence (cc-pVXZ) basis sets [89]. These basis sets are better tuned for post Hartree-Fock methods. The X parameter decides the number of functions for the valence electrons [89].
- The augmented correlation-consistent (aug-cc-pVXZ) basis sets [90]. The cc-pVXZ basis sets are designed for ground state calculations, but are inferior when it comes to describing excited states. The aug-cc-pVXZ basis functions alleviates some of this by incuding diffuse functions for the outer valence electrons [6]. The parameter X is the same as in the case of the cc-pVXZ basis set.

To reuse the basis sets from PySCF [18] and Psi4 [19] we have created a class `CustomSystem` which lets us build a `QuantumSystem`-class by manually setting the matrix elements. We can thus ask PySCF and Psi4 to use their well-optimized methods to generate basis sets and reuse these in our solvers. In this thesis we will only use basis sets from PySCF and we therefore only describe the interface towards this library.

We have created three interface functions which sets up a `CustomSystem` of atomic orbitals, restricted molecular orbitals, and unrestricted molecular orbitals respectively. The two latter methods use the restricted and unrestricted

[2] Even in the Born-Oppenheimer approximation.

Hartree-Fock solvers of PySCF. There are two main input parameters to these functions and that is `molecule` and `basis`. The former is a string describing the atom or molecule. In case of an atom it is enough to write the chemical symbol for the atom, e.g., `"he"` for Helium. For molecules the coordinates of the atoms contained in the system must be included. In the case of diatomic molecules we can then specify a bond distance along a specific axis, e.g., `f"h 0 0 0; h 0 0 1.2"` for the H_2 molecule with the bond distance 1.2 specified in atomic units along the z-axis. The basis strings share the same format as discussed above, e.g., to specify the usage of aug-cc-pVDZ, we pass in the string `"aug-ccpvdz"` as the basis.

8.3 Particle density

From subsection 3.8.2 we know how to compute the one-body particle density once we have found the one-body density matrix from a specific solver. For variational methods where the dual state of $|\phi_p\rangle$ is the adjoint $\langle\phi_p|$ we can use the expression in Equation 3.156. However, as we are focusing much of our work on the bi-variational formulation of coupled-cluster we will implement the more general particle-density calculation

$$\rho(x) = \tilde{\phi}_q(x)\rho_p^q\phi_p(x), \tag{8.30}$$

where $\tilde{\phi}_q(x)$ is the bi-variational dual state of $\phi_p(x)$. For the Hartree-Fock methods and configuration interaction solvers we choose $\tilde{\phi}_q(x) = \phi_q^*(x)$ and we have recovered the original expression for the particle density as seen in Equation 3.156. In Program 1 we have included the code used to compute the particle density given a one-body density matrix denoted `rho_qp`, and the set of orbitals `bra_spf` and `ket_spf` as the bra- and ket-states respectively. We let the first index (the rows) of the orbital arrays denote the orbital index p, q, etc, whereas the remaining indices define the evaluation of the function on a d-dimensional grid $x \in \mathbb{C}^d$.

8.4 Change of basis

Much of what we do in this thesis is related to basis transformations. Either by diagonalization of the one-body Hamiltonian, an initial Hartree-Fock calculation, or in the orbital rotations in the non-orthogonal and orbital-adaptive coupled-cluster methods. A basis transformation can in general be represented by

$$|\psi_p\rangle = C_{\alpha p}\,|\phi_\alpha\rangle\,, \tag{8.31}$$

Program 1 In this listing we have added a function computing the particle density on an arbitrary grid that the orbitals are evaluated on.

```
def compute_particle_density(rho_qp, bra_spf, ket_spf):
    rho = np.zeros(ket_spf.shape[1:], dtype=ket_spf.dtype)
    spf_slice = slice(0, ket_spf.shape[0])

    for _i in np.ndindex(rho.shape):
        i = (spf_slice, *_i)
        rho[_i] += np.dot(bra_spf[i], np.dot(rho_qp, ket_spf[i]))

    return rho
```

where we use greek indices to denote a basis of K orbitals $\{\phi_\alpha\}$ and latin letters for the basis of L transformed orbitals $\{\psi_p\}$, and where $\mathbf{C} \in \mathbb{C}^{K\times L}$ is a complex matrix with the coefficients necessary for the transformation.

Having found the coefficient matrix $\mathbf{C}$ we can change basis for all the existing matrix elements stored in the `QuantumSystem`-class. We will also here assume for the sake of generality that the dual states $\tilde{\psi}_p$ and $\tilde{\phi}_\alpha$ are not necessarily the adjoints of ψ_p and ϕ_α. This means that

$$\langle\tilde{\psi}_p| = \tilde{C}_{p\alpha}\langle\tilde{\phi}_\alpha|\,. \tag{8.32}$$

Take extra note of the ordering of the indices in the coefficients in the dual basis transformation. In the case of adjoint states we have the familiar $\tilde{C}_{p\alpha} = C^*_{\alpha p}$. From the list of contents in `QuantumSystem` at the top of this chapter, we have three types of basis transformations that we need to support to fully change our system. We need to be able to change basis for one- and two-body matrix elements, and for the single-particle functions.

We denote arbitrary one-body matrix elements of the one-body matrix $\mathbf{h}$ in the original orbital basis by

$$h_{\alpha\beta} \equiv \langle\tilde{\phi}_\alpha|\hat{h}|\phi_\beta\rangle\,. \tag{8.33}$$

Transforming to the new basis set we have

$$\tilde{h}_{pq} = \langle\tilde{\psi}_p|\hat{h}|\psi_q\rangle = \tilde{C}_{p\alpha}h_{\alpha\beta}C_{\beta q} \implies \tilde{\mathbf{h}} = \tilde{\mathbf{C}}\mathbf{h}\mathbf{C}, \tag{8.34}$$

where $\tilde{\mathbf{h}}$ is the transformed one-body elements. An implementation of the change of basis for the one-body elements is shown in Program 2. In the case of the dipole moments we store these as an array of one-body elements, one for every dimension, which means that we need to transform each axis using the algorithm in Program 2. For the two-body elements we denote the elements by

$$u^{\alpha\beta}_{\gamma\delta} \equiv \langle\tilde{\phi}_\alpha\tilde{\phi}_\beta|\hat{u}|\phi_\gamma\phi_\delta\rangle\,, \tag{8.35}$$

Program 2 This function changes basis for the one-body matrix elements given a coefficient matrix `c` and an optional dual coefficient matrix `c_tilde`.

```
def transform_one_body_elements(h, c, c_tilde=None):
    if c_tilde is None:
        c_tilde = c.conj().T

    return c_tilde @ h @ c
```

where we do not care if the elements are antisymmetric or not as it does not change the basis transformation. The transformation can now be done by

$$\tilde{u}_{rs}^{pq} = \langle \psi_p \psi_q | \hat{u} | \psi_r \psi_s \rangle = \tilde{C}_{p\alpha} \tilde{C}_{q\beta} u_{\gamma\delta}^{\alpha\beta} C_{\gamma r} C_{\delta s}. \tag{8.36}$$

In Program 3 we demonstrate the function which changes the basis for the two-body elements. We make use of temporary storage of a two-body matrix `_u` which lowers the cost of the basis transformation from $\mathcal{O}(L^8)$ to $\mathcal{O}(L^5)$. For

Program 3 This function changes the basis of the two-body elements given a coefficient matrix `c` and an optional dual matrix `c_tilde`.

```
def transform_two_body_elements(u, c, c_tilde=None):
    if c_tilde is None:
        c_tilde = c.conj().T

    # abcd, ds -> abcs
    _u = np.tensordot(u, c, axes=(3, 0))
    # abcs, cr -> absr -> abrs
    _u = np.tensordot(_u, c, axes=(2, 0)).transpose(0, 1, 3, 2)
    # abrs, qb -> arsq -> aqrs
    _u = np.tensordot(_u, c_tilde, axes=(1, 1)).transpose(
        0, 3, 1, 2
    )
    # pa, aqrs -> pqrs
    _u = np.tensordot(c_tilde, _u, axes=(1, 0))

    return _u
```

the single-particle functions the basis transformation is performed by Equation 8.31 and Equation 8.32 where the states are projected on a grid. We represent all the single-particle states as a $d+1$-dimensional array, where the first axis denotes which single-particle state we are looking at, and the d-remaining axes denotes the grid. In Program 4 we show the member function of `QuantumSystem` for changing the single-particle state basis.

Program 4 Here we list the member function in `QuantumSystem` that transforms the single-particle states given a coefficient matrix `c` and an optional dual matrix `c_tilde`. The single-particle states are denoted `self._spf` and `self._bra_spf` in case of a dual state that is not the adjoint state.

```
class QuantumSystem:
    # Code removed for clarity

    def change_basis_spf(self, c, c_tilde=None):
        if c_tilde is not None:
            # In case of bi-orthogonal basis sets, we create an
            # extra set of single-particle functions for
            # the bra-side
            self._bra_spf = self.np.tensordot(
                c_tilde,
                self._spf.conj()
                if self._bra_spf is None else self._bra_spf,
                axes=((1), (0)),
            )

        self._spf = self.np.tensordot(
            c, self._spf, axes=((0), (0))
        )
```

8.5 Spin-doubling

The basis sets we are exploring are always formulated as spatial orbitals without any spin component. Furthermore, we look at spin-independent Hamiltonians for the most part[3] and a restricted solution can be used where we incorporate the spin by reusing the doubly occupied orbitals. We will use this to some extent for the restricted Hartree-Fock solver which will be discussed in subsection 9.1.5. However, most of the methods we have implemented make no assumption on the spin-orbitals other than there being two spin-components, and therefore allow general spin-orbitals as discussed in subsection 3.5.1. This means that after we have created our basis sets, we include spin by making the system doubly degenerate in each orbital.

The ordering of the spin-orbitals are important as some solvers exploit the spin-degeneracy and therefore need to know how the spin-orbitals are ordered. We have chosen a solution which is far from optimal, but which is reasonable as long as we have an even number of particles with the same amount of particles in each spin direction. We use the convention that orbitals are ordered in an increasing order based on their single-particle eigenenergy.[4]

[3] We explore a spin-dependent laser field to some extent as will be demonstrated in the results.

[4] This is the ordering that is returned by NumPy when diagonalizing the one-body Hamil-

We then double the length of each orbital axis in the single-particle functions,[5] the one-body- and two-body Hamiltonians, and all other matrix elements. Next we repeat each orbital twice so that even indices correspond to a certain spin direction and odd indices to the other direction. We are able to achieve this quite succintly using the Kronecker-product and slicing in NumPy. In Program 5 we demonstrate a snippet which adds spin to a set of orbitals defined on an arbitrary grid. For the one-body elements we use the function

Program 5 Spin-doubling of the single-particle functions.

```
class QuantumSystem:
    # Code removed for clarity

    def change_to_spin_orbital_basis(self, anti_symmetrize=True):
        # Code removed for clarity

        if not self._spf is None:
            new_shape = [
                self._spf.shape[0] * 2, *self._spf.shape[1:]
            ]

            spf = self.np.zeros(
                tuple(new_shape), dtype=self._spf.dtype
            )
            spf[::2] += self._spf
            spf[1::2] += self._spf

            self._spf = spf
            assert self._spf.shape[0] == self.l
```

listed in Program 6. The two-body elements requires us to do some more work as the Kronecker product gets applied to the two last indices of the array. We also want the product to be applied to pairwise indices that interact in the two-body integrals. This requires some transposing of the elements, and is shown in Program 7.

Program 6 Function adding spin to one-body matrix elements, that is, matrices.

```
def add_spin_one_body(h):
    return np.kron(h, np.eye(2))
```

A more general solution – and which should be implemented in the future – is to create spin-blocks with each spin direction following each other as this

tonian.

[5] Except for the grid axes.

Program 7 Function adding spin to the two-body elements.

```
def add_spin_two_body(_u):
    u = _u.transpose(1, 3, 0, 2)
    u = np.kron(u, np.eye(2))
    u = u.transpose(2, 3, 0, 1)
    u = np.kron(u, np.eye(2))
    u = u.transpose(0, 2, 1, 3)

    return u
```

allows for an unequal number of particles in each spin direction. This is the solution that needs to be taken for the unrestricted Hartree-Fock method when changing basis.

8.6 Time evolution operators

The only time evolution operators used in this thesis are dipole lasers in the length gauge. We have implemented this by allowing `QuantumSystem` to have a pointer to a `TimeEvolutionOperator`-class, where `LaserField` is a subclass. The `LaserField`-class takes in the parameter `laser_pulse` and an optional `polarization_vector`. The former parameter is the electric field of the laser including the envelope function, whereas the latter defines which axis to polarize along. By default the polarization vector is set along the x-axis, that is, the first axis. Note that `QuantumSystem` so far does not have a charge which means that for negative charge either the pulse or the polarization vector needs to incorporate this sign. Both `laser_pulse` and `polarization_vector` can be constants or functions of a single parameter; time. We restrict our attention to a constant linear polarization, but we use time-dependent laser pulses. To specify a laser pulse, the user creates a function or a class with a `__call__`-method which takes in a single parameter as time. This function should return the electric field at the given time including the envelope function.

8.7 Measuring the dipole moment

In order to measure the dipole moment in time we use the one-body density matrix from the given solver to compute

$$\langle \mathbf{d}(t) \rangle = \rho_p^q(t) \mathbf{d}_q^p, \tag{8.37}$$

where the time-dependence is kept in the one-body density matrix. For the time-dependent Hartree-Fock method and for the orbital-adaptive time-

dependent coupled-cluster methods we have to make sure that we change basis at each time step before computing the trace of the one-body density matrix and the dipole moment. This yields a time-dependent dipole moment. Note also that we choose a specific axis of the dipole moment.

Chapter 9

Solver implementations

In this chapter we will discuss various implementation aspects of the *ab initio* solvers discussed in chapter 4 through chapter 5 and chapter 6.

9.1 Hartree-Fock

In section 4.1 we showed how the variational principle of the Hartree-Fock ansatz led to the canonical Hartree-Fock equations, where the molecular orbitals are the primary unknowns. Here we will demonstrate how we can find solvable equations for the molecular orbitals starting from an initial basis of atomic orbitals. We will in the following demonstrate three different procedures related to the restrictions put on the spin-orbitals as discussed in subsection 3.5.1. First we will discuss a general Hartree-Fock method which puts no restrictions on the molecular orbitals. This method leads to the molecular orbitals being described as general spin-orbitals as shown in Equation 3.80. The second method is known as the *restricted Hartree-Fock* method as it limits the molecuar orbitals to restricted spin-orbitals as in Equation 3.82. Finally, we will demonstrate the *unrestricted Hartree-Fock method* yielding unrestricted spin-orbitals for the molecular orbitals as shown in Equation 3.81.

9.1.1 Hartree-Fock with general spin-orbitals

Given a basis of K known non-orthonormal atomic orbitals $\{\chi_\alpha\}$, we wish to find an orthonomal basis of L molecular orbitals $\{\phi_p\}$ satisfying the canonical Hartree-Fock equations. We can transform from the known atomic orbital basis to the unknown molecular orbital basis by

$$|\phi_p\rangle = C_{\alpha p} |\chi_\alpha\rangle , \tag{9.1}$$

where $\mathbf{C} \in \mathbb{C}^{K \times L}$ is now our unknown coefficient matrix. The orthonormality condition of the molecular orbitals can now be formulated as

$$\langle \phi_p | \phi_q \rangle = C^*_{\alpha p} C_{\beta q} \langle \chi_\alpha | \chi_\beta \rangle = C^*_{\alpha p} s_{\alpha\beta} C_{\beta q} = \delta_{pq}, \tag{9.2}$$

where $s_{\alpha\beta}$ is the matrix elements of the overlap matrix $\mathbf{S} \in \mathbb{C}^{K \times K}$ of the atomic orbitals. In the case of an orthonormal basis of atomic orbitals, the overlap matrix $\mathbf{S} \in \mathbb{C}^{K \times K}$ reduces to the identity matrix. By left-projecting with a state from our atomic orbital basis onto the canonical Hartree-Fock equations, we obtain

$$\langle \chi_\alpha | \hat{f} | \phi_q \rangle = \epsilon_q \langle \chi_\alpha | \phi_q \rangle \implies f_{\alpha\beta} C_{\beta q} = \epsilon_q C_{\beta q} s_{\alpha\beta} \implies \mathbf{FC} = \mathbf{SC}\boldsymbol{\epsilon}, \tag{9.3}$$

where we have denoted the matrix elements of the Fock operator in the atomic orbital basis by

$$\langle \chi_\alpha | \hat{f} | \chi_\beta \rangle \equiv f_{\alpha\beta}, \tag{9.4}$$

and where $\mathbf{F} \in \mathbb{C}^{K \times K}$ is the *Fock matrix* consisting of the matrix elements defined in Equation 9.4. The diagonal matrix $\boldsymbol{\epsilon} = \text{diag}(\epsilon_1, \ldots, \epsilon_L)$ is the matrix with the orbital eigenenergies from the canonical Hartree-Fock equation. The orbital eigenenergies are indeed energies, but they are *not* the eigenenergy of the total Hamiltonian. Rather they are similar to the eigenergies of the one-body Hamiltonian, but with the Fock operator representing a one-body Hamiltonian containing a potential built from the mean-field interaction in the many-body problem. The equations in Equation 9.3 are known as the *Roothaan-Hall* equations [91, 92]. The Roothaan-Hall equations constitute a generalized eigenvalue equation.[1] These equations represent a computational improvement to the integro-differential equations that come from the canonical Hartree-Fock equations.

In Python we solve the Roothaan-Hall equations using SymPy's linear algebra routine `scipy.linalg.eigh` which solves both ordinary and generalized eigenvalue equations for symmetric and Hermitian matrices [70], viz.

```
epsilon, C = scipy.linalg.eigh(fock_matrix, s)
```

where `s` is the overlap matrix. Our solution does not discriminate whether the atomic orbitals are orthornomal or not. We always solve the generalized eigenvalue equation, and therefore pass in the idenity matrix as the overlap matrix in case of an orthonormal atomic orbital basis.

[1] The grammar sounds highly speculative as we talk about the Roothaan-Hall *equations* reducing to a single *equation*.

9.1.2 Constructing the general Fock matrix

An important point to note is that the Fock matrix elements depends on both the atomic and the molecular orbitals. That is,

$$f_{\alpha\beta} = \langle\chi_\alpha|\hat{f}|\chi_\beta\rangle = \langle\chi_\alpha|\hat{h}|\chi_\beta\rangle + \langle\chi_\alpha\phi_j|\hat{u}|\chi_\beta\phi_j\rangle_{AS}\,, \tag{9.5}$$

where j only sums over the occupied indices in the molecular orbital basis as discussed in subsection 3.6.2. We notice that only the antisymmetric two-body elements depend on the molecular orbitals. Formulating the matrix elements in terms of the known atomic orbitals and the coefficient matrix we get

$$\langle\chi_\alpha\phi_j|\hat{u}|\chi_\beta\phi_j\rangle = C^*_{\gamma j}C_{\delta j}\,\langle\chi_\alpha\chi_\gamma|\hat{u}|\chi_\beta\chi_\delta\rangle\,, \tag{9.6}$$

$$\langle\chi_\alpha\phi_j|\hat{u}|\phi_j\chi_\beta\rangle = C^*_{\gamma j}C_{\delta j}\,\langle\chi_\alpha\chi_\gamma|\hat{u}|\chi_\delta\chi_\beta\rangle\,. \tag{9.7}$$

The product of the coefficient matrices inspires the introduction of the density matrix of the occupied orbitals

$$D_{\delta\gamma} \equiv C^*_{\gamma j}C_{\delta j} \implies \mathbf{D} = \mathbf{C}_o\mathbf{C}_o^\dagger, \tag{9.8}$$

where $\mathbf{D} \in \mathbb{C}^{K\times K}$, and we have denoted the occupied coefficient matrices by $\mathbf{C}_o \in \mathbb{C}^{K\times N}$. We can compute the density matrix in Python by

```
o = slice(0, n)
density_matrix = C[:, o] @ C[:, 0].conj().T
```

where `n` is the number of occupied particles and `o` is a slice with the indices of the occupied states. We can then write the matrix elements of the Fock operator in terms of the atomic orbitals and the density matrix as

$$f_{\alpha\beta} = \langle\chi_\alpha|\hat{h}|\chi_\beta\rangle + D_{\delta\gamma}\,\langle\chi_\alpha\chi_\gamma|\hat{u}|\chi_\beta\chi_\delta\rangle_{AS}\,. \tag{9.9}$$

We use NumPy's tensor contraction routine `np.tensordot` to contract the density matrix and the two-body antisymmetric matrix. The Fock matrix can thus be constructed by

```
fock_matrix = (
    h + np.tensordot(density_matrix, u, axes=((0, 1), (3, 1)))
)
```

where `h` is the one-body matrix elements, `u` the antisymmetric two-body elements with the memory ordered by reading the indices from left to right, and `density_matrix` the density matrix.

General Hartree-Fock energy

The Hartree-Fock energy can be found by inserting the expansion of the molecular orbitals in terms of the atomic orbitals and the coefficient matrices into the energy functional from Equation 4.4. This yields

$$E = D_{\beta\alpha} \langle \chi_\alpha | \hat{h} | \chi_\beta \rangle + \frac{1}{2} D_{\gamma\alpha} D_{\delta\beta} \langle \chi_\alpha \chi_\beta | \hat{u} | \chi_\gamma \chi_\delta \rangle_{AS}, \tag{9.10}$$

where we have contracted the occupied coefficient matrices into density matrices. In Python we compute the energy by

```
energy = np.trace(np.dot(density_matrix, h))
term = 0.5 * np.tensordot(
    density_matrix, u, axes=((0, 1), (2, 0))
)
energy += np.trace(np.dot(density_matrix, term))
```

where `term` is used as a temporary storage for the contraction of one of the density matrices with the antisymmetric two-body elements.

General Hartree-Fock one-body density matrix

The one-body density matrix elements is given by

$$\rho_p^q = \langle \Phi | \hat{c}_p^\dagger \hat{c}_q | \Phi \rangle = \delta_{p \in o} C_{\alpha p}^* s_{\alpha\beta} C_{\beta q} = \delta_{p \in o} \delta_{pq}, \tag{9.11}$$

where we have labelled the set of occupied indices in the Slater determinants by $o = \{1, \ldots N\}$. We can represent the one-body density matrix as a block matrix by

$$\boldsymbol{\rho} = \begin{pmatrix} \mathbb{1}_{N \times N} & 0_{N \times M} \\ 0_{M \times N} & 0_{M \times M} \end{pmatrix}, \tag{9.12}$$

where $M = L - N$ is the number of virtual basis states. We compute the one-body density matrix by

```
o = slice(0, n)
rho_qp = np.zeros_like(h)
rho_qp[o, o] = C[:, o].conj().T @ s @ C[:, o]
```

where `n` is the number of occupied particles and `o` is a slice with the occupied indices.

9.1.3 Self-consistent field procedure

Now, in order for us to solve the Roothaan-Hall equations, we need an expression for the Fock matrix. However, the Fock matrix depends on the coefficients found from solving the Roothaan-Hall equations. In order to get

around this pickle, we use *self-consistent field iterations* to gradually converge towards a solution to the Roothaan-Hall equations. We denote matrices at a specific step i by a superscript (i), e.g., the Fock matrix at step i is denoted $\mathbf{F}^{(i)}$. If there are no superscripts that means the matrix is independent of the self-consistent iterations. The self-consistent field method for the Roothaan-Hall equations is then given by,

$$\mathbf{F}^{(i)}\mathbf{C}^{(i+1)} = \mathbf{S}\mathbf{C}^{(i+1)}\boldsymbol{\epsilon}^{(i+1)}. \tag{9.13}$$

Here $\mathbf{F}^{(i)}$ is built from the coefficient matrices at the previous time step, i.e., $\mathbf{C}^{(i)}$. The generalized eigenvalue equation is solved in the same manner as described in subsection 9.1.1 yielding the coefficient matrix and the orbital eigenenergies for the next time step.

To start the self-consistent iterations we need an initial value for the Fock matrix. We choose $\mathbf{F}^{(0)} = \mathbf{h}$, i.e., we set the initial Fock matrix to be the one-body Hamiltonian matrix. The self-consistent procedure can now be explained by the following steps:

1. Construct the Fock matrix $\mathbf{F}^{(i)}$ from Equation 9.9, or from the initial state if $i = 0$.

2. Solve Equation 9.13 to find $\mathbf{C}^{(i+1)}$ and $\boldsymbol{\epsilon}^{(i+1)}$.

3. Build the density matrix $\mathbf{D}^{(i+1)}$ from the occupied coefficient matrices as in Equation 9.8.

4. Check for convergence.

The convergence of the self-consistent iterations are determined by the change in energy and the change in the density matrix between two consecutive steps. That is, for two given tolerances δ_E and δ_D, we say that the iterations have converged when both

$$\Delta E = E^{(i+1)} - E^{(i)} < \delta_E, \tag{9.14}$$

$$\|\Delta\mathbf{D}\|_F = \left\|\mathbf{D}^{(i+1)} - \mathbf{D}^{(i)}\right\|_F < \delta_D. \tag{9.15}$$

are satisfied. The matrix norm is given by the Frobenius norm.

9.1.4 Convergence acceleration

The self-consistent field iterations are not guaranteed to converge. By utlizing the convergence acceleration techniques discussed in section 7.3 we can

often remedy some of these problems. We define $\mathbf{F}^{(i)}$ as the measured quantity, and the newly built $\mathbf{F}^{(i+1)}$ as our predicted quantity. The error vector is constructed from

$$\boldsymbol{e}_i = \mathbf{F}^{(i)}\mathbf{D}^{(i)}\mathbf{S} - \mathbf{S}\mathbf{D}^{(i)}\mathbf{F}^{(i)}. \tag{9.16}$$

The error vector is only used for the DIIS acceleration and ignored in the alpha filter. We use the estimated Fock matrix from the alpha filter or DIIS as our new Fock matrix before starting the next round in the self-consistent field iterations.

9.1.5 The restricted Hartree-Fock method

In the restricted Hartree-Fock method we make the assumption that each spin direction is doubly occupied by an orbital. This can be a valid assumption if the Hamiltonian is spin-independent[2]. To be even more specific, we will look at the *closed-shell restricted Hartree-Fock* method, i.e., each spin-orbital *must* be doubly occupied and each energy shell must be completely filled. This corresponds to the spin-restricted spin-orbitals from Equation 3.82. For a basis of L spin-orbitals we get L/2 orbitals, where L must be an even number. We label the states by

$$\phi_P(x) = \varphi_p(\mathbf{r})\sigma(m_s) \implies |\phi_P\rangle = |\varphi_p\sigma\rangle\,, \tag{9.17}$$

where $P \in \{1,\ldots,L\}$ and $p \in \{1,\ldots,L/2\}$. That is, we use capital letters to refer to composite indices and lowercase letters for the orbitals. We write the ground state Slater determinant as

$$|\Phi\rangle = |\phi_1\phi_2\ldots\phi_{N-1}\phi_N\rangle = |(\varphi_1\alpha)(\varphi_1\beta)\ldots(\varphi_{N/2}\alpha)(\varphi_{N/2}\beta)\rangle\,, \tag{9.18}$$

where N is an even number of particles. The requirement that the molecular orbitals should be orthonormal is kept in the restricted Hartree-Fock method. As a consequence both the spin basis functions and the orbitals are orthonormal,

$$\langle\phi_P|\phi_Q\rangle = \langle\sigma|\tau\rangle\,\langle\varphi_p|\varphi_q\rangle = \delta_{\sigma\tau}\delta_{pq} = \delta_{PQ}. \tag{9.19}$$

Inserting the restricted spin-orbitals into the canonical Hartree-Fock equation we get,

$$\hat{f}\,|\phi_P\rangle = \epsilon_P\,|\phi_P\rangle \implies \hat{f}\,|\varphi_p\sigma\rangle = \epsilon_p\,|\varphi_p\sigma\rangle\,. \tag{9.20}$$

[2]We write *can* as there are situations where the Hamiltonian is spin-independent, but subject to conditions where the spin-symmetry of the restricted spin-orbitals break.

By projecting onto a molecular orbital we demonstrate how we can construct the Fock matrix elements when the Hamiltonian is spin-independent. This gives

$$\langle \phi_P | \hat{f} | \phi_Q \rangle = \langle \phi_P | \hat{h} | \phi_Q \rangle + \langle \phi_P \phi_J | \hat{u} | \phi_Q \phi_J \rangle_{AS} \,. \tag{9.21}$$

For the one-body Hamiltonian part of the Fock matrix elements we get

$$\langle \phi_P | \hat{h} | \phi_Q \rangle = \delta_{\sigma\tau} \langle \varphi_p | \hat{h} | \varphi_q \rangle \,. \tag{9.22}$$

For the two-body part, we split up the antisymmetric elements into its constituent parts and show the spin-dependence in each terms separately. We start with the Coulomb operator giving

$$\langle \phi_P \phi_J | \hat{u} | \phi_Q \phi_J \rangle = \langle \sigma | \tau \rangle \, \langle \nu | \nu \rangle \, \langle \varphi_p \varphi_j | \hat{u} | \varphi_q \varphi_j \rangle = 2\delta_{\sigma\tau} \langle \varphi_p | \hat{J} | \varphi_q \rangle \,, \tag{9.23}$$

where we have introduced the Coulomb operator from Equation 4.24, and summed over the spin-dependence $|\nu\rangle$ from the two occupied orbitals in the two-body elements. That is,

$$\langle \nu | \nu \rangle = \delta_{\nu\nu} = 2. \tag{9.24}$$

The second term in the antisymmetric two-body elements is the exchange operator

$$\langle \phi_P \phi_J | \hat{u} | \phi_J \phi_Q \rangle = \langle \sigma | \nu \rangle \, \langle \nu | \tau \rangle \, \langle \varphi_p \varphi_j | \hat{u} | \varphi_j \varphi_q \rangle = \delta_{\sigma\tau} \langle \varphi_p | \hat{K} | \varphi_q \rangle \,, \tag{9.25}$$

where we have used the completeness relation for the spin of the occupied molecular orbitals, viz.

$$|\nu\rangle\langle\nu| = \mathbb{1} \in \mathbb{R}^{2\times 2}. \tag{9.26}$$

Collecting the terms, we get the Fock matrix elements

$$\langle \phi_P | \hat{f} | \phi_Q \rangle = \delta_{\sigma\tau} \Big[\langle \varphi_p | \hat{h} | \varphi_q \rangle + 2 \langle \varphi_p | \hat{J} | \varphi_q \rangle - \langle \varphi_p | \hat{K} | \varphi_q \rangle \Big] \tag{9.27}$$

$$= \delta_{\sigma\tau} \langle \varphi_p | \hat{f} | \varphi_q \rangle \,, \tag{9.28}$$

where we see that the spin-dependence has been removed from the orbital integrals. We can therefore restrict ourselves to the orbital integrals for the Fock matrix elements. This means that we only need to look for coefficients for the molecular orbitals in terms of a known atomic orbital basis without spin. That is,

$$|\varphi_p\rangle = C_{\alpha p} \, |\chi_\alpha\rangle \,, \tag{9.29}$$

where $\{\chi_\alpha\}$ is our spin-independent basis of K known atomic orbitals. By projecting the atomic orbitals onto the canonical Hartree-Fock equations we will again be left with the Roothaan-Hall equations as seen in Equation 9.3.

9.1.6 Constructing the restricted Fock matrix

The difference between the restricted and the general Hartree-Fock methods lies in our calculation of the Fock matrix elements in the atomic orbital basis. We now have that

$$f_{\alpha\beta} \equiv \langle \chi_\alpha | \hat{f} | \chi_\beta \rangle = \langle \chi_\alpha | \hat{h} | \chi_\beta \rangle + 2 \langle \chi_\alpha | \hat{J} | \chi_\beta \rangle - \langle \chi_\alpha | \hat{K} | \chi_\beta \rangle , \tag{9.30}$$

where the Coulomb and the exchange operator depends on the full spin-dependent molecular orbitals. Looking at these two operators separately we have

$$\langle \chi_\alpha | \hat{J} | \chi_\beta \rangle = C^*_{j\gamma} C_{j\delta} \langle \chi_\alpha \chi_\gamma | \hat{u} | \chi_\beta \chi_\delta \rangle = C^*_{j\gamma} C_{j\delta} I^{\alpha\gamma}_{\beta\delta}, \tag{9.31}$$

$$\langle \chi_\alpha | \hat{K} | \chi_\beta \rangle = C^*_{j\gamma} C_{j\delta} \langle \chi_\alpha \chi_\gamma | \hat{u} | \chi_\delta \chi_\beta \rangle = C^*_{j\gamma} C_{j\delta} I^{\alpha\gamma}_{\delta\beta}, \tag{9.32}$$

where we have introduced the tensor notation for the elements of the two-body operator to be

$$I^{\alpha\beta}_{\gamma\delta} \equiv \langle \chi_\alpha \chi_\beta | \hat{u} | \chi_\gamma \chi_\delta \rangle , \tag{9.33}$$

where the greek letters indicate that the elements are expressed in the atomic orbital basis. Note that these elements are not antisymmetric as opposed to $u^{\alpha\beta}_{\gamma\delta}$. We also introduce the restricted density matrix

$$D_{\beta\alpha} \equiv 2 C^*_{\alpha i} C_{\beta i}, \tag{9.34}$$

where $i \in \{1, \ldots, N/2\}$, and N is the number of particles. In Python we compute the density matrix in the same way as done for the general Hartree-Fock method, but now we choose the slice over the occupied indices to be `o = slice(0, n //2)`, and multiply the density matrix by a factor 2. The restricted Fock matrix elements in the atomic orbital basis can now be written

$$f_{\alpha\beta} = h_{\alpha\beta} + D_{\delta\gamma} \left[I^{\alpha\gamma}_{\beta\delta} - \frac{1}{2} I^{\alpha\gamma}_{\delta\beta} \right], \tag{9.35}$$

In Python we compute the restricted Fock matrix by

```
fock_matrix = (
    h
    + np.tensordot(density_matrix, I, axes=((0, 1), (3, 1)))
    - 0.5 * np.tensordot(
        density_matrix, I, axes=((0, 1), (2, 1))
    )
)
```

where `density_matrix` is now the restricted density matrix and `I` are the two-body elements. Furthermore, the one-body Hamiltonian `h` is now spin-independent. By proceeding with the self-consistent field iterations solving the Roothaan-Hall equations with Equation 9.35 as the definition of the Fock matrix elements, we find the orbital coefficient matrix $\mathbf{C} \in \mathbb{C}^{K \times L/2}$ which we use to transform to the restricted molecular orbitals. Once transformed, we are at liberty to introduce spin-redundancy to open up for non-restricted post Hartree-Fock methods, e.g., the coupled-cluster method.

Restricted Hartree-Fock energy

We can compute the ground-state restricted Hartree-Fock energy by inserting our expression for the restricted molecular orbitals into the energy functional in Equation 4.4. This yields

$$E = D_{\beta\alpha} \left\{ h_{\alpha\beta} + \frac{1}{2} D_{\delta\gamma} \left(I^{\alpha\gamma}_{\beta\delta} - \frac{1}{2} I^{\alpha\gamma}_{\delta\beta} \right) \right\}. \tag{9.36}$$

We compute the energy in Python by the snippet shown in Program 8. The

Program 8 In this snippet we demonstrate how to compute the restricted Hartree-Fock energy from Equation 9.36.

```
# term_{ab} <- D_{dc} I^{ac}_{bd}
term = np.tensordot(
    density_matrix, I, axes=((0, 1), (3, 1))
)
# term_{ab} <- term_{ab} -0.5 * D_{dc} I^{ac}_{db}
term -= 0.5 * np.tensordot(
    density_matrix, I, axes=((0, 1), (2, 1))
)

# term_{ab} <- h_{ab} + 0.5 term_{ab}
term = h + 0.5 * term

# energy = D_{ba} term_{ab}
energy = np.trace(np.dot(term, density_matrix))
```

one-body density matrix in the restricted Hartree-Fock method is computed in the same way as for the general Hartree-Fock method, but with the restricted coefficients and an extra factor from the double occupancy.

9.1.7 The unrestricted Hartree-Fock method

The unrestricted Hartree-Fock method allows the molecular orbitals to have independent orbitals for each spin direction. Hence, we assume that the

molecular orbitals can be described by spin-unrestricted spin-orbitals as seen in Equation 3.81. Introducing indices for the different molecular orbitals, we denote the spin-unrestricted molecular orbitals by

$$\phi_P(x) = \varphi_p^\sigma(\mathbf{r})\sigma(m_s) \implies |\phi_P\rangle = |\varphi_p^\sigma\sigma\rangle\,, \tag{9.37}$$

where $P \in \{1,\ldots,L\}$, $\sigma \in \{\alpha,\beta\}$, and $p \in \{1,\ldots,L_\sigma\}$. We have that $L = L_\alpha + L_\beta$, and we have refrained from labelling the lower case orbital indices as they always occur with a spin index. Note that there is no implicit sum over the label σ in the orbital φ_p^σ and the spin-function $\sigma(m_s)$. We can collect the orbitals in two sets $\{\varphi_p^\sigma\}$, one for each spin direction. The ground state Slater determinant can then be written as

$$|\Phi\rangle = |\phi_1\phi_2\ldots\phi_{N-1}\phi_N\rangle = |(\varphi_1^\alpha\alpha)\ldots(\varphi_{N_\alpha}^\alpha\alpha)(\varphi_1^\beta\beta)\ldots(\varphi_{N_\beta}^\beta\beta)\rangle\,, \tag{9.38}$$

where N_σ is the number of particles with spin $\sigma(m_s)$. Note the ordering of the spin-orbitals in the determinant. As the two sets of orbitals can be of different sizes, we can no longer be sure that there is an even number of spin states. We therefore stack the spin-orbitals after one another instead of interlacing them by odd and even positions. The orthonormality of the molecular orbitals is given by

$$\langle\phi_P|\phi_Q\rangle = \delta_{PQ} = \langle\sigma|\tau\rangle\,\langle\varphi_p^\sigma|\varphi_q^\tau\rangle\,, \tag{9.39}$$

where the overlap between two orbitals with differing spin is not necessarily zero. However, if the two spin directions are the same, i.e., $\sigma = \tau$, we get

$$\langle\varphi_p^\sigma|\varphi_q^\sigma\rangle = \delta_{pq}. \tag{9.40}$$

Inserting the unrestricted spin-orbitals into the canonical Hartree-Fock equations yield

$$\hat{f}\,|\phi_P\rangle = \epsilon_P\,|\phi_P\rangle \implies \hat{f}\,|\varphi_p^\sigma\sigma\rangle = \epsilon_p^\sigma\,|\varphi_p^\sigma\sigma\rangle\,, \tag{9.41}$$

which demonstrates how each spin-component yields a different equation as the Fock eigenenergies ϵ_p^α is in general different from ϵ_p^β. By projecting onto another molecular orbital as in Equation 9.21 we demonstrate how the spin yields two separate Fock matrices, one for each spin direction.[3] The one-body elements in the molecular orbital basis is given by

$$\langle\phi_P|\hat{h}|\phi_Q\rangle = \delta_{\sigma\tau}\,\langle\varphi_p^\sigma|\hat{h}|\varphi_q^\tau\rangle\,, \tag{9.42}$$

[3]Note that this assumes a spin-independent Hamiltonian.

while the Coulomb operator from the two-body elements is given by

$$\langle \phi_P \phi_J | \hat{u} | \phi_Q \phi_J \rangle = \delta_{\sigma\tau} \sum_{\rho \in \{\alpha,\beta\}} \langle \varphi_p^\sigma | \hat{J}^\rho | \varphi_q^\sigma \rangle . \tag{9.43}$$

We note that this term provides a coupling between the orbitals in both spin directions as we get a sum over the two spin directions. This is not the case for the exchange operator from the antisymmetric two-body elements. We have

$$\langle \phi_P \phi_J | \hat{u} | \phi_J \phi_Q \rangle = \delta_{\sigma\tau} \langle \varphi_p^\sigma | \hat{K}^\sigma | \varphi_q^\tau \rangle . \tag{9.44}$$

Collecting all the terms in order to find the Fock matrix, we get

$$\langle \phi_P | \hat{f} | \phi_Q \rangle = \delta_{\sigma\tau} \left[\langle \varphi_p^\sigma | \hat{h} | \varphi_q^\tau \rangle + \sum_{\rho \in \{\alpha,\beta\}} \langle \varphi_p^\sigma | \hat{J}^\rho | \varphi_q^\tau \rangle - \langle \varphi_p^\sigma | \hat{K}^\sigma | \varphi_q^\tau \rangle \right]. \tag{9.45}$$

This demonstrates how the spin yields two different Fock matrices from the canonical Hartree-Fock equations. That is,

$$\langle \varphi_p^\sigma | \hat{f}^\sigma | \varphi_q^\sigma \rangle = \langle \varphi_p^\sigma | \hat{h} | \varphi_q^\sigma \rangle + \sum_{\rho \in \{\alpha,\beta\}} \langle \varphi_p^\sigma | \hat{J}^\rho | \varphi_q^\sigma \rangle - \langle \varphi_p^\sigma | \hat{K}^\sigma | \varphi_q^\sigma \rangle , \tag{9.46}$$

where the spin label on the Fock matrix corresponds to the spin label of the exchange operator. We now look for a set of coefficients for the orbitals in each spin direction in terms of our original atomic orbital basis,

$$|\varphi_p^\sigma\rangle = C_{\kappa p}^\sigma |\chi_\kappa\rangle , \tag{9.47}$$

where we use the greek letters κ, λ, μ, and ν for the atomic orbitals to avoid confusion with the spin-functions $\alpha(m_s)$ and $\beta(m_s)$. Before we demonstrate how we can generate a set of equations in order to find the coefficient matrices $\mathbf{C}^\sigma \in \mathbb{C}^{K \times L_\sigma}$, we motivate the spin-labelling of the Fock matrices in the atomic orbital basis. We define

$$f_{\kappa\lambda}^\sigma \equiv \langle \chi_\kappa | \hat{f}^\sigma | \chi_\lambda \rangle = h_{\kappa\lambda} + \sum_{\rho \in \{\alpha,\beta\}} D_{\nu\mu}^\rho I_{\lambda\nu}^{\kappa\mu} - D_{\nu\mu}^\sigma I_{\nu\lambda}^{\kappa\mu}, \tag{9.48}$$

where the density matrix along a certain spin direction is defined similarly to the density matrices in the general Hartree-Fock method. Left-projecting the atomic orbital basis on the canonical Hartree-Fock equations acting on an orbital in the unrestricted regime yields

$$\langle \chi_\kappa | \hat{f}^\sigma | \varphi_p^\sigma \rangle = \epsilon_p^\sigma \langle \chi_\kappa | \varphi_p^\sigma \rangle \implies C_{\lambda p}^\sigma \langle \chi_\kappa | \hat{f}^\sigma | \chi_\lambda \rangle = C_{\lambda p}^\sigma \epsilon_p^\sigma \langle \chi_\kappa | \chi_\lambda \rangle \tag{9.49}$$

$$\implies f_{\kappa\lambda}^\sigma C_{\lambda p}^\sigma = s_{\kappa\lambda} C_{\lambda p}^\sigma \epsilon_p^\sigma \implies \mathbf{F}^\sigma \mathbf{C}^\sigma = \mathbf{S} \mathbf{C}^\sigma \boldsymbol{\epsilon}^\sigma. \tag{9.50}$$

These coupled equations constitute the *Pople-Nesbet equations*. They resemble the Roothaan-Hall equations seen in the two previous methods in that they are generalized eigenvalue equations, but now we solve two sets of eigenvalue equations simultaneously. Note that the coupling between the two spin directions occurs in the Fock matrix via the Coulomb operator. The self-consistent field iterations for the unrestricted Hartree-Fock method remains the same, but now we iterate equations for both spin directions at the same time.

The unrestricted Hartree-Fock energy

Inserting our expression for the molecular orbitals into the energy functional we find the unrestricted Hartree-Fock energy,

$$E = \sum_{\sigma\in\{\alpha,\beta\}} \left\{ D^{\sigma}_{\lambda\kappa} h_{\kappa\lambda} + \frac{1}{2} \sum_{\tau\in\{\alpha,\beta\}} D^{\sigma}_{\mu\kappa} D^{\tau}_{\nu\lambda} I^{\kappa\lambda}_{\mu\nu} - \frac{1}{2} D^{\sigma}_{\mu\kappa} D^{\sigma}_{\nu\lambda} I^{\kappa\lambda}_{\nu\mu} \right\}. \tag{9.51}$$

9.1.8 Time evolution

Due to time limitations we have only implemented a time-dependent general Hartree-Fock method. From Equation 4.49 we know that we can write the time evolution of the molecular orbitals by,

$$i\hbar \frac{\partial}{\partial t} |\phi_i(t)\rangle = \hat{f}(t) |\phi_i(t)\rangle . \tag{9.52}$$

We can now insert the linear combination for the molecular orbitals in terms of the known atomic orbital basis. The time evolution of the molecular orbitals is kept in the coefficients leaving the atomic orbital basis static in time. This gives

$$i\hbar \frac{\partial}{\partial t} C_{\alpha i}(t) |\chi_\alpha\rangle = \hat{f}(t) C_{\alpha i}(t) |\chi_\alpha\rangle . \tag{9.53}$$

Left projecting with another state from the atomic orbitals we can rewrite the previous equation to

$$i\hbar \frac{\partial}{\partial t} C_{\alpha i}(t) \langle\chi_\beta|\chi_\alpha\rangle = C_{\alpha i}(t) \langle\chi_\beta|\hat{f}(t)|\chi_\alpha\rangle \tag{9.54}$$

$$\implies i\hbar \dot{C}_{\alpha i} s_{\beta\alpha} = C_{\alpha i}(t) f_{\beta\alpha}(t) \implies i\hbar \mathbf{S}\dot{\mathbf{C}} = \mathbf{F}(t)\mathbf{C}(t), \tag{9.55}$$

where the time-dependent Fock matrix $\mathbf{F}(t)$ contains the matrix elements

$$f_{\beta\alpha}(t) = \langle\chi_\beta|\hat{f}(t)|\chi_\alpha\rangle . \tag{9.56}$$

We restrict ourselves to orthonormal atomic orbital basis sets as we start the time evolution after performing a ground state Hartree-Fock calculation and transforming to the orthonormal molecular orbital basis. Using atomic units we can then write Equation 9.55 as,

$$\dot{\mathbf{C}} = -i\mathbf{F}(t)\mathbf{C}(t). \tag{9.57}$$

In case of non-orthogonal atomic orbitals, the orthonormalization procedure described in subsection 3.5.2 can be used to make the orbitals orthonormal prior to starting the time evolution. As discussed in section 7.4 we need to convert $\dot{\mathbf{C}}$ to a vector. Using NumPy we store the result from the right-hand side as a two-dimensional array and we can use the function `np.ravel` to convert the two-dimensional array to a contiguous, flattened, one-dimensional array. We use the member function `reshape` to go from the flattened array back to the two-dimensional form.

9.1.9 Time-dependent energy

The time-dependent energy is computed in exactly the same way as for the general Hartree-Fock method. We therefore reuse this functionality, but use the time-dependent coefficients for the density matrices.

9.1.10 Time-dependent overlap

From subsection 3.6.7 we an expression for the overlap of two Slater determinants. Due to the orthonormality of the atomic orbital basis, the time-dependent overlap is given by

$$P(t, t_0) = \left| \langle \Phi(t) | \Phi(t_0) \rangle \right|^2 = \left| \det(\mathbf{C}^\dagger(t)\mathbf{C}(t_0)) \right|^2, \tag{9.58}$$

where $\mathbf{C}(t)$ is the coefficient matrix of the time evolved states.

9.2 Configuration interaction

As the main goal of this thesis has been to implement coupled-cluster solvers, the configuration interaction solver has not been worked at to such a large degree. The motivation for implementing a full configuration interaction solver for small systems is to compare our approximate methods to an – within the computational space – exact method. We have therefore implemented a "naïve" configuration interaction solver where we create the full Slater determinant space and store it in memory. From this we also create the full Hamiltonian matrix $\mathbf{H}$. Our implementation thus quickly absorbs too much

memory and therefore limits the number of particles and basis functions that can be explored. To improve on the current scheme, an implementation of the *direct CI* methods [6, 93] along with only storing non-zero elements in $\mathbf{H}$ will yield a more powerful method supporting more particles and basis functions.

9.2.1 Constructing the Slater determinant basis

We represent the Slater determinants as NumPy-arrays [69] of bit strings using unsigned integers. The reason for choosing NumPy-arrays is that we are ble to use Numba [83] to speed up much of the explicit for-loops. Unfortunately this means that we have to the bit-twiddling manually. The default choice is to use `np.uint64`, i.e., 64-bit unsigned integers with room for 64 single-particle states, but other options such as 32-bit and 16-bit unsignd integers are available. If we have a system with $L > 64$ we add more integers in the array thus allowing for an integer mutiple of 64 single-particle states at a time. Let b be the number of bits in an integer, then the number of integers needed for a single Slater determinant N_i is given by

$$N_i = \left\lfloor \frac{L}{b} \right\rfloor + q, \tag{9.59}$$

where q is either one or zero,

$$q = \begin{cases} 1 & L \mod b > 0, \\ 0 & L \mod b = 0, \end{cases} \tag{9.60}$$

where $L \mod b$ is the remainder of the integer division. The number of Slater determinants N_s is given by a recursive function $N_s(S)$ depending on the order S of the truncation,

$$N_s(S) = \begin{cases} 1, & S = 0, \\ N_s(S-1)\frac{(N-[S-1])(M-[S-1])}{S^2}, & S > 0. \end{cases} \tag{9.61}$$

Here N is the number of particles, $M = L - N$ is the number of virtual states, and we have denoted the order S as an integer where 1 represents singles, 2 doubles, and so forth. This formula counts the number of ways N particles can be distributed among M positions moving S particles at a time. For a given truncation level, e.g., singles-and-doubles (CISD), the number of Slater determinants is then

$$N_s = N_s(2) + N_s(1) + N_s(0), \tag{9.62}$$

where $N_s(0) = 1$ counts the reference state. In Table 9.1 we demonstrate how the number of Slater determinants increase as a function of truncation

Table 9.1: In this table we demonstrate how the number of Slater determinants N_s increases as a function of truncation level for $N = 4$ and $L = 80$. We have also included the number of bytes needed to store the Slater determinants using `np.uint64`, i.e., 64-bit unsigned integers to represent the determinants, and the size of the Hamiltonian matrix in bytes where we assume 128-bit complex numbers as elements. The storage cost of the Hamiltonian matrix for CIS was 0.001 GB, which does not show up in the designated decimal point.

Truncation	N_s	Determinant storage [B]	Hamiltonian storage [GB]
CIS	305	2440	0.0
CISD	17405	139240	4.5
CISDT	298605	2388840	1328.7
CISDTQ	1581580	12652640	37273.7

for a fixed number of particles. The storage cost of the Hamiltonian matrix $\mathbf{H}$ explodes when going from the CIS truncation to the CISDTQ level as the memory cost increases by 7 orders of magnitude.

In our code we construct the Slater determinant basis by creating the reference determinant where we set the N first bits in the array of unsigned integers and then create $N_s - 1$ copies of this state. The setting of a single-particle state in a bit string is done using the binary OR command. An example of the setting of single-particle states represented as bits is shown in Program 9. Other options are to use the binary XOR operation, but whichever one is chosen some care must be shown as bugs can arise if the single-particle state is

Program 9 An example of how set the single-particle state 68 in a binary state array `state` using `np.uint64` integers to represent determinants.

```
# Value of state
# state == [0b0, 0b0]

# The number of bits in an integer
BITSTRING_SIZE = 64
# Compute the integer index in state
elem_i = 68 // BITSTRING_SIZE

# Set the fourth bit in the second integer in state
state[elem_i] |= 1 << (4 - elem_i * BITSTRING_SIZE)

# New value of state
# state == [0b0, 0b10000] == [0, 16]
```

already set. In the case of the OR operation this does not change the state, but the XOR operation will remove the state. For this reason we use the XOR operation in order to unset a bit, i.e., remove a single-particle state.

The higher excited determinants are created by exciting the reference determinant in a recursive fashion. The excitation operator for a single Slater determinant is shown in Program 10. This function excites all single-particle

Program 10 Function used to represent a series of excitation operators $\hat{X}_i^a$, neglecting the sign.

```
@numba.njit(cache=True, nogil=True, fastmath=True)
def _excite_state(state, o_remove, v_insert):
    for i, a in zip(o_remove, v_insert):
        elem_i = i // BITSTRING_SIZE
        elem_a = a // BITSTRING_SIZE

        state[elem_i] ^= 1 << (i - elem_i * BITSTRING_SIZE)
        state[elem_a] |= 1 << (a - elem_a * BITSTRING_SIZE)
```

states in the array `o_remove` to the single-particle states in `v_insert`. Note that the Slater determinants are interpreted as being in canonical ordering and we ignore the sign handling when creating the basis of determinants. The signs are thus handled when computing matrix elements. To populate the `o_remove`- and `v_insert`-arrays, we have a function which recursively adds an occupied index into `o_remove` and then proceeds to add all the virtual indices in order into `v_insert`, before calling the excitation function defined in Program 10. The full recursive procedure is shown in Program 11. The entire implementation of the configuration interaction method is uniquely defined by the basis of Slater determinants. This means that after a truncation order has been chosen and the basis of Slater determinants has been constructed, everything that follows will be solved in the same manner independently of the truncation level.

9.2.2 Constructing the Hamiltonian matrix

The arguably most effective "first-order" optimization that can be performed for the configuration interaction method is to implement the Slater-Condon rules when evaluating matrix elements of operator strings, as opposed to brute force evaluation of the action of the second quantized operators on a determinant. When constructing the Hamiltonian matrix $\mathbf{H}$ with one- and two-body operators, we wish to evaluate the matrix elements

$$H_{IJ} = \langle \Phi_I | \hat{H} | \Phi_J \rangle = h_q^p \langle \Phi_I | \hat{c}_p^\dagger \hat{c}_q | \Phi_J \rangle + \frac{1}{4} u_{rs}^{pq} \langle \Phi_I | \hat{c}_p^\dagger \hat{c}_q^\dagger \hat{c}_r \hat{c}_s | \Phi_J \rangle , \tag{9.63}$$

Program 11 Function creating all excited determinants of a given order `order`.

```
@numba.njit(cache=True, nogil=True, fastmath=True)
def _create_excited_states(
    n, l, states, index, order, o_remove, v_insert
):
    if order == 0:
        _excite_state(states[index], o_remove, v_insert)
        return index + 1

    i_start = (
        0 if len(o_remove) == order else o_remove[order] + 1
    )
    a_start = (
        n if len(v_insert) == order else v_insert[order] + 1
    )

    for i in range(i_start, n):
        o_remove[order - 1] = i
        for a in range(a_start, l):
            v_insert[order - 1] = a

            index = _create_excited_states(
                n,
                l,
                states,
                index,
                order - 1,
                o_remove,
                v_insert,
            )

    return index
```

using the Slater-Condon rules defined in Lemma 3.2 and Lemma 3.3. Given two Slater determinants $|\Phi_I\rangle$ and $|\Phi_J\rangle$ which we represent as two occupation number states $|\mathbf{n}\rangle$ and $|\mathbf{m}\rangle$, respectively, we need ways to evaluate the following:

- The sign given by the phase,

$$(\Gamma_-)_p^{\mathbf{n}} = \prod_{i=1}^{p-1} (-1)^{n_i}, \tag{9.64}$$

  as defined in Definition 3.2.

- The Kronecker-Delta $\delta_{p\in\mathbf{n}}$ checking if the single-particle state p is an occupied state in $|\mathbf{n}\rangle$.

- The difference $|\mathbf{n} - \mathbf{m}|$, between the two determinants $|\mathbf{n}\rangle$ and $|\mathbf{m}\rangle$.

- The position of a set bit to a single-particle index p in order to find the correct matrix elements in h_q^p and u_{rs}^{pq}.

For the sign calculation we use the product for the phase $(\Gamma_-)_i^{\mathbf{n}}$ defined in Definition 3.2 by counting the number of set bits k at positions below i, and computing $(-1)^k$. An implementation of this sign calculation is shown in Program 12. The implementation of the Kronecker-Delta is shown in Program 13. To compute the difference between the two determinants we start by using the XOR operation to find the specific bits that are set in either $\mathbf{n}$

Program 12 Function computing the sign of the action of a creation or annihilation operator for index `p` on a determinant `state`. This is the binary implementation of the phase defined in Definition 3.2.

```
@numba.njit(cache=True, nogil=True, fastmath=True)
def compute_sign(state, p):
    elem_i = 0
    k = 0

    for i in range(p):
        if (i - elem_i * BITSTRING_SIZE) >= BITSTRING_SIZE:
            elem_i += 1

        k += (
            state[elem_i] >> (i - elem_i * BITSTRING_SIZE)
        ) & 1

    return (-1) ** k
```

Program 13 Implementation of the Kronecker-Delta $\delta_{p \in \mathbf{n}}$.

```
@numba.njit(cache=True, nogil=True, fastmath=True)
def occupied_index(state, p):
    elem_p = p // BITSTRING_SIZE

    return (
        state[elem_p] & (1 << (p - elem_p * BITSTRING_SIZE))
    ) != 0
```

or $\mathbf{m}$, but not both. Next, we count the number of set bits in this difference state. The counting of set bits in an integer is a topic which has been explored in some depth in the field of computer science and has led to some very efficient algorithms. We use the population count algorithm [94] shown in Program 14. Now, counting the number of set bits in the difference-state

Program 14 Implementation of the popcount algorithm for 64-bit integers.

```
# Constants used by the popcount_64 algorithm
m_1 = 0x5555_5555_5555_5555
m_2 = 0x3333_3333_3333_3333
m_4 = 0x0F0F_0F0F_0F0F_0F0F
h_01 = 0x0101_0101_0101_0101


@numba.njit(cache=True, nogil=True, fastmath=True)
def popcount_64(num):
    num -= (num >> 1) & m_1
    num = (num & m_2) + ((num >> 2) & m_2)
    num = (num + (num >> 4)) & m_4

    return (num * h_01) >> 56
```

from $|\mathbf{n}\rangle$ XOR $|\mathbf{m}\rangle$ yields the difference $|\mathbf{n} - \mathbf{m}|$. The function in Program 15 computes the difference between two determinants. To compute the index of a set bit in a bitstring we iterate over all bit positions in the bitstring and right-shift the bits before using the binary AND operation to check if the rightmost bit is set. Once we encounter a bit, the iteration counter contains the index of the bit. An implementation of this scheme is shown in Program 16.

9.2.3 Diagonalization

Having constructed the full Hamiltonian matrix $\mathbf{H} \in \mathbb{C}^{N_s \times N_s}$ the next step is to diagonalize the matrix in order to get the eigenenergies $\mathbf{E} = \text{diag}(E_1, \ldots, E_{N_s})$ and the eigenvectors, i.e., the coefficients for the eigenstates, $\mathbf{C} \in \mathbb{C}^{N_s \times N_s}$. As

Program 15 Function counting the difference in the number of single-particle states in two Slater determinants.

```
@numba.njit(cache=True, nogil=True, fastmath=True)
def state_diff(state_i, state_j):
    diff = state_i ^ state_j

    num_bits = 0
    for elem in diff:
        num_bits += popcount_64(elem)

    return num_bits
```

Program 16 Function computing the index of a set bit in Slater determinant. The parameter `index_num` decides if we should find the first (0), second (1), or higher, set bits.

```
@numba.njit(cache=True, nogil=True, fastmath=True)
def get_index(state, index_num=0):
    index = 0

    for elem_p in range(len(state)):
        for p in range(BITSTRING_SIZE):
            if (state[elem_p] >> p) & 0b1 != 0:
                if index_num == 0:
                    return index

                index_num -= 1

            index += 1

    return -1
```

stated in chapter 5, we restrict our attention to orthonormal single-particle states and hence orthonormal Slater determinants. We therefore need to solve the eigenvalue equation

$$\mathbf{HC} = \mathbf{EC}. \tag{9.65}$$

The Hamiltonian matrix is Hermitian and we can therefore use the function `np.linalg.eigh` [69], which uses the LAPACK-routines [95] `_syevd` and `_heevd` for symmetric and Hermitian matrices respectively, to solve the eigenvalue equation. This will yield the full spectrum of $\mathbf{H}$ and will often prove a limiting factor in terms of computational complexity as the number of FLOPS required to solve this equation scales as $\mathcal{O}(N_s^3)$.

As an alternative to the full spectrum we can use a sparse eigenvalue solver. We use the function `scipy.sparse.linalg.eigsh` from SymPy [70] which is a wrapper around the ARPACK routines SSEUPD and DSEUPD [96] implementing the Implictly Restarted Lanczos Method with a theoretical complexity of $\mathcal{O}(N_s^2)$. This lets us specify how many eigenpairs k we wish to compute, which is then found iteratively.

The eigensolvers given by NumPy [69] and SciPy [70] sorts the eigenvalues in an ascending order with the eigenvectors sorted in the same fashion, and with the eigenvectors unitary. This means that the ground state energy is found as the first element of the eigenvalues.

9.2.4 One-body density matrix

Having diagonalized the Hamiltonian matrix we can compute the one-body density matrix of the system. For a given eigenstate $|\Psi_I\rangle$ we compute the one-body density matrix by

$$\rho_{I\,p}^{\;q} = \langle \Psi_I | \hat{c}_p^\dagger \hat{c}_q | \Psi_I \rangle = C_{JI}^* C_{KI} \langle \Phi_J | \hat{c}_p^\dagger \hat{c}_q | \Phi_K \rangle \,. \tag{9.66}$$

As matrix elements of the one-body density matrix are given by a pair of creation and annihilation operators we can use the Slater-Condon rules for one-body operators to evaluate the overlap. This results in virtually the same implementation as for the one-body Hamiltonian, but with a new one-body operator given by the coefficient vector $\mathbf{c}_I$ for a specific eigenstate $|\Psi_I\rangle$. Note that $\mathbf{c}_I \in \mathbb{C}^{N_s}$ and that the indices into this vector is given by the same indices as for the Slater determinants, unlike the single-particle indices used for the one-body density matrix and the one-body Hamiltonian.

9.2.5 Time evolution

Having solved the ground state problem, we move on to the dynamics of the configuration interaction method. Choosing an initial state with a given coefficient vector $\mathbf{c}(0) \in \mathbb{C}^{N_s}$, either from the ground state problem or from some

other method, we proceed to solve the differential equation demonstrated in Equation 5.30. In atomic units this corresponds to solving

$$\dot{\mathbf{c}}(t) = -i\mathbf{H}(t)\mathbf{c}(t), \tag{9.67}$$

which we see is already a vector and therefore be directly fed into the numerical integrators described in section 7.4. Our task is now to construct the time-dependent Hamiltonian matrix. In general we can construct the time-dependent matrix elements from

$$H_{IJ}(t) = h_q^p(t) \langle \Phi_I | \hat{c}_p^\dagger \hat{c}_q | \Phi_J \rangle + \frac{1}{4} w_{rs}^{pq}(t) \langle \Phi_I | \hat{c}_p^\dagger \hat{c}_q^\dagger \hat{c}_s \hat{c}_r | \Phi_J \rangle . \tag{9.68}$$

and reuse the Slater-Condon rules to evaluate the one- and two-body operators. Our implementation does programmatically support a time-dependent two-body operator, but this is not something that we will use. Therefore, by only including time-dependent one-body operators, an optimization is to store two copies of the full Hamiltonian matrix,[4] and only re-compute the time-dependent one-body contributions. We define the two sets of matrix elements for the Hamiltonian matrix by

$$(\hat{H}_1)_{IJ}(t) \equiv \langle \Phi_I | \hat{h}(t) | \Phi_J \rangle , \tag{9.69}$$

$$(\hat{H}_2)_{IJ}(t) \equiv \langle \Phi_I | \hat{w}(t) | \Phi_J \rangle . \tag{9.70}$$

Setting $\hat{w}(t) = \hat{w}$ we now compute the Hamiltonian matrix from

$$\mathbf{H}(t) = \mathbf{H}_1(t) + \mathbf{H}_2, \tag{9.71}$$

where we only construct a new $\mathbf{H}_1(t)$ – using the Slater-Condon rules for the one-body operator – at every time step.

9.2.6 Time-dependent energy

For a time-evolved state $|\Psi(t)\rangle$ with a time-evolved Hamiltonian $\hat{H}(t)$, we can compute the energy of the state at a certain time t by

$$E(t) = \frac{\langle \Psi(t) | \hat{H}(t) | \Psi(t) \rangle}{\langle \Psi(t) | \Psi(t) \rangle}, \tag{9.72}$$

where we have included an explicit normalization due to potential drift in the coefficients from the time evolution using numerical integrators. Expanding

[4] This might seem a little odd as we have already argued at length of how the Hamiltonian matrix is the bottleneck of the implementation, but remember that our focus is on the dynamics of quantum-mechanical systems and we are therefore quite limited in the size of the systems we can explore. This means that we will seldom look at very large systems and we can often store the full Hamiltonian matrix, and copies, in memory.

the time-evolved state in the static basis of Slater determinants with time-dependent coefficients, $\mathbf{c}(t)$, we find the time-dependent energy to be

$$E(t) = \frac{c_I^*(t)\,\langle\Phi_I|\hat{H}(t)|\Phi_J\rangle\,c_J(t)}{c_I^*(t)c_I(t)} = \frac{\mathbf{c}^\dagger(t)\mathbf{H}(t)\mathbf{c}(t)}{\mathbf{c}^\dagger(t)\mathbf{c}(t)}. \tag{9.73}$$

9.2.7 Time-dependent overlap

We compute the time-dependent overlap by

$$P(t,t_0) = \frac{\left|\,\langle\Psi(t)|\Psi(t_0)\rangle\,\right|^2}{\langle\Psi(t)|\Psi(t)\rangle\;\langle\Psi(t_0)|\Psi(t_0)\rangle} = \frac{\left|\mathbf{c}^\dagger(t)\mathbf{c}(t_0)\right|^2}{\left|\mathbf{c}(t)\right|^2\left|\mathbf{c}(t_0)\right|^2}, \tag{9.74}$$

where we again include an explicit normalization term in case of drift in the normalization due to the integrator.

9.3 Coupled-cluster

In this thesis we have implemented a set of coupled-cluster solvers, they are:

- The coupled-cluster doubles (CCD) and the coupled-cluster singles-and-doubles (CCSD) methods with static orbitals. This includes both time-independent and time-dependent solvers.

- The non-orthogonal coupled-cluster doubles (NOCCD) ground state solver. Note that we often call this solver for the orbital-adaptive coupled-cluster doubles method (OACCD). This solver was written by Myhre [21] and given to use as part of an ongoing article on the stability of time-dependent coupled-cluster methods. We still describe the implementation in some detail as we had to integrate the solution into our library.

- The orbital-adaptive time-dependent coupled-cluster doubles (OATD-CCD) method. This method uses the OACCD method as an initial ground state solver.

Our coupled-cluster library tries in as large degree as possible to reuse routines for the different solvers as this makes optimization more efficient, that is, we only need to optizime a specific function once, instead of once per solver.

9.3.1 Ground state solvers with static orbitals

From chapter 6 we know that the projected amplitude equations from Equation 6.10 should be satisfied once we have found the optimal τ_μ-amplitudes. However, in order to find the optimal amplitudes we employ an iterative *quasi-Newton* method which avoids the need for computing the Jacobian matrix and solving a linear equation as in Newton's method [6]. We define the left-hand side of Equation 6.10 with the normal-ordered Hamiltonian to be

$$\Omega_\mu(\boldsymbol{\tau}^{(i)}) = \langle \Phi_\mu | \exp(-\hat{T}^{(i)}) \hat{H}_N \exp(\hat{T}^{(i)}) | \Phi \rangle \,, \tag{9.75}$$

where $\boldsymbol{\tau}^{(i)}$ is the collection of cluster amplitudes at iteration i and μ denotes an excitation level. Note that we treat Ω_μ as a tensor of rank μ in order to collect all elements from a cluster of rank μ. In section B.2 the τ-amplitude equations are listed for the doubles (CCD) and singles-and-doubles (CCSD) truncation levels.

In the quasi-Newton method we now solve [6, 97]

$$\Delta\tau_\mu^{(i)} = \frac{\Omega_\mu(\boldsymbol{\tau}^{(i)})}{D_\mu}, \tag{9.76}$$

in order to find the change in the amplitudes between two iterations. In the former equation μ serves as a label and should not be summed. The division is also interpreted as an element-wise division. Now, D_μ is a tensor of rank μ and serves as an approximation to the Jacobian matrix in case of a full fledged Newton's method [6]. For the singles and doubles amplitudes we have the tensors

$$D_i^a \equiv \epsilon_i - \epsilon_a, \tag{9.77}$$

$$D_{ij}^{ab} \equiv \epsilon_i + \epsilon_j - \epsilon_a - \epsilon_b, \tag{9.78}$$

where $\epsilon = \mathrm{diag}(\epsilon_1, \ldots, \epsilon_L)$ are the diagonal elements of the normal-ordered Fock matrix. In order for Equation 9.76 to be well-defined we require that none of the elements in D_μ are zero. This is ensured as long as we have a well-defined single-reference problem as [98]

$$\epsilon_i \neq \epsilon_a, \tag{9.79}$$

for all $i \in \{1, \ldots, N\}$ and $a \in \{N+1, \ldots, L\}$ when the single-reference assumption holds. However, do note that the lack of infinite precision on a computer means that we can get instabillities if we approach a system that is almost degenerate across the Fermi vacuum, that is, if we are almost in a multireference situation. We are now able to compute the next iteration of the cluster amplitudes by

$$\boldsymbol{\tau}^{(i+1)} = \boldsymbol{\tau}^{(i)} + \Delta\boldsymbol{\tau}^{(i)}, \tag{9.80}$$

where we collect all the cluster amplitudes together when computing the improved estimate. We order the τ-amplitudes with the virtual indices first, for example the doubles amplitudes is given by

$$\tau_{ij}^{ab} \rightarrow \texttt{t\_2[a, b, i, j]}, \tag{9.81}$$

as NumPy arrays. To determine if we have found a converged set of cluster amplitude we compute the Frobenius norm of each set of amplitudes using NumPy, and checking whether or not we have a value below a set threshold. An alternative is to compute the energy in every iteration of the cluster amplitudes and determining convergence based on the difference in energy between each step.

Having found converged $\boldsymbol{\tau}$-amplitudes we turn our attention to the Lagrange multipliers, also known as the $\boldsymbol{\lambda}$-amplitudes. The procedure is virtually the same as for the $\boldsymbol{\tau}$-amplitudes, but now we solve for the stationary condition in Equation 6.46. That is,

$$\Omega_\mu(\boldsymbol{\tau}, \boldsymbol{\lambda}^{(i)}) = \langle \Phi | (\mathbb{1} + \hat{\Lambda}^{(i)}) \exp(-\hat{T}) \left[\hat{H}, \hat{X}_\mu\right] \exp(\hat{T}) | \Phi \rangle \tag{9.82}$$

where $\boldsymbol{\tau}$ are now the converged $\boldsymbol{\tau}$-amplitudes. The equations for CCD and CCSD are listed in section B.3. Reusing the quasi-Newton method we compute

$$\Delta\lambda_\mu^{(i)} = \frac{\Omega_\mu(\boldsymbol{\tau}, \boldsymbol{\lambda}^{(i)})}{D_\mu}, \tag{9.83}$$

where the D_μ is the same tensor as for the τ-amplitudes, but with the occupied and the virtual indices reversed. That is, we order the indices of the λ-amplitudes in the opposite order from the τ-amplitudes, e.g., the doubles amplitudes are

$$\lambda_{ab}^{ij} \rightarrow \texttt{l\_2[i, j, a, b]}, \tag{9.84}$$

using NumPy arrays. We compute the next iteration of the λ-amplitudes from

$$\boldsymbol{\lambda}^{(i+1)} = \boldsymbol{\lambda}^{(i)} + \Delta\boldsymbol{\lambda}^{(i)}. \tag{9.85}$$

The convergence criteria for $\boldsymbol{\lambda}$ is the same as for the $\boldsymbol{\tau}$-amplitudes, i.e., we check if the Frobenius norm of each amplitude set is below a certain threshold.

9.3.2 Convergence acceleration

As discussed in section 7.3 the quasi-Newtion method can suffer from convergence instabillities. We can therefore use the alpha filter from subsection 7.3.1 and the DIIS technique from subsection 7.3.2 to accelerate the convergence. In order to use these techniques as they stand we need to define the predicted estimate z_i to use in the alpha filter and the error vectors in DIIS.

Alpha filter

For the alpha filter we define our predicted estimate to be

$$\boldsymbol{z}^{(i)} = \boldsymbol{\tau}^{(i)} + \Delta\boldsymbol{\tau}^{(i)}, \tag{9.86}$$

for the τ-amplitudes. The measurement is thus $\boldsymbol{\tau}^{(i)}$. Moving to the λ-amplitudes we define the predicted estimate similarly, viz.

$$\boldsymbol{z}^{(i)} = \boldsymbol{\lambda}^{(i)} + \Delta\boldsymbol{\lambda}^{(i)}, \tag{9.87}$$

and with the measurement as $\lambda^{(i)}$. This means that we need to represent our amplitude tensors as vectors, and in the case of more than one set of amplitudes we need to concatenate these vectors on top of one another. By letting $\alpha \to 1$ we include less and less of the next iteration. Setting $\alpha = 0$ we remove the convergence acceleration entirely.

DIIS

For the DIIS algorithm described in subsection 7.3.2 we define our error vectors to be

$$\boldsymbol{e}_i = \boldsymbol{\Omega}^{(i)}, \tag{9.88}$$

for both amplitude sets. This choice is made as we know that $\boldsymbol{\Omega} \to 0$ when we reach convergence and have found the optimized amplitudes. Thus the least squares minimization of the error vectors should yield the optimal converged amplitudes. The measured vector $\mathbf{p}_{i+1}$ is given by

$$\mathbf{p}_{i+1} = \boldsymbol{\tau}^{(i)} + \Delta\boldsymbol{\tau}^{(i)}, \tag{9.89}$$

for the τ-amplitudes and similarly for the λ-amplitudes. The extrapolated value from the DIIS algorithm is chosen as the new amplitude before starting the next iteration of the quasi-Newton method.

9.3.3 Non-orthogonal ground state solver

The non-orthogonal coupled-cluster doubles (NOCCD/OACCD) method has been implemented by Myhre as part of his article "Demonstrating that the nonorthogonal orbital optimized coupled cluster model converges to full configuration interaction" [21] and has been implemented into our framework by the author. We wish to use the quasi-Newton method for the orbital rotations κ in a similar fashion as for the cluster amplitudes in subsection 9.3.1. From

the stationary conditions in Equation 6.63 and Equation 6.64, we can compute the change in the orbital rotations by [62]

$$\Delta(\kappa^u)^{(i)} = -\frac{1}{D^a_i} \left. \frac{\partial L(\boldsymbol{\tau}, \boldsymbol{\lambda}, \kappa^u, \kappa^d)}{\partial \kappa^d} \right|_{\kappa=0}, \tag{9.90}$$

$$\Delta(\kappa^d)^{(i)} = -\frac{1}{D^i_a} \left. \frac{\partial L(\boldsymbol{\tau}, \boldsymbol{\lambda}, \kappa^u, \kappa^d)}{\partial \kappa^u} \right|_{\kappa=0}, \tag{9.91}$$

where the index placement of the $\mathbf{D}$-matrix should be noted. The stationary conditions for κ^u and κ^d are listed in section B.5. This lets us compute the next iteration of the rotations in the quasi-Newton method by

$$(\kappa^u)^{(i+1)} = (\kappa^u)^{(i)} + \Delta(\kappa^u)^{(i)}, \tag{9.92}$$

$$(\kappa^d)^{(i+1)} = (\kappa^d)^{(i)} + \Delta(\kappa^d)^{(i)}. \tag{9.93}$$

As discussed in subsection 6.1.8 the ground state algorithm for the NOCCD method can be formulated as [21, 62]:

1. Compute the orbital transformation matrices by

$$\mathbf{S} = \exp(\boldsymbol{\kappa}), \qquad \tilde{\mathbf{S}} = \exp(-\boldsymbol{\kappa}), \tag{9.94}$$

   where we use the matrix exponential function `scipy.linalg.expm` from SciPy [68] to compute the exponential of the $\boldsymbol{\kappa}$-matrices. Initially we set $\boldsymbol{\kappa} = \mathbb{1}$.

2. Change from the original atomic orbital basis to the new non-orthogonal basis using $\mathbf{S}$ and $\tilde{\mathbf{S}}$ as coefficient matrices for the ket and bra states respectively, as discussed in section 8.4.

3. Solve the τ and λ equations as described in subsection 9.3.1. Note that as we have transformed to the new non-orthogonal basis we need to recompute the D_μ-matrices.

4. Compute the stationary conditions for the orbital rotations from Equation 6.63 and Equation 6.64, and build the next $\boldsymbol{\kappa}$ from the new matrices $(\kappa^u)^{(i+1)}$ and $(\kappa^d)^{(i+1)}$ found from the quasi-Newton method.

We start the initial minimization using $\boldsymbol{\kappa} = \mathbb{1}$. This means that the initial iterations of the τ- and λ-amplitudes are the same as for the CCD-method, and if we are looking at a system where the CCD-method has "extreme" convergence issues, [5] the NOCCD-method will also follow the same diverging trend.

[5] By "extreme" convergence issues we mean so severe problems that the first iteration of the cluster amplitudes yield residuals that blow up and clearly diverges.

Now, the convergence criteria for the NOCCD method is slightly different than in the static ground state solvers. The method uses a semi-adaptive convergence scheme where we initially let the cluster amplitudes converge to a very low tolerance, i.e., a non-precise convergence. We then compute the new orbital rotations using the quasi-Newton method with optional convergence acceleration, e.g., DIIS. The convergence critera of the orbital rotations are found from the Frobenius norm of $\Delta(\kappa^u)^{(i)}$ and $\Delta(\kappa^d)^{(i)}$ as these should be zero in the optimal basis. Now we update the convergence criteria of the cluster amplitudes by multiplying the smallest orbital residual and multiplying it with some pre-defined factor. Choosing the largest tolerance criterion, either the newly computed tolerance from the orbital rotations, or some predefined termination tolerance we repeat the steps numerated above. Once the residuals of the orbital matrices are below the termination tolerance, we say that the method has converged.

9.3.4 Computing the coupled-cluster energy

In the case of "pure" ground state calculations for CCD and CCSD where we are only interested in the energy, we can compute the projected coupled-cluster energy from Equation 6.19. However, for the NOCCD-method we compute the full Lagrangian from Equation 6.61. As we continually transform to the new basis in the NOCCD-method this is equivalent to the coupled-cluster Lagrangian in Equation 6.42. This Lagrangian can also be used for the CCD- and CCSD-methods once we have found the optimal values for $\boldsymbol{\lambda}$. These are listed in section B.4.

9.3.5 Density matrices

Having found the converged τ- and λ-amplitudes we can compute the one- and two-body density matrices as discussed in subsection 6.1.7. These values only depend on the cluster amplitudes which means that NOCCD can reuse the density matrices from the static CCD-method. We have listed the tensor contractions involved for the one- and two-body density matrices in the CCD-method, and the one-body density matrix for the CCSD-method in Appendix C.

9.3.6 Time evolution with static orbitals

From Equation 6.72 and Equation 6.74 we find the equations of motion for the amplitudes. To evolve the amplitudes in time using a numerical integration

scheme we compute

$$\partial_t \tau_\mu = -i \langle \Phi_\mu | \exp(-\hat{T}(t)) \hat{H}(t) \exp(\hat{T}(t)) | \Phi \rangle , \tag{9.95}$$

$$\partial_t \lambda_\mu = i \langle \Phi | (\mathbb{1} + \hat{\Lambda}(t)) \exp(-\hat{T}(t)) \left[\hat{H}(t), \hat{X}_\mu \right] \exp(\hat{T}(t)) | \Phi \rangle , \tag{9.96}$$

where we have set $\hbar = 1$ in atomic units. Sans the imaginary number and sign these are just the τ- and λ-amplitude equations as used in the time-independent case. However, the Hamiltonian and the amplitudes themselves are the time-evolved states. The explicit tensor contractions for CCD and CCSD are listed in section B.2 and section B.3.

Now, the integration schemes assume a vector of derivatives instead of a set of rank 2 and rank 4 tensors. We therefore ravel the amplitude tensors using `np.ravel` from NumPy to represent them as a one-dimensional array. We then concatenate the arrays as a single long one-dimensional array. However, we have formulated all our amplitude equations using the rank 2 and 4 tensors and we must transform the input vector with amplitudes from the integration schemes to the correct shape of the amplitudes when solving the right-hand sides. To do this we have created a Python class called `AmplitudeContainer` which defines convenience functions handling the reshaping of the amplitudes. This class was originally intended to provide operators such as `__add__`, `__mul__`, etc, to allow direct manipulation of the amplitudes inside the containers when calling differential equation solvers. This worked relatively right out of the box for the Runge-Kutta 4 scheme, but once we included the Gauss-integrator with more complex manipulations of the solution vector we were forced to move to the – in hindsight – much smarter solution of making all the amplitudes into a single vector.

Using the Python dunder method `__iter__` we make `AmplitudeContainer` into a generator object, viz.

```
class AmplitudeContainer:
    # Code removed for clarity

    def __iter__(self):
        yield self._t
        yield self._l

    def unpack(self):
        yield from self._t
        yield from self._l
```

where `self._t` and `self._l` are Python lists with the τ- and λ-amplitudes respectively. The latter method `unpack` allows us to iterate over all the amplitudes in a for-loop. For CCSD `self._t` will be a list of three amplitudes, τ_0, τ_i^a and τ_{ij}^{ab}, where the τ_0 is the phase defined in section 6.5. The `self._l`-list will contain the two amplitudes λ_a^i and λ_{ab}^{ij}. The method for stacking all the

amplitudes into a vector is now given by Program 17. The inverse operation

Program 17 Function in `AmplitudeContainer` building a single vector with all coupled-cluster ampltides stacked on top of one another.

```
class AmplitudeContainer:
    # Code removed for clarity

    def asarray(self):
        np = self.np

        amp_vec = np.zeros(self.n)
        start_index = 0
        stop_index = 0

        for amp in self.unpack():
            start_index = stop_index
            stop_index += amp.size

            try:
                amp_vec[start_index:stop_index] += amp.ravel()
            except TypeError:
                amp_vec = amp_vec.astype(amp.dtype)
                amp_vec[start_index:stop_index] += amp.ravel()

        return amp_vec
```

where we go from a vector of amplitudes to two sets of amplitudes is demonstrated in Program 18. Note that this is a static method which means that the function is available outside an instance of the container object. This lets us build the container by comparing with an existing container denoted `u` where we assume that the dimensionality are the same in both containers.

9.3.7 Time-dependent energy

The time-dependent energy for the coupled-cluster method is computed in exactly the same way as for the variational ground state solvers, that is, by computing the Lagrangian from Equation 6.42. We have listed the Lagrangian for CCD and CCSD in section B.4.

9.3.8 Time-dependent overlap

Due to the dual state of $|\Psi\rangle$ in coupled-cluster not being the adjoint, we have that

$$\langle\tilde{\Psi}|\Psi\rangle \neq \langle\Psi|\tilde{\Psi}\rangle^* . \tag{9.97}$$

Program 18 Function in `AmplitudeContainer` building lists amplitudes and reshaping them into the correct rank.

```
class AmplitudeContainer:
    # Code removed for clarity

    @staticmethod
    def from_array(u, arr):
        np = u.np

        args = []
        start_index = 0
        stop_index = 0

        for amps in u:
            inner = []

            if type(amps) == list:
                for amp in amps:
                    start_index = stop_index
                    stop_index += amp.size

                    inner.append(
                        arr[start_index:stop_index].reshape(
                            amp.shape
                        )
                    )
            else:
                start_index = stop_index
                stop_index += amps.size
                inner = arr[start_index:stop_index].reshape(
                    amps.shape
                )

            args.append(inner)

        return type(u)(*args, np=np)
```

This means that there is an inherent ambiguity in the calculation of the autocorrelation as defined Equation 2.146 where $A(t, t_0) \neq A^*(t_0, t)$. To get around this we force hermiticity by computing the autocorrelation from [22]

$$A(t, t_0) \equiv \frac{1}{2}\left(\langle \tilde{\Psi}(t)|\Psi(t_0)\rangle + \langle \tilde{\Psi}(t_0)|\Psi(t)\rangle^* \right). \tag{9.98}$$

The time-dependent overlap can then be found by

$$P(t, t_0) = \left|A(t, t_0)\right|^2. \tag{9.99}$$

In Appendix D we have added explicit tensor contractions for both CCD and CCSD in order to compute the coupled-cluster autocorrelation.

9.3.9 Orbital-adaptive time evolution

We have in this thesis implemented the doubles truncation of the orbital-adaptive time-dependent coupled-cluster family; the OATDCCD-method. This method uses the NOCCD-method as its ground state solver due to the lack of an existing ground state OACCD-method [14]. Thus, after we have computed the ground state using the NOCCD-method, we change to this basis using the converged $\mathbf{S}$ and $\tilde{\mathbf{S}}$ as coefficient matrices with the latter serving as the left-hand coefficients.

To propagate the cluster amplitudes and the orbitals in time we start by noticing that

$$\mathcal{E}[\boldsymbol{\tau}, \boldsymbol{\lambda}, \Phi, \tilde{\Phi}] = \langle \tilde{\Psi}|\Big(\hat{H} - i\hbar\hat{\eta}\Big)|\Psi\rangle = \langle \tilde{\Psi}|\hat{H}|\Psi\rangle\,, \tag{9.100}$$

in the doubles approximation. This is a consequence of the gauge condition imposed on the orbital rotations with the occupied-occupied and virtual-virtual blocks of η_q^p being zero, viz.

$$\eta_b^a = \eta_j^i = 0, \tag{9.101}$$

and from the CCD one-body density matrix. In section C.1 we demonstrate that

$$\rho_i^a = \rho_a^i = 0, \tag{9.102}$$

which means that

$$\langle \tilde{\Psi}|\hat{\eta}|\Psi\rangle = \eta_q^p \langle \tilde{\Psi}|\hat{a}_p^\dagger \hat{\tilde{a}}_q|\Psi\rangle = \eta_q^p \rho_p^q = 0. \tag{9.103}$$

This means that the right-hand side evaluation in the OATDCCD-method now consists of evaluating the τ- and λ-amplitudes similarly as in the time-dependent static orbital coupled-cluster methods and we can reuse the machinery from the TDCCD-method to propagate the amplitudes. We then

move on to evolving the orbitals in time. This means that we must solve the P-space and Q-space equations as discussed in section 6.3. The equations of motion for the orbitals can then be expressed as [14]

$$\partial_t |\phi_p\rangle = (\hat{P} + \hat{Q})\partial_t |\phi_p\rangle = \eta_p^q |\phi_q\rangle + \hat{Q}\partial_t |\phi_p\rangle , \tag{9.104}$$

$$\partial_t \langle\tilde{\phi}_p| = \partial_t \langle\tilde{\phi}_p| (\hat{P} + \hat{Q}) = -\eta_q^p \langle\tilde{\phi}_q| + \partial_t \langle\tilde{\phi}_p| \hat{Q}, \tag{9.105}$$

where we in the second equation used that

$$\eta_q^p = \langle\tilde{\phi}_p|\partial_t|\phi_q\rangle = -\left(\partial_t \langle\tilde{\phi}_p|\right) |\phi_q\rangle . \tag{9.106}$$

We start by solving the P-space equations, which means that we need to compute the one- and two-body density matrices. These are listed in Appendix C. From the right-hand sides of Equation 6.124 and Equation 6.125 we can construct the two matrices R_a^i and R_i^a respectively, that is,

$$R_a^i = h_a^p \rho_p^i - h_q^i \rho_a^q + \frac{1}{2} u_{is}^{pq} \rho_{pq}^{as} - \frac{1}{2} u_{rs}^{aq} \rho_{iq}^{sr}, \tag{9.107}$$

$$\tilde{R}_i^a = h_i^p \rho_p^a - h_q^a \rho_i^q + \frac{1}{2} u_{is}^{pq} \rho_{pq}^{sa} - \frac{1}{2} u_{rs}^{aq} \rho_{iq}^{sr}, \tag{9.108}$$

where we note that $\partial_t \rho_i^a = 0$ in the doubles approximation. Next we construct the coefficient matrix $\mathbf{A}$ by

$$A_{aj}^{ib} \equiv \delta_a^b \rho_j^i - \delta_j^i \rho_a^b. \tag{9.109}$$

We can now formulate the P-space equations quite succintly by

$$i A_{aj}^{ib} \eta_b^j = R_a^i, \tag{9.110}$$

$$-i \eta_j^b A_{bi}^{ja} = \tilde{R}_i^a, \tag{9.111}$$

where atomic units are assumed. Here Equation 9.110 and Equation 9.111 are two linear equations for η_b^j and η_j^b respectively. To solve these equations we can either create compound indices such that $\boldsymbol{\eta}$, $\mathbf{R}$, and $\tilde{\mathbf{R}}$ become vectors, and similarly for $\mathbf{A}$ as a matrix. We use NumPy's method `np.linalg.tensorsolve` [69] to solve the linear equation more or less as they stand and let NumPy handle the dimensionality transformations. However, we do need to transpose the axes in the A_{aj}^{ib} array as we use a fixed ordering of the elements. For Equation 9.110 we have

$$A_{aj}^{ib} \to A_{jb}^{ai} \equiv \mathbf{A}_r, \tag{9.112}$$

whereas for Equation 9.111 we do

$$A_{aj}^{ib} \to A_{ai}^{bj} \equiv \mathbf{A}_l. \tag{9.113}$$

As matrices and vectors this then translates to the matrix equations

$$i\mathbf{A}_r\boldsymbol{\eta} = \mathbf{R}, \tag{9.114}$$

$$-i\tilde{\boldsymbol{\eta}}\mathbf{A}_l = \tilde{\mathbf{R}}, \tag{9.115}$$

where we have marked the virtual-occupied block of η_q^p by a tilde to distinguish it from merely the transpose of the occupied-virtual block. Solving both these equations yield the two non-zero blocks of η_q^p.

Having found η_q^p we can now solve the Q-space equations found in Equation 6.132 and Equation 6.135. Recalling that

$$\hat{Q} \equiv \mathbb{1} - \hat{P} = \mathbb{1} - |\phi_p\rangle\langle\tilde{\phi}_p|, \tag{9.116}$$

where the sum over the orbitals can be truncated to further lower the computational cost of the OATDCCD-method. In this thesis we have not included any studies where we truncate the orbital basis further. The Q-space equations therefore simplifies as the right-hand side of Equation 6.132 and Equation 6.135 will be zero. A demonstration of this fact is shown in section B.6. The Q-space equations thus reduce to

$$i\rho_p^q \hat{Q}\partial_t |\phi_q\rangle = 0 \implies \partial_t |\phi_q\rangle = \eta_q^r |\phi_r\rangle, \tag{9.117}$$

$$-i\rho_p^q \left(\partial_t \langle\tilde{\phi}_q|\right) \hat{Q} = 0 \implies \partial_t \langle\tilde{\phi}_q| = -\langle\tilde{\phi}_r|\eta_r^q. \tag{9.118}$$

We denote the biorthonormal basis of single-particle states from NOCCD by $\{\chi_\alpha\}$ where we have

$$\langle\tilde{\chi}_\alpha|\chi_\beta\rangle = \delta_{\alpha\beta}. \tag{9.119}$$

The time-dependent orbitals can then be constructed from the ground state orbitals by

$$|\phi_p(t)\rangle = C_{\alpha p}(t)\,|\chi_\alpha\rangle, \tag{9.120}$$

$$\langle\tilde{\phi}_p(t)| = \tilde{C}_{p\alpha}(t)\,\langle\tilde{\chi}_\alpha|, \tag{9.121}$$

where the time-dependence is kept in the coefficients. The equations of motion for the coefficients is then found by projecting onto the ground state orbital basis. This gives

$$\dot{C}_{\alpha q} = C_{\alpha r}\eta_q^r \implies \dot{\mathbf{C}} = \mathbf{C}\boldsymbol{\eta}, \tag{9.122}$$

$$\dot{\tilde{C}}_{q\alpha} = -\eta_r^q \tilde{C}_{r\alpha} \implies \dot{\tilde{\mathbf{C}}} = -\boldsymbol{\eta}\tilde{\mathbf{C}}, \tag{9.123}$$

where we denote the derivative of the coefficient matrices in time by a dot.

In order to use known numerical integration schemes we collect all the amplitudes and the coefficients together in a single vector as done for the

Program 19 Iterator and unpacking methods for `OACCVector`.

```
class OACCVector(AmplitudeContainer):
    # Code removed for clarity

    def __iter__(self):
        yield self._t
        yield self._l
        yield self._C
        yield self._C_tilde

    def unpack(self):
        yield from super().unpack()
        yield self._C
        yield self._C_tilde
```

regular time-dependent coupled-cluster methods. In fact, we are able to reuse the `AmplitudeContainer`-class by creating a subclass called `OACCVector` which only needs new `__iter__` and `unpack` methods thanks to the generality of `AmplitudeContainer`. These are listed in Program 19. We are then able to reuse the `asarray` and `from_array` methods from `AmplitudeContainer`. Thus we can reuse the already implemented differential equation solvers.

9.3.10 Measuring quantities

More or less all measurable quantities can be computed in the same manner as for the regular time-dependent coupled-cluster method, but we must remember to change the basis of the matrix elements as discussed in section 8.4.

9.3.11 Time-dependent overlap

A significant drawback of the orbital-adaptive time-dependent coupled-cluster family of methods are their inability to compute the time-dependent overlap, or the autocorrelation, in polynomial time. The main reason for this is that the overlap is computed at two separate times which yield two different sets of operators. We can see this from

$$|\phi_p(t)\rangle = \hat{d}_p^\dagger(t)\,|-\rangle = C_{\alpha p}(t)\,|\chi_\alpha\rangle = C_{\alpha p}(t)\hat{d}_\alpha^\dagger(0)\,|-\rangle \tag{9.124}$$

$$\implies \hat{d}_p^\dagger(t) = C_{\alpha p}(t)\hat{d}_\alpha^\dagger(0), \tag{9.125}$$

$$\implies \hat{\tilde{d}}_p(t) = \tilde{C}_{p\alpha}(t)\hat{\tilde{d}}_\alpha(0), \tag{9.126}$$

where we have expressed the time-evolved biorthonormal second quantized operators as a linear combination of the initial operators. Now, the biorthonor-

mality condition is only maintained at equal times which means that

$$\left\{\hat{d}_p^\dagger(t), \hat{\tilde{d}}_q(t_0)\right\} \neq \delta_{pq}, \tag{9.127}$$

in general. To get around this we express all operators in terms of the initial operators and use the coefficient matrices to keep track of the time-dependence. Looking at the doubles cluster amplitudes we then have

$$\hat{T}_2(t) = \tau_{ij}^{ab}(t)\hat{d}_a^\dagger(t)\hat{d}_b^\dagger(t)\hat{\tilde{d}}_j(t)\hat{\tilde{d}}_i(t) = \tau_{\gamma\delta}^{\alpha\beta}(t)\hat{d}_\alpha^\dagger(0)\hat{d}_\beta^\dagger(0)\hat{\tilde{d}}_\delta(0)\hat{\tilde{d}}_\gamma(0), \tag{9.128}$$

where we have defined the transformed cluster amplitudes

$$\tau_{\gamma\delta}^{\alpha\beta}(t) \equiv \tau_{ij}^{ab}(t)C_{\alpha a}(t)C_{\beta b}(t)\tilde{C}_{j\delta}(t)\tilde{C}_{i\gamma}(t). \tag{9.129}$$

An imporant point to note in Equation 9.128 is that the sum over the greek indices run over the entire basis set of initial orbitals $\{\chi_\alpha\}$. This means that the $\hat{T}$-operators no longer are excitation operators in the usual sense, and similarly for the $\hat{\Lambda}$-operators no longer being relaxation operators. At equal times the biorthonormality condition is fulfilled by the coefficients. As this is not the case for unequal times, the overlap can be found by

$$\langle\tilde{\Psi}(t)|\Psi(t_0)\rangle = \langle\tilde{\Phi}(t)|(\mathbb{1} + \hat{\Lambda}(t))\exp(-\hat{T}(t))\exp(\hat{T}(t_0))|\Phi(t_0)\rangle, \tag{9.130}$$

where the unequal times in the reference determinants remove our ability to use the Fermi vacuum formalism as the right and left reference determinants are defined in terms of different second quantized operators. This problem resembles the variational formulation of the coupled-cluster method as discussed in subsection 6.1.5.

This means that we are unable to compute the spectrum of energy levels of a system. However, we are still able to compute the energy transitions using the dipole moment.

Part III

Results

Chapter 10

Validation

> Testing shows the presence, not the absence of bugs.
>
> — Edsger Wybe Dijkstra

As the quote by E. W. Dijkstra so succintly puts, testing will only reveal the presence of bugs and there are most likely bugs present in the developed code that we are unable to locate. However, continuous testing over time will help make sure that new additions and evolution of existing code will not break at a later time. Our codes have contribution from several authors and we have therefore implemented a wide range of unit tests where these make sense, integration tests running longer simulations and checking the results against known results. In fact, both the studies in this chapter are implemented as tests in a more brief version to make sure that changes to the code should still reproduce what we present in this chapter. To ensure continuous testing – and deployment of the documentation – we use Travis CI.[1] This means that all changes to the git-repositories run through the test-suites automatically and checks that known values are reproduced.

The focus in this thesis is on time evolution of quantum mechanical systems, and as such we will mainly look at time-dependent phenomena with little focus on ground state solutions. However, note that several known ground state values, in particular for one- and two-dimensional quantum dots, are implemented as tests. In this chapter we wish to demonstrate that our implementations work as expected by reproducing known results from the literature. We will in this section limit our attention to small systems.

[1] See: `https://travis-ci.com/`

10.1 The one-dimensional harmonic oscillator

An excellent starting point for validation is the one-dimensional harmonic oscillator using the discretized one-dimensional quantum dot system as discussed in section 8.1. A study done by Zanghellini *et al.* [99] explores the multi-configuration time-dependent Hartree-Fock method on the one-dimensional harmonic oscillator system for two particles compared to a semi-analytic result.[2] In this study the confining potential is given by the harmonic oscillator potential,

$$\hat{v} = \frac{1}{2}\omega^2\hat{x}^2, \tag{10.1}$$

where atomic units are used. Zanghellini *et al.* uses a monochromatic, dipole, laser field described by

$$E(t) = E_0 \sin(\Omega t)\hat{x}, \tag{10.2}$$

which is active for the entire simulation. The Coulomb interaction is described by the shielded Coulomb interaction from Equation 8.21 with $\alpha = 1$ and the screening parameter set to $a = 0.25$. In the simulation done by Zanghellini *et al.* the parameters are chosen to be $\omega = 0.25$, $E_0 = 1$, and $\Omega = 8\omega$. The simulation is run on a one-dimensional grid where $x \in [-10, 10]$. We use a relatively small basis of $L = 20$ spin-orbitals, that is, the $L/2 = 10$ first one-dimensional harmonic oscillator orbitals found by diagonalizing the one-body Hamiltonian. The time evolution is run for $t = 4\tau$ where τ is a cycle of the laser given by

$$\tau = \frac{2\pi}{\Omega}. \tag{10.3}$$

We use an integration time step of $\Delta t = 1 \times 10^{-2}$ and the Gauss-integrator with $s = 3$ and a fix-point convergence threshold of $\epsilon = 1 \times 10^{-6}$.

We will reproduce part of the study done by Zanghellini *et al.* using the following methods: time-dependent Hartree-Fock (TDHF), time-dependent configuration interaction with doubles and singles-and-doubles excitations (TDCID and TDCISD), and time-dependent coupled-cluster with doubles and singles-and-doubles excitations (TDCCD and TDCCSD), as well as the their ground state counterparts. We do not include the non-orthogonal coupled-cluster doubles (NOCCD) nor the orbital-adaptive time-dependent coupled-cluster doubles (OATDCCD) methods, as part of the study is a comparison of the time-dependent overlap which we have not implemented for the latter method as dicussed in subsection 9.3.11. In Figure 10.1 we plot the ground

[2] Semi-analytic as the time evolution is solved numerically.

Table 10.1: In this table we list the ground state energies computed for the one-dimensional harmonic oscillator. The values are rounded to four decimal places.

Method	Energy [E_h]	Relative error
HF	1.1798	0.4306
CID	1.0516	0.2751
CCD	1.0516	0.2751
CID-HF	0.8384	0.0166
CCD-HF	0.8384	0.0166
CISD	0.8253	0.0007
CCSD	0.8253	0.0007

state particle densities using the general Hartree-Fock method and CISD, i.e., full configuration interaction for two particles. In the lower plot in Figure 10.1 we demonstrate that CCSD reproduces the exact solution for the particle density as achieved from configuration interaction to a high precision by computing the absolute difference between each point on the grid, that is,

$$\left|\Delta\rho(x,0)\right| = \left|\rho_{\mathrm{CISD}}(x,0) - \rho_{\mathrm{CCSD}}(x,0)\right|. \tag{10.4}$$

We have listed the ground state energies in Table 10.1 for the different solver methods. We compute the relative error by

$$e_{\mathrm{rel}} = \frac{|E - E_{\mathrm{ref}}|}{|E_{\mathrm{ref}}|}, \tag{10.5}$$

where $E_{\mathrm{ref}} = 0.8247\,E_h$ as the exact value from Zanghellini *et al.* [99]. Note that the relative error is computed for the rounded values.

In Figure 10.2 we show the time-dependent overlap for two one-dimensional quantum dots subject to the same dipole laser as in the study done by Zanghellini *et al.* [99]. We also show how TDCCSD reproduces the exact TDCISD solution to a large degree by computing the absolute difference between the overlap from TDCISD and TDCCSD. By inspection we see that both the particle density in Figure 10.1 and the time-dependent overlap in Figure 10.2 resembles the results from Zanghellini *et al.* [99], and we conclude that TDHF, TDCISD, and TDCCSD work as expected with the latter two methods serving as exact solutions within the finite single-particle space we explore.

Before moving on to more exotic systems, we will look shortly at the performance of CCD and CID applied to the same one-dimensional harmonic

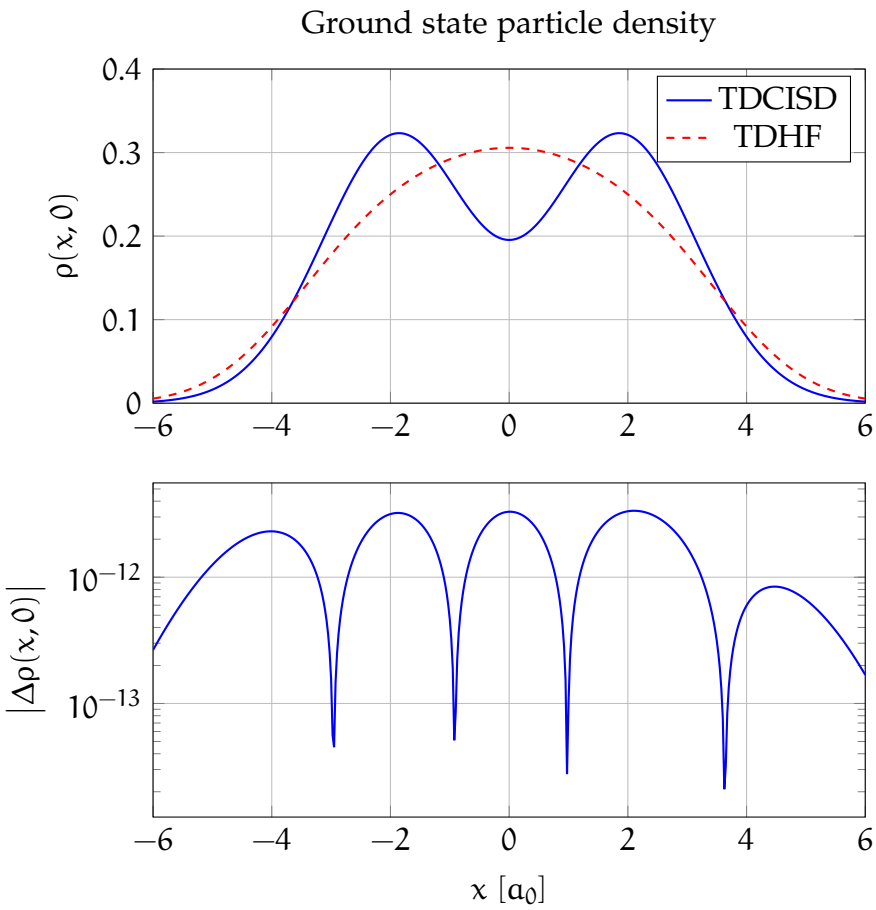

Figure 10.1: In the top figure we have reproduced Figure 1. in the study done by Zanghellini *et al.* [99], that is, we have plotted the particle density for two one-dimensional quantum dots in an harmonic oscillator trap using full-configuration interaction and a general Hartree-Fock solver. In the lower figure we have plotted the absolute difference between the particle densities from the full-configuration interaction and coupled-cluster with singles-and-doubles methods.

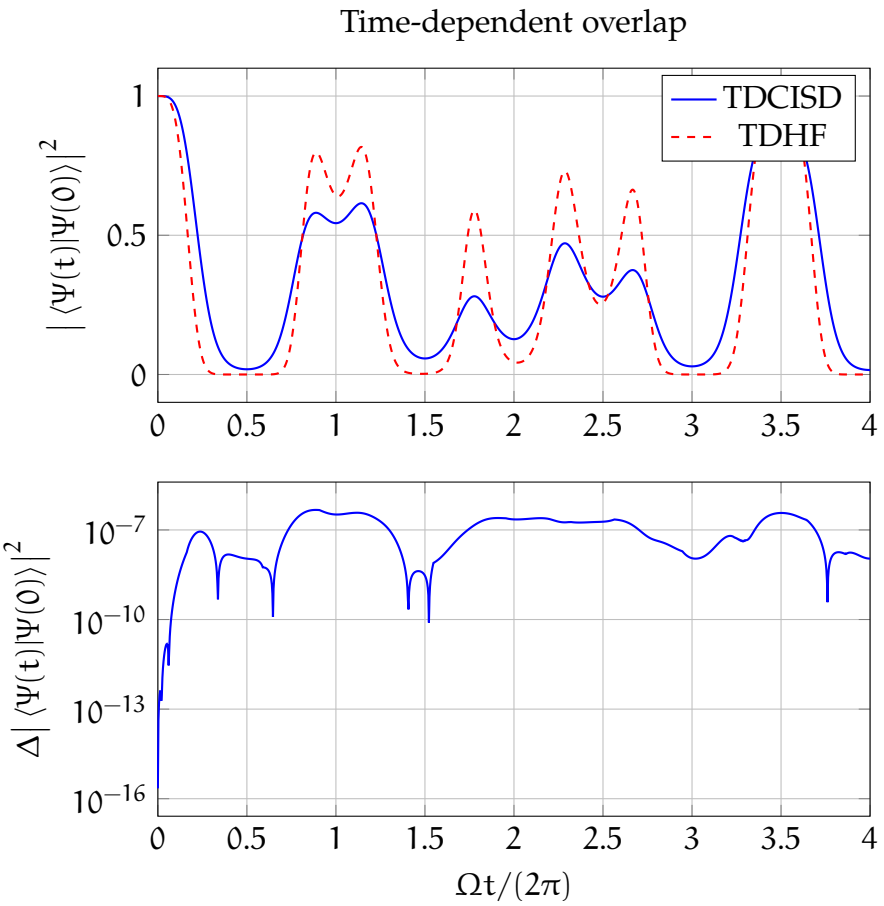

Figure 10.2: In the top figure we have plotted the time-dependent overlap between the initial ground state $|\Psi(0)\rangle$ and the state $|\Psi(t)\rangle$ at a later time. We compare the time-dependent general Hartree-Fock method and the time-dependent full configuration interaction method. The figure is a reproduction of Figure 2. in the study done by Zanghellini *et al.* [99]. In the lower figure we show the absolute difference in the overlap between the time-dependent full configuration interaction method and the time-dependent coupled-cluster method with singles and doubles.

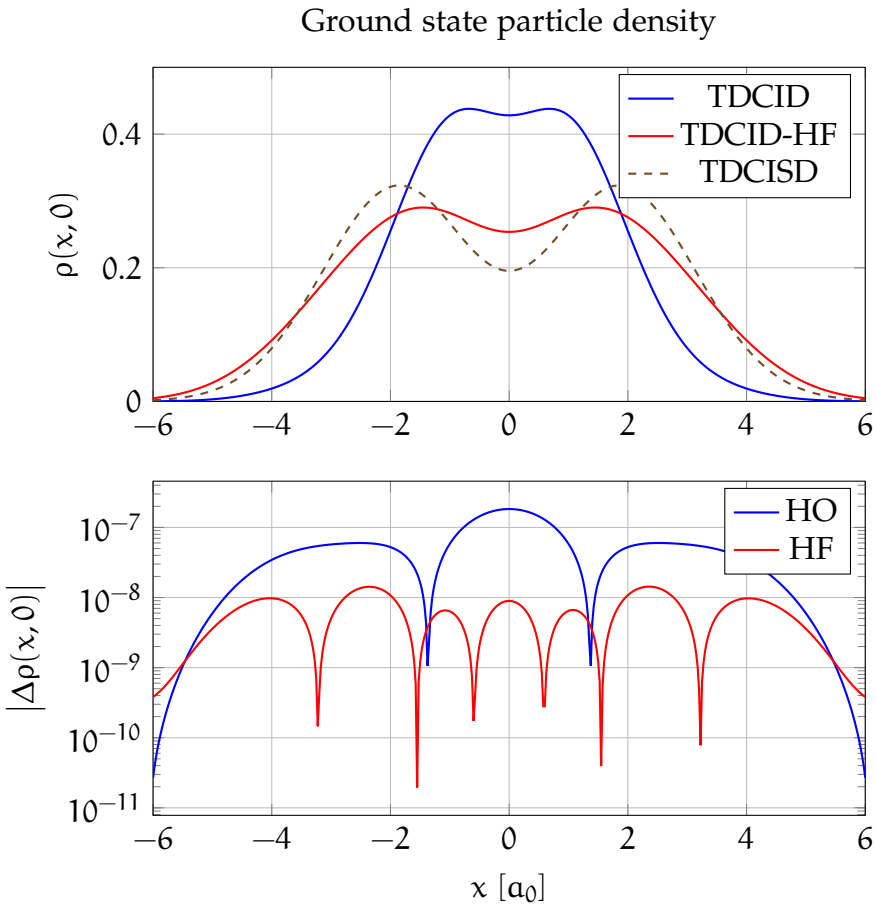

Figure 10.3: In this figure we try to reproduce Figure 10.1 using plain CID and CID with a Hartree-Fock basis. The lower figure shows the absolute difference between CCD and CID with a harmonic oscillator (HO) basis and a Hartree-Fock (HF) basis.

oscillator system. The reason for doing this is to demonstrate the importance of the singles excitation operator. Looking at Figure 10.3 we can see how the doubles approximations CID and CCD with the harmonic oscillator basis are quite far from the full configuration interaction benchmark. Performing a Hartree-Fock calulation and transforming to the new molecular orbital basis we see that CID and CCD are much better at reproducing the full configuration interaction result. This demonstrates the effectiveness of Brillouin's theorem by moving to the optimal single-reference determinant found in Hartree-Fock. However, we see that this does not completely remove the need for a singles operator as the result for CID and CCD in the molecular orbital basis are still quite far from the exact results.

In Figure 10.4 we show how TDCID and TDCCD with and without a Hartree-Fock basis is unable to give a good reconstruction of the exact so-

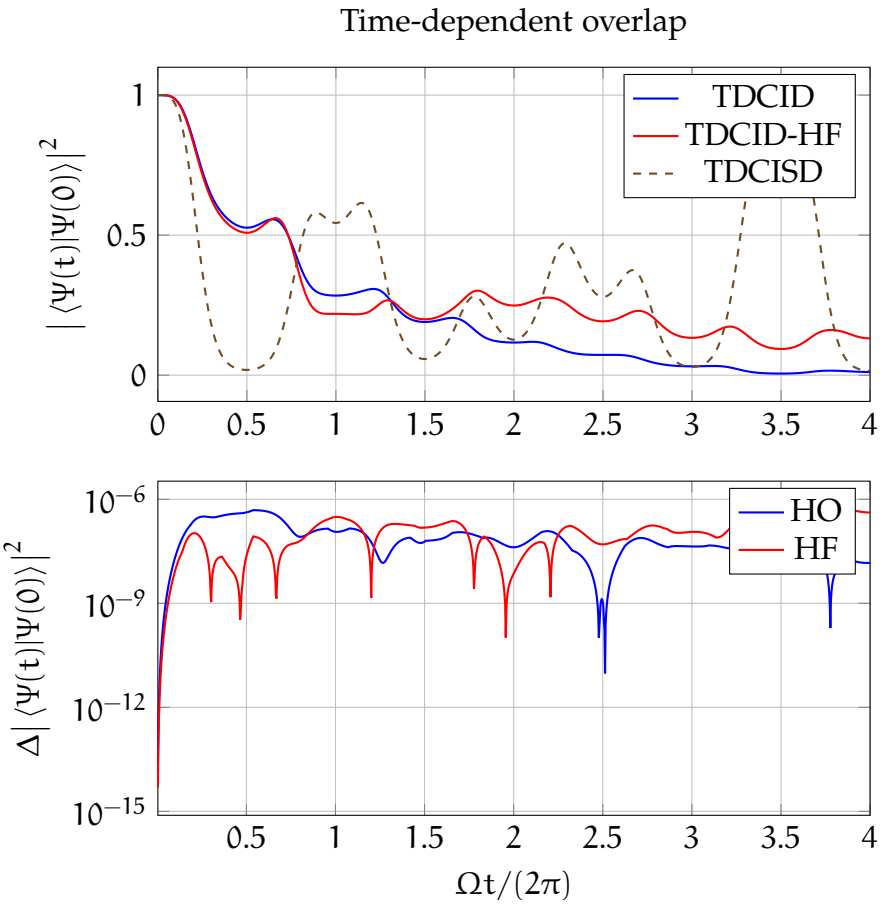

Figure 10.4: Here we reproduce Figure 10.2 with the doubles approximations CID and CCD using both the original harmonic oscillator (HO) basis, and the Hartree-Fock (HF) basis. In the lower figure we demonstrate the absolute error between CID and CCD using both basis sets.

lution from full configuration interaction. The lack of singles excitations become glaringly apparent once we start the time evolution of the system. This can be seen as an effect of the laser field being described by a singles operator. It is therefore likely that a singles-excitation operator best describes this interaction and the doubles approximation will have problems properly depicting the dynamics. In fact, comparing with Figure 10.2 we see that TDHF gives a qualitatively much better approximation to the exact results. This demonstrates that the singles approximation is essential for the laser driven dynamics we explore.

We therefore conclude that the pure doubles approximations are inferior at describing the dipole laser fields we explore and we will therefore not use these for any significant results in the remainder of this thesis.

10.2 Two-electron molecule

In a study on the optical response of molecules subject to an intense laser fields done by Li *et al.* [100] a comparison of the time-dependent Hartree-Fock method and the time-dependent full configuration interaction[3] is performed. This provides us with an ample opportunity to repeat the experiments in order for us to verify our methods. We will therefore reproduce parts of the study done by Li *et al.* using TDHF, TDCISD, TDCCSD, and OATDCCD.

We will look at the smallest molecule H_2, that is, the Hydrogen-molecule with two electrons. This means that TDCISD, TDCCSD, and OATDCCD should produce exact results for the single-particle basis that is used. We express H_2 in 14 Gaussian type orbitals, that is, the 6-311++G(d, p) basis set, with an equilibrium geometry of $R_e = 0.7354\,\text{Å} \approx 1.3897\,a_0$. We use PySCF [18] to create the basis set with the string `"6-311++Gss"`. We center the molecule around the origin with each atom located at $\pm R_e/2$ in the z-direction zero for the x- and y-direction. We then make the basis set doubly occupied by including spin. We perform a ground state calculation using the general Hartree-Fock solver and transform to this basis. We then do ground state computations using the time-independent version of the specific solvers berfore starting the time evolution. The laser pulse used by Li *et al.* is

$$\mathbf{E}(t) = \hat{\mathbf{d}} \cdot \mathbf{f}(t) \sin(\omega t), \tag{10.6}$$

where the envelope function is given by $\mathbf{f}(t) = f(t)\boldsymbol{\epsilon}$ with $\boldsymbol{\epsilon}$ as the polarization vector. The envelope is described by

$$f(t) = \begin{cases} (\omega t/2\pi)E_m, & \omega t \in [0, 2\pi], \\ E_m, & \omega t \in [2\pi, 4\pi], \\ [3 - \omega t/(2\pi)]E_m, & \omega t \in [4\pi, 6\pi], \\ 0, & \omega t \neq [0, 6\pi], \end{cases} \tag{10.7}$$

where we set $E_m = 0.07\,E_h \approx 1.72 \times 10^{14}\,W/cm^2$ and $\omega = 0.1\,E_h/\hbar$ which corresponds to a wavelength of $\lambda = 456\,nm$. We run the simulation for a total of $t_f = 225\,\hbar/E_h$ with the laser turned on from the start. We use the Gauss-integrator as discussed in subsection 7.4.3 with $s = 3$, a fix-point convergence threshold of $\epsilon = 1 \times 10^{-6}$, and an integration time step of $\Delta t = 1 \times 10^{-2}\,\hbar/E_h$. In our programs the dipole moment is defined with a positive sign, which means that we need to introduce a negative sign in the envelope or the polarization vector to include the negative charge of the electrons. We have chosen to set the polarization vector along the negative z-direction.

[3] Note that Li *et al.* denotes the time-dependent full-configuration interaction method by: "the time-dependent Schrödinger equation".

A plot of the instantaneous dipole moment of H_2 is shown in Figure 10.5. A by-eye comparison of the top figure in Figure 10.5 with figure 4 in "A time-dependent Hartree–Fock approach for studying the electronic optical response of molecules in intense fields" [100] shows that we are in perfect agreement with the results of Li *et al.*. In the lower figure we show the absolute error in the induced dipole moment as calculated by the TDCCSD and OATDCCD methods compared with the exact full configuration interaction solution. As the error between the TDCISD, and TDCCSD and OATDCCD are smaller than the convergence threshold of the Gauss-integrator, we conclude that TDCCSD and OATDCCD reproduce the exact results to a satisfying degree. The TDHF-method is several orders of magnitude off from the coupled-cluster methods, but it is interesting to note in the top figure in Figure 10.5 that the time-dependent Hartree-Fock method performs qualitatively well. There are small discrepancies visible to the eye, but at the intensity we use for our laser the mean-field approximation performs excellently. However, we expect that as the intensity increases, this method will prove inferior to the correlated methods.

10.3 Summing up the validation

We have now demonstrated that the bulk of our methods perform as expected and give satisfying results for small systems. Furthermore, we have demonstrated that the self-made one-dimensional system and the interface towards PySCF [18] are working. We have also demonstrated that we support several dipole laser fields and that we can compute various quantities from all methods. Recalling the words of E. W. Dijkstra we do note that we have not proven our methods to be free of bugs, but at least we have demonstrated that a wide range of our code works as expected.

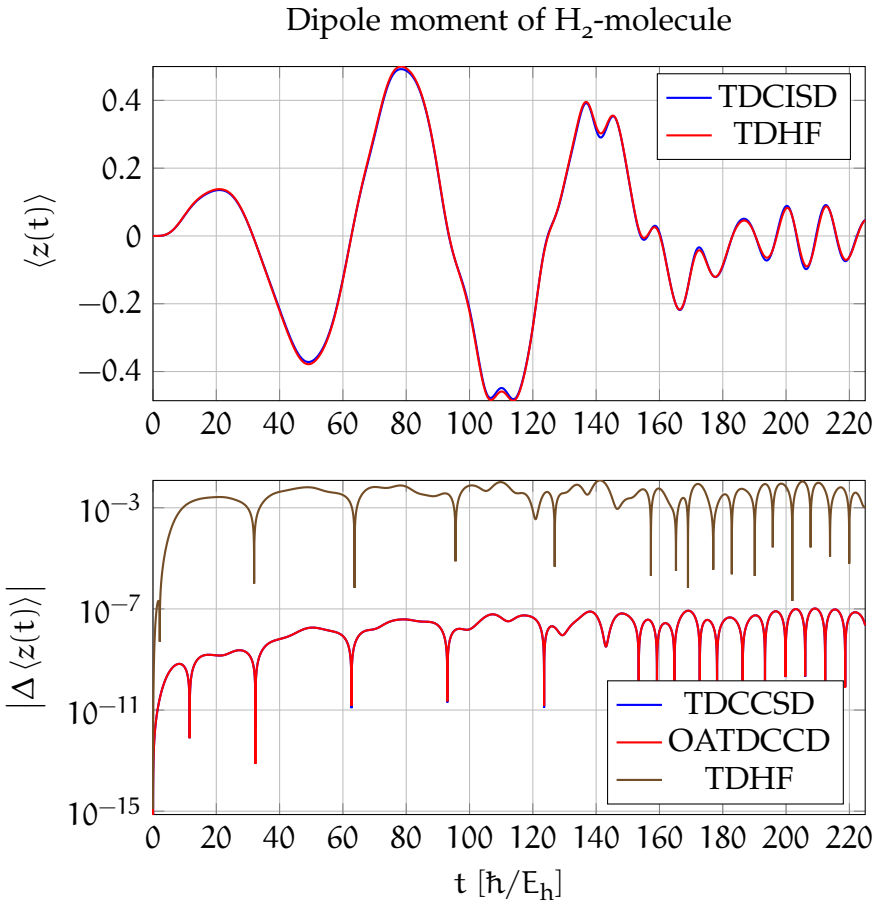

Figure 10.5: In the top figure we have plotted the instantaneous dipole by radiating a H_2 molecule with a dipole laser. The lower figure shows the absolute error of the dipole using the TDHF, TDCCSD, and OATDCCD methods compared to the TDCISD solver.

Chapter 11

Stability of the coupled-cluster methods

In this chapter we will explore some aspects of the stability of the implemented coupled-cluster methods. We also seek to answer the question of why we should even consider the conceptually more complicated orbital-adaptive time-dependent coupled-cluster methods as opposed to the known time-dependent coupled-cluster methods with static orbitals.

11.1 Why bother with orbital rotations?

In chapter 10 we demonstrated how both TDCCSD and OATDCCD provided excellent agreement with exact solution for the 2-particle systems. An important question to answer is then why we should even bother implementing OATDCCD, when TDCCSD seems to suffice. Especially so, as we in our implementation do not truncate the single-particle basis for OATDCCD. This is one of its strengths as an approximation to the multi-configuration time-dependent Hartree-Fock family of methods. Removing this strength from OATDCCD seems to leave us with a method that performs just as well as the TDCCSD method. As part of the original motivation for this thesis, we wished to study the OATDCCD-method as an academic study of a rather novel method. However, as pointed out by Pedersen & Kvaal [22], the TDCCSD-method is *unstable* when simulating a system subject to a strong external field. This is even the case for 2-particle systems where TDCCSD is formally exact within the finite single-particle basis. Pedersen & Kvaal conjectured that the inclusion of orbital rotations might alleviate the stability issues experienced by TDCCSD, and we will here verify that this is indeed the case.

We will use exactly the same fields, atoms, and parameters as Pedersen &

Kvaal. The dipole laser pulse is given by

$$\mathbf{E}(t) = \mathbf{E}\cos(\omega t)G(t), \tag{11.1}$$

where the envelope function $G(t)$ is given by

$$G(t) = \sin^2(\pi t/t_d). \tag{11.2}$$

Here t_d is the duration of the laser pulse and the envelope is active for $t \in [0, t_d]$. Note that atomic units are assumed throughout this study. We let the negative charge of the electrons occur in the polarization vector. The atoms we look at are He (Helium) and Be (Beryllium) in the cc-pVDZ-basis, and we will use TDFCI (TDCISDTQ) simulations as the ground truth. We will run the simulations using both TDCCSD and OATDCCD with the restricted Hartree-Fock reference determinant from PySCF as our reference state. We set $t_d = 5\,\hbar/E_h$ and run the simulation for $t_f = 10\,\hbar/E_h$. We have chosen a rather crude time step of $\Delta t = 1 \times 10^{-2}\,\hbar/E_h$, but for the Gauss-integrator with $s = 3$ and $\epsilon = 1 \times 10^{-6}$ this should be acceptable. The frequency for He is set to $\omega_{He} = 2.873\,564\,3\,E_h/\hbar$, and for Be we have $\omega_{Be} = 0.206\,817\,5\,E_h/\hbar$ in accordance with Pedersen & Kvaal [22]. As we merely wish to demonstrate that OATDCCD is stable where TDCCSD is not, we only look at the most intense case with an electric field strength of $E_{He} = 100\,E_h/(ea_0)$ for He and $E_{Be} = 1\,E_h/(ea_0)$ for Be.

As there are no expressions for the autocorrelation of the OATDCCD-method, we are unable to compare with the autocorrelation as done in the article by Pedersen & Kvaal. Therefore, as part of the stability analysis we will sample the Frobenius norm of the cluster amplitudes, and the time-dependent overlap with the reference determinant as discussed in section 6.5. We will compare this with the weight of the reference determinant in the TDFCI simulations, i.e., $\left|c_0(t)\right|^2$, the zeroth compononent in the TDFCI coefficient vector.

In Figure 11.1 we see the results from the simulation of He. We see that the dashed line with the results from the TDCCSD-method for the time-dependent overlap and the time-dependent energy stops after a short time, at $t \approx 0.87\,\hbar/E_h$. This was where the Gauss-integrator crashed due to a non-converging fix-point iteration. We see that this point more or less exactly matches the point where the overlap with reference state becomes close to zero as conjectured. Furthermore, by looking at the lowermost palette we see a perfect correlation with the norm of the TDCCSD-amplitudes sky-rocketing when the overlap goes to zero. We can push this simulation through by lowering the time step, but we have left this out of the study as we wish to demonstrate that OATDCCD is stable for the given time step. A too low time step would result in an extremely impractical simulation where the time to reach any reasonable length scales would take orders of magnitude more simulation time.

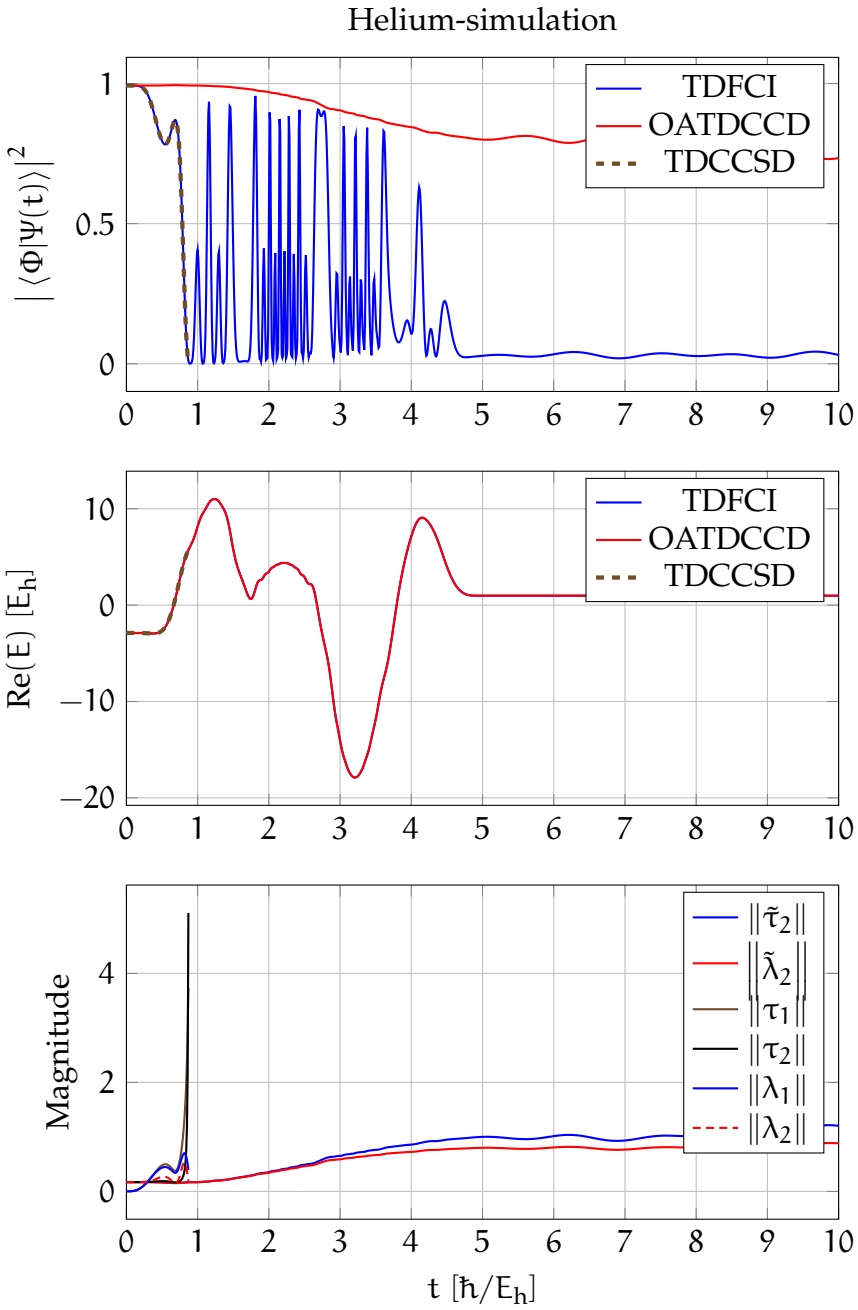

Figure 11.1: In these figures we have plotted the overlap with the reference state in time, and the real part of the time-dependent energy of the three solvers TDFCI (TDCISD), TDCCSD, and OATDCCD for the He system. In the lowermost palette we have plotted the magnitude of the cluster amplitudes and the Lagrange multipliers for OATDCCD (marked with a tilde) and TDCCSD.

In Figure 11.2 the results from the simulation of Be is shown. Again the same behaviour as for the simulation of He is exhibited; once the overlap with the reference determinant becomes small, the amplitudes sky-rocket and the TDCCSD-method crashes. In both simulations we see that the TDFCI solutions drops down to a low overlap with the reference state, but this is not a problem for the TDFCI-methods as they can always remove the weigth of the reference state. This does however demonstrate that the initial Hartree-Fock reference determinant is poor choice for the intense fields we explore in these simulations. It is more interesting to see how the OATDCCD-method seems completely unaffected by the choice of a poor reference state as it is able to rotate to a new set of orbitals thereby creating a much better reference state. We also see his behavior in the norm of the amplitudes of the OATDCCD-method. The more optimal reference determinant seems to remove the stress from the amplitudes and OATDCCD does not seem to exhibit the same stability issues in the simulations we have demonstrated in Figure 11.1 and Figure 11.2.

We do not however state that the OATDCCD-method is infinitely stable as there are several situations which we believe would break the simulation, e.g., a near multireference state, oscillations between two (almost) equally good reference states. In short, if there does not exist a single good reference state, we believe the OATDCCD-method will suffer the same fate as for the TDCCSD-method.

11.2 Summing up the stability analysis

We have now demonstrated why the OATDCCD-method is an important method for dynamics of many-body systems as it provides a more stable solver than the TDCCSD-method. A further study of this phenomenon will not included in this thesis as the author is participating in an ongoing work on the stability of the OATDCCD-method titled "Numerically stable time-dependent coupled-cluster simulations of many-electron dynamics in intense laser pulses" [66]. In the following we will not look at stability issues in more detail, but rather focus on the application of the methods to various systems.

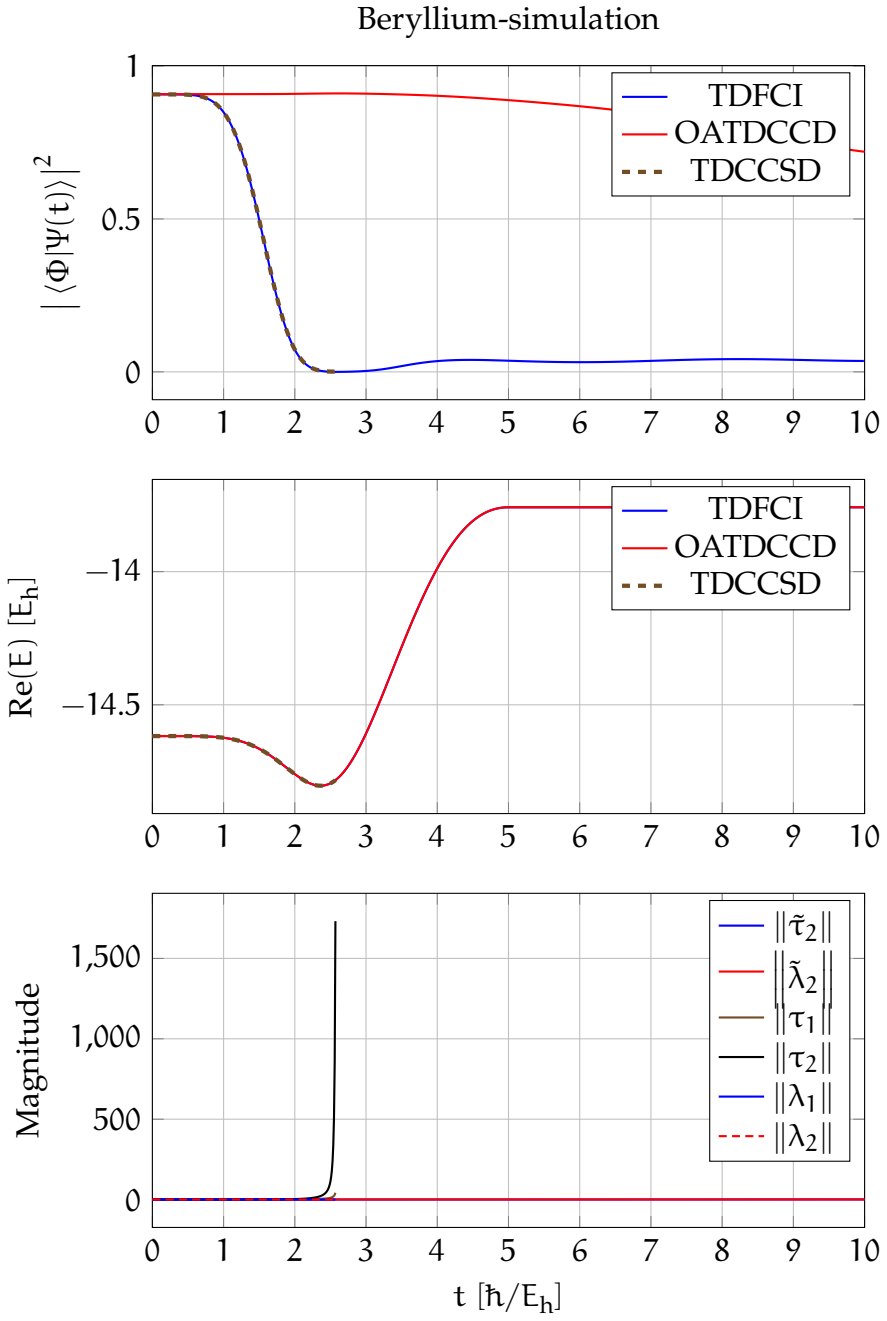

Figure 11.2: In these figures we have plotted the overlap with the reference state in time, and the real part of the time-dependent energy of the three solvers TDFCI (TDCISD), TDCCSD, and OATDCCD for the Be system. The lower palette exhibits the magnitude of the cluster amplitudes and the Lagrange multipliers for OATDCCD (marked with a tilde) and TDCCSD.

Chapter 12

Applications

Having verified that our implementations work on smaller systems in chapter 10 and demonstrated the strength of the orbital-adaptive coupled-cluster methods in chapter 11 we now seek to push the methods by exploring more complicated systems. Our goal is to firmly establish that we are able to explore larger systems than can be done with the full configuration interaction method and the multi-configuration Hartree-Fock method, while achieving a quality of the results beyond what is possible with the mean-field approximation using Hartree-Fock. Furthermore, we wish to demonstrate the versatility of our methods by studying exotic systems such as spin-dependent laser field interactions and ionization of the one-dimensional Beryllium-atom. Note that we in this chapter do little to no conscious effort in terms of optimization as the default setup of the solvers often yield more than good enough results. This means that we can focus as much as possible on the physics of the problems.

12.1 Electronic spectra of molecules

In an article by Nest *et al.* [101] the multiconfiguration time-dependent Hartree-Fock method was tested on a system of lithium hydride and methane subject to a dipole laser pulse with a sine-squared envelope on the form[1]

$$\mathbf{E}(t) = -\boldsymbol{\epsilon} E(t) \sin^2\big(\pi t/T\big) = -\boldsymbol{\epsilon} E_0 \sin(\omega t) \sin^2\big(\pi t/T\big), \tag{12.1}$$

where $\boldsymbol{\epsilon}$ is the polarization vector, ω is the frequency corresponding to a photon energy of $E_\nu = 5.44\,eV$. The negative sign in the polarization vector comes from the charge of the electrons. The laser field is active for $t \in [0, T]$ where $T = 1\,fs$, and the intensity of the laser field is chosen to

[1] Note that Nest *et al.* [101] does not explicitly add a formula for the laser, but based on their description we infer the form of the laser.

Table 12.1: In this table we show the conversions used to move from the SI units given in the article by Nest *et al.* [101] to the atomic units used in the simulation.

Quantity	SI units	Atomic units
E_ν	$5.44\,eV$	$1.999\,163 \times 10^{-1}\,E_h$
I	$3.5 \times 10^{12}\,W/cm^2$	$9.973\,085 \times 10^{-5}\,I_a$
t	$1\,fs$	$4.134\,137 \times 10^{1}\,\hbar/E_h$

be $I = 3.5 \times 10^{12}\,W/cm^2$. The simulation is run for $100\,fs$ with a time step of[2] $\Delta t = 1 \times 10^{-2}\,\hbar/E_h$ using the Gauss-integrator with $s = 3$ and $\epsilon = 1 \times 10^{-6}$. A word of caution, when reproducing the results in this article some care must be taken when converting to atomic units for the frequency, time, and the intensity of the laser as it is not clear how much one should round the numbers. We have used the Python library *Pint* [102] to convert from SI units to atomic units as they stand in the text without any rounding. These conversions are summarized in Table 12.1. The corresponding frequency in atomic units of the laser specified by the photon energy E_ν in Table 12.1 is $\omega = 1.999\,163 \times 10^{-1}\,E_h/\hbar$. The electric field strength from the intensity is found to be $E = 9.986\,533 \times 10^{-4}\,E_h/(ea_0)$.

We repeat the study for the LiH molecule as done by Nest *et al.* [101]. We use a bond-length of $3.08\,a_0$ in the z-direction between the lithium and the hydrogen atoms with the basis 6-31G*. To specify this basis in PySCF we pass in the string `"6-31Gs"`. We use the TDHF, TDCCSD, and the OATDCCD solvers in this study and we sample the dipole moment for each method. Computing the Fourier transform of the dipole moment after the laser is turned off yields the absorption spectra of LiH. We run two simulations; one where we polarize the laser along the z-direction and measure along the same axis, and another simulation where we do the same in the x-direction.

In Figure 12.1 we have included the Fourier transform of the sampled dipole moment in x- and z-direction in time, respectively. These plots show the absorption spectra for the LiH molecule. For the z-direction it is important to note that the LiH molecule with the bonding set in the z-direction has a non-zero dipole moment. This makes the absorption spectra include a constant zero frequency component. We have removed this component from the figures by using the function `scipy.signal.detrend` [68]. In Table 12.2 we have used the function `scipy.signal.find_peaks` [68] to locate the transition energies for the Fourier specter of the dipole moment polarized along

[2]Note that we specify the time step in atomic units as we convert all the SI units to atomic units when doing the simulation.

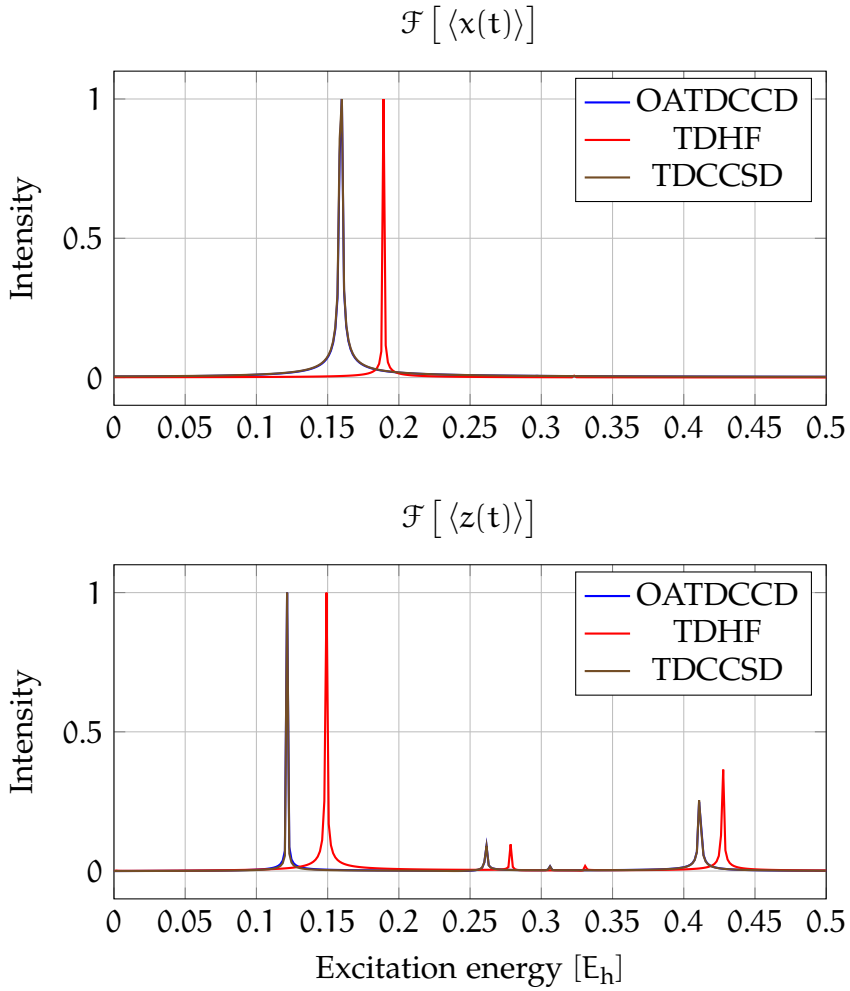

Figure 12.1: In these figures we show the Fourier transform of the dipole moment in x-and y-direction of the LiH molecule using time-dependent Hartree-Fock, time-dependent coupled-cluster with singles and doubles, orbital-adaptive time-dependent coupled cluster with doubles excitations. The top figure shows the results in x-direction and the lower in z-direction.

Table 12.2: Transition energies from peaks in Fourier specter of the dipole moment of LiH in the x-direction as seen in the top palette of Figure 12.1. The peaks are counted from left to right.

Solver	Peak [n]	ΔE [E_h]	ΔE [eV]
TDHF	1	0.1892	5.1491
	2	0.3231	8.7912
TDCCSD	1	0.1600	4.3537
	2	0.2969	8.0795
OATDCCD	1	0.1600	4.3537
	2	0.2969	8.0795

the x-direction. We have done the same in Table 12.3 for the z-direction. Note that we have set a threshold for the minimum height of the peaks to 5×10^{-3} to avoid some noisy signals.[3]

For the sake of comparison we have also used CISD to compute the excited energy levels. By subtracting the ground state energy from each excited energy level we find the transition energies from the ground state to a higher state, and we are able to compare with the results in Table 12.2 and Table 12.3. However, this will include all transition energies, even those that are beyond the dipole allowed transitions. We therefore wish to filter out all higher-order transitions as we are only looking for dipole allowed effects. Now, the way we verify if a transition is an allowed dipole transition[4] once we have the spectrum (E_K, Ψ_K) from the CISD-Hamiltonian, is to compute a transition one-body density matrix defined as

$$(\rho_{IJ})^q_p \equiv \langle \Psi_I | \hat{c}^\dagger_p \hat{c}_q | \Psi_J \rangle = C^*_{KI} C_{LJ} \langle \Phi_K | \hat{c}^\dagger_p \hat{c}_q | \Phi_L \rangle , \tag{12.2}$$

where the name stems from the fact that we can reuse the one-body density matrix routine, but now with two different coefficient vectors $\mathbf{C}_I$ and $\mathbf{C}_J$. To verify if an energy transition between two states Ψ_I and Ψ_J are allowed in the dipole approximation we compute

$$\left| \mathbf{d}^p_q (\rho_{IJ})^q_p \right| > 0, \tag{12.3}$$

where a non-zero – or, numerically non-zero – value means that the transition is allowed along the axis that has a non-zero value. Note that the

[3] This value was chosen by trial and error where we inspected the figures –especially for the z-direction – in Figure 12.1 to see that all peaks are in the results at the approximate correct location.

[4] Within the CISD-approximation.

Table 12.3: Transition energies from the peaks in the Fourier specter of the dipole moment of LiH in the z-direction as seen in the bottom palette of Figure 12.1. The peaks are counted from left to right.

Solver	Peak [n]	ΔE [E_h]	ΔE [eV]
TDHF	1	0.1492	4.0607
	2	0.2785	7.5772
	3	0.3308	9.0005
	4	0.4277	11.6379
TDCCSD	1	0.1215	3.3072
	2	0.2615	7.1167
	3	0.3061	8.3307
	4	0.4108	11.1774
OATDCCD	1	0.1215	3.3072
	2	0.2615	7.1167
	3	0.3061	8.3307
	4	0.4108	11.1774

Table 12.4: Here we see the allowed dipole transitions from the ground state $I = 0$ to a higher excited state J. We have only included results from the first 40 states in the spectrum from the CISD-Hamiltonian.

Transition	Direction	ΔE [E_h]	ΔE [eV]
$0 \to 4$	z	0.1218	3.3138
$0 \to 11$	x, y	0.1595	4.3398
$0 \to 12$	x, y	0.1595	4.3398
$0 \to 16$	z	0.2613	7.1108
$0 \to 23$	x, y	0.2970	8.0814
$0 \to 24$	x, y	0.2970	8.0814
$0 \to 28$	z	0.3060	8.3275
$0 \to 32$	z	0.4115	11.1974
$0 \to 33$	z	0.5310	14.4485

absolute value in Equation 12.3 should be interpreted as an elementwise absolute value for each spatial component in $\mathbf{d}_q^p$. Using these techniques to locate allowed transitions, we map the lowest lying allowed dipole transitions for the LiH molecule using CISD in the restricted Hartree-Fock basis in Table 12.4. Comparing the results from Table 12.2 and Table 12.3 with the results from CISD in Table 12.4 we see that TDCCSD and OATDCCD are in excellent agreement with the transition energies from the spectrum of the CISD-Hamiltonian. However, there are small discrepancies which we expect as all three methods approximate the four-particle system of LiH molecule with at most two-particle excitation operators. We also see that OATDCCD and TDCCSD yields exactly the same dipole transition energies within the precision that we have kept for these results. It is a little hard to determine if the coupled-cluster methods perform better than CISD as the energies are simultaneously higher and lower at different energy levels. An important point to note is that even though CISD is found using the variational principle thus guaranteeing an upper bound to the energy, the *energy difference* does not have this requirement. That is, the ground state energy and an excited state are both an upper bound to the their respective energy, but the excited state might be closer to the exact energy therefore making the difference smaller than what it should be. Furthermore, we know that OATDCCD and TDCCSD are more correlated than CISD and should in theory yield better results, however, the transition energies from the coupled-cluster methods depends on a lot of factors such as the time step of the integrator and the sampling time

when computing the Fourier transform of the dipole moment signal. But, within two decimal places the results from the coupled-cluster methods and CISD are in perfect agreement.

As an extra point, the converged ground state energies[5] for CISD, TD-CCSD, and OATDCCD are

$$E_0 = -8.9772\,E_h. \tag{12.4}$$

The methods therefore seemingly perform just as well on the LiH system. However, we see that we are able to achieve a lower ground state energy than reported by Nest *et al.* [101].

There is no doubt that TDHF is quite far off in terms of the dipole transition energies when loooking at Table 12.2 and Table 12.3. This demonstrates the expected behavior as discussed in section 10.2 that the TDHF will falter once the laser fields intesifies and the correlations in the atoms and molecules becomes larger. To properly explain the dynamics of even a 4-particle system we need something better than the signle-determinant mean-field approximation achieved from TDHF. The fact that TDHF is so far off shows promise in that the real-time coupled-cluster methods can be used to improve on many reported results achieved from using TDHF.

12.2 Spectra of noble gasses

Before moving on to more exotic systems we wish to demonstrate one of the main goals in this thesis, and that is to prove that the implemented methods are able to explore larger systems than what can achieved with the full configuration interaction method. We therefore wish to demonstrate some simulations for the Ne and Ar atoms in exactly the same laser field as in the study done by Nest *et al.* [101] shown in Equation 12.1, but with a higher frequency. We have chosen a frequency ω corresponding to a laser wavelength of $\lambda = 200\,nm$ and let the envelope last for a full cycle, that is, $T = 2\pi/\omega$. We have chosen this frequency as this lets us simulate a full cycle of the laser in a relatively short time, thus letting the atoms oscillate for a long time after the laser is turned off.

Due to the size of the atoms, $N = 10$ for Ne and $N = 18$ for Ar, the evolution of the system takes a substantial amount of time. We have used two different basis sets: cc-pVDZ and aug-cc-pVDZ for both atoms. We specify these basis sets in PySCF [18] by the strings `"ccpvdz"` and `"aug-ccpvdz"` respectively. For Ne the basis set cc-pVDZ yields $L = 28$ spin-orbitals and aug-cc-pVDZ contains $L = 46$ spin-orbitals. Similarly for Ar we get $L = 36$ spin-orbitals for cc-pVDZ and $L = 54$ for aug-cc-pVDZ. In other words, the

[5]This energy is excluding the nuclear repulsion as reported by Nest *et al.* [101].

Table 12.5: Ground state energies for Ne and Ar in both cc-pVDZ and aug-cc-pVDZ using OATDCCD and TDCCSD. The convergence tolerance for all amplitudes in both methods were set to 1×10^{-6}.

Atom	Basis	Solver	E [E_h]	E [eV]
Ne	cc-pVDZ	OATDCCD	−128.6796	−3501.5501
		TDCCSD	−128.6796	−3501.5513
	aug-cc-pVDZ	OATDCCD	−128.7082	−3502.3294
		TDCCSD	−128.7085	−3502.3364
Ar	cc-pVDZ	OATDCCD	−526.9562	−14339.2093
		TDCCSD	−526.9562	−14339.2094
	aug-cc-pVDZ	OATDCCD	−526.9725	−14339.6511
		TDCCSD	−526.9725	−14339.6519

basis sets are still quite small, but due to the number of particles the runs using our non-optimized code are still slow. Ideally we would like to run all simulations for 100 fs with a time step of $\Delta t = 1 \times 10^{-2}\,\hbar/E_h$, but in practice the larger basis sets did limit the length of the simulations. We managed to run Ne in cc-pVDZ using OATDCCD for the full duration, but all other runs were truncated to 25 fs, or in the case of Ar in aug-cc-pVDZ, were cut-off due to exceeding the max time of a week at the Abel compute cluster. We used the Gauss-integrator with $s = 3$ and $\epsilon = 1 \times 10^{-6}$ as convegence threshold for the fix-point iterations.

All runs are done using the OATDCCD-method and we have repeated the runs for Ne in both basis sets using TDCCSD as well. The ground state energies are listed in Table 12.5. In Figure 12.2 we have plotted the absorption spectra for Ne using both basis sets. The corresponding dipole allowed transition energies are listed in Table 12.6. As discussed in section 8.2, to properly model dynamics we need an augmented basis set with diffues basis functions beyond the ground state optimized correlation consistent basis sets. We can see this in the transition energies found from cc-pVDZ as they are far higher than the same transitions in aug-cc-pVDZ. In the article "Gauge invariant coupled cluster response theory using optimized nonorthogonal orbitals" by Pedersen *et al.* [60] they report both ground state results and the first allowed dipole transition for Ne in aug-cc-pVDZ.[6] For the ground state energies we have used the exact same methods, i.e., the CCSD and NOCCD ground state

[6]They report results for more basis sets, but we can compare with this basis set in particular.

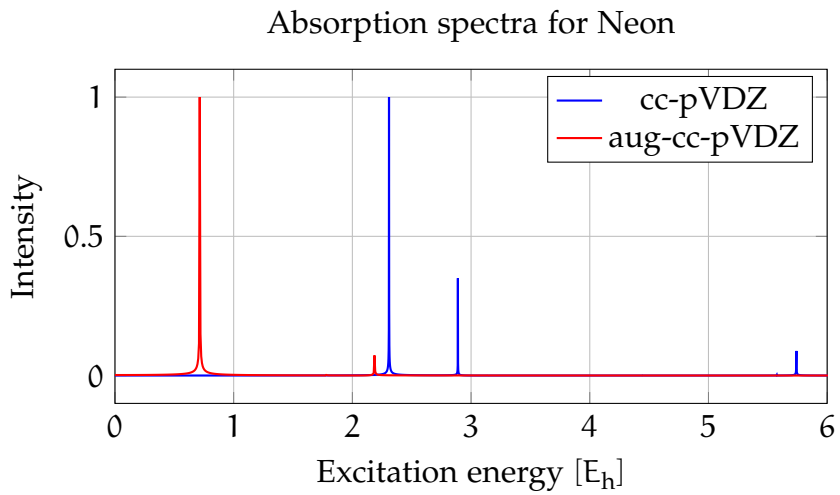

Figure 12.2: In this figure we have plotted the Fourier transform of the expectation value of the dipole moment in z-direction of the Ne atom in both cc-pVDZ and aug-cc-pVDZ using OATDCCD. The results for TDCCSD are visually indistinguishable and we have therefore refrained from plotting these. The peaks for both basis sets and using both solvers are listed in Table 12.6.

solvers, and we see that we agree with the results found by Pedersen *et al.* [60] to three decimal places for Ne in the aug-cc-pVDZ basis. In Table 12.6 we also see that OATDCCD and TDCCSD report similar values for the first allowed dipole transition of Ne in aug-cc-pVDZ basis as reported by Pedersen *et al.* [60] using linear response theory with CCSD and NOCCD. The time-dependent NOCCD-method should be equal to OATDCCD if we let the right-hand side of the Q-space equations in OATDCCD be zero.[7] We also see the same behvior as reported by Pedersen *et al.* [60] that OATDCCD reports a higher value for the transition energy than TDCCSD. However, the second allowed dipole transition in Table 12.6 for Ne in the aug-cc-pVDZ basis is not reported elsewhere.

Mostly as a test of the applicability of our developed codes, we repeat the same study we did for Ne on the Ar atom. We restrict our attention to the OATDCCD method for no other reason than time limitations.[8] In Figure 12.3 we have plotted the absorption spectra of Ar in both the cc-PVDZ and the aug-cc-pVDZ basis. The results from the latter basis does not have a good resolution due to relatively few samples after the laser pulse was switched off, but we are able to see a trend. In Table 12.7 we have listed the dipole allowed

[7] This is one of the reasons why we use NOCCD as the ground state solver for OATDCCD.

[8] The inclusion of results using TDCCSD should absolutely have been done, but this will have to be explored at a later time.

Table 12.6: Dipole transitions for Ne in both basis sets. We have numbered the peaks from left to right from the plot in Figure 12.2.

Basis	Solver	Peak [n]	ΔE [E_h]	ΔE [eV]
cc-pVDZ	TDCCSD	1	2.3116	62.9005
		2	2.8879	78.5830
		3	5.7507	156.4842
	OATDCCD	1	2.3087	62.8237
		2	2.8890	78.6130
		3	5.7412	156.2261
aug-cc-pVDZ	TDCCSD	1	0.7003	19.0567
		2	2.1700	59.0489
	OATDCCD	1	0.7141	19.4327
		2	2.1863	59.4913

Table 12.7: Dipole allowed transition energies for Ar in cc-pVDZ and aug-cc-pVDZ basis along the z-axis using the OATDCCD-method.

Basis	Solver	Peak [n]	ΔE [E_h]	ΔE [eV]
cc-pVDZ	OATDCCD	1	1.1118	30.2549
		2	1.4746	40.1254
		3	1.6323	44.4168
aug-cc-pVDZ	OATDCCD	1	0.4677	12.7275

transition energies for all the peaks that we see in Figure 12.3. Recalling that the cc-pVDZ basis gave a much higher transition energy than for the aug-cc-pVDZ basis for Ne we see the same result for Ar. Note that we have been unable to locate any results for the first allowed dipole transitino for Ar in the aug-cc-pVDZ basis and we therefore merely report it in Table 12.7.

12.3 Spin-dependent laser pulses

We have so far demonstrated that our implemented methods reproduce known results from the literature on a wide range of systems. Furthermore, we have demonstrated that we can run large simulations up to $N = 18$ (Ar) in a modest basis set. However, we now wish to demonstrate that our implemented

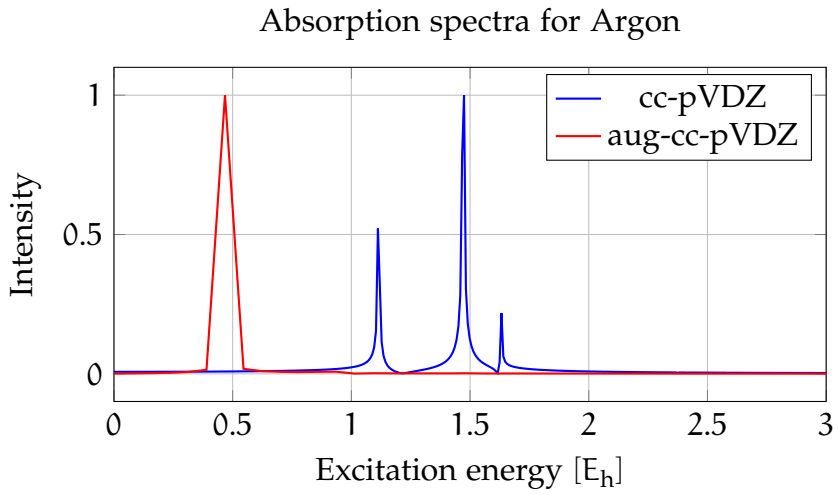

Figure 12.3: In this figure we have plotted the Fourier transform of the expectation value of the dipole moment in z-direction of the Ar atom in both cc-pVDZ and aug-cc-pVDZ using OATDCCD. The peaks for both basis sets and using both solvers are listed in Table 12.7.

methods are able to simulate systems with a *spin-dependent* Hamiltonian. Doing this will demonstrate that we are able to simulate systems with a spin-dependent magnetic field.

In a study by Isborn & Li [103], the authors explored a spin-dependent laser field to see singlet-triplet transitions which are invisible to a spin-symmetric field. This study is performed using the time-dependent unrestricted Hartree-Fock (TDUHF) method and time-dependent density functional theory. We have not implemented a TDUHF-method and will therefore use our regular TDHF code with general spin-orbitals and the OATDCCD-method.

The laser pulse used by Isborn & Li [103] is given by

$$\mathbf{E}(t) = E_m \boldsymbol{\epsilon} \sin(\omega t), \tag{12.5}$$

where we polarize in the negative z-direction to include the charge of the electrons. The field is active for $t \in [0, T]$ with $T = 6\pi/\omega$, i.e., the field is active for three cycles of the laser frequency. The frequency is set to $\omega = 0.06\,E_h/\hbar$, the integration time step to $\Delta t = 1 \times 10^{-2}\,\hbar/E_h$ and we let the simulation run for a total of $50\,fs$. We simulate the three molecules H_2, LiH, and CO with the two basis sets STO-3G and 6-31G**. The laser field strength for H_2 was set to $E_m = 0.1$, and for LiH and CO to $E_m = 0.01$. Furthermore, a hickup in the (self-made) caching scheme used on the Abel computing cluster led to the seven days long run for CO in the 6-31G** basis using OATDCCD being deleted. Thus, our results for CO will only be in the smaller STO-3G basis set. A frutstrating fact in the article by Isborn & Li [103] is that the

Table 12.8: Equilibrium bond lengths for diatomic molecules used in the study on spin-dependent laser fields [104]. Note that the values for LiH are reused from the study by Nest *et al.* [101], and converted to pm for the sake of completeness.

Molecule	R_e [pm]	R_e [a_0]
H_2	74	1.40
LiH	163	3.08
CO	143	2.70

bonding length of the molecules used are not reported. We therefore assume that Isborn & Li [103] used the equilibrium bond-lengths in the z-direction for all three molecules. These are listed in Table 12.8. In order to make the applied field spin-dependent we have chosen a solution where we set the dipole moment matrix elements corresponding to a specific spin direction to zero and leave the other spin direction as it is. A demonstration of the dipole matrix elements of the H_2 molecule in the 6-31G** basis is shown in Figure 12.4. By using the matrix elements on the right in Figure 12.4 we effectively use a spin-dependent laser field applied to all spins in the up-direction.[9]

In Figure 12.5 we have plotted the absorption spectra of H_2 using both basis sets and both TDHF and OATDCCD. We have also included absorption spectra using a spin-dependent field as the dashed lines in Figure 12.5. As expected from the study done by Isborn & Li [103] we see that the spin-dependency adds an extra peak at a lower energy level than the first allowed dipole transition. This is the first singlet to triplet allowed dipole transition in H_2.

In Table 12.9 we have listed the transition energies found from the peaks in Figure 12.5. For the H_2 molecule we can use CISD, i.e., FCI in this case, to compute the entire spectrum and locate the allowed dipole transitions using the same technique as discussed in section 12.1. Furthermore, using the spin-reduced dipole matrix elements we should be able to locate the allowed singlet-triplet transitions. In Table 12.10 we have listed all allowed dipole transitions in both basis sets for H_2. We have denoted singlet allowed transitions – where it is understood that the same transition is allowed in the spin-dependent case as well – specifically to demonstrate which peaks we expect to see for the singlet only transitions. Comparing Table 12.10 with the results in Table 12.9 we are able to locate the energy transitions in the results

[9]Note that which indices correspond to "up" or "down" is completely arbitrary, we just need a name for the odd and even indices.

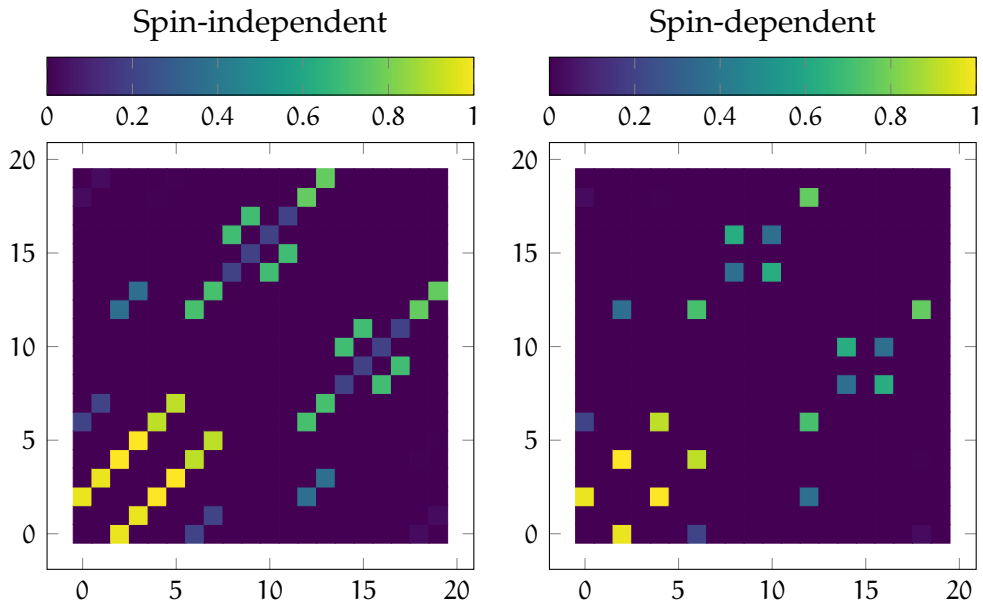

Figure 12.4: In these figures we have plotted the dipole matrix elements along z-direction, that is, z_q^p, for H_2 in the 6-31G** basis. The image on the left is of the full dipole matrix elements whereas the image on the left shows the same matrix elements, but with all odd indices set to zero which means that we are left with the dipole matrix elements for the spin-up direction. Note that we have scaled the values to be between 0 and 1 by taking the elementwise absolute value of z and dividing by the max value in the matrix.

Table 12.9: Dipole transition energy levels for the H_2 molecule in both the STO-3G and the 6-31G** basis sets using TDHF and OATDCCD. These results are found from the visible peaks in Figure 12.5.

Basis	Solver	Singlet allowed	ΔE [E_h]	ΔE [eV]
STO-3G	TDHF	no	0.5574	15.1687
		yes	0.9315	25.3464
	OATDCCD	no	0.6078	16.5395
		yes	0.9675	26.3262
6-31G**	TDHF	no	0.3632	9.8841
		yes	0.5466	14.8751
	OATDCCD	no	0.4028	10.9611
		yes	0.5539	15.0715

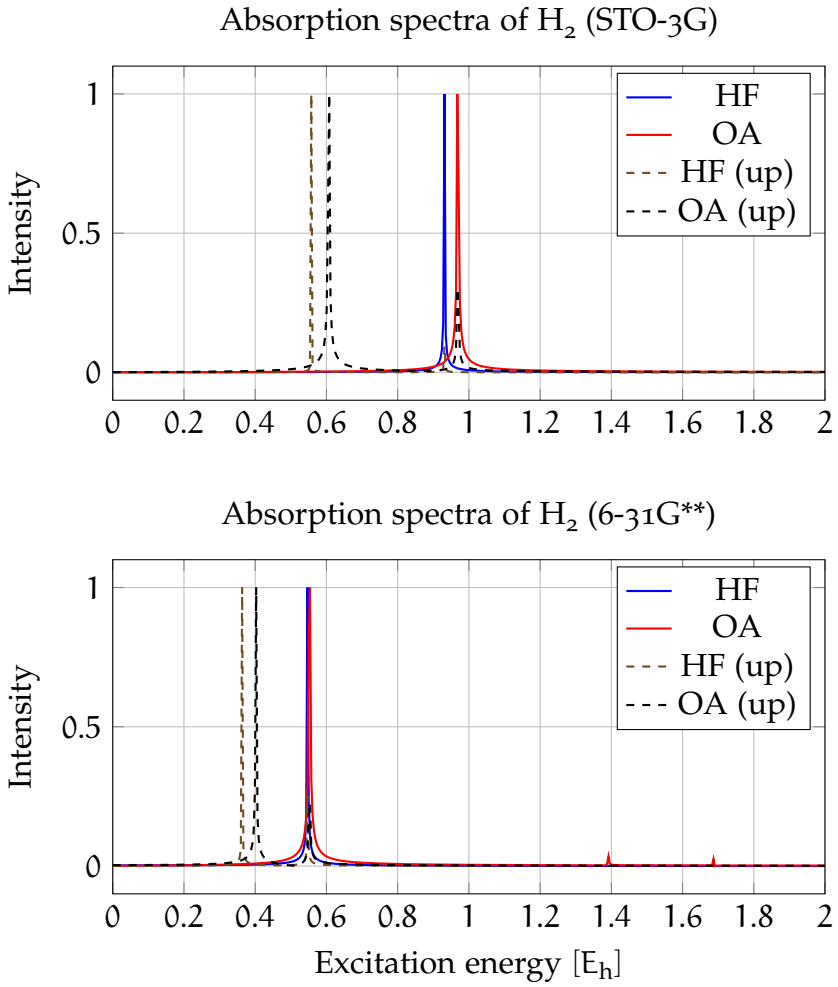

Figure 12.5: In these figures we have plotted the absorption spectra of H_2 subject to a laser field using the TDHF (HF) and the OATDCCD (OA) methods. The label "up" denotes a spin-dependent field along one of the spin-functions. No extra label means that the field is spin-indepdenent.

Table 12.10: Dipole allowed transitions for H_2 in both basis sets computed using CISD. The transition is from the ground state $I = 0$ to a higher excited state J. We have limited the transition energies to $\Delta E \leqslant 1\,E_h$ for the 6-31G** basis. Spin-independent transitions, i.e., singlet-to-singlet transitions, are denoted with a "yes" under the column "Singlet allowed". These transitions are also allowed in the spin-dependent case.

Basis	Transition	Singlet allowed	ΔE [E_h]	ΔE [eV]
STO-3G	$0 \to 1$	no	0.6065	16.5040
	$0 \to 3$	no	0.6065	16.5040
	$0 \to 4$	yes	0.9689	26.3660
6-31G**	$0 \to 1$	no	0.4020	10.9403
	$0 \to 2$	no	0.4020	10.9403
	$0 \to 3$	no	0.4020	10.9403
	$0 \to 4$	yes	0.5523	15.0277

from OATDCCD. We note that the energies are not exactly the same – even though both CISD and OATDCCD are formally exact within the given basis for $N = 2$ particles – but as the methods for discovering these energy transitions are so vastly different as discussed in section 12.1 we conclude that these energies are the same. Comparing with the results from Isborn & Li [103] we see that TDHF is close to their results using TDUHF. However, we conjecture that the discrepancies are mainly a result of Isborn & Li [103] using the presumably more stable TDUHF method for spin-dependent laser fields. We also note that our results using the more exact methods OATDCCD and CISD have higher transition energies than the results achieved from TDHF. It seems that both TDHF and TDUHF predict a lower transition energy than what is correct.

From Table 12.10 we see that the degenerate transitions in the STO-3G basis $0 \to 1$ and $0 \to 3$ are triplet-only allowed transitions, but the interesting thing is that the transition $0 \to 2$ is also a transition with the same energy level. However, the latter transition is *not* a dipole-allowed triplet transition. In the 6-31G** basis the triplet transitions opens up for all transitions up to the fourth excited state within the energy levels we explore.

Repeating the same exercise for the LiH system we have the absorption spectra for both the spin-dependent and spin-independent fields in the STO-3G and the 6-31G** basis sets in Figure 12.6. We see that the signal from these simulations is rather noisy. Tabulating the values in Figure 12.6 we get the results shown in Table 12.11. Unlike the H_2 molecule we see that the values in Table 12.11 contains significantly more noise, especially for the transition energies found using the TDHF-method. The transition energy in Table 12.11 denoted with a "†" is included as it is, but we conjecture that it should really

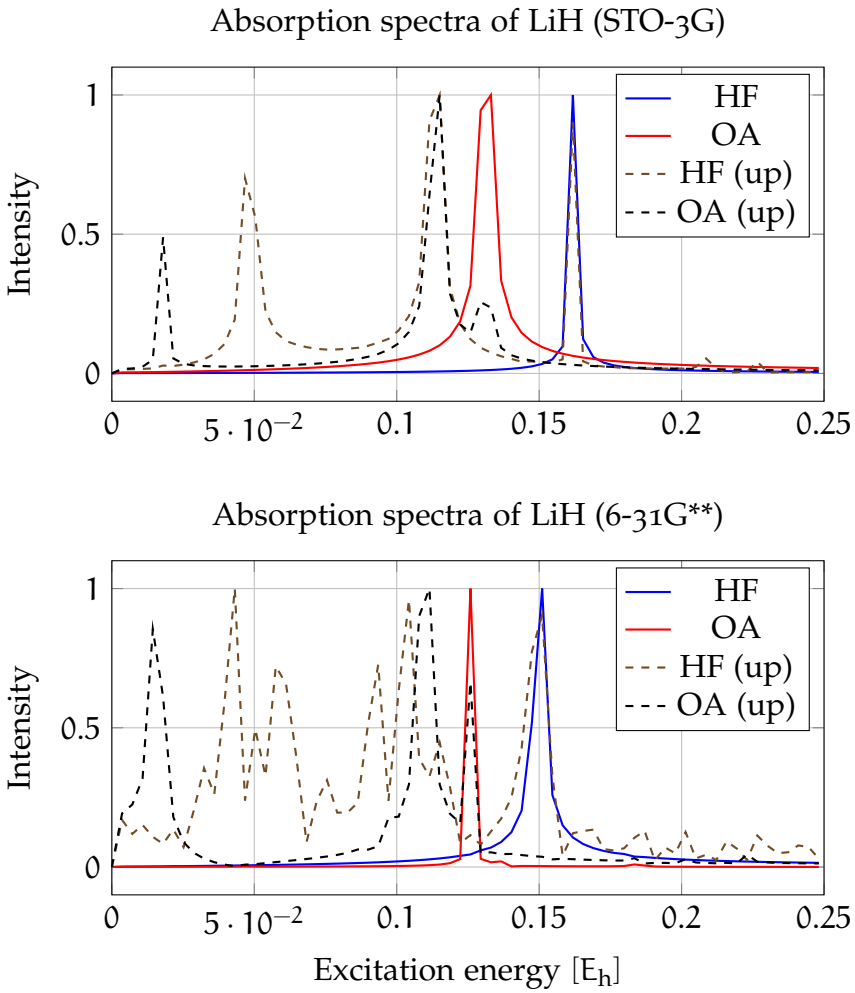

Figure 12.6: In these figures we have plotted the absorption spectra of LiH subject to a laser field using the TDHF (HF) and the OATDCCD (OA) methods. The label "up" denotes a spin-dependent field along one of the spin-functions. No extra label means that the field is spin-indepdenent.

Table 12.11: Dipole transition energy levels for the LiH molecule in both the STO-3G and the 6-31G** basis sets using TDHF and OATDCCD. These results are found from the peaks in Figure 12.6 with a threshold that the peaks must have a larger intensity than 0.2.

Basis	Solver	Singlet allowed	ΔE [E_h]	ΔE [eV]
STO-3G	TDHF	no	$0.0468^{\diamond}$	1.2722
		no	0.1151	3.1316
		yes	0.1618	4.4038
	OATDCCD	no	$0.0180^{\diamond}$	0.4893
		no	0.1151	3.1316
		no	$0.1295^{\dagger}$	3.5231
		yes	0.1331	3.6210
6-31**	TDHF	no	$0.0324^{\ddagger}$	0.8808
		no	$0.0432^{\ddagger}$	1.1743
		no	$0.0503^{\ddagger}$	1.3701
		no	$0.0575^{\ddagger}$	1.5658
		no	$0.0755^{\ddagger}$	2.0551
		no	$0.0935^{\ddagger}$	2.5444
		no	$0.1043^{\ddagger}$	2.8380
		no	0.1151	3.1316
		yes	0.1510	4.1102
	OATDCCD	no	$0.0144^{\diamond}$	0.3915
		no	0.1115	3.0339
		yes	0.1259	3.4253

Table 12.12: Dipole allowed transitions for LiH in both basis sets computed using CISD. We use the notation $[J - K]$ to denote a range of excited states. We only include results for $\Delta E \leqslant 0.25\, E_h$.

Basis	Transition	Singlet allowed	ΔE $[E_h]$	ΔE $[eV]$
STO-3G	$0 \rightarrow [1-3]$	no	0.1138	3.0959
	$0 \rightarrow 4$	yes	0.1313	3.5741
6-31G**	$0 \rightarrow [1-3]$	no	0.1099	2.9894
	$0 \rightarrow 4$	yes	0.1259	3.4261
	$0 \rightarrow [13-15]$	no	0.2222	6.0468

be the singlet-allowed transition listed just below. This as the peaks in the upper palette of Figure 12.6 show that the two peaks coincide, but due to few samples they do not overlap perfectly. The values for TDHF in Table 12.11 denoted with a "‡" are clearly noise. Furthermore, comparing with Isborn & Li [103] we see that only the two values that are not denoted with a "‡" are the actual dipole transition energies we should see. However, they are so weak that they occur below the noise and would not have been discovered unless we knew what we were looking for. This demonstrates that the TDHF-method is unable to describe the spin-dependent field. As Isborn & Li [103] were able to get better measurements we believe that the usage of a TDUHF-method would recover the desired results. This would be an interesting study to explore, but we have not had the time to implement the TDUHF-method. The values in Table 12.11 marked with a "⋄" are most likely the results of dipole transitions between two excited states. We see that they are present in plots of Isborn & Li [103] as well, and we leave them as they are.

Computing the dipole allowed transitions using the CISD-method we get the results shown in Table 12.12. The TDHF results in Table 12.11 that are not marked as noise compare well with the results from Isborn & Li [103] whereas the OATDCCD results are comparable to the results from CISD in Table 12.12. However, they are not the same for the same reasons as discussed in the two previous studies using this technique. Finally, in Figure 12.7 we have listed the results from the CO simulations in the STO-3G basis. Here we clearly see how TDHF really struggles with the spin-dependent field. In Table 12.13 we have tabulated the peaks from Figure 12.7. The results from the TDHF-method, especially for the spin-dependent field, are hard to make sense of. They seemingly only consist of noisy data and by comparing with the results found by Isborn & Li [103] we see that there are little to no comparison of the results. For OATDCCD we trust our data a little more, but it is again hard to compare with the results from Isborn & Li [103] as they use TDUHF and TDDFT. Also, what is strange is that we only see a single clear peak once the

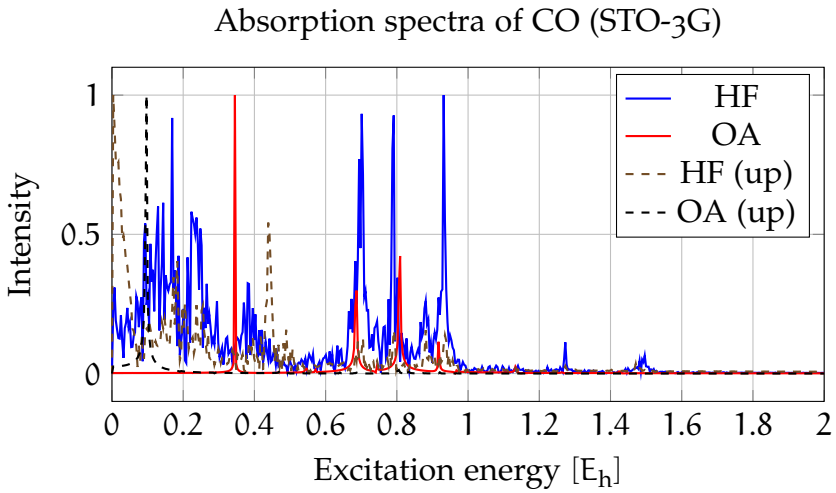

Figure 12.7: In these figures we have plotted the absorption spectra of CO subject to a laser field using the TDHF (HF) and the OATDCCD (OA) methods. The label "up" denotes a spin-dependent field along one of the spin-functions. No extra label means that the field is spin-indepdenent.

spin-dependent field is active, and this value is much lower than any results reported by Isborn & Li [103].

The inclusion of a spin-dependent laser field demonstrates that we are able to take a step further and include magnetic fields with spin-orbit coupling in future work. In Winther-Larsen's work, a demonstration of an orbital angular magnetic field is showcased [17], but we wish in the future to include the spin-dependence as well.

12.4 Ionization of one-dimensional atoms

The process of modelling ionization of electrons in atoms is a hot topic [80, 105–108]. It is also of the utmost importance when doing laser driven dynamics as at some point or another we will use a field which in reality would rip the electrons away from the atoms and molecules. An accurate description of this process is therefore important in order to model real experiments, which after all, is what we are trying to do.

In a study done by Miyagi & Bojer Madsen [80] they explored the dynamics of one-dimensional atoms subject to a dipole laser. This study provides us with an excellent benchmark to observe a form of ionization and see if this is reproducible in our formalism. Note that Miyagi & Bojer Madsen [80] use a discrete-variable-representation basis (DVR) [80, 106] which is why they include an absorbing potential. Our solution differs from this as we use the static one-dimensional quantum dot basis with a one-dimensional atom

Table 12.13: Dipole transition energy levels for the CO molecule in the STO-3G basis using TDHF and OATDCCD. These results are found from the peaks in Figure 12.7 with a threshold that the peaks must have a larger intensity than 0.05 for the OATDCCD-method and 0.8 for the TDHF-method.

Basis	Solver	Singlet allowed	ΔE [E_h]	ΔE [eV]
STO-3G	TDHF	no	0.0036	0.0979
		yes	0.1690	4.5996
		yes	0.7013	19.0833
		yes	0.7912	21.5299
		yes	0.9315	25.3465
	OATDCCD	no	0.0971	2.6423
		yes	0.3453	9.3949
		yes	0.6869	18.6919
		yes	0.8092	22.0193
		yes	0.9171	24.9552

potential. In a position basis with Hartree atomic units, the one-body Hamiltonian is given by [80]

$$h(x,t) = -\frac{1}{2}\frac{d^2}{dx^2} - \frac{Z}{\sqrt{x^2+1}} + xF(t) - iW(x), \tag{12.6}$$

where $Z = N_e$ – the number of electrons in the system – and $W(x)$ is the absorbing potential, which we will set to zero. The second term gives rise to the naming of these systems as one-dimensional atoms as this term serves as the electron-nuclear interaction in the atomic Hamiltonian, but with the three-dimensional position replaced with x. One of the interesting aspects of the one-dimensional atoms is that many open-shell systems such as Carbon (C) becomes closed shell systems in the one-dimensional case. We will limit our study to the one-dimensional Beryllium (Be) system with $N = 4$ electrons in a closed shell.

The laser pulse $F(t)$ used by Miyagi & Bojer Madsen is given by [80]

$$F(t) = -\frac{dA(t)}{dt} = -\frac{d}{dt}\left[\frac{F_0}{\omega}\sin^2\left(\frac{\pi t}{T}\right)\sin(\omega t)\right] \tag{12.7}$$

$$= -\sin\left(\frac{\pi t}{T}\right)\left[\omega\sin\left(\frac{\pi t}{T}\right)\cos(\omega t) + \frac{2\pi}{T}\cos\left(\frac{\pi t}{T}\right)\sin(\omega t)\right], \tag{12.8}$$

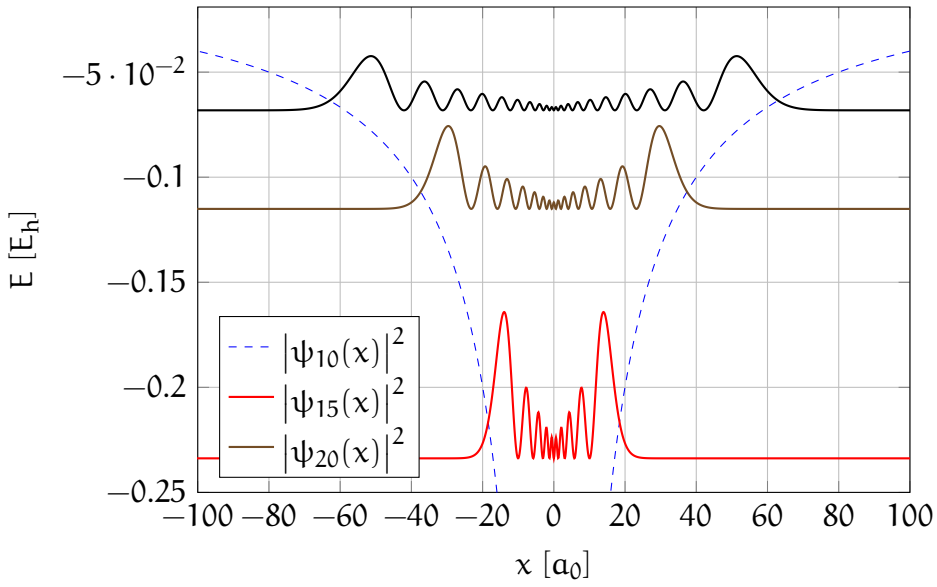

Figure 12.8: In this figure we have plotted some of the high lying single-particle functions squared and scaled by their eigenenergy inside the one-dimensional Beryllium potential. We have only included a select few single-particle functions to avoid the figure being too cluttered.

where the field is active for $t \in [0, T]$. The Coulomb interaction is given by Equation 8.21 with a shielding parameter of $a = 1$ and $\alpha = 1$. To compare with the study by Miyagi & Bojer Madsen [80] we will run for $T = 331\,\hbar/E_h$ with $\Delta t = 1 \times 10^{-2}\,\hbar/E_h$ which corresponds to $n_t = 33100$ time steps. This computation is rather involved and we will therefore limit ourselves to the time-dependent Hartree-Fock method and the orbital-adaptive time-dependent coupled-cluster method as the full-configuration interaction method becomes quite expensive. In fact, for $N = 4$ and $L = 40$ we have to create a Hamiltonian matrix with 91390^2 elements, each of size 16 B as we use complex numbers. To solve this system we require a more efficient implementation of the configuration interaction method which is out of scope for this thesis.

Using the same definition as Sato *et al.* [106], we define ionization as all components outside a radius of $20\,a_0$ from the center of the nucleus [16, 106]. We can then measure the amount of ionization by computing the particle density outside this radius, or conversely, the amount of particle density still inside the nucleus. However, note that as we use static orbitals, we are dependent on having a large enough basis set to actually observe ionization. In Figure 12.8 we see the highest lying orbitals we have used in the one-dimensional Beryllium system. We see that unless we include more than 10 orbitals we will not include states that are outside the radius of $20\,a_0$. To

demonstrate this we have in Figure 12.9 plotted the particle density using a basis of $L/2 = 10$ orbitals. Looking at the lower palette of Figure 12.9 we see that the system is still fairly confined. This shows how this basis does not allow any significant particle density outside the nucleus. We can also see this from Figure 12.8 as $L = 20$ means the highest single-particle function used is $\psi_{10}(x)$ which is clearly confined in the potential well. Looking at Figure 12.10 we see the same one-dimensional Be system with a basis set of $L = 40$ spin-orbitals. It is apparent that the system undergoes a larger degree of ionization with more of the particle density further away from the central potential. This is also seen in Figure 12.8 as $L = 40$ includes the state $\psi_{20}(x)$ which is more dispersed. Comparing with the results reported by Miyagi & Bojer Madsen [80] we see that we are able to perform qualitatively just as well. In Figure 12.10 we see that the OATDCCD-method is able to describe a larger degree of ionization than TDHF. However, it is reasonable to believe that with either a larger basis set, or a basis set with time-dependency on the grid we might get an even large degree of ionization. As it stands the particles can never escape the potential and once they have reached the edge of their extent – as seen in Figure 12.8 – they can only be reflected. This will then lead to the electrons oscillating in the well, when they should in fact have escaped the trapping potential all together.

If we were to describe ionization in three dimensions we would either need a combination of diffues or continuum states which can describe ionization. An alternative is the use of a DVR basis [80, 106], but this would need a clever grid solution as the three dimensional grid quickly becomes a memory and computational clog.

12.5 Summing up the applications

We have in this chapter explored several studies done on atoms and molecules using real-time methods. We have found our implemented methods to be comparable to what has been reported in the literature. We have demonstrated how the methods can be applied to larger systems such as Ar, and discussed how more time must be spent on the optimization of our code for systems of $N = 18$ particles to be practical.

We went on to look at more academic studies where we explored a spin-depedent laser field as a taste of what can be done with the addition of spin-orbit coupling. Finally, we explored the highly interesting topic of ionization in a one-dimensional atomic system highlighting how the implemented code can be used to describe these type of effects.

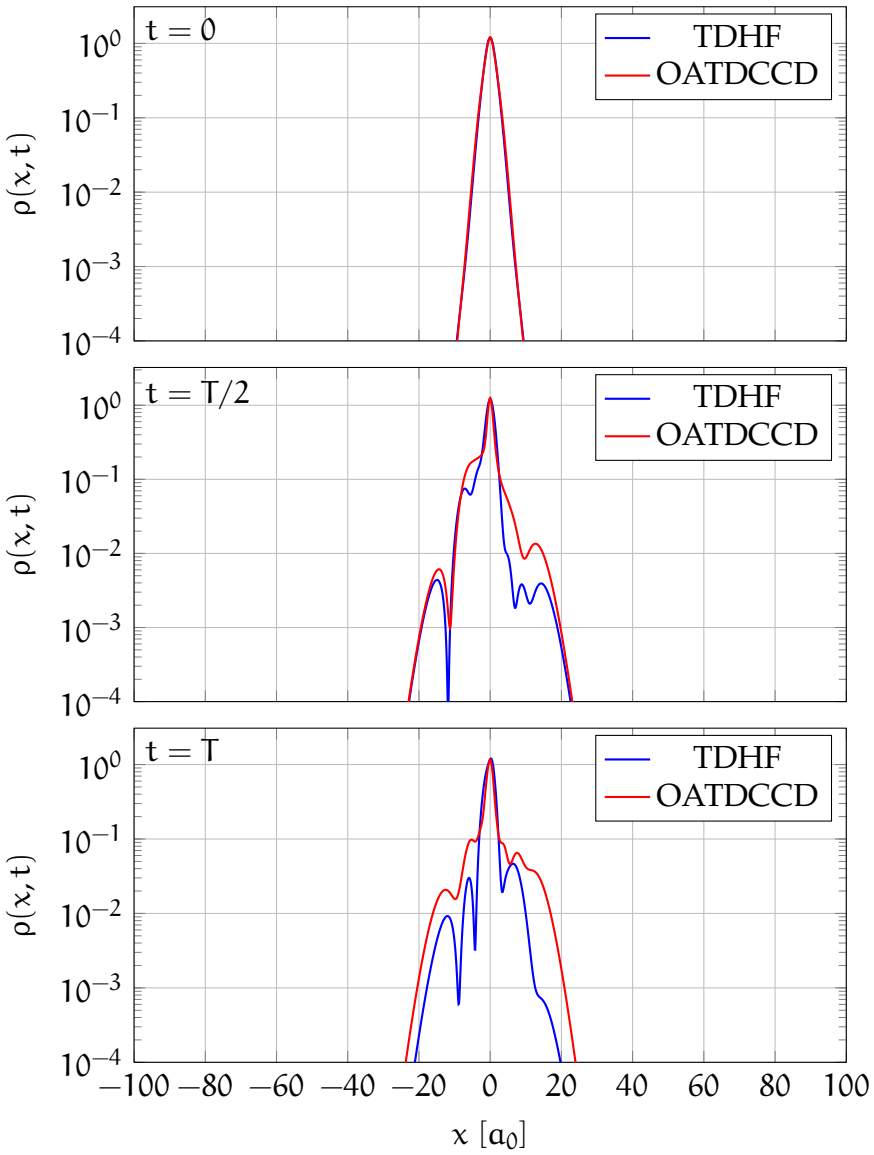

Figure 12.9: In these figures we plot the particle density for the initial ground state, after half the simulation has been run and for the final state of the one-dimensional Be system. For these figures we have $L = 20$ spin-orbitals, that is, $L/2 = 10$ orbitals. The y-axis has been truncated at $y = 1 \times 10^{-4}$ to avoid including noise in the figures.

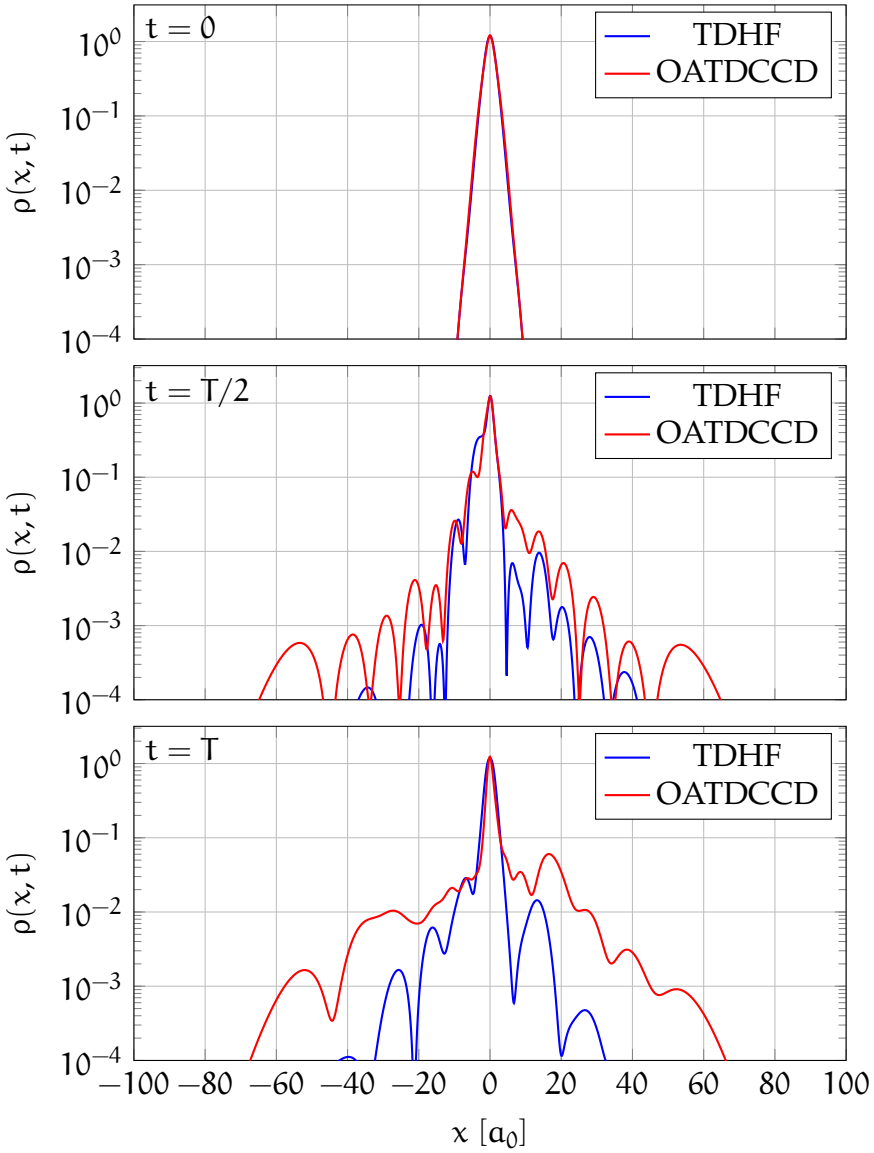

Figure 12.10: These figures show the same situation as in Figure 12.9 but for $L = 40$ spin-orbitals. We have truncated the y-axis to $y = 1 \times 10^{-4}$ as lower values include more noise and provides no more insight.

Part IV

Summary remarks

Chapter 13

Conclusions and perspective

Our initial goal of this thesis was to implement time-dependent coupled-cluster doubles (CCD/TDCCD), singles-and-doubles (CCSD/TDCCSD), and orbital-adaptive time-dependent coupled-cluster doubles (NOCCD/OATDCCD) methods. These were to be tested on one- and two-dimensional single and double quantum dots. However, due to the novelty of the OATDCCD method this thesis diverged to a new set of goals. We therefore switched focus to the stability of real-time coupled-cluster methods – which in itself is a rather new research area – with collaborators at the Hylleraas Center. This will lead to a forthcoming publication [66]. The focus is on atoms and molecules as these systems are more applicable and common among quantum chemists than quantum dots. Also, due to the close collaboration with Winther-Larsen [17] this proved a natural divergence on the systems to be explored on our separate theses. To fully challenge and explore the coupled-cluster methods we have implemented a set of Hartree-Fock (HF/RHF/UHF/TDHF) solvers and configuration interaction (CISD.../TDCISD...) methods which allow us to improve and compare results from the coupled-cluster solvers.

In this thesis we have described the implementation of the TDHF, TDCI and TDCC/OATDCCD methods along with descriptions on how to represent the quantum systems we are exploring. We have demonstrated that our methods work as expected by comparing with known results from the scientific literature. We have also compared the various truncation levels of the coupled-cluster[1] and the configuration interaction methods, and demonstrated how the Hartree-Fock approach can be used to improve these results by providing an optimal single reference state. We then moved on to demonstrate that orbital-adaptive time-dependent coupled-cluster doubles is more stable than time-dependent coupled-cluster singles-and-doubles subject to very intense fields. We demonstrated that the inclusion of explicit orbital rotations – as

[1] Up to and including the CCSD truncation level.

conjectured by Pedersen & Kvaal [22] – made the method more robust for the Helium and Beryllium systems subject to very intense laser field than with static orbitals in the regular time-dependent coupled-cluster method.

Having verified that our implemented methods worked as expected we went on to apply the methodology to four different topics.

1. We explored the LiH molecule subject to a laser field polarized along the x- and z-direction and measured absorption energies using TDHF, TDCCSD, and OATDCCD. This was a study done by Nest *et al.* [101], and we were able to reproduce their results. We also used CISD to compute all dipole-allowed transition energies from the ground state to higher excited states. This allows us to compare the coupled-cluster results with transitions from higher lying levels than reported by Nest *et al.* [101].

2. We then set out to demonstrate that the coupled-cluster formulation lets us explore systems that are much larger than what is possible using full configuration interaction theory. We chose to explore the absorption energies of Ne and Ar, that is, atoms with $N = 10$ and $N = 18$ particles respectively. We used two different basis sets and thereby also demonstrated that in order to get good results we require a diffuse correlation consistent basis set (aug-cc-pVDZ). The results for Ne were compared with existing works. We were unable to find comparable results for Ar, but we report the first dipole allowed transition in the aug-cc-pVDZ basis to be $\Delta E = 0.4677\,E_h$.

3. Having demonstrated the applicability of the implemented methods, we set out to demonstrate its versatility as well. We modelled a spin-dependent laser field as done by Isborn & Li [103]. We were able to achieve comparable results using OATDCCD, but we also showed how the general TDHF-method failed to reproduce the results from TDUHF reported by Isborn & Li [103] for larger molecules.

4. Finally we explored ionization in a one-dimensional Beryllium atom. We demonstrated how the choice of basis limits the amount of ionization. We noted that if one is to consider ionization in a three-dimensional system more flexible basis sets should be utilized.

All in all we have demonstrated that our implemented libraries are robust and that they can be applied to a wide range of physical and chemical systems. Furthermore, this conclusion should be seen in conjunction with the results from the work of Winther-Larsen [17] as we have used the same framework applied to different systems. We have limited the discussion of the quantum dots in this thesis, but these are explored in detail by Winther-Larsen. Also,

as part of these theses there is an ongoing publication where we apply these methods to more exotic systems of quantum dots [109].

13.1 Future prospects

Even though we have demonstrated a wide range of applications, there is still a vast amount of studies that can be done in lieu of this work. The future prospects from this thesis can be divided into two parts: the continued development of the methods and solvers, and the application of the methods to unexplored systems. We will discuss these two prospect categories separately.

13.1.1 Development of the libraries

In this thesis we have explored a significant amount of methodology and techniques used in real-time electronic many-body theories, but we have in no way exhausted the space of possibilities. Furthermore, much of our work is written in such a way that we wish to inspire continued development by other students and researchers, and we will hopefully be able to publish a software specification. But as such, we will here list some topics we deem interesting to explore and include in the implemented methods.

- CuPy [72] is a Python library resembling NumPy [69] in both use and content, however CuPy is an implementation of arrays and linear algebra on a graphics processing unit (GPU). Our libraries were originally set up to allow for the usage of CuPy, but due to a few shortcomings we have not had the time to fully integrate this into our systems. This should absolutely be explored further as this will almost surely increase the speed of the methods.

- There are excellent differential equation libraries such as SciPy [68] and diffeqpy [77] which would remove the need for self-implemented solvers as these can potentially lead to bugs and are most likely not properly optimized. However, do note that for the same reasons as discussed in subsection 7.4.2, we want our integrators to be symplectic, and SciPy does not have any implemented symplectic solvers. Diffeqpy on the other hand contains quite a few solvers which are symplectic. A proper interface towards either or both of these libraries should be implemented and a thorough study of the effects of various solvers can be explored.

- To properly study ionization we should investigate grid-based basis sets [16, 80, 106]. This allows for a more flexible description away from

equilibrium. In particular the discrete-variable-representation as used by Miyagi & Bojer Madsen [80] is of interest.

- The inclusion of triples amplitudes in TDCCSDT and OATDCCD is of interest. In the latter case this would include a substantial increase in complexity in the orbital equations. However, the OATDCCDT-method has – to the authors knowledge – *never* been implemented.

- One of the main obstacles – in the authors opinion – for an effective workflow with the implemented libraries are: the reimplementation of methods used to sample various quantities, e.g., the dipole moment, and the occasional manual optimization to ensure convergence. We have stressed a philosophy where all methods should behave in a similar way, that is, they compute the ground state, and they open up for propagation. All quantities should have a similar interface when it comes to measurement, but occasionally time and lack of creativity have hindered this philosophy leading to small discrepancies in the interfaces between the different methods. This is frustrating as each sampling script must be tailored to fit each method.

  The second obstacle with manual optimization should be improved by using adaptive techniques allowing for automatic improvement of convergence thresholds. For example, using a gradient descent method to improve upon a converged state. Directly related to this is also an attempt at implementing the Kalman filter as an improvement to the alpha filter discussed in section 7.3.

13.1.2 Application to physical and chemical systems

We have in this thesis and the thesis by Winther-Larsen [17] demonstrated a wide range of applications of the libraries we have developed. One of the main difficulties in writing this thesis has been the downscaling of the amount of results to present. There is a multitude of systems that we have not had the time to include between the four covers that our theses consist of. Along with our work there are also two manuscripts in preparation. The first manuscript concerns itself with the stability of time-dependent coupled-cluster methods [66] and serves as a follow up to the work by Pedersen & Kvaal [22]. The second manuscript is an extensive study on the time evolution of quantum dots [109] and seeks to apply the developed framework to studies on various quantum dot systems. Therefore, it is not surprising that much of this work will be presented in later studies as part of Winther-Larsen's and my own PhD-studies at the Centre for Computing in Science Education.

- Interesting systems to include are: three-dimensional quantum dots,

magnetic fields with spin-coupling, and exploration, and relativistic systems.

- Large systems of atoms and molecules are often restricted to Hartree-Fock simulations. Real-time simulations of any such system could potentially lead to new results.
- In the work of Winther-Larsen [17] the inclusion of an orbital-dependent magnetic field is done. By including a spin-dependent magnetic field this could potentially lead to interesting physics. In section 12.3 we saw some examples of a spin-dependent laser field leading to "exotic" transitions.
- Studies of nuclear systems and nuclear reactions such as fission and fusion are immensely interesting. The exploration of such phenomena using real-time coupled-cluster methods holds great promise for applying *ab initio* approaches to these challenging topics.
- In section 12.2 we demonstrated the importance of basis sets when it comes to the quality of the results achieved from dynamical systems. A proper study of this has been left out of this thesis, but is of fundamental interest.
- We have in this thesis limited our attention to laser fields described in the dipole approximation. The inclusion of higher-order multipoles could potentially let us move into the high-energy regime of Röntgen and the like. This would also require relativistic considerations as well.

Part V

Appendices

Appendix A

Quantum Mechanics

In this appendix we will add proofs and derivations of expressions arising from the theory chapters on quantum mechanics and many-body theory.

A.1 Gauge invariant electromagnetic Hamiltonian

Given the semi-classical Hamiltonian on the form

$$\hat{H} = -\frac{\hbar^2}{2m}\boldsymbol{\nabla}^2 + v(\mathbf{r}) + i\hbar\frac{q}{2m}\left[\boldsymbol{A}\cdot\boldsymbol{\nabla} + \boldsymbol{\nabla}\cdot\boldsymbol{A}\right] + \frac{q^2}{2m}\boldsymbol{A}^2 + q\phi, \tag{A.1}$$

where $\boldsymbol{A}$ and ϕ are the classical description of the electromagnetic vector and scalar potentials respectively, we wish to show that under the gauge transformations

$$\boldsymbol{A} \to \boldsymbol{A}' = \boldsymbol{A} + \boldsymbol{\nabla} f, \tag{A.2}$$

$$\phi \to \phi' = \phi - \frac{\partial f}{\partial t}, \tag{A.3}$$

$$\psi \to \psi' = \exp\left[\frac{iq}{\hbar} f\right]\psi, \tag{A.4}$$

as listed in Equation 2.110 to Equation 2.112, the time-dependent Schrödinger equation is invariant. We start by looking at the gradient and the Laplace operator on the gauge transformed wave function.

$$\boldsymbol{\nabla}\psi' = \exp\left[\frac{iq}{\hbar} f\right]\left[\frac{iq}{\hbar}\left(\boldsymbol{\nabla} f\right) + \boldsymbol{\nabla}\right]\psi, \tag{A.5}$$

$$\boldsymbol{\nabla}^2\psi' = \exp\left[\frac{iq}{\hbar} f\right]\left[\frac{iq}{\hbar}\left(\boldsymbol{\nabla} f\right) + \boldsymbol{\nabla}\right]^2\psi, \tag{A.6}$$

$$\tag{A.7}$$

where the nabla-operator works on everything to its right unless it is in a paranthesis. This means that one must include the product rule with the wave function ψ for the squared bracket. The potential $v(\mathbf{r})$ does not include derivatives and therefore leaves the state ψ' unchanged. For the third term we get

$$\boldsymbol{A}' \cdot \boldsymbol{\nabla}\psi' + \boldsymbol{\nabla} \cdot \left(\boldsymbol{A}'\psi'\right) = 2\boldsymbol{A}' \cdot \boldsymbol{\nabla}\psi' + \left(\boldsymbol{\nabla} \cdot \boldsymbol{A}'\right)\psi'. \tag{A.8}$$

The former of these two terms yield

$$2\boldsymbol{A}' \cdot \boldsymbol{\nabla}\psi' = 2\exp\left[\frac{iq}{\hbar}f\right]\left[\frac{iq}{\hbar}\boldsymbol{A} \cdot (\boldsymbol{\nabla}f) + \boldsymbol{A} \cdot \boldsymbol{\nabla} + \frac{iq}{\hbar}(\boldsymbol{\nabla}f)^2 + (\boldsymbol{\nabla}f) \cdot \boldsymbol{\nabla}\right]\psi, \tag{A.9}$$

and the latter gives

$$\left(\boldsymbol{\nabla} \cdot \boldsymbol{A}'\right)\psi' = \exp\left[\frac{iq}{\hbar}f\right]\left[(\boldsymbol{\nabla} \cdot \boldsymbol{A}) + \left(\boldsymbol{\nabla}^2 f\right)\right]\psi. \tag{A.10}$$

The term squared in the vector potential yields

$$\left(\boldsymbol{A}'\right)^2\psi' = \exp\left[\frac{iq}{\hbar}f\right]\left[\boldsymbol{A}^2 + 2\boldsymbol{A} \cdot (\boldsymbol{\nabla}f) + (\boldsymbol{\nabla}f)^2\right]\psi. \tag{A.11}$$

For the scalar potential we get

$$\phi'\psi' = \exp\left[\frac{iq}{\hbar}f\right]\left[\phi - \frac{\partial f}{\partial t}\right]\psi. \tag{A.12}$$

The left-hand side of the time-dependent Schrödinger equation gives

$$\frac{\partial}{\partial t}\psi' = \exp\left[\frac{iq}{\hbar}f\right]\left[\frac{iq}{\hbar}\frac{\partial f}{\partial t} + \frac{\partial}{\partial t}\right]\psi. \tag{A.13}$$

Noting that all terms in the time-dependent Schrödinger equation contains the exponential function from ψ' we can remove this term on both sides. Starting with the scalar potential and the left-hand side of the time-dependent Schrödinger equation, we have that

$$i\hbar\frac{\partial}{\partial t}\psi' \supset v(\mathbf{r})\psi' + q\phi'\psi' \implies i\hbar\frac{\partial}{\partial t}\psi \supset v(\mathbf{r})\psi + q\phi\psi, \tag{A.14}$$

where we have used the notation $\supset$ to denote a term in the right-hand side of the Schrödinger equation, and included the potential term. To go from here we collect all terms that contain the function f. For the kinetic term we have

$$-\frac{\hbar^2}{2m}\boldsymbol{\nabla}^2\psi' \supset \left[\frac{q^2}{2m}(\boldsymbol{\nabla}f)^2 - \frac{iq\hbar}{m}(\boldsymbol{\nabla}f) \cdot \boldsymbol{\nabla} - \frac{iq\hbar}{2m}\left(\boldsymbol{\nabla}^2 f\right)\right]\psi, \tag{A.15}$$

where we have multiplied in the constant factor to recognize equal terms.

$$\frac{iq\hbar}{2m}\left[\mathbf{A}'\cdot\boldsymbol{\nabla}+\boldsymbol{\nabla}\cdot\mathbf{A}'\right]\psi' \supset \left[-\frac{q^2}{m}\mathbf{A}\cdot(\boldsymbol{\nabla}f)-\frac{q^2}{m}(\boldsymbol{\nabla}f)^2 + \frac{iq\hbar}{m}(\boldsymbol{\nabla}f)\cdot\boldsymbol{\nabla}+\frac{iq\hbar}{2m}\left(\boldsymbol{\nabla}^2 f\right)\right]\psi. \tag{A.16}$$

Finally, the squared term contains the function f in the following places

$$\frac{q^2}{2m}\left(\mathbf{A}'\right)^2\psi' \supset \left[\frac{q^2}{m}\mathbf{A}\cdot(\boldsymbol{\nabla}f)+\frac{q^2}{2m}(\boldsymbol{\nabla}f)^2\right]\psi. \tag{A.17}$$

We are thus able to see that all terms containing the function f cancel and can conclude that Equation 2.110 through Equation 2.112 are gauge transformations for the electromagnetic potentials and the wave function that leave the time-dependent Schrödinger equation invariant.

A.2 Positive definite overlap matrix

Consider an atomic orbital basis of L single-particle states $\{\chi_\alpha\}$ where the overlap is given by

$$s_{\alpha\beta} = \langle\chi_\alpha|\chi_\beta\rangle = \int dx \chi_\alpha^*(x)\chi_\beta(x) \neq \delta_{\alpha\beta}. \tag{A.18}$$

The overlap matrix $\mathbf{S}\in\mathbb{C}^{L\times L}$ constructed from the overlap elements above is Hermitian by construction. This means that there exists a unitary matrix $\mathbf{U}\in\mathbb{C}^{L\times L}$ which diagonalizes the overlap matrix, viz.

$$\mathbf{U}^\dagger\mathbf{S}\mathbf{U} = \mathbf{s}, \tag{A.19}$$

where $\mathbf{s}$ is a diagonal matrix with the eigenvalues λ_i of $\mathbf{S}$. We now wish to show that $\mathbf{S}$ is positive definite.

Proof. Defining $\mathbf{u}_i\in\mathbb{C}^L$ as the i'th column of $\mathbf{U}$ we have that

$$\mathbf{u}_i^\dagger\mathbf{S}\mathbf{u}_i = u_{\alpha i}^* s_{\alpha\beta} u_{\beta i} = \int dx \left(u_{\alpha i}\chi_\alpha(x)\right)\left(\chi_\beta(x)u_{\beta i}\right) \tag{A.20}$$

$$= \int dx \psi_i^*(x)\psi_i(x) = \langle\psi_i|\psi_i\rangle = \lambda_i > 0, \tag{A.21}$$

as the normalization of ψ_i dictates that the inner product with itself must be greater than zero. This demonstrates that $\mathbf{S}$ is positive definite. □

Now, as $\mathbf{S}$ is positive definite, we have that the eigenvalues $\lambda_i > 0$.

A.3 Orbital rotations

We prove Lemma 3.4.

Proof. Let $\{\phi_i\}$ be an orthonormal basis of L atomic orbitals. We can then do a unitary transformation from this basis to a new basis $\{\psi_i\}$ of L single-particle states by

$$|\psi_i\rangle = U_{ji}\,|\phi_j\rangle\,, \tag{A.22}$$

where U_{ji} is an element in the unitary matrix $\mathbf{U} \in \mathbb{C}^{L\times L}$. For a set of coordinates $\mathbf{x} = \{x_1, \ldots, x_N\}$, we write

$$\psi_{ij} \equiv \psi_j(x_i) = \langle x_i|\psi_j\rangle\,, \tag{A.23}$$

and equivalently for ϕ_{ij}. Projecting onto the coordinate basis we can write Equation A.22 as

$$\psi_{ki} = U_{ji}\phi_{kj} \implies \mathbf{\Psi} = \mathbf{\Phi U}, \tag{A.24}$$

where the matrices $\mathbf{\Psi}$, $\mathbf{\Phi}$, and $\mathbf{U}$ are the matrices with elements

$$\mathbf{\Psi} = \begin{pmatrix} \psi_{11} & \psi_{12} & \cdots & \psi_{1N} \\ \vdots & \vdots & \ddots & \vdots \\ \psi_{N1} & \psi_{N2} & \cdots & \psi_{NN} \end{pmatrix}, \tag{A.25}$$

$$\mathbf{\Phi} = \begin{pmatrix} \phi_{11} & \phi_{12} & \cdots & \phi_{1N} \\ \vdots & \vdots & \ddots & \vdots \\ \phi_{N1} & \phi_{N2} & \cdots & \phi_{NN} \end{pmatrix}, \tag{A.26}$$

$$\mathbf{U} = \begin{pmatrix} U_{11} & U_{12} & \cdots & U_{1N} \\ \vdots & \vdots & \ddots & \vdots \\ U_{N1} & U_{N2} & \cdots & U_{NN} \end{pmatrix}. \tag{A.27}$$

The Slater determinants projected onto the coordinates $\mathbf{x}$ can now be found by

$$\Psi(\mathbf{x}) = \langle \mathbf{x}|\Psi\rangle = \frac{1}{\sqrt{N!}}\det(\mathbf{\Psi}), \tag{A.28}$$

and similarly for $\Phi(\mathbf{x})$. We can now write the unitary transformation from $\Phi(\mathbf{x})$ to $\Psi(\mathbf{x})$ as

$$\Psi(\mathbf{x}) = \frac{1}{\sqrt{N!}}\det(\mathbf{U\Phi}) = \det(\mathbf{U})\Phi(\mathbf{x}), \tag{A.29}$$

where we used that the determinant of a product is the product of the determinants. Since $\mathbf{U}$ is unitary we have that the squared determinant of $\mathbf{U}$ will 1, as can be seen by using the product rule of determinants described above. This means that

$$\det(\mathbf{U}) = \exp[i\phi], \tag{A.30}$$

that is, the determinant of a unitary matrix becomes a complex phase factor. In other words, $\Psi(\mathbf{x})$ will differ from $\Phi(\mathbf{x})$ by at most a complex phase factor and

$$\langle\Psi|\Psi\rangle = \left\|\det(U)\right\|^2 \langle\Phi|\Phi\rangle = \langle\Phi|\Phi\rangle = \mathbb{1}, \tag{A.31}$$

and the lemma is proved. □

A.4 Deriving the reference energy

Let $\{\phi_p\}$ be an orthonormal basis of L single-particle states with the N first states occupied in the reference state $|\Phi\rangle$, we compute the reference energy from Equation 3.142. We use Wick's theorem with normal ordering relative to the Fermi vacuum, that is, we treat the reference state as our vacuum state. Starting with the one-body operator, we get

$$\hat{h} = h_q^p \hat{c}_p^\dagger \hat{c}_q = h_q^p \left(\{\hat{c}_p^\dagger \hat{c}_q\} + \hat{c}_p^\dagger \hat{c}_q \right) = h_q^p \{\hat{c}_p^\dagger \hat{c}_q\} + h_q^p \delta_{p\in O} \delta_{pq}, \tag{A.32}$$

where we use $\delta_{p\in O}$ to denote that the general index p must be contained in the set of occupied indices $O = \{1, \ldots, N\}$. This notation is similar to the one used by Crawford & Schaefer III in "An Introduction to Coupled Cluster Theory for Computational Chemists"[50]. We call the first term, the *normal-ordered one-body Hamiltonian*,

$$\hat{h}_N \equiv h_q^p \{\hat{c}_p^\dagger \hat{c}_q\}. \tag{A.33}$$

Computing the expectation value of the one-body Hamiltonian on the reference state, we get

$$\langle\Phi|\hat{h}|\Phi\rangle = \langle\Phi|\hat{h}_N|\Phi\rangle + h_q^p \delta_{p\in O}\delta_{pq} \langle\Phi|\Phi\rangle = 0 + h_i^i. \tag{A.34}$$

To see why the former term becomes zero, we have to consider the four combinations of indices that can be summed over in the operators. From subsection 3.6.2 we know that only terms with both occupied or both virtual indices will contribute to the expectation value. As the operators are normal-ordered

relative to the Fermi vacuum they will destroy the reference state by either creating a particle that is already present in the reference state, or destroying a particle that is not in the reference state. The expectation value of the two-body term is given by

$$\langle \Phi|\hat{u}|\Phi\rangle = \frac{1}{4} u_{rs}^{pq} \langle \Phi|\hat{c}_p^\dagger \hat{c}_q^\dagger \hat{c}_s \hat{c}_r|\Phi\rangle \,. \tag{A.35}$$

For brevity, we will only write out the operator strings.

$$\begin{aligned}
\hat{c}_p^\dagger \hat{c}_q^\dagger \hat{c}_s \hat{c}_r &= \overbrace{\hat{c}_p^\dagger \hat{c}_q^\dagger \hat{c}_s \hat{c}_r} + \overbrace{\hat{c}_p^\dagger \hat{c}_q^\dagger \hat{c}_s \hat{c}_r} + \overbrace{\{\hat{c}_p^\dagger \hat{c}_q^\dagger \hat{c}_s \hat{c}_r\}} + \overbrace{\{\hat{c}_p^\dagger \hat{c}_q^\dagger \hat{c}_s \hat{c}_r\}} \\
&\quad + \overbrace{\{\hat{c}_p^\dagger \hat{c}_q^\dagger \hat{c}_s \hat{c}_r\}} + \overbrace{\{\hat{c}_p^\dagger \hat{c}_q^\dagger \hat{c}_s \hat{c}_r\}} + \{\hat{c}_p^\dagger \hat{c}_q^\dagger \hat{c}_s \hat{c}_r\} \qquad \text{(A.36)} \\
&= -\delta_{p\in O}\delta_{q\in O}\delta_{ps}\delta_{qr} + \delta_{p\in O}\delta_{q\in O}\delta_{pr}\delta_{qs} - \delta_{p\in O}\delta_{ps}\{\hat{c}_q^\dagger \hat{c}_r\} \\
&\quad + \delta_{p\in O}\delta_{pr}\{\hat{c}_q^\dagger \hat{c}_s\} + \delta_{q\in O}\delta_{qs}\{\hat{c}_p^\dagger \hat{c}_r\} - \delta_{q\in O}\delta_{qr}\{\hat{c}_p^\dagger \hat{c}_s\} \\
&\quad + \{\hat{c}_p^\dagger \hat{c}_q^\dagger \hat{c}_s \hat{c}_r\}. \qquad \text{(A.37)}
\end{aligned}$$

For the same reason as with the expectation value of the one-body operator, all terms with a normal-ordered pair of creation and annihilation operators will be zero. This means that we are left with the two fully contracted terms and the normal-ordered product with two pairs of creation and annihilation operators. We note that there exists a combination of indices which will *not* destroy the reference even though the operators are normal-ordered. This occurs when both creation operators act on virtual states and the two annihilation operators act on occupied states, viz.

$$\{\hat{c}_a^\dagger \hat{c}_b^\dagger \hat{c}_j \hat{c}_i\} |\Phi\rangle = A |\Phi_{ij}^{ab}\rangle \,, \tag{A.38}$$

where A is some phase factor. In other words, this combination of operators will leave the reference state excited, but due to the orthonormality of the basis states, the overlap between the reference state and the excited state will be zero. We are thus left with

$$\begin{aligned}
\langle \Phi|\hat{u}|\Phi\rangle &= \frac{1}{4} u_{rs}^{pq} \left\{ -\delta_{p\in O}\delta_{q\in O}\delta_{ps}\delta_{qr} + \delta_{p\in O}\delta_{q\in O}\delta_{pr}\delta_{qs} \right\} \langle \Phi|\Phi\rangle \qquad \text{(A.39)} \\
&= -\frac{1}{4} u_{ji}^{ij} + \frac{1}{4} u_{ij}^{ij} = \frac{1}{2} u_{ij}^{ij}, \qquad \text{(A.40)}
\end{aligned}$$

where we have used the anti-symmetry of the two-body tensor to collect the two remaining terms, that is, $u_{ij}^{ij} = -u_{ji}^{ij}$. In total we are left with the reference energy of the electronic Hamiltonian

$$E_0 = \langle \Phi|\hat{H}|\Phi\rangle = \langle \Phi|\hat{h}|\Phi\rangle + \langle \Phi|\hat{u}|\Phi\rangle = h_i^i + \frac{1}{2} u_{ij}^{ij}, \tag{A.41}$$

which is what we wanted to show.

A.5 The normal-ordered Hamiltonian

Given an orthonormal basis of L single-particle states $\{\phi_p\}$, with the N first states occupied in the reference state $|\Phi\rangle$, we can construct the normal-ordered Hamiltonian, $\hat{H}_N$, relative to the Fermi vacuum by using Wick's theorem. Starting with the one-body Hamiltonian, we know from Equation A.32 that we can write the one-body Hamiltonian as

$$\hat{h} = \hat{h}_N + h_i^i, \tag{A.42}$$

where $\hat{h}_N$ is the normal-ordered one-body Hamiltonian from Equation A.33. For the two-body operator, we use Equation A.37 and perform the summation. This gives

$$\begin{aligned}\hat{u} = &-\frac{1}{4}u_{ji}^{ij} + \frac{1}{4}u_{ij}^{ij} - \frac{1}{4}u_{ri}^{iq}\{\hat{c}_q^\dagger \hat{c}_r\} + \frac{1}{4}u_{is}^{iq}\{\hat{c}_q^\dagger \hat{c}_s\} \\ &+ \frac{1}{4}u_{rj}^{pj}\{\hat{c}_p^\dagger \hat{c}_r\} - \frac{1}{4}u_{js}^{pj}\{\hat{c}_p^\dagger \hat{c}_s\} + \frac{1}{4}u_{rs}^{pq}\{\hat{c}_p^\dagger \hat{c}_q^\dagger \hat{c}_s \hat{c}_r\}.\end{aligned} \tag{A.43}$$

Using the antisymmetric properties of the antisymmetric two-body matrix elements,

$$u_{rs}^{pq} = -u_{rs}^{qp} = -u_{sr}^{pq} = u_{sr}^{qp}, \tag{A.44}$$

and relabeling some of the indidces, we can collect terms and rewrite the two-body operator to

$$\hat{u} = \frac{1}{2}u_{ij}^{ij} + u_{qi}^{pi}\{\hat{c}_p^\dagger \hat{c}_q\} + \hat{u}_N. \tag{A.45}$$

Here we have introduced the *normal-ordered two-body operator* to be

$$\hat{u}_N \equiv \frac{1}{4}u_{rs}^{pq}\{\hat{c}_p^\dagger \hat{c}_q^\dagger \hat{c}_s \hat{c}_r\}. \tag{A.46}$$

Combining the one- and two-body operators, we get the full Hamiltonian

$$\hat{H} = \hat{h} + \hat{u} = h_i^i + \frac{1}{2}u_{ij}^{ij} + \left(h_q^p + u_{qi}^{pi}\right)\{\hat{c}_p^\dagger \hat{c}_q\} + \frac{1}{4}u_{rs}^{pq}\{\hat{c}_p^\dagger \hat{c}_q^\dagger \hat{c}_s \hat{c}_r\}, \tag{A.47}$$

where we have collected the constant terms, the one-body terms and the two-body term. We recognize the two first constant terms as the reference energy from Equation 3.142. The two next terms constitute the normal-ordered Fock operator given by

$$\hat{f}_N \equiv \left(h_q^p + u_{qi}^{pi}\right)\{\hat{c}_p^\dagger \hat{c}_q\} \equiv f_q^p\{\hat{c}_p^\dagger \hat{c}_q\}. \tag{A.48}$$

Inserted into the full Hamiltonian we are able to discern the normal-ordered Hamiltonian.

$$\hat{H} = E_0 + \hat{f}_N + \hat{u}_N \equiv E_0 + \hat{H}_N. \tag{A.49}$$

In terms of the second quantized operator the normal-ordered Hamiltonian is given by

$$\hat{H}_N = \hat{f}_N + \hat{u}_N = f^p_q \{\hat{c}^\dagger_p \hat{c}_q\} + \frac{1}{4} u^{pq}_{rs} \{\hat{c}^\dagger_p \hat{c}^\dagger_q \hat{c}_s \hat{c}_r\}. \tag{A.50}$$

The normal-ordered Hamiltonian relative to the Fermi vacuum is defined in such a manner that

$$\langle \Phi | \hat{H}_N | \Phi \rangle = \langle \Phi | \hat{f}_N | \Phi \rangle + \langle \Phi | \hat{u}_N | \Phi \rangle = 0. \tag{A.51}$$

You can convince yourself of this by noting that the only terms that do not destroy the reference state must leave it excited. For an orthonormal basis of Slater determinants, this will necessarily leave the overlap between the reference state and an excited state zero.

A.6 Many-body operators in second quantization

We will in this section demonstrate the representation of the one- and two-body operators as matrix elements of single-particle functions and second quantized operators. We let $\hat{Q}_1$ be a one-body operator acting on a single single-particle state at a time,

$$\hat{Q}_1 = \sum_{i=1}^{N} \hat{q}(i), \tag{A.52}$$

where $\hat{q}(i)$ acts on particle state i and ignores the other states. As a tensor product we can write this particular operator by

$$\hat{q}(i) = \mathbb{1} \otimes \cdots \otimes \hat{q} \otimes \cdots \otimes \mathbb{1} = \mathbb{1}^{\otimes(i-1)} \otimes \hat{q} \otimes \mathbb{1}^{\otimes(N-(i+1))} \tag{A.53}$$

that is, a tensor product of identity operators except for position i where the one-body operator $\hat{q}$ is located. Let $\{\phi_p\}$ be a basis of L single-particle states. We can then find the action of $\hat{q}$ on a single-particle state,

$$\hat{q} |\phi_i\rangle = \sum_{p=1}^{L} |\phi_p\rangle \langle \phi_p | \hat{q} | \phi_i \rangle \equiv \sum_{p=1}^{L} q^p_i |\phi_p\rangle, \tag{A.54}$$

where we have used the resolution of the identity. Furthermore, we have re-instated explicit sums for the moment to avoid confusion. As the one-body operator acts on a single single-particle state at a time, the operator will commute with the permutation operator $\hat{P}_\sigma$. We can construct an N-particle Slater determinant by the antisymmetrizer $\hat{A}$ shown in Equation 3.92. Acting with $\hat{Q}_1$ on the Slater determinant, we get

$$\hat{Q}_1 |\Phi\rangle = \hat{Q}_1 |\phi_1 \dots \phi_N\rangle = \frac{1}{\sqrt{N!}} \sum_{\sigma \in S_N} (-1)^{|\sigma|} \hat{P}_\sigma \sum_{i=1}^{N} \hat{q}(i) \bigotimes_{j=1}^{N} |\phi_j\rangle , \tag{A.55}$$

where we have moved the one-body operator to the far right. We have also represented the Slater determinant as a single ket with the occupied single-particle states inside, similar to the occupation number representation in the section on Fock space. Concentrating on the action of the one-body operator on the product state, we can write

$$\sum_{i=1}^{N} \hat{q}(i) \bigotimes_{j=1}^{N} |\phi_j\rangle = \sum_{i=1}^{N} \sum_{p=1}^{L} q_i^p \left(\bigotimes_{j=1}^{i-1} |\phi_j\rangle \right) \otimes |\phi_p\rangle \otimes \left(\bigotimes_{j=i+1}^{N} |\phi_j\rangle \right) , \tag{A.56}$$

where the single-particle state $|\phi_i\rangle$ has been replaced in the product state by the single-particle state $|\phi_p\rangle$. Moving the matrix elements outside the antisymmetrizer we get a sum over Slater determinants which we write

$$\hat{Q}_1 |\Phi\rangle = \sum_{p=1}^{L} \sum_{i=1}^{N} q_i^p |\phi_1 \dots \phi_p \dots \phi_N\rangle , \tag{A.57}$$

where the placement of ϕ_p depends on the index i as we replace ϕ_i with ϕ_p. This means that we ignore the canonical ordering of the determinants for now, but this can be included after ϕ_p has been inserted. We will however not sort the state after the removal and insertion of a new single-particle state. Having moved the matrix elements of $\hat{q}(i)$ outside the antisymmetrizer we see that

$$|\phi_1 \dots \phi_{i-1} \phi_p \phi_{i+1} \dots \phi_N\rangle = \hat{c}_p^\dagger \hat{c}_i |\phi_1 \dots \phi_N\rangle = \hat{c}_p^\dagger \hat{c}_i |\Phi\rangle = \hat{c}_p^\dagger \hat{c}_q |\Phi\rangle , \tag{A.58}$$

where we in the last equality used that $\hat{c}_a |\Phi\rangle = 0$ using the Fermi vacuum formalism and therefore $\hat{c}_i |\Phi\rangle = \hat{c}_q |\Phi\rangle$. We also see that the sum over p is independent of the sum over q (where we went from $i \to q$), and we write

$$\hat{Q}_1 |\Phi\rangle = \sum_{p=1}^{L} \sum_{q=1}^{L} q_q^p \hat{c}_p^\dagger \hat{c}_q |\Phi\rangle , \tag{A.59}$$

Removing the explicit sums and extracting the operator without the reference determinant, we then have

$$\hat{Q}_1 = q_q^p \hat{c}_p^\dagger \hat{c}_q, \tag{A.60}$$

where the matrix elements q_q^p can be found in a basis of given single-particle states ϕ_p by

$$q_q^p \equiv \langle \phi_p | \hat{q} | \phi_q \rangle = \int dx \phi_p^*(x) \hat{q} \phi_q(x), \tag{A.61}$$

which is what we wanted to show.

The two-body operator $\hat{Q}_2$ is given by

$$\hat{Q}_2 = \sum_{i<j}^{N} \hat{q}(i,j), \tag{A.62}$$

where the sum runs over all pairs (i,j) for N particles and we treat $i < j$. The two-body operator is harder to represent in an explicit tensor representation as opposed to the one-body operator in Equation A.53. This is due to there being two operators acting on two separate single-particle states, but the results being connected. We will therefore describe the action of the two-body operator on a product state of two single-particle states by

$$\hat{q}(i,j) \, |\phi_i\rangle \otimes |\phi_j\rangle = \sum_{p,q=1}^{L} q_{ij}^{pq} \, |\phi_p\rangle \otimes |\phi_q\rangle \, , \tag{A.63}$$

where we have used the resolution of the identity for both single-particle states in the product state. The two-body matrix elements are given by

$$q_{ij}^{pq} \equiv \langle \phi_p \phi_q | \hat{q}(i,j) | \phi_i \phi_j \rangle \tag{A.64}$$

$$= \int dx_1 dx_2 \phi_p^*(x_1) \phi_q^*(x_2) \hat{q}(i,j) \phi_i(x_1) \phi_j(x_2), \tag{A.65}$$

where some care must be shown for the notation of the matrix elements in the definition of the two-body elements as we use $|\phi_i \phi_j\rangle = |\phi_i\rangle \otimes |\phi_j\rangle$ to denote a product state in the matrix elements. However, outside the matrix elements, this notation will denote a Slater determinant in the occupation number representation. Note the symmetry of the integral that

$$q_{ij}^{pq} = q_{ji}^{qp}, \tag{A.66}$$

as the ordering of the two integrals is arbitrary. The two-body operator will also commute with the permutation operator $\hat{P}_\sigma$ as the ordering of the pairs

does not matter when all pairs are included. The action of the two-body operator on a Slater determinant can thus be written

$$\hat{Q}_2 |\Phi\rangle = \sum_{i<j}^{N} \sum_{p,q=1}^{L} q_{ij}^{pq} |\phi_1 \dots \phi_p \dots \phi_q \dots \phi_N\rangle , \tag{A.67}$$

where ϕ_p is at position i and ϕ_q at j. Again we ignore canonical ordering after the new single-particle states have been inserted. From Equation A.67 we see that the insertion and removal of the single-particle states can be described by the second quantized operator string $\hat{c}_p^\dagger \hat{c}_q^\dagger \hat{c}_j \hat{c}_i$ as we first remove single-particle state ϕ_i, then ϕ_j before inserting ϕ_q and then ϕ_p.[1] This ensures that after the total operator string has been evaluated, no sign-change has occured. Now, including $i = j$ introduces no extra elements as $\hat{c}_j \hat{c}_i$ will destroy the reference determinant. Furthermore, due to the symmetry of the two-body elements from Equation A.66 we have that including $i > j$ in the summation will introduce double counting of the same states as for $i < j$ thus this can be added at the cost of a factor $1/2$. Finally, as in the case of the one-body operators, changing the limit on the sum over i and j from N to L will not introduce any new elements as $\hat{c}_r \hat{c}_s$ will destroy the reference whenever $r > N$ and $s > N$. In total we can then write the action of the two-body operator on a Slater determinant,

$$\hat{Q}_2 |\Phi\rangle = q_{rs}^{pq} \hat{c}_p^\dagger \hat{c}_q^\dagger \hat{c}_s \hat{c}_r |\Phi\rangle , \tag{A.68}$$

where we have removed the explicit summations and all sums run over the entire number of basis states. Without the determinant we have the operator given by

$$\hat{Q}_2 = q_{rs}^{pq} \hat{c}_p^\dagger \hat{c}_q^\dagger \hat{c}_s \hat{c}_r, \tag{A.69}$$

which is the same form as in the second term of Equation 3.110.

A.7 Hermitian Lagrange multipliers

We prove that the Lagrange mutlipliers in Equation 4.5 can be chosen Hermitian.

Proof. We follow closely the derivation done by Mayer [44], we start by noticing that the constraint is Hermitian, i.e.,

$$\langle \phi_i | \phi_j \rangle - \delta_{ij} = \langle \phi_j | \phi_i \rangle^* - \delta_{ji}. \tag{A.70}$$

[1] Note the ordering of the annihilation operators.

As of now we have two independent Lagrange multipliers; one for the overlap $\langle\phi_i|\phi_j\rangle$ and another for the the complex conjugate $\langle\phi_j|\phi_i\rangle$. We can formulate the constraint for the real and imaginary part separately,

$$\mathrm{Re}\left\{\langle\phi_i|\phi_j\rangle\right\} = \frac{1}{2}\left\{\langle\phi_i|\phi_j\rangle + \langle\phi_j|\phi_i\rangle\right\} = 0, \tag{A.71}$$

$$\mathrm{Im}\left\{\langle\phi_i|\phi_j\rangle\right\} = \frac{1}{2i}\left\{\langle\phi_i|\phi_j\rangle - \langle\phi_j|\phi_i\rangle\right\} = 0. \tag{A.72}$$

Introducing two separate Lagrange multipliers μ_{ij} and ν_{ij} for the two latter conditions, we get

$$\begin{aligned}\mu_{ij}\,\mathrm{Re}\left\{\langle\phi_i|\phi_j\rangle\right\} + \nu_{ij}\,\mathrm{Im}\left\{\langle\phi_i|\phi_j\rangle\right\} = \frac{1}{2}\left[\mu_{ij} - i\nu_{ij}\right]\,\langle\phi_i|\phi_j\rangle \\ + \frac{1}{2}\left[\mu_{ij} + i\nu_{ij}\right]\,\langle\phi_j|\phi_i\rangle\,.\end{aligned} \tag{A.73}$$

We now choose our combined Lagrange multipliers to be

$$\lambda_{ji} = -\frac{1}{2}\left[\mu_{ij} - i\nu_{ij}\right], \tag{A.74}$$

$$\lambda_{ij} = -\frac{1}{2}\left[\mu_{ij} + i\nu_{ij}\right], \tag{A.75}$$

which implies that $\lambda_{ji} = \lambda_{ij}^*$, which is what we wanted to show. □

Appendix B

Coupled-cluster equations

In this appendix we will show the explicit equations used in the coupled-cluster methods for different truncation levels.

B.1 Energy equations

In this section we derive the projected coupled-cluster correlation energy from the normal-ordered Hamiltonian. This consists of the linear contribution in Equation 6.17 and the squared contribution in Equation 6.18. As stated in subsection 6.1.2, we need only concern ourselves with the case where the cluster operator is given by

$$\hat{T} = \hat{T}_1 + \hat{T}_2 = \tau_i^a \{\hat{c}_a^\dagger \hat{c}_i\} + \frac{1}{4}\tau_{ij}^{ab}\{\hat{c}_a^\dagger \hat{c}_b^\dagger \hat{c}_j \hat{c}_i\}, \tag{B.1}$$

where we note that the cluster operators are normal-ordered by construction. Looking at the energy contribution linear in the cluster operator we get

$$\begin{aligned}\langle\Phi|\left[\hat{H}_N\hat{T}\right]_c|\Phi\rangle &= \langle\Phi|\left[\hat{H}_N\hat{T}_1\right]_c|\Phi\rangle + \langle\Phi|\left[\hat{H}_N\hat{T}_2\right]_c|\Phi\rangle &\text{(B.2)}\\ &= \langle\Phi|\left[\hat{f}_N\hat{T}_1\right]_c|\Phi\rangle + \langle\Phi|\left[\hat{u}_N\hat{T}_2\right]_c|\Phi\rangle\,, &\text{(B.3)}\end{aligned}$$

where we only keep the non-zero contributions in the last line. As we are projecting onto the reference determinant, we are dependent on the operators being fully contracted. This means that all non-contracted operators will destroy the overlap. Hence, the doubles cluster operator cannot couple with the Fock-operator nor can a single singles cluster operator couple with the two-body-operator. Looking at each operator pair separately we get

$$\begin{aligned}\langle\Phi|\left[\hat{f}_N\hat{T}_1\right]_c|\Phi\rangle &= f_q^p\tau_i^a\,\langle\Phi|\{\hat{c}_p^\dagger\hat{c}_q\}\{\hat{c}_a^\dagger\hat{c}_i\}|\Phi\rangle = f_q^p\tau_i^a\,\langle\Phi|\{\hat{c}_p^\dagger\hat{c}_q\hat{c}_a^\dagger\hat{c}_i\}|\Phi\rangle &\text{(B.4)}\\ &= f_q^p\tau_i^a\delta_{qa}\delta_{pi} = f_a^i\tau_i^a. &\text{(B.5)}\end{aligned}$$

The doubles cluster operator on the two-body Hamiltonian yields

$$\langle\Phi|\left[\hat{u}_N\hat{T}_2\right]_c|\Phi\rangle = \frac{1}{16}u_{rs}^{pq}\tau_{ij}^{ab}\,\langle\Phi|\left\{\hat{c}_p^\dagger\hat{c}_q^\dagger\hat{c}_s\hat{c}_r\right\}\left\{\hat{c}_a^\dagger\hat{c}_b^\dagger\hat{c}_j\hat{c}_i\right\}|\Phi\rangle\,. \tag{B.6}$$

For the sake of brevity we will restrict our attention to the operator strings that are non-zero when utilizing Wick's theorem.

$$\begin{aligned}\left\{\hat{c}_p^\dagger\hat{c}_q^\dagger\hat{c}_s\hat{c}_r\right\}\left\{\hat{c}_a^\dagger\hat{c}_b^\dagger\hat{c}_j\hat{c}_i\right\} &= \overbrace{\left\{\hat{c}_p^\dagger\hat{c}_q^\dagger\hat{c}_s\hat{c}_r\hat{c}_a^\dagger\hat{c}_b^\dagger\hat{c}_j\hat{c}_i\right\}} + \overbrace{\left\{\hat{c}_p^\dagger\hat{c}_q^\dagger\hat{c}_s\hat{c}_r\hat{c}_a^\dagger\hat{c}_b^\dagger\hat{c}_j\hat{c}_i\right\}} \\ &\quad + \overbrace{\left\{\hat{c}_p^\dagger\hat{c}_q^\dagger\hat{c}_s\hat{c}_r\hat{c}_a^\dagger\hat{c}_b^\dagger\hat{c}_j\hat{c}_i\right\}} + \overbrace{\left\{\hat{c}_p^\dagger\hat{c}_q^\dagger\hat{c}_s\hat{c}_r\hat{c}_a^\dagger\hat{c}_b^\dagger\hat{c}_j\hat{c}_i\right\}} \qquad \text{(B.7)} \\ &= \delta_{ra}\delta_{sb}\delta_{qj}\delta_{pi} - \delta_{rb}\delta_{sa}\delta_{qj}\delta_{pi} \\ &\quad - \delta_{ra}\delta_{sb}\delta_{qi}\delta_{pj} + \delta_{rb}\delta_{sa}\delta_{qi}\delta_{pj}. \qquad \text{(B.8)}\end{aligned}$$

Inserting the Kronecker-delta functions back into the energy contribution and summing, we get

$$\langle\Phi|\left[\hat{u}_N\hat{T}_2\right]_c|\Phi\rangle = \frac{1}{16}\left[u_{ab}^{ij} - u_{ba}^{ij} - u_{ab}^{ji} + u_{ba}^{ji}\right]\tau_{ij}^{ab} = \frac{1}{4}u_{ab}^{ij}\tau_{ij}^{ab}, \tag{B.9}$$

where we have used the antisymmetric properties of the two-body elements to collect all four terms.

Moving on to the squared cluster operator contribution we note that the only non-zero contribution to the energy can come from the singles cluster operator as this provides a doubly excited state from the reference state. This also means that we can only get a coupling with the two-body operator. We are thus left with

$$\begin{aligned}\langle\Phi|\left[\hat{u}_N\hat{T}_1^2\right]_c|\Phi\rangle &= \frac{1}{4}u_{rs}^{pq}\tau_i^a\tau_j^b\,\langle\Phi|\left\{\hat{c}_p^\dagger\hat{c}_q^\dagger\hat{c}_s\hat{c}_r\right\}\left\{\hat{c}_a^\dagger\hat{c}_i\right\}\left\{\hat{c}_b^\dagger\hat{c}_j\right\}|\Phi\rangle \qquad \text{(B.10)} \\ &= u_{ab}^{ij}\tau_i^a\tau_j^b, \qquad \text{(B.11)}\end{aligned}$$

where we note that the same contractions as in the previous term is performed for the squared cluster operators. Collecting all the contributions to the correlation energy we get

$$\begin{aligned}\langle\Phi|\bar{H}_N|\Phi\rangle &= \langle\Phi|\left[\hat{H}_N\hat{T}\right]_c|\Phi\rangle + \frac{1}{2!}\langle\Phi|\left[\hat{H}_N\hat{T}^2\right]_c|\Phi\rangle \qquad \text{(B.12)} \\ &= f_a^i\tau_i^a + \frac{1}{2}u_{ab}^{ij}\left(\tau_{ij}^{ab} + \tau_i^a\tau_j^b\right), \qquad \text{(B.13)}\end{aligned}$$

which is what we wanted to show.

B.2 Coupled-cluster τ-amplitude equations

We use the amplitude expressions from the book *Many-Body Methods in Chemistry and Physics* [10] for the τ-amplitudes. The task at hand is to evaluate

$$\Omega_\mu(\boldsymbol{\tau}) = \langle \Phi_\mu | \exp(-\hat{T}) \hat{H}_N \exp(\hat{T}) | \Phi \rangle \,, \tag{B.14}$$

for the CCD approximation with $\hat{T} = \hat{T}_2$ and CCSD with $\hat{T} = \hat{T}_1 + \hat{T}_2$. We denote the number of basis functions by L, the number of particles by N, and the number virtual states by $M = L - N$. We assume that $N < L/2$ so that it is better to replace a contraction along a virtual index with an occupied index. Furthermore, we assume that the tensor contractions are performed as binary operations where the ordering of the contractions involving the lowest cost are performed. The permutation operator $P(ab)$ is defined by the action

$$f_c^b \tau_{ij}^{ac} P(ab) = f_c^b \tau_{ij}^{ac} - f_c^a \tau_{ij}^{bc}, \tag{B.15}$$

that is, it subtracts the same term, but with two indices replaced.

The CCD τ-amplitudes are shown in Table B.1. For the CCSD τ-amplitudes we have the doubles amplitudes from CCD in Table B.1 along with the new doubles terms in Table B.3. Note that term D8a in Table B.3 is different by a sign from the one in *Many-Body Methods in Chemistry and Physics* as the latter contains a typo. In Table B.2 we show the singles amplitude contributions for CCSD.

Table B.2: Terms and intermediates included in the CCSD τ_1-amplitudes. Empty lines continue from the line above.

Label	Intermediate	Term	Complexity
S1		f_i^a	$\mathcal{O}(MN)$
S2a		$f_c^k \tau_{ik}^{ac}$	$\mathcal{O}(M^2N^2)$
S2b		$\frac{1}{2} u_{cd}^{ak} \tau_{ik}^{cd}$	$\mathcal{O}(M^3N^2)$
S2c		$-\frac{1}{2} u_{ic}^{kl} \tau_{kl}^{ac}$	$\mathcal{O}(M^2N^3)$
S3a		$f_c^a \tau_i^c$	$\mathcal{O}(M^2N)$
S3b		$-f_i^k \tau_k^a$	$\mathcal{O}(MN^2)$
S3c		$u_{ic}^{ak} \tau_k^c$	$\mathcal{O}(M^2N^2)$
S4a	$W_{di}^{kl} = -\frac{1}{2} u_{cd}^{kl} \tau_i^c$	$\tau_{kl}^{ad} W_{di}^{kl}$	$\mathcal{O}(M^2N^3)$
S4b	$W_i^k = -\frac{1}{2} u_{cd}^{kl} \tau_{il}^{cd}$	$\tau_k^a W_i^k$	$\mathcal{O}(M^2N^3)$

Table B.2: (continued)

Label	Intermediate	Term	Complexity
S4c	$W_d^l = u_{cd}^{kl}\tau_k^c$	$W_d^l\tau_{li}^{da}$	$\mathcal{O}(M^2N^2)$
S5a	$W_i^k = -f_c^k\tau_i^c$	$\tau_k^a W_i^k$	$\mathcal{O}(MN^2)$
S5b	$W_{di}^{ak} = u_{cd}^{ak}\tau_i^c$	$W_{di}^{ak}\tau_k^d$	$\mathcal{O}(M^3N^2)$
S5c	$W_i^k = -u_{ic}^{kl}\tau_l^c$	$\tau_k^a W_i^k$	$\mathcal{O}(MN^3)$
S6	$W_c^k = -u_{cd}^{kl}\tau_l^d$		
	$W_i^k = W_c^k\tau_i^c$	$\tau_k^a W_i^k$	$\mathcal{O}(M^2N^2)$

Table B.3: New terms included in the CCSD τ_2-amplitudes. These terms should be added along with the ones from CCD in Table B.1. Empty lines continue from the line above.

Label	Intermediate	Term	Complexity
D4a		$u_{cj}^{ab}\tau_i^c P(ij)$	$\mathcal{O}(M^3N^2)$
D4b		$-u_{ij}^{kb}\tau_k^a P(ab)$	$\mathcal{O}(M^2N^3)$
D5a	$W_i^k = f_c^k\tau_i^c$	$-t_{kj}^{ab}W_i^k P(ij)$	$\mathcal{O}(M^2N^3)$
D5b	$W_c^a = \tau_k^a f_c^k$	$-W_c^a\tau_{ij}^{cb}P(ab)$	$\mathcal{O}(M^3N^2)$
D5c	$W_{di}^{ak} = u_{cd}^{ak}\tau_i^c$	$W_{di}^{ak}\tau_{kj}^{db}P(ab)P(ij)$	$\mathcal{O}(M^3N^3)$
D5d	$W_{ic}^{al} = \tau_k^a u_{ic}^{kl}$	$-W_{ic}^{al}\tau_{lj}^{cb}P(ab)P(ij)$	$\mathcal{O}(M^3N^3)$
D5e	$W_{ij}^{kb} = u_{cd}^{kb}\tau_{ij}^{cd}$	$-\frac{1}{2}\tau_k^a W_{ij}^{kb}P(ab)$	$\mathcal{O}(M^3N^3)$
D5f	$W_{ji}^{kl} = u_{cj}^{kl}\tau_i^c$	$\frac{1}{2}\tau_{kl}^{ab}W_{ji}^{kl}P(ij)$	$\mathcal{O}(M^2N^4)$
D5g	$W_d^a = u_{cd}^{ka}\tau_k^c$	$W_d^a\tau_{ij}^{db}P(ab)$	$\mathcal{O}(M^3N^2)$
D5h	$W_i^l = u_{ci}^{kl}\tau_k^c$	$-\tau_{lj}^{ab}W_i^l P(ij)$	$\mathcal{O}(M^2N^3)$
D6a	$W_{di}^{ab} = u_{cd}^{ab}\tau_i^c$	$W_{di}^{ab}\tau_j^d$	$\mathcal{O}(M^4N)$
D6b	$W_{ij}^{bk} = \tau_l^b u_{ij}^{kl}$	$\tau_k^a W_{ij}^{bk}$	$\mathcal{O}(M^2N^3)$
D6c	$W_{ji}^{kb} = -u_{cj}^{kb}\tau_i^c$	$\tau_k^a W_{ji}^{kb}P(ab)P(ij)$	$\mathcal{O}(M^2N^3)$

Table B.3: (continued)

Label	Intermediate	Term	Complexity
D7a	$W^{kl}_{di} = \frac{1}{2} u^{kl}_{cd} \tau^c_i$		
	$W^{kl}_{ij} = W^{kl}_{di} \tau^d_j$	$\tau^{ab}_{kl} W^{kl}_{ij}$	$\mathcal{O}(M^2N^4)$
D7b	$W^{kl}_{ij} = \frac{1}{2} u^{kl}_{cd} \tau^{cd}_{ij}$		
	$W^{bk}_{ij} = \tau^b_l W^{kl}_{ij}$	$\tau^a_k W^{bk}_{ij}$	$\mathcal{O}(M^2N^4)$
D7c	$W^{al}_{cd} = -\tau^a_k u^{kl}_{cd}$		
	$W^{al}_{di} = W^{al}_{cd} \tau^c_i$	$W^{al}_{di} \tau^{db}_{lj} P(ij) P(ab)$	$\mathcal{O}(M^3N^3)$
D7d	$W^l_d = -u^{kl}_{cd} \tau^c_k$		
	$W^l_i = W^l_d \tau^d_i$	$\tau^{ab}_{lj} W^l_i P(ij)$	$\mathcal{O}(M^2N^3)$
D7e	$W^l_d = -u^{kl}_{cd} \tau^c_k$		
	$W^a_d = \tau^a_l W^l_d$	$W^a_d \tau^{db}_{ij} P(ab)$	$\mathcal{O}(M^3N^2)$
D8a	$W^{kb}_{di} = -u^{kb}_{cd} \tau^c_i$		
	$W^{kb}_{ij} = W^{kb}_{di} \tau^d_j$	$\tau^a_k W^{kb}_{ij} P(ab)$	$\mathcal{O}(M^3N^2)$
D8b	$W^{kl}_{ji} = u^{kl}_{cj} \tau^c_i$		
	$W^{bk}_{ji} = \tau^b_l W^{kl}_{ji}$	$\tau^a_k W^{bk}_{ji} P(ij)$	$\mathcal{O}(M^2N^3)$
D9	$W^{kl}_{di} = u^{kl}_{cd} \tau^c_i$		
	$W^{kl}_{ij} = W^{kl}_{di} \tau^d_j$		
	$W^{bk}_{ij} = \tau^b_l W^{kl}_{ij}$	$\tau^a_k W^{bk}_{ij}$	$\mathcal{O}(M^2N^3)$

B.3 Coupled-cluster λ-amplitude equations

Using SymPy [70] we are able to efficiently create amplitude equations by programmatically evaluating Wick's theorem. The labelling of the terms in the equations are inspired by the naming convention used in *Many-Body Methods in Chemistry and Physics* [10], but with slight modifications. The first letter, either "S" or "D", denotes a singles or a doubles contribution respectively. The number is used to collect terms with a similar structure, e.g., contractions between a singles amplitude, a doubles amplitude, and the two-body

Table B.1: Terms and intermediates included in the CCD τ-amplitudes.

Label	Intermediate	Term	Complexity
D1		u_{ij}^{ab}	$\mathcal{O}(M^2N^2)$
D2a		$f_c^b \tau_{ij}^{ac} P(ab)$	$\mathcal{O}(M^3N^2)$
D2b		$-f_j^k \tau_{ik}^{ab} P(ij)$	$\mathcal{O}(M^2N^3)$
D2c		$\frac{1}{2}\tau_{ij}^{cd} u_{cd}^{ab}$	$\mathcal{O}(M^4N^2)$
D2d		$\frac{1}{2}\tau_{kl}^{ab} u_{ij}^{kl}$	$\mathcal{O}(M^2N^4)$
D2e		$\tau_{ik}^{ac} u_{cj}^{kb} P(ab)P(ij)$	$\mathcal{O}(M^3N^3)$
D3a	$W_{ij}^{kl} = \frac{1}{4}\tau_{ij}^{cd} u_{cd}^{kl}$	$\tau_{kl}^{ab} W_{ij}^{kl}$	$\mathcal{O}(M^2N^4)$
D3b	$W_{jc}^{bk} = \tau_{jl}^{bd} u_{cd}^{kl}$	$\tau_{ik}^{ac} W_{jc}^{bk} P(ij)$	$\mathcal{O}(M^3N^3)$
D3c	$W_i^l = \frac{1}{2}\tau_{ik}^{dc} u_{cd}^{kl}$	$-\tau_{lj}^{ab} W_i^l P(ij)$	$\mathcal{O}(M^2N^3)$
D3d	$W_d^a = \frac{1}{2}\tau_{lk}^{ac} u_{cd}^{kl}$	$-\tau_{ij}^{db} W_d^a P(ab)$	$\mathcal{O}(M^3N^2)$

Hamiltonian will share the same number. To differentiate the different terms with the same type of contractions we tack on a second letter which is increased alphabetically. However, the number and the second letter do not have a deeper meaning as in the work by Shavitt & Bartlett [10].

Table B.4: Terms included in the CCD λ_2-amplitudes. Empty lines continue from the line above.

Label	Intermediate	Term	Complexity
D1		u_{ab}^{ij}	$\mathcal{O}(M^2N^2)$
D2a		$\frac{1}{2}\lambda_{ab}^{kl} u_{kl}^{ij}$	$\mathcal{O}(M^2N^4)$
D2b		$\frac{1}{2}\lambda_{dc}^{ij} u_{ab}^{dc}$	$\mathcal{O}(M^4N^2)$
D2c		$-f_a^c \lambda_{bc}^{ij} P(ab)$	$\mathcal{O}(M^3N^2)$
D2d		$f_k^i \lambda_{ab}^{jk} P(ij)$	$\mathcal{O}(M^2N^3)$
D2e		$\lambda_{bc}^{jk} u_{ak}^{ic} P(ab)P(ij)$	$\mathcal{O}(M^3N^3)$
D3a	$W_a^c = \frac{1}{2}\tau_{kl}^{dc} u_{ad}^{kl}$	$-\lambda_{bc}^{ij} W_a^c P(ab)$	$\mathcal{O}(M^3N^2)$
D3b	$W_{kl}^{ij} = \frac{1}{4}\lambda_{dc}^{ij} \tau_{kl}^{dc}$	$W_{kl}^{ij} u_{ab}^{kl}$	$\mathcal{O}(M^2N^4)$

Table B.4: (continued)

Label	Intermediate	Term	Complexity
D3c	$W_k^i = \frac{1}{2}\tau_{kl}^{dc} u_{dc}^{il}$	$\lambda_{ab}^{jk} W_k^i P(ij)$	$\mathcal{O}(M^2N^3)$
D3d	$W_{bl}^{jd} = \lambda_{bc}^{jk} \tau_{kl}^{dc}$	$-W_{bl}^{jd} u_{ad}^{il} P(ab)P(ij)$	$\mathcal{O}(M^3N^3)$
D3e	$W_l^j = \frac{1}{2}\lambda_{dc}^{jk} \tau_{kl}^{dc}$	$W_l^j u_{ab}^{il} P(ij)$	$\mathcal{O}(M^2N^3)$
D3f	$W_{kl}^{ij} = \frac{1}{4}\tau_{kl}^{dc} u_{dc}^{ij}$	$\lambda_{ab}^{kl} W_{kl}^{ij}$	$\mathcal{O}(M^2N^4)$
D3g	$W_b^d = \frac{1}{2}\lambda_{bc}^{kl} \tau_{kl}^{dc}$	$-W_b^d u_{ad}^{ij} P(ab)$	$\mathcal{O}(M^3N^2)$

Table B.5: Terms included in the CCSD λ_1-amplitudes. Empty lines continue from the line above.

Label	Intermediate	Term	Complexity
S1		f_a^i	$\mathcal{O}(MN)$
S2a		$\lambda_b^i f_a^b$	$\mathcal{O}(M^2N)$
S2b		$f_j^i \lambda_a^j$	$\mathcal{O}(MN^2)$
S3a		$\lambda_b^j u_{aj}^{ib}$	$\mathcal{O}(M^2N^2)$
S3b		$-\tau_j^b u_{ab}^{ij}$	$\mathcal{O}(M^2N^2)$
S4a		$\frac{1}{2}\lambda_{bc}^{ij} u_{aj}^{bc}$	$\mathcal{O}(M^3N^2)$
S4b		$-\frac{1}{2}\lambda_{ab}^{jk} u_{jk}^{ib}$	$\mathcal{O}(M^2N^3)$
S5a	$W_a^b = \tau_j^c u_{ac}^{bj}$	$\lambda_b^i W_a^b$	$\mathcal{O}(M^3N)$
S5b	$W_j^i = \tau_k^b u_{bj}^{ik}$	$W_j^i \lambda_a^j$	$\mathcal{O}(MN^3)$
S5c	$W_b^c = \tau_j^c \lambda_b^j$	$u_{ac}^{ib} W_b^c$	$\mathcal{O}(M^3N)$
S5d	$W_k^j = -\lambda_b^j \tau_k^b$	$u_{aj}^{ik} W_k^j$	$\mathcal{O}(MN^3)$
S6a	$W_{ck}^{ij} = \lambda_{bc}^{ij} \tau_k^b$	$W_{ck}^{ij} u_{aj}^{ck}$	$\mathcal{O}(M^2N^3)$
S6b	$W_{ad}^{ij} = \frac{1}{2}\lambda_{bc}^{ij} u_{ad}^{bc}$	$W_{ad}^{ij} \tau_j^d$	$\mathcal{O}(M^4N^2)$
S6c	$W_{al}^{jk} = \frac{1}{2}\lambda_{ab}^{jk} \tau_\lambda^b$	$u_{jk}^{il} W_{al}^{jk}$	$\mathcal{O}(MN^4)$
S6d	$W_c^d = \frac{1}{2}\tau_{jk}^{bd} \lambda_{bc}^{jk}$	$u_{ad}^{ic} W_c^d$	$\mathcal{O}(M^3N^2)$

Table B.5: (continued)

Label	Intermediate	Term	Complexity
S7	$W_k^c = \lambda_b^j \tau_{jk}^{bc}$	$W_k^c u_{ac}^{ik}$	$\mathcal{O}(M^2N^2)$
S8a	$W_a^b = -\tau_j^b \lambda_a^j$	$f_b^i W_a^b$	$\mathcal{O}(M^2N)$
S8b	$W_j^i = -\lambda_b^i \tau_j^b$	$W_j^i f_a^j$	$\mathcal{O}(MN^2)$
S9a	$W_{dk}^{ic} = -\lambda_{bc}^{ij} \tau_{jk}^{bd}$	$W_{dk}^{ic} u_{ad}^{ck}$	$\mathcal{O}(M^3N^3)$
S9b	$W_{ab}^{ck} = -\tau_j^c \lambda_{ab}^{jk}$	$u_{ck}^{ib} W_{ab}^{ck}$	$\mathcal{O}(M^3N^2)$
S9c	$W_{cl}^{ka} = -\lambda_{ab}^{jk} \tau_{jl}^{bc}$	$u_{ck}^{il} W_{cl}^{ka}$	$\mathcal{O}(M^3N^3)$
S10a	$W_a^b = -\frac{1}{2} \tau_{jk}^{bc} \lambda_{ac}^{jk}$	$f_b^i W_a^b$	$\mathcal{O}(M^3N^2)$
S10b	$W_j^i = -\frac{1}{2} \lambda_{bc}^{ik} \tau_{jk}^{bc}$	$W_j^i f_a^j$	$\mathcal{O}(M^2N^3)$
S10c	$W_a^b = -\frac{1}{2} \tau_{jk}^{bc} u_{ac}^{jk}$	$\lambda_b^i W_a^b$	$\mathcal{O}(M^3N^2)$
S10d	$W_j^i = -\frac{1}{2} u_{bc}^{ik} \tau_{jk}^{bc}$	$W_j^i \lambda_a^j$	$\mathcal{O}(M^2N^3)$
S10e	$W_\lambda^k = -\frac{1}{2} \lambda_{bc}^{jk} \tau_{jl}^{bc}$	$W_\lambda^k u_{ak}^{il}$	$\mathcal{O}(M^2N^3)$
S10f	$W_{jk}^{ib} = -\frac{1}{4} u_{cd}^{ib} \tau_{jk}^{cd}$	$W_{jk}^{ib} \lambda_{ab}^{jk}$	$\mathcal{O}(M^3N^3)$
S10g	$W_{kl}^{ij} = \frac{1}{4} \lambda_{bc}^{ij} \tau_{kl}^{bc}$	$W_{kl}^{ij} u_{aj}^{kl}$	$\mathcal{O}(M^2N^4)$
S11a	$W_{ck}^{ij} = \lambda_{bc}^{ij} \tau_k^b$		
	$W_{kd}^{ic} = W_{ck}^{ij} \tau_j^d$	$W_{kd}^{ic} u_{ad}^{ck}$	$\mathcal{O}(M^3N^2)$
S11b	$W_{al}^{jk} = \lambda_{ab}^{jk} \tau_\lambda^b$		
	$W_{ja}^{ic} = u_{ck}^{il} W_{al}^{jk}$	$W_{ja}^{ic} \tau_j^c$	$\mathcal{O}(M^2N^4)$
S11c	$W_{cj}^{ib} = \frac{1}{2} u_{cd}^{ib} \tau_j^d$		
	$W_{jk}^{ib} = W_{cj}^{ib} \tau_k^c$	$W_{jk}^{ib} \lambda_{ab}^{jk}$	$\mathcal{O}(M^3N^2)$
S11d	$W_{cl}^{jk} = \frac{1}{2} \lambda_{bc}^{jk} \tau_\lambda^b$		
	$W_d^\lambda = W_{cl}^{jk} \tau_{jk}^{cd}$	$W_d^\lambda u_{ad}^{il}$	$\mathcal{O}(M^2N^3)$
S11e	$W_{cd}^{kb} = \frac{1}{2} \lambda_{bc}^{jk} \tau_j^d$		
	$W_\lambda^d = W_{cd}^{kb} \tau_{kl}^{bc}$	$W_\lambda^d u_{ad}^{il}$	$\mathcal{O}(M^3N^2)$
S11f	$W_j^i = -\lambda_b^i \tau_j^b$		
	$Z_a^j = u_{ac}^{jk} \tau_k^c$	$W_j^i Z_a^j$	$\mathcal{O}(M^2N^2)$

Table B.5: (continued)

Label	Intermediate	Term	Complexity
S11g	$W_b^i = -u_{bc}^{ik}\tau_k^c$		
	$W_j^i = W_b^i\tau_j^b$	$W_j^i\lambda_a^j$	$\mathcal{O}(M^2N^2)$
S11h	$W_k^j = -\lambda_b^j\tau_k^b$		
	$W_k^c = \tau_j^c W_k^j$	$u_{ac}^{ik}W_k^c$	$\mathcal{O}(M^2N^2)$
S11i	$W_{ck}^{ij} = -\lambda_{bc}^{ij}\tau_k^b$		
	$W_{dl}^{ik} = W_{ck}^{ij}\tau_{jl}^{cd}$	$W_{dl}^{ik}u_{ad}^{kl}$	$\mathcal{O}(M^2N^3)$
S11j	$W_{bc}^{ka} = -\lambda_{ab}^{jk}\tau_j^c$		
	$W_{dl}^{ac} = W_{bc}^{ka}\tau_{kl}^{bd}$	$u_{cd}^{il}W_{dl}^{ac}$	$\mathcal{O}(M^4N^2)$
S11k	$W_{cl}^{ij} = -\frac{1}{2}\lambda_{bc}^{ij}\tau_\lambda^b$		
	$w_{lk}^{ij} = w_{cl}^{ij}\tau_k^c$	$W_{lk}^{ij}u_{aj}^{kl}$	$\mathcal{O}(M^2N^3)$
S11l	$W_\lambda^i = -\frac{1}{2}\lambda_{bc}^{ij}\tau_{jl}^{bc}$		
	$Z_a^\lambda = \tau_k^d u_{ad}^{kl}$	$W_\lambda^i Z_a^\lambda$	$\mathcal{O}(M^2N^3)$
S11m	$W_a^d = -\frac{1}{2}\tau_{jk}^{bd}\lambda_{ab}^{jk}$		
	$Z_d^i = \tau_\lambda^c u_{cd}^{il}$	$Z_d^i W_a^d$	$\mathcal{O}(M^3N^2)$
S11n	$W_{kl}^{ij} = \frac{1}{4}\lambda_{bc}^{ij}\tau_{kl}^{bc}$		
	$Z_{aj}^{kl} = u_{ad}^{kl}\tau_j^d$	$W_{kl}^{ij}Z_{aj}^{kl}$	$\mathcal{O}(M^2N^4)$
S11o	$W_{jk}^{il} = \frac{1}{4}u_{cd}^{il}\tau_{jk}^{cd}$		
	$W_{ab}^{il} = W_{jk}^{il}\lambda_{ab}^{jk}$	$W_{ab}^{il}\tau_\lambda^b$	$\mathcal{O}(M^2N^4)$
S12a	$W_{cl}^{ij} = -\frac{1}{2}\lambda_{bc}^{ij}\tau_\lambda^b$		
	$W_{lk}^{ij} = W_{cl}^{ij}\tau_k^c$		
	$W_{kd}^{il} = W_{lk}^{ij}\tau_j^d$	$W_{kd}^{il}u_{ad}^{kl}$	$\mathcal{O}(M^2N^3)$
S12b	$W_{al}^{jk} = -\frac{1}{2}\lambda_{ab}^{jk}\tau_\lambda^b$		
	$W_{lc}^{ja} = W_{al}^{jk}\tau_k^c$		
	$W_{cd}^{al} = W_{lc}^{ja}\tau_j^d$	$u_{cd}^{il}W_{cd}^{al}$	$\mathcal{O}(M^3N^2)$

Table B.6: New terms included in the CCSD λ_2-amplitudes. These terms should be added along with the ones from CCD in Table B.4. Empty lines continue from the line above.

Label	Intermediate	Term	Complexity
D4a	$W_{dk}^{ij} = l_{cd}^{ij} t_k^c$	$W_{dk}^{ij} u_{ab}^{dk}$	$\mathcal{O}(M^3N^3)$
D4b	$W_{kl}^{ij} = t_k^c u_{cl}^{ij}$	$W_{kl}^{ij} l_{ab}^{kl}$	$\mathcal{O}(M^2N^4)$
D5a		$l_a^k u_{bk}^{ij} P(ab)$	$\mathcal{O}(M^2N^3)$
D5b		$-l_c^i u_{ab}^{jc} P(ij)$	$\mathcal{O}(M^3N^2)$
D7a		$f_a^i \lambda_b^j P(ab)P(ij)$	$\mathcal{O}(M^2N^2)$
D7b	$W_k^i = f_c^i \tau_k^c$	$W_k^i \lambda_{ab}^{jk} P(ij)$	$\mathcal{O}(M^2N^3)$
D7c	$W_a^c = \tau_k^c f_a^k$	$\lambda_{bc}^{ij} W_a^c P(ab)$	$\mathcal{O}(M^3N^2)$
D8a	$W_k^i = \lambda_c^i \tau_k^c$	$W_k^i u_{ab}^{jk} P(ij)$	$\mathcal{O}(M^2N^3)$
D8b	$W_a^c = \tau_k^c \lambda_a^k$	$u_{bc}^{ij} W_a^c P(ab)$	$\mathcal{O}(M^3N^2)$
D8c	$W_b^c = \tau_k^d u_{bd}^{ck}$	$\lambda_{ac}^{ij} W_b^c P(ab)$	$\mathcal{O}(M^3N^2)$
D8d	$W_k^j = \tau_\lambda^c u_{ck}^{jl}$	$W_k^j \lambda_{ab}^{ik} P(ij)$	$\mathcal{O}(M^2N^3)$
D10a	$W_{ab}^{dl} = -\frac{1}{2} \tau_k^d \lambda_{ab}^{kl}$		
	$W_{ab}^{cd} = \tau_\lambda^c W_{ab}^{dl}$	$u_{cd}^{ij} W_{ab}^{cd}$	$\mathcal{O}(M^4N^2)$
D10b	$W_{dl}^{ij} = -\frac{1}{2} \lambda_{cd}^{ij} \tau_\lambda^c$		
	$W_{lk}^{ij} = W_{dl}^{ij} \tau_k^d$	$W_{lk}^{ij} u_{ab}^{kl}$	$\mathcal{O}(M^2N^4)$
D11a	$W_b^j = \tau_k^c u_{bc}^{jk}$	$\lambda_a^i W_b^j P(ab)P(ij)$	$\mathcal{O}(M^2N^3)$
D11b	$W_{ac}^{di} = \tau_k^d \lambda_{ac}^{ik}$	$W_{ac}^{di} u_{bd}^{jc} P(ab)P(ij)$	$\mathcal{O}(M^4N^2)$
D11c	$W_{al}^{ik} = -\lambda_{ac}^{ik} \tau_\lambda^c$	$W_{al}^{ik} u_{bk}^{jl} P(ab)P(ij)$	$\mathcal{O}(M^2N^4)$
D12a	$W_b^k = -\tau_\lambda^d u_{bd}^{kl}$		
	$W_b^c = \tau_k^c W_b^k$	$\lambda_{ac}^{ij} W_b^c P(ab)$	$\mathcal{O}(M^3N^2)$
D12b	$W_c^j = -\tau_\lambda^d u_{cd}^{jl}$		
	$W_k^j = W_c^j \tau_k^c$	$\lambda_{ab}^{ik} W_k^j P(ij)$	$\mathcal{O}(M^2N^3)$
D12c	$W_{bk}^{jl} = -u_{bd}^{jl} \tau_k^d$		
	$W_{bk}^{cj} = \tau_\lambda^c W_{bk}^{jl}$	$\lambda_{ac}^{ik} W_{bk}^{cj} P(ab)P(ij)$	$\mathcal{O}(M^3N^3)$

B.4 Coupled-cluster Lagrangian

The coupled-cluster doubles Lagrangian is given by

$$\begin{aligned} L(\boldsymbol{\tau},\boldsymbol{\lambda}) = {} & \frac{\lambda_{ab}^{ij} u_{ij}^{ab}}{4} + \frac{\tau_{ij}^{ab} u_{ab}^{ij}}{4} + \frac{f_b^a \lambda_{ac}^{ij} \tau_{ij}^{bc}}{2} \\ & - \lambda_{ab}^{ij} \tau_{ik}^{ac} u_{cj}^{bk} - \frac{f_i^j \lambda_{ab}^{ik} \tau_{jk}^{ab}}{2} + \frac{\lambda_{ab}^{ij} \tau_{kl}^{ab} u_{ij}^{kl}}{8} \\ & + \frac{\lambda_{ab}^{ij} \tau_{ij}^{cd} u_{cd}^{ab}}{8} - \frac{\lambda_{ab}^{ij} \tau_{jk}^{ac} \tau_{il}^{bd} u_{cd}^{kl}}{2} - \frac{\lambda_{ab}^{ij} \tau_{kl}^{ac} \tau_{ij}^{bd} u_{cd}^{kl}}{4} \\ & + \frac{\lambda_{ab}^{ij} \tau_{il}^{ab} \tau_{jk}^{cd} u_{cd}^{kl}}{8} + \frac{\lambda_{ab}^{ij} \tau_{jk}^{ab} \tau_{il}^{cd} u_{cd}^{kl}}{8} + \frac{\lambda_{ab}^{ij} \tau_{kl}^{ab} \tau_{ij}^{cd} u_{cd}^{kl}}{16}. \end{aligned} \tag{B.16}$$

The coupled-cluster singles-and-doubles Lagrangian is given by

$$
\begin{aligned}
L(\boldsymbol{\tau},\boldsymbol{\lambda}) = {} & f_i^a\lambda_a^i + f_a^i\tau_i^a + \frac{\lambda_{ab}^{ij}u_{ij}^{ab}}{4} + \frac{\tau_{ij}^{ab}u_{ab}^{ij}}{4} + f_b^a\lambda_a^i\tau_i^b \\
& + f_a^i\lambda_b^j\tau_{ij}^{ab} + \frac{f_b^a\lambda_{ac}^{ij}\tau_{ij}^{bc}}{2} + \frac{\lambda_a^i\tau_{jk}^{ab}u_{bi}^{jk}}{2} + \frac{\lambda_a^i\tau_{ij}^{bc}u_{bc}^{aj}}{2} \\
& + \frac{\lambda_{ab}^{ij}\tau_k^a u_{ij}^{bk}}{2} + \frac{\lambda_{ab}^{ij}\tau_i^c u_{cj}^{ab}}{2} - f_i^j\lambda_a^i\tau_j^a - \lambda_a^i\tau_j^b u_{bi}^{aj} \\
& - \lambda_{ab}^{ij}\tau_{ik}^{ac}u_{cj}^{bk} - \frac{f_i^j\lambda_{ab}^{ik}\tau_{jk}^{ab}}{2} - \frac{\tau_j^a\tau_i^b u_{ab}^{ij}}{2} + \frac{\lambda_{ab}^{ij}\tau_{kl}^{ab}u_{ij}^{kl}}{8} \\
& + \frac{\lambda_{ab}^{ij}\tau_{ij}^{cd}u_{cd}^{ab}}{8} + \lambda_a^i\tau_j^a\tau_k^b u_{bi}^{jk} + \lambda_a^i\tau_i^b\tau_j^c u_{bc}^{aj} + \lambda_a^i\tau_j^b\tau_{ik}^{ac}u_{bc}^{jk} \\
& + \lambda_{ab}^{ij}\tau_k^a\tau_i^c u_{cj}^{bk} - f_a^i\lambda_b^j\tau_j^a\tau_i^b - \lambda_{ab}^{ij}\tau_k^a\tau_{il}^{bc}u_{cj}^{kl} - \lambda_{ab}^{ij}\tau_i^c\tau_{jk}^{ad}u_{cd}^{bk} \\
& - \frac{f_a^i\lambda_{bc}^{jk}\tau_j^a\tau_{ik}^{bc}}{2} - \frac{f_a^i\lambda_{bc}^{jk}\tau_i^b\tau_{jk}^{ac}}{2} - \frac{\lambda_a^i\tau_j^a\tau_{ik}^{bc}u_{bc}^{jk}}{2} - \frac{\lambda_a^i\tau_i^b\tau_{jk}^{ac}u_{bc}^{jk}}{2} \\
& - \frac{\lambda_{ab}^{ij}\tau_k^c\tau_{il}^{ab}u_{cj}^{kl}}{2} - \frac{\lambda_{ab}^{ij}\tau_k^c\tau_{ij}^{ad}u_{cd}^{bk}}{2} - \frac{\lambda_{ab}^{ij}\tau_{jk}^{ac}\tau_{il}^{bd}u_{cd}^{kl}}{2} \\
& - \frac{\lambda_{ab}^{ij}\tau_l^a\tau_k^b u_{ij}^{kl}}{4} - \frac{\lambda_{ab}^{ij}\tau_j^c\tau_i^d u_{cd}^{ab}}{4} - \frac{\lambda_{ab}^{ij}\tau_{kl}^{ac}\tau_{ij}^{bd}u_{cd}^{kl}}{4} \\
& + \frac{\lambda_{ab}^{ij}\tau_k^a\tau_{ij}^{cd}u_{cd}^{bk}}{4} + \frac{\lambda_{ab}^{ij}\tau_i^c\tau_{kl}^{ab}u_{cj}^{kl}}{4} + \frac{\lambda_{ab}^{ij}\tau_{il}^{ab}\tau_{jk}^{cd}u_{cd}^{kl}}{8} \\
& + \frac{\lambda_{ab}^{ij}\tau_{jk}^{ab}\tau_{il}^{cd}u_{cd}^{kl}}{8} + \frac{\lambda_{ab}^{ij}\tau_{kl}^{ab}\tau_{ij}^{cd}u_{cd}^{kl}}{16} - \lambda_a^i\tau_k^a\tau_j^b\tau_i^c u_{bc}^{jk} \\
& - \lambda_{ab}^{ij}\tau_k^a\tau_i^c\tau_{jl}^{bd}u_{cd}^{kl} - \frac{\lambda_{ab}^{ij}\tau_k^a\tau_j^c\tau_i^d u_{cd}^{bk}}{2} - \frac{\lambda_{ab}^{ij}\tau_k^a\tau_l^c\tau_{ij}^{bd}u_{cd}^{kl}}{2} \\
& - \frac{\lambda_{ab}^{ij}\tau_l^a\tau_k^b\tau_i^c u_{cj}^{kl}}{2} - \frac{\lambda_{ab}^{ij}\tau_i^c\tau_k^d\tau_{jl}^{ab}u_{cd}^{kl}}{2} - \frac{\lambda_{ab}^{ij}\tau_l^a\tau_k^b\tau_{ij}^{cd}u_{cd}^{kl}}{8} \\
& - \frac{\lambda_{ab}^{ij}\tau_j^c\tau_i^d\tau_{kl}^{ab}u_{cd}^{kl}}{8}\frac{\lambda_{ab}^{ij}\tau_l^a\tau_k^b\tau_j^c\tau_i^d u_{cd}^{kl}}{4}.
\end{aligned}
\tag{B.17}
$$

The same consideration in terms of intermediates should used when computing the Lagrangian as well.

B.5 Non-orthogonal orbital equations

Here we list the stationary conditions for κ^u and κ^d as used in the non-orthogonal coupled-cluster doubles method. For $\Delta\kappa^d$ we have [21]

$$\begin{aligned}(\Delta\kappa^d)^I_A = &-\frac{\lambda^{lk}_{cd}\tau^{cd}_{mk}u^{Im}_{Al}}{2} - \frac{\lambda^{lk}_{cd}\tau^{ec}_{lk}u^{Id}_{Ae}}{2} + \frac{\lambda^{lk}_{Ac}\tau^{cd}_{lk}f^I_d}{2}\\ &- \lambda^{lk}_{Ac}\tau^{cd}_{mk}u^{Im}_{dl} - \frac{\lambda^{lk}_{Ac}\tau^{ed}_{lk}u^{Ic}_{ed}}{4} - \frac{\lambda^{lk}_{Ac}u^{Ic}_{lk}}{2}\\ &- \frac{\lambda^{Ik}_{cd}\tau^{cd}_{lk}f^l_A}{2} + \frac{\lambda^{Ik}_{cd}\tau^{cd}_{ml}u^{ml}_{Ak}}{4} - \lambda^{Ik}_{cd}\tau^{ec}_{lk}u^{dl}_{Ae}\\ &+ \frac{\lambda^{Ik}_{cd}u^{cd}_{Ak}}{2} + f^I_A,\end{aligned} \tag{B.18}$$

where Myhre [21] uses capital letters to denote indices which will not get contracted. For $\Delta\kappa^u$ we get [21]

$$\begin{aligned}(\Delta\kappa^u)^A_I = &\frac{\lambda^{lk}_{cd}\tau^{cd}_{mk}}{4}\tau^{ef}_{Il}u^{Am}_{ef} - \frac{\lambda^{lk}_{cd}\tau^{Ae}_{ln}}{2}\tau^{cd}_{mk}u^{mn}_{Ie} + \frac{\lambda^{lk}_{cd}\tau^{cd}_{mk}}{2}u^{Am}_{Il}\\ &+ \frac{\lambda^{lk}_{cd}\tau^{Ae}_{lk}}{8}\tau^{cd}_{mn}u^{mn}_{Ie} + \frac{\lambda^{lk}_{cd}\tau^{cd}_{Ik}}{2}f^A_l + \frac{\lambda^{lk}_{cd}\tau^{cd}_{Il}}{4}\tau^{ef}_{mk}u^{Am}_{ef}\\ &- \frac{\lambda^{lk}_{cd}\tau^{cd}_{Im}}{8}\tau^{ef}_{lk}u^{Am}_{ef} - \frac{\lambda^{lk}_{cd}\tau^{cd}_{Im}}{4}u^{Am}_{lk} + \frac{\lambda^{lk}_{cd}\tau^{ec}_{lk}}{2}\tau^{fd}_{Im}u^{Am}_{ef}\\ &+ \frac{\lambda^{lk}_{cd}\tau^{Ad}_{mn}}{4}\tau^{ec}_{lk}u^{mn}_{Ie} + \frac{\lambda^{lk}_{cd}\tau^{ec}_{lk}}{2}u^{Ad}_{Ie} - \lambda^{lk}_{cd}\tau^{ec}_{mk}\tau^{fd}_{Il}u^{Am}_{ef}\\ &- \lambda^{lk}_{cd}\tau^{ec}_{mk}\tau^{Ad}_{ln}u^{mn}_{Ie} + \frac{\lambda^{lk}_{cd}\tau^{Ad}_{lk}}{4}\tau^{ec}_{mn}u^{mn}_{Ie} + \lambda^{lk}_{cd}\tau^{ec}_{Ik}u^{Ad}_{el}\\ &- \frac{\lambda^{lk}_{cd}\tau^{Ac}_{lk}}{2}f^d_I + \lambda^{lk}_{cd}\tau^{Ac}_{mk}u^{dm}_{Il} + \frac{\lambda^{lk}_{cd}\tau^{Ae}_{lk}}{4}u^{cd}_{Ie}\\ &- \frac{\tau^{cd}_{Ik}u^{Ak}_{cd}}{2} + \frac{\tau^{Ac}_{lk}u^{lk}_{Ic}}{2} - f^A_I.\end{aligned} \tag{B.19}$$

B.6 Untruncated Q-space equations

Let $\{\chi_\alpha\}$ be an initial biorthonormal single-particle basis with the corresponding dual states such that

$$|\phi_p\rangle = C_{\alpha p}\,|\chi_\alpha\rangle\,, \tag{B.20}$$

$$\langle\tilde{\phi}_p| = \tilde{C}_{p\alpha}\,\langle\tilde{\chi}_\alpha|\,, \tag{B.21}$$

are the time-evolved biorthonormal orbitals in the OATDCC-method. It is important to note that we are now in a position where we can truncate the

number of basis states $\{\phi_p\}$. That is, if we let $p \in \{1, \ldots, L\}$ we can choose a $K \leqslant L$ such that $p \in \{1, \ldots, K\}$ and thus lower the number of orbitals that we need to evolve in time. The time-dependency is kept in the coefficients and we have that

$$\langle \tilde{\phi}_p | \phi_q \rangle = \tilde{C}_{p\alpha} C_{q\beta} \langle \tilde{\chi}_\alpha | \chi_\beta \rangle = \tilde{C}_{p\alpha} C_{q\alpha} = \delta_{pq}, \tag{B.22}$$

at equal times. Now, if we do not truncate the basis of time-evolved orbitals $\{\phi_p\}$, i.e., $K = L$, we have the inverse transformation

$$|\chi_\beta\rangle = \delta_{\alpha\beta} |\chi_\alpha\rangle = \tilde{C}_{p\beta} C_{\alpha p} |\chi_\alpha\rangle = \tilde{C}_{p\beta} |\phi_p\rangle, \tag{B.23}$$

$$\langle \tilde{\chi}_\beta | = \delta_{\beta\alpha} \langle \tilde{\chi}_\alpha | = \tilde{C}_{p\alpha} C_{\beta p} \langle \tilde{\chi}_\alpha | = C_{\beta p} \langle \phi_p |. \tag{B.24}$$

In order to find equations for the coefficients using Equation 6.132 and Equation 6.135 we left-project the former equation with $\langle \tilde{\chi}_\alpha |$ and right-project the latter equation with $|\chi_\alpha\rangle$. Looking at the one-body Hamiltonian term from Equation 6.132 we have

$$\rho_p^q \langle \tilde{\chi}_\alpha | \hat{Q} \hat{h} | \phi_q \rangle = \rho_p^q \langle \tilde{\chi}_\alpha | \hat{h} | \phi_q \rangle - \rho_p^q h_q^r \langle \tilde{\chi}_\alpha | \phi_r \rangle \tag{B.25}$$

$$= \rho_p^q h_q^r C_{\alpha r} - \rho_p^q h_q^r C_{\beta r} \delta_{\alpha\beta} = 0, \tag{B.26}$$

if the basis set over the time-evolved orbitals is untruncated. This exact same cancellation will occur for the two-body Hamiltonian term in Equation 6.132 as well as both the one- and two-body Hamiltonian terms in Equation 6.135.

Appendix C

Coupled-cluster density matrices

From Equation 6.53 we have an expression for the coupled-cluster one-body density matrices ρ_p^q from the left- and right-hand coupled-cluster wave functions,

$$\rho_p^q = \langle\tilde{\Psi}|\hat{c}_p^\dagger \hat{c}_q|\Psi\rangle = \langle\Phi|(\mathbb{1} + \hat{\Lambda})\exp(-\hat{T})\hat{c}_p^\dagger \hat{c}_q \exp(\hat{T})|\Phi\rangle\,. \tag{C.1}$$

Note that we here restrict ourselves to the case of static orbitals, however, the expressions turn out to be the same for the case of orbital-adaptive orbitals due to the bi-orthonormality of the bi-variational second quantized operators. In order to find an expression for the one-body density matrices in terms of the λ- and τ-amplitudes we wish to use Wick's theorem. We start by splitting up the left-hand wave function into two terms.

$$\rho_p^q = \langle\Phi|\exp(-\hat{T})\hat{c}_p^\dagger \hat{c}_q \exp(\hat{T})|\Phi\rangle + \langle\Phi|\hat{\Lambda}\exp(-\hat{T})\hat{c}_p^\dagger \hat{c}_q \exp(\hat{T})|\Phi\rangle\,. \tag{C.2}$$

Next we expand the exponentials and use the Baker-Campbell-Hausdorff formula. This lets us write

$$\exp(-\hat{T})\hat{c}_p^\dagger \hat{c}_q \exp(\hat{T}) = \hat{c}_p^\dagger \hat{c}_q + \left[\hat{c}_p^\dagger \hat{c}_q, \hat{T}\right] + \frac{1}{2!}\left[\left[\hat{c}_p^\dagger \hat{c}_q, \hat{T}\right], \hat{T}\right] + \ldots. \tag{C.3}$$

To determine how many terms to include we have to look at the number of excitations that will be performed by the excitation operators $\hat{T}$ and relaxation operators $\hat{\Lambda}$. We know that $\hat{T}$ will at least excite the reference by 1. The combined operator $\hat{c}_p^\dagger \hat{c}_q$ is able to excite and relax the reference with at most 1, or leave it unchanged. The relaxation operator $\hat{\Lambda}$ will at least relax the reference by 1. As our basis of Slater determinants are orthonormal the only non-zero contributions to ρ_p^q will be the operator combinations that leave the reference unchanged after applying the total operator product. For the first term in ρ_p^q this leaves us with

$$\langle\Phi|\exp(-\hat{T})\hat{c}_p^\dagger \hat{c}_q \exp(\hat{T})|\Phi\rangle = \langle\Phi|\hat{c}_p^\dagger \hat{c}_q|\Phi\rangle + \langle\Phi|\hat{c}_p^\dagger \hat{c}_q \hat{T}|\Phi\rangle\,, \tag{C.4}$$

where we have only kept the first term in the first commutator for the Baker-Campbell-Hausdorff expansion as the second term in the first commutator will leave the state excited thus annihilating the overlap. For the term in the one-body density matrix with the Lagrange multipliers, we find

$$\langle\Phi|\hat{\Lambda}\exp(-\hat{T})\hat{c}_p^\dagger\hat{c}_q\exp(\hat{T})|\Phi\rangle = \langle\Phi|\hat{\Lambda}\hat{c}_p^\dagger\hat{c}_q|\Phi\rangle + \langle\Phi|\hat{\Lambda}\left[\hat{c}_p^\dagger\hat{c}_q,\hat{T}\right]|\Phi\rangle + \frac{1}{2!}\langle\Phi|\hat{\Lambda}\left[\left[\hat{c}_p^\dagger\hat{c}_q,\hat{T}\right],\hat{T}\right]|\Phi\rangle + \ldots. \quad \text{(C.5)}$$

Depending on the truncation level of the coupled-cluster equations, e.g., singles, doubles etc, this will provide a natural truncation for Equation C.5.

C.1 Doubles one-body density matrix

In the doubles truncation, the only contribution to Equation C.5 will be

$$\langle\Phi|\,\hat{\Lambda}e^{-\hat{T}}\hat{c}_p^\dagger\hat{c}_q e^{\hat{T}}\,|\Phi\rangle = \langle\Phi|\,\hat{\Lambda}\left[\hat{c}_p^\dagger\hat{c}_q,\hat{T}\right]\,|\Phi\rangle\,. \quad \text{(C.6)}$$

This happens as the first term in Equation C.5 will at best leave the reference relaxed by 1 as $\hat{c}_p^\dagger\hat{c}_q$ can only excite a single particle. The next commutator will suffer the same effect, but in reverse. Two $\hat{T}$ operators will leave the reference in a $+4$ state, $\hat{c}_p^\dagger\hat{c}_q$ will at best relax this to a $+3$ state. Then, $\hat{\Lambda}$, will only be able to relax the total down to a $+1$, thus annihilating the overlap. The one-body density matrix for coupled cluster doubles is then

$$\rho_p^q = \langle\Phi|\,\hat{c}_p^\dagger\hat{c}_q\,|\Phi\rangle + \langle\Phi|\left[\hat{c}_p^\dagger\hat{c}_q,\hat{T}\right]\,|\Phi\rangle + \langle\Phi|\,\hat{\Lambda}\left[\hat{c}_p^\dagger\hat{c}_q,\hat{T}\right]\,|\Phi\rangle \quad \text{(C.7)}$$

$$= \delta_j^q\delta_p^i\left(\delta_i^j + \frac{1}{2}l_{ab}^{ik}t_{kj}^{ab}\right) - \frac{1}{2}\delta_b^q\delta_p^a l_{ac}^{ij}t_{ij}^{cb}. \quad \text{(C.8)}$$

We note that there are no contribution to the terms with an occupied and a virtual index, that is, $\rho_a^i = \rho_i^a = 0$. This is a direct consequence of the lack of single excitations. The density operators $\hat{c}_a^\dagger\hat{c}_i$ and $\hat{c}_i^\dagger\hat{c}_a$ will excite and relax a single particle respectively. But, $\hat{\Lambda}$ and $\hat{T}$ only works on pairs therefore leaving the reference oddly excited or relaxed thus annihilating the overlap.

C.2 Doubles two-body density matrix

We find the two-body density matrix in the doubles approximation from the article by Kvaal [14]. These are given by Equation 6.54. Using the same block

format as Kvaal [14], we have

$$\rho_{ij}^{kl} = P(ij)\delta_{ki}\delta_{lj} - \frac{1}{2}P(ij)P(kl)\delta_{ki}\lambda_{cd}^{lm}\tau_{jm}^{cd} + \frac{1}{2}\lambda_{cd}^{kl}\tau_{ij}^{cd}, \tag{C.9}$$

for the occupied block, and we stress that m and n are occupied indices in the Fermi vacuum sense. We then have

$$\begin{aligned}\rho_{ij}^{ab} = &-\frac{1}{2}P(ab)\lambda_{cd}^{kl}\tau_{ij}^{ac}\tau_{kl}^{bd} + P(ij)\lambda_{cd}^{kl}\tau_{ik}^{ac}\tau_{jl}^{bd} \\ &+ \frac{1}{2}P(ij)\lambda_{cd}^{kl}\tau_{il}^{ab}\tau_{jk}^{cd} + \frac{1}{4}\lambda_{cd}^{kl}\tau_{kl}^{ab}\tau_{ij}^{cd} + \tau_{ij}^{ab},\end{aligned} \tag{C.10}$$

$$\rho_{ia}^{jb} = \frac{1}{2}\delta_{ji}\lambda_{ac}^{kl}\tau_{kl}^{bc} - \lambda_{ac}^{jk}\tau_{ik}^{bc}, \tag{C.11}$$

where the antisymmetry of the two-body density matrix elements yield

$$\rho_{ia}^{jb} = -\rho_{ia}^{bj} = -\rho_{ai}^{jb} = \rho_{ai}^{bj}. \tag{C.12}$$

The two final terms are

$$\rho_{ab}^{ij} = \lambda_{ab}^{ij}, \qquad \rho_{ab}^{cd} = \frac{1}{2}\lambda_{ab}^{ij}\tau_{ij}^{cd}. \tag{C.13}$$

C.3 Singles-and-doubles one-body density matrix

For coupled-cluster singles-and-doubles Equation C.5 will truncate at the double commutator as written. Employing SymPy[70] we can compute an expression for the one-body density matrices.

$$\begin{aligned}\rho_p^q = &\langle\Phi|\,\hat{c}_p^\dagger\hat{c}_q\,|\Phi\rangle + \langle\Phi|\left[\hat{c}_p^\dagger\hat{c}_q, \hat{T}\right]|\Phi\rangle + \langle\Phi|\,\hat{\Lambda}\hat{c}_p^\dagger\hat{c}_q\,|\Phi\rangle \\ &+ \langle\Phi|\,\hat{\Lambda}\left[\hat{c}_p^\dagger\hat{c}_q, \hat{T}\right]|\Phi\rangle + \frac{1}{2!}\langle\Phi|\,\hat{\Lambda}\left[\left[\hat{c}_p^\dagger\hat{c}_q, \hat{T}\right], \hat{T}\right]|\Phi\rangle\end{aligned} \tag{C.14}$$

$$\begin{aligned}= &\delta_p^a\delta_b^q\left(l_a^i t_i^b + \frac{1}{2}l_{ac}^{ij}t_{ij}^{bc}\right) + \delta_p^a\delta_i^q l_a^i + \delta_j^q\delta_p^i\left(\delta_i^j - l_a^j t_i^a + \frac{1}{2}l_{ab}^{jk}t_{ki}^{ab}\right) \\ &+ \delta_a^q\delta_p^i\left(t_i^a + l_b^j\left[t_{ij}^{ab} - t_i^b t_j^a\right] + \frac{1}{2}t_i^b l_{cb}^{kj}t_{kj}^{ac} - \frac{1}{2}t_j^a l_{cb}^{kj}t_{ki}^{cb}\right).\end{aligned} \tag{C.15}$$

In this expression we have only kept the fully contracted terms. SymPy sets the indices arbitrarily so the expression shown in Equation C.15 has been factorized and had a relabeling of the indices for improved readability.

Appendix D

Coupled-cluster autocorrelation

We compute the autocorrelation of any wave function from an initial state at time t_0 to a later time t by

$$P(t_0 \to t) \equiv \left| \langle \psi(t) | \psi(t_0) \rangle \right|^2. \tag{D.1}$$

That is, we compute the squared overlap between the initial state $|\psi(t_0)\rangle$ and the final state $|\psi(t)\rangle$. In the bi-variational formulation of Hilbert space, where the left- and right-hand states of the coupled-cluster wave function differ, some care must be taken as to how the autocorrelation should be computed.

$$P(t_0 \to t) \equiv \left| \langle \tilde{\Psi}(t) | \Psi(t_0) \rangle \right|^2 = \langle \tilde{\Psi}(t) | \Psi(t_0) \rangle \, \langle \tilde{\Psi}(t_0) | \Psi(t) \rangle \,, \tag{D.2}$$

where we note that the two latter terms no logner are complex conjugates of one another. This is a consequence of the bi-variational principle. For clarity we set $t_0 = 0$ and define $|\Psi(0)\rangle$ as the coupled cluster ground state, and $\langle \tilde{\Psi}(0)|$ as the left-hand ground state. Restricting ourselves to the case of time-independent spin-orbitals, we need to evolve the λ- and τ-amplitudes in time. We thus have to find an expression for the inner product of

$$\langle \tilde{\Psi}(t) | \Psi(0) \rangle = \langle \Phi | \Big[\mathbb{1} + \hat{\Lambda}(t) \Big] \exp(-\hat{T}(t)) \exp(\hat{T}) | \Phi \rangle \,, \tag{D.3}$$

and where the second inner product can be found by replacing the time-dependence of the amplitudes to the other state. Note that $\hat{T}(t) \neq \hat{T}$ and $\hat{\Lambda}(t) \neq \hat{\Lambda}$. We split up the $\Big[\mathbb{1} + \hat{\Lambda}\Big]$-term, and expand the exponentials. The term with $\mathbb{1}$ will only give back the overlap between the reference states. As $\hat{T}$ provides a net excitation of at least 1 and $\hat{\Lambda}$ a net relaxation of at least 1,[1]

[1] Note that this applies to the time-dependent versions of these operators as well. It is only the amplitudes that are time-dependent and not the creation nor the annihilation operators.

only terms with a combination of $\hat{\Lambda}$ and $\hat{T}$ will survive.

$$\langle\tilde{\Psi}(t)|\Psi(0)\rangle = 1 + \langle\Phi|\hat{\Lambda}(t)\exp(-\hat{T}(t))\exp(\hat{T})|\Phi\rangle \tag{D.4}$$

$$= 1 + \sum_{n=0}^{\infty}\sum_{m=0}^{\infty}\frac{(-1)^n}{n!m!}\langle\Phi|\hat{\Lambda}(t)\hat{T}^n(t)\hat{T}^m|\Phi\rangle\,, \tag{D.5}$$

where the alternating sign comes from the left-hand side, time-dependent, cluster operator. To find explicit expressions for the autocorrelation, we need to look at specific truncation levels for the cluster operators.

D.1 Doubles autocorrelation

In the doubles approximation $\hat{T}$ and $\hat{\Lambda}$ yield a net excitation and relaxation of 2, respectively. This means that $n, m \in \{0, 1\}$ as any higher exponentials will leave the reference excited after the action of $\hat{\Lambda}$. Furthermore, for $n = m = 0$, $\hat{\Lambda}$ will annihilate the reference as it acts as a relaxation operator on the Fermi vacuum. We also have for $n = m = 1$ the reference will be left doubly excited thus annihilating the overlap. This leaves us with

$$\langle\tilde{\Psi}(t)|\Psi(0)\rangle = 1 + \langle\Phi|\hat{\Lambda}(t)\left[-\hat{T}(t) + \hat{T}\right]|\Phi\rangle\,, \tag{D.6}$$

Using SymPy [70] to compute Wick's theorem and only keeping fully contracted terms, we get

$$\langle\tilde{\Psi}(t)|\Psi(0)\rangle = 1 + \frac{1}{4}\tau_{ij}^{ab}\lambda_{ab}^{ij}(t) - \frac{1}{4}\lambda_{ab}^{ij}(t)\tau_{ij}^{ab}(t). \tag{D.7}$$

The bi-variational conjugate of this equation consists of removing the time-dependence from the λ-amplitudes and switching the time-dependence in the τ-amplitudes.

D.2 Singles-and-doubles autocorrelation

Restricting ourselves to the singles and doubles approximation we have that the $\hat{T}$ operator can yield a net excitation of 1 and 2, whereas $\hat{\Lambda}$ can give a net relaxation of 1 and 2. This truncates the infinite sums in Equation D.5 to $n, m \in \{0, 1, 2\}$. Note however that for $n = m = 0$, $\hat{\Lambda}$ will annihilate the Fermi vacuum. We are then left with

$$\langle\tilde{\Psi}(t)|\Psi(0)\rangle = 1 + \langle\Phi|\hat{\Lambda}(t)\left[-\hat{T}(t) + \hat{T} - \hat{T}(t)\hat{T} + \frac{1}{2}\hat{T}(t)^2 + \frac{1}{2}\hat{T}^2\right]|\Phi\rangle\,. \tag{D.8}$$

Using SymPy [70] to compute this expression using Wick's theorem and only keeping the fully contracted terms, we find

$$\langle\tilde{\Psi}(t)|\Psi(0)\rangle = 1 + \lambda_a^i(t)\left[\tau_i^a - \tau_i^a(t)\right] + \lambda_{ab}^{ij}(t)\left[\frac{1}{4}\tau_{ij}^{ab} - \frac{1}{2}\tau_j^a\tau_i^b - \tau_i^a(t)\tau_j^b - \frac{1}{2}\tau_j^a(t)\tau_i^b(t) - \frac{1}{4}\tau_{ij}^{ab}(t)\right] \tag{D.9}$$

and the bi-variational conjugate of this equation by switching the time-dependence of the amplitudes.

Bibliography

1. Landreman, M. A Nontrivial Manifesto. *Physics Today* **58,** 52 (2005).
2. Hartree, D. R. The Wave Mechanics of an Atom with a Non-Coulomb Central Field. Part I. Theory and Methods. *Mathematical Proceedings of the Cambridge Philosophical Society* **24,** 89 (1928).
3. Szabo, A. & Ostlund, N. S. *Modern Quantum Chemistry: Intro to Advanced Electronic Structure Theory* (Dover publications, 1996).
4. Ullrich, C. A. *Time-Dependent Density-Functional Theory. Concepts and Applications* (Oxford University Press, 2011).
5. Hjorth-Jensen, M., Lombardo, M. P. & van Kolck, U. *An advanced course in computational nuclear physics* in *Lecture Notes in Physics* **936** (Springer International Publishing, 2017).
6. Helgaker, T., Jørgensen, P. & Olsen, J. *Molecular Electronic-Structure Theory* (John Wiley & Sons, Ltd, 2000).
7. Coester, F. Bound states of a many-particle system. *Nuclear Physics* **7,** 421 (1958).
8. Goings, J. J., Lestrange, P. J. & Li, X. Real-time time-dependent electronic structure theory. *Wiley Interdisciplinary Reviews: Computational Molecular Science* **8,** e1341 (2018).
9. Joachain, C. J., Kylstra, N. J. & Potvliege, R. M. *Atoms in Intense Laser Fields* (Cambridge University Press, 2009).
10. Shavitt, I. & Bartlett, R. J. *Many-Body Methods in Chemistry and Physics. MBPT and Coupled-Cluster Theory* ISBN: 978-0-511-59683-4 (Cambridge University Press, 2009).
11. Hagen, G., Papenbrock, T., Hjorth-Jensen, M. & Dean, D. J. Coupled-cluster computations of atomic nuclei. *Reports on Progress in Physics* **77,** 096302 (2014).
12. Gauss, J. & Stanton, J. F. Coupled-cluster calculations of nuclear magnetic resonance chemical shifts. *The Journal of Chemical Physics* **103,** 3561 (1995).

13. Lohne, M. P., Hagen, G., Hjorth-Jensen, M., Kvaal, S. & Pederiva, F. Ab initio computation of the energies of circular quantum dots. *Physical Review B* **84,** 115302 (2011).
14. Kvaal, S. Ab initio quantum dynamics using coupled-cluster. *The Journal of Chemical Physics* **136,** 194109 (2012).
15. Kvaal, S. Variational formulations of the coupled-cluster method in quantum chemistry. *Molecular Physics* **111,** 1100 (2013).
16. Hochstuhl, D., Hinz, C. & Bonitz, M. Time-dependent multiconfiguration methods for the numerical simulation of photoionization processes of many-electron atoms. *The European Physical Journal Special Topics* **223,** 177 (2014).
17. Winther-Larsen, S. G. *AQUADUCT* Ab Initio *Quantum Dynamics Using Coupled Cluster in Time* MA thesis (University of Oslo, 2019).
18. Sun, Q. *et al.* PySCF: the Python-based simulations of chemistry framework. *Wiley Interdisciplinary Reviews: Computational Molecular Science* **8,** e1340 (2018).
19. Parrish, R. M. *et al.* Psi4 1.1: An Open-Source Electronic Structure Program Emphasizing Automation, Advanced Libraries, and Interoperability. *Journal of Chemical Theory and Computation* **13,** 3185 (2017).
20. Kristiansen, H. E. *Time Evolution of Quantum Mechanical Many-Body Systems* MA thesis (University of Oslo, 2017).
21. Myhre, R. H. Demonstrating that the nonorthogonal orbital optimized coupled cluster model converges to full configuration interaction. *The Journal of Chemical Physics* **148,** 094110 (2018).
22. Pedersen, T. B. & Kvaal, S. Symplectic integration and physical interpretation of time-dependent coupled-cluster theory. *The Journal of Chemical Physics* **150,** 144106 (2019).
23. Dirac, P. A. M. *The principles of quantum mechanics* (Oxford university press, 1981).
24. Von Neumann, J. *Mathematical foundations of quantum mechanics* (Princeton university press, 2018).
25. Salasnich, L. *Quantum Physics of Light and Matter* (Springer, 2017).
26. Leinaas, J. M. *Modern Quantum Mechanics. Lecture notes - FYS4110* (2018).
27. Dirac, P. A. M. A new notation for quantum mechanics. *Mathematical Proceedings of the Cambridge Philosophical Society* **35,** 416 (1939).
28. Griffiths, D. J. *Introduction to Quantum Mechanics* (Cambridge University Press, 2017).

29. Kvaal, S. *Lecture notes for FYS-KJM4480 - Quantum mechanics for many-particle systems* 2017.
30. Jost, J. & Jost Li-Jost, X. *Calculus of variations* (Cambridge University Press, 1998).
31. Feynman, R. P. Forces in Molecules. *Physical Review* **56,** 340 (4 1939).
32. Kramer, P. & Saraceno, M. *Geometry of the time-dependent variational principle in quantum mechanics* (Springer, 1981).
33. Frenkel, Y. I. *Wave Mechanics: Advanced General Theory* (Oxford at the Clarendon Press, 1934).
34. Bladel, J. V. Lorenz or Lorentz? *IEEE Antennas and Propagation Magazine* **33,** 69 (1991).
35. Robinett, R. W. Quantum wave packet revivals. *Physics Reports* **392,** 1 (2004).
36. Leinaas, J. M. & Myrheim, J. On the theory of identical particles. *Il Nuovo Cimento B (1971-1996)* **37,** 1 (1977).
37. Fraleigh, J. B. *A first course in abstract algebra* (Pearson Education Inc., 2003).
38. Wick, G. C. The Evaluation of the Collision Matrix. *Physical Review* **80,** 268 (2 1950).
39. Slater, J. C. The Theory of Complex Spectra. *Physical Review* **34,** 1293 (10 1929).
40. Condon, E. U. The Theory of Complex Spectra. *Physical Review* **36,** 1121 (7 1930).
41. Wikipedia contributors. *Slater–Condon rules — Wikipedia, The Free Encyclopedia* [Online; accessed 6-August-2019]. 2014.
42. Thouless, D. Stability conditions and nuclear rotations in the Hartree-Fock theory. *Nuclear Physics* **21,** 225 (1960).
43. Born, M. & Oppenheimer, R. Zur Quantentheorie der Molekeln. *Annalen der Physik* **389,** 457 (1927).
44. Mayer, I. *Simple Theorems, Proofs, and Derivations in Quantum Chemistry* (Springer, 2003).
45. Löwdin, P. O. Quantum Theory of Many-Particle Systems. I. Physical Interpretations by Means of Density Matrices, Natural Spin-Orbitals, and Convergence Problems in the Method of Configurational Interaction. *Physical Review* **97,** 1474 (1955).
46. Høgberget, J. *Quantum monte-carlo studies of generalized many-body systems* MA thesis (University of Oslo, 2013).

47. Lyche, T. *Lecture Notes for Mat-inf 4130* 2017.

48. Mayer, I. On Löwdin's method of symmetric orthogonalization*. Löwdin's Method of Symmetric Orthogonalization. *International Journal of Quantum Chemistry* **90,** 63 (2002).

49. Karwowski, J. in *Methods in Computational Molecular Physics* (eds Wilson, S. & Diercksen, G.) 65 (Springer US, 1992).

50. Crawford, T. D. & Schaefer III, H. F. in *Reviews in Computational Chemistry, Volume 14* (eds Lipkowitz, K. B. & Boyd, D. B.) 33 (John Wiley & Sons, Ltd, 2007).

51. Pople, J. A., Binkley, J. S. & Seeger, R. Theoretical models incorporating electron correlation. *International Journal of Quantum Chemistry* **10,** 1 (1976).

52. Nooijen, M., Shamasundar, K. R. & Mukherjee, D. Reflections on size-extensivity, size-consistency and generalized extensivity in many-body theory. *Molecular Physics* **103,** 2277 (2005).

53. Monkhorst, H. J. Calculation of properties with the coupled-cluster method. *International Journal of Quantum Chemistry* **12,** 421 (1977).

54. Čížek, J. On the Correlation Problem in Atomic and Molecular Systems. Calculation of Wavefunction Components in Ursell-Type Expansion Using Quantum-Field Theoretical Methods. *The Journal of Chemical Physics* **45,** 4256 (1966).

55. Fink, M. A new method for evaluating the density matrix and its application to the ground state form factors of 4He and 16O. *Nuclear Physics A* **221,** 163 (1974).

56. Helgaker, T. & Jørgensen, P. Configuration-interaction energy derivatives in a fully variational formulation. *Theoretica chimica acta* **75,** 111 (1989).

57. Arponen, J. Variational principles and linked-cluster exp S expansions for static and dynamic many-body problems. *Annals of Physics* **151,** 311 (1983).

58. Löwdin, P. O., Froelich, P. & Mishra, M. Some properties of the bivariational Hartree–Fock scheme for complex symmetric many-particle operators. *International Journal of Quantum Chemistry* **36,** 93 (1989).

59. Pedersen, T. B., Koch, H. & Hättig, C. Gauge invariant coupled cluster response theory. *The Journal of Chemical Physics* **110,** 8318 (1999).

60. Pedersen, T. B., Fernández, B. & Koch, H. Gauge invariant coupled cluster response theory using optimized nonorthogonal orbitals. *The Journal of Chemical Physics* **114,** 6983 (2001).

61. Balian, R. & Brezin, E. Nonunitary bogoliubov transformations and extension of Wick's theorem. *Il Nuovo Cimento B* **64,** 37 (1969).

62. Bozkaya, U., Turney, J. M., Yamaguchi, Y., Schaefer, H. F. & Sherrill, C. D. Quadratically convergent algorithm for orbital optimization in the orbital-optimized coupled-cluster doubles method and in orbital-optimized second-order Møller-Plesset perturbation theory. *The Journal of Chemical Physics* **135,** 104103 (2011).

63. Hoodbhoy, P. & Negele, J. W. Time-dependent coupled-cluster approximation to nuclear dynamics. I. Application to a solvable model. *Physical Review C* **18,** 2380 (5 1978).

64. Hoodbhoy, P. & Negele, J. W. Time-dependent coupled-cluster approximation to nuclear dynamics. II. General formulation. *Physical Review C* **19,** 1971 (5 1979).

65. Huber, C. & Klamroth, T. Explicitly time-dependent coupled cluster singles doubles calculations of laser-driven many-electron dynamics. *The Journal of Chemical Physics* **134,** 054113 (2011).

66. Kristiansen, H. E., Schøyen, Ø. S., Kvaal, S. & Pedersen, T. B. Numerically stable time-dependent coupled-cluster simulations of many-electron dynamics in intense laser pulses. *To be determined.* Manuscript in preparation (2019).

67. Van Rossum, G. & Drake Jr, F. L. *Python tutorial* (Centrum voor Wiskunde en Informatica Amsterdam, The Netherlands, 1995).

68. Jones, E., Oliphant, T. E., Peterson, P., *et al. SciPy: Open source scientific tools for Python* 2001. `http://www.scipy.org/`.

69. Oliphant, T. E. *A guide to NumPy* (Trelgol Publishing USA, 2006).

70. Meurer, A. *et al.* SymPy: Symbolic computing in Python. *PeerJ Computer Science* **3,** e103 (Jan. 2017).

71. Dask Development Team. *Dask: Library for dynamic task scheduling* (2016). `https://dask.org`.

72. Nishino, R. O. Y. U. D. & Loomis, S. H. C. *CuPy: A NumPy-Compatible Library for NVIDIA GPU Calculations* (2017). `https://cupy.chainer.org/`.

73. Brookner, E. *Tracking and Kalman filtering made easy* (Wiley Online Library, 1998).

74. Pulay, P. Convergence acceleration of iterative sequences. the case of scf iteration. *Chemical Physics Letters* **73,** 393 (1980).

75. Pulay, P. Improved SCF convergence acceleration. *Journal of Computational Chemistry* **3,** 556 (1982).

76. Shepard, R. & Minkoff, M. Some comments on the DIIS method. *Molecular Physics* **105,** 2839 (2007).

77. Rackauckas, C. & Nie, Q. DifferentialEquations.jl – A Performant and Feature-Rich Ecosystem for Solving Differential Equations in Julia. *Journal of Open Research Software* **5,** 15 (2017).

78. Mørken, K. M. *Numerical Algorithms and Digital Representation* 2017.

79. Magnus, W. On the exponential solution of differential equations for a linear operator. *Communications on Pure and Applied Mathematics* **7,** 649 (1954).

80. Miyagi, H. & Bojer Madsen, L. Time-dependent restricted-active-space self-consistent-field singles method for many-electron dynamics. *The Journal of Chemical Physics* **140,** 164309 (2014).

81. Yuan, F. *et al.* Addition and removal energies of circular quantum dots. *The Journal of Chemical Physics* **147,** 164109 (2017).

82. Anisimovas, E. & Matulis, A. Energy spectra of few-electron quantum dots. *Journal of Physics: Condensed Matter* **10,** 601 (1998).

83. Lam, S. K., Pitrou, A. & Seibert, S. *Numba: A LLVM-based Python JIT Compiler* in *Proceedings of the Second Workshop on the LLVM Compiler Infrastructure in HPC* (ACM, 2015), 7.

84. Lattner, C. & Adve, V. *LLVM: A Compilation Framework for Lifelong Program Analysis & Transformation* in *Proceedings of the International Symposium on Code Generation and Optimization: Feedback-directed and Runtime Optimization* (IEEE Computer Society, 2004), 75.

85. Su, Q. & Eberly, J. H. Model atom for multiphoton physics. *Physical Review A* **44,** 5997 (9 1991).

86. Garcia de la Vega, J. M. & Miguel, B. in *Introduction to advanced topics of computational chemistry* (eds Montero, L. A., Diaz, L. A. & Bader, R.) 41 (2003).

87. Hehre, W. J., Stewart, R. F. & Pople, J. A. Self-Consistent Molecular-Orbital Methods. I. Use of Gaussian Expansions of Slater-Type Atomic Orbitals. *The Journal of Chemical Physics* **51,** 2657 (1969).

88. Ditchfield, R., Hehre, W. J. & Pople, J. A. Self-Consistent Molecular-Orbital Methods. IX. An Extended Gaussian-Type Basis for Molecular-Orbital Studies of Organic Molecules. *The Journal of Chemical Physics* **54,** 724 (1971).

89. Dunning, T. H. Gaussian basis sets for use in correlated molecular calculations. I. The atoms boron through neon and hydrogen. *The Journal of Chemical Physics* **90,** 1007 (1989).

90. Kendall, R. A., Dunning, T. H. & Harrison, R. J. Electron affinities of the first-row atoms revisited. Systematic basis sets and wave functions. *The Journal of Chemical Physics* **96,** 6796 (1992).

91. Roothaan, C. C. J. New Developments in Molecular Orbital Theory. *Reviews of Modern Physics* **23,** 69 (1951).

92. Hall, G. G. & Lennard-Jones, J. E. The molecular orbital theory of chemical valency VIII. A method of calculating ionization potentials. *Proceedings of the Royal Society of London. Series A. Mathematical and Physical Sciences* **205,** 541 (1951).

93. Olsen, V. K. B. *Full configuration interaction simulation of quantum dots* MA thesis (University of Oslo, 2012).

94. Muła, W., Kurz, N. & Lemire, D. Faster Population Counts Using AVX2 Instructions. *The Computer Journal* **61,** 111 (2017).

95. Anderson, E. *et al. LAPACK Users' Guide* (Society for Industrial and Applied Mathematics, 1999).

96. Lehoucq, R. B., Sorensen, D. C. & Yang, C. *ARPACK Users' Guide: Solution of Large Scale Eigenvalue Problems by Implicitly Restarted Arnoldi Methods.* 1997.

97. Bartlett, R. J. & Purvis, G. D. Many-body perturbation theory, coupled-pair many-electron theory, and the importance of quadruple excitations for the correlation problem. *International Journal of Quantum Chemistry* **14,** 561 (1978).

98. Cramer, C. J. *Essentials of Computational Chemistry: Theories and Models* (John Wiley & Sons, Chichester, England, 2004).

99. Zanghellini, J., Kitzler, M., Brabec, T. & Scrinzi, A. Testing the multi-configuration time-dependent Hartree–Fock method. *Journal of Physics B: Atomic, Molecular and Optical Physics* **37,** 763 (2004).

100. Li, X. *et al.* A time-dependent Hartree–Fock approach for studying the electronic optical response of molecules in intense fields. *Physical Chemistry Chemical Physics* **7,** 233 (2 2005).

101. Nest, M., Padmanaban, R. & Saalfrank, P. Time-dependent approach to electronically excited states of molecules with the multiconfiguration time-dependent Hartree-Fock method. *The Journal of Chemical Physics* **126,** 214106 (2007).

102. Grecco, H. *Pint* `https://github.com/hgrecco/pint`. 2019.

103. Isborn, C. M. & Li, X. Singlet–Triplet Transitions in Real-Time Time-Dependent Hartree–Fock/Density Functional Theory. *Journal of Chemical Theory and Computation* **5,** 2415 (2009).

104. Chieh, C. P. *Bond Lengths and Energies* [Online; accessed 31-August-2019]. 2019. https://chem.libretexts.org/Bookshelves/Physical_and_Theoretical_Chemistry_Textbook_Maps/Supplemental_Modules_(Physical_and_Theoretical_Chemistry)/Chemical_Bonding/Fundamentals_of_Chemical_Bonding/Chemical_Bonds/Bond_Lengths_and_Energies.

105. Kosloff, R. & Kosloff, D. Absorbing boundaries for wave propagation problems. *Journal of Computational Physics* **63,** 363 (1986).

106. Sato, T. *et al.* Time-dependent complete-active-space self-consistent-field method for atoms: Application to high-order harmonic generation. *Physical Review A* **94,** 023405 (2 2016).

107. Sawada, R., Sato, T. & Ishikawa, K. L. Analysis of strong-field enhanced ionization of molecules using Bohmian trajectories. *Physical Review A* **90,** 023404 (2 2014).

108. Sato, T. & Ishikawa, K. L. The structure of approximate two electron wavefunctions in intense laser driven ionization dynamics. *Journal of Physics B: Atomic, Molecular and Optical Physics* **47,** 204031 (2014).

109. Kristiansen, H. E., Schøyen, Ø. S., Winther-Larsen, S. G. & Hjorth-Jensen, M. Time Evolution of Quantum Dot Systems. *To be determined.* Manuscript in preparation (2019).